

Bioinspired Modification and Functionalization of Hydrogels for Applications in Biomedicine

Biologisch-inspirierte Modifizierung und Funktionalisierung von Hydrogelen für Anwendungen in der Biomedizin



Doctoral thesis for a doctoral degree
at the Graduate School of Life Sciences,
Julius-Maximilians-University Würzburg,
Section Biomedicine

submitted by

Matthias Beudert

From

Bad Kissingen

Würzburg, 2022



Submitted on:

Members of the Thesis Committee

Chairperson: Prof. Dr. Carmen Villmann

Primary Supervisor: Prof. Dr. Tessa Lühmann

Supervisor (Second): Prof. Dr. Robert Luxenhofer

Supervisor (Third): Prof. Dr. Felix Engel

Date of Public Defence:

Date of Receipt of Certificates:

The presented work has been carried out as a member of the Graduate School of Life Science under the supervision of Professor Dr. Dr. Lorenz Meinel and Prof. Dr. Tessa Lühmann at the Chair of Drug Formulation and Delivery at the Institute for Pharmacy and Food Chemistry of the Julius Maximilian University of Wuerzburg between November 2017 and April 2022

Table of Content

Acknowledgments	III
List of Publications	V
Other Scientific Contributions	VI
Abbreviations	VII
1. Introduction	1
1.1 The Extracellular Matrix as a Role Model for Biomaterials	1
1.2 Hydrogels – Design and Application in Biomedicine	3
1.3. Hydrogel Conjugation Strategies	4
1.3.1. Covalent Hydrogel Crosslinking	4
1.3.2. Bioconjugation Strategies	5
1.4. Applications	8
1.4.1. Hydrogels as Wound Sealants	8
1.4.2. Hydrogels in Biofabrication	9
1.4.3. Hydrogels in Controlled Drug Delivery	11
2. Summary	14
3. Zusammenfassung	16
4. Chapter 1: From Thermogelling Hydrogel Towards Functional Bioinks: Controlled Modification and Cytocompatible Crosslinking	18
5. Chapter 2: Merging Bioresponsive Release of Insulin-like Growth Factor I with 3D Printable Thermogelling Hydrogels	49
6. Chapter 3: Fibrin Sealants – Today and Tomorrow	77
7. Chapter 4: Molecular Engineering of Fibrinogen for Improved Stability Towards Plasmin Degradation	91
8. Materials & Methods	138
9. Discussion & Outlook	139
9.1 Thermogelling POx/POzi Hydrogels for Drug Delivery and Biofabrication.....	139
9.2 Development of Improved Fibrin Sealants for Wound Closure.....	142
10. References	146
Declaration of Authorship	157
Affidavit	162
Eidesstattliche Erklärung	162
Curriculum vitae	163

Acknowledgments

Zu Beginn möchte ich mich ausdrücklich bei Prof. Dr. Dr. Lorenz Meinel dafür bedanken, dass er mir die Möglichkeit gegeben hat, meine Dissertation an seinem Lehrstuhl anzufertigen, was mir erlaubte an zukunftssträchtigen und faszinierenden Themen zu forschen. Außerdem weiß ich seine stets fachlich kompetente Beratung zu schätzen, die mir sowohl wissenschaftlich als auch persönlich geholfen hat. Zusätzlich möchte ich mich für seine volle Unterstützung bedanken, weitere Möglichkeiten der Fortbildung außerhalb der Universität zu verfolgen.

Großer Dank gilt außerdem meiner Betreuerin Prof. Dr. Tessa Lühmann, die mir während dieser Zeit mit Rat und Tat zur Seite stand, mich unterstützte und immer ein offenes Ohr für mich hatte. Ihr Vertrauen in meine Fähigkeiten erlaubte mir, mich zu entfalten und die Projekte frei und eigenständig voranzutreiben, was mich persönlich gefordert, aber auch sehr positiv geprägt hat.

Des Weiteren möchte ich mich bei Prof. Dr. Robert Luxenhofer und Prof. Dr. Felix Engel dafür bedanken, meine Promotion im Rahmen der *Graduate School of Life Science* begleitet zu haben. In unseren Meetings setzen sie immer wieder neue Impulse, die die gemeinsamen Projekte entschieden vorantrieben. Zusätzlicher Dank gebührt in diesem Zusammenhang auch dem gesamten Team der *Graduate School of Life Science* für die Unterstützung und Hilfe während der Doktorarbeit.

Mein Dank gilt außerdem meinen Kooperationspartnern, durch die ich Einblicke in neue Themenfelder erhalten habe und die maßgeblich zum Erfolg dieser Arbeit beigetragen haben. Dies gilt zudem für Prof. Dr. Andreas Schlosser and Stephanie Lamer vom Rudolf-Virchow-Zentrum sowie Prof. Dr. Jürgen Seibel und Juliane Adelman vom Institut für organische Chemie in Würzburg, die mich bei massenspektrometrischen Analysen unterstützt haben. In diesem Zusammenhang ist außerdem Lars Schönemann vom Rudolf-Virchow-Zentrum durch seine Hilfe und seinen Rat bei Klonierungs-Experimenten hervorzuheben.

Dank gilt dem Forschungsverbund SFB TRR225 für die Einsicht in neue Themenfelder und die Erfahrungen, die ich auf gemeinsamen Konferenzen und Tagungen gewinnen konnte, die mich sowohl wissenschaftlich als auch persönlich vorangebracht haben. Hervorzuheben sind hierbei vor allem Dr. Lukas Hahn und Prof. Dr. Robert Luxenhofer für die erfolgreiche Zusammenarbeit beim Teilprojekt A03 des SFB TRR225.

Besonderer Dank gilt all meinen Kolleginnen und Kollegen am Lehrstuhl für Pharmazeutische Pharmazie und Technologie in Würzburg, die mich über die Jahre auf dieser Reise begleitet haben. Speziell möchte ich mich hier bei Marco Saedtler, Tobias Miesler und Katharina Dodt für ihre Freundschaft und Unterstützung v.a. zu Beginn der Doktorarbeit bedanken. Niklas Hauptstein möchte ich für die wertvollen Diskussion im Büro wie auch die zahlreichen weiteren außeruniversitären Aktivitäten danken. Spezieller Dank gilt zudem Simon Hanio und Björn ter Mors für die Kicker-Duelle, Kaffee-Pausen, Gespräche, Feiern und die insgesamt unvergessliche Zeit zusammen in Würzburg. Hervorzuheben ist außerdem Marcus Gutmann für seine durchgängige Unterstützung und Hilfe in wissenschaftlichen Bereichen sowie die enge Freundschaft.

Zum Schluss möchte ich mich bei meiner Familie für ihre bedingungslose Unterstützung während dieser Zeit bedanken. Durch euch bin ich zu der Person geworden, die ich bin. Ihr habt mir stets alle Freiheiten gelassen, mich zu entfalten und meinen eigenen Weg zu finden. Abschließend möchte ich mich bei meiner Partnerin Judith bedanken. Du warst während der ganzen Zeit, sowohl in Höhen als auch Tiefen, immer an meiner Seite. Ohne dich wäre diese Arbeit nicht möglich gewesen.

List of Publications

Beudert, M.; Gutmann, M.; Lühmann, T.; Meinel, L., Fibrin Sealants: Challenges and Solutions. *ACS Biomater Sci Eng* 2022, 8 (6), 2220-2231.

Beudert, M.; Hahn, L.; Horn, A. H. C.; Hauptstein, N.; Sticht, H.; Meinel, L.; Luxenhofer, R.; Gutmann, M.; Lühmann, T., Merging bioresponsive release of insulin-like growth factor I with 3D printable thermogelling hydrogels. *J Control Release* **2022**, 347, 115-126.

Hahn, L.; **Beudert, M.;** Gutmann, M.; Keßler, L.; Stahlhut, P.; Fischer, L.; Karakaya, E.; Lorson, T.; Thievensen, I.; Detsch, R.; Lühmann, T.; Luxenhofer, R., From Thermogelling Hydrogels toward Functional Bioinks: Controlled Modification and Cytocompatible Crosslinking. *Macromol Biosci* **2021**, e2100122.

Hasselmann, S.; Hahn, L.; Lorson, T.; Schätzlein, E.; Sébastien, I.; **Beudert, M.;** Lühmann, T.; Neubauer, J. C.; SEXTL, G.; Luxenhofer, R.; Heinrich, D., Freeform direct laser writing of versatile topological 3D scaffolds enabled by intrinsic support hydrogel. *Materials Horizons* **2021**, 8 (12), 3334-3344.

Hahn, L.; Maier, M.; Stahlhut, P.; **Beudert, M.;** Flegler, V.; Forster, S.; Altmann, A.; Toppe, F.; Fischer, K.; Seiffert, S.; Bottcher, B.; Lühmann, T.; Luxenhofer, R., Inverse Thermogelation of Aqueous Triblock Copolymer Solutions into Macroporous Shear-Thinning 3D Printable Inks. *ACS Appl Mater Interfaces* **2020**, 12 (11), 12445-12456.

Lübtow, M. M.; Mrlik, M.; Hahn, L.; Altmann, A.; **Beudert, M.;** Lühmann, T.; Luxenhofer, R., Temperature-Dependent Rheological and Viscoelastic Investigation of a Poly(2-methyl-2-oxazoline)-b-poly(2-iso-butyl-2-oxazoline)-b-poly(2-methyl-2-oxazoline)-Based Thermogelling Hydrogel. *J. Funct Biomater*. *J Funct Biomater* **2019**, 10 (3), 36.

Fischer, J. C.; Lin, C. C.; Heidegger, S.; Wintges, A.; Schlapschy, M.; **Beudert, M.;** Combs, S. E.; Bassermann, F.; Skerra, A.; Haas, T.; Poeck, H., Regeneration After Radiation- and Immune-Mediated Tissue Injury Is Not Enhanced by Type III Interferon Signaling. *Int J Radiat Oncol Biol Phys* **2019**, 103 (4), 970-976. (work done during master program at the Technical University of Munich)

Other Scientific Contributions

Beudert, M.; et al., “3D printable poly(2-oxazoline) hydrogels for bioresponsive release of insulin-like growth factor I.” Scientific talk at the DPhG Annual meeting **2021**.

Beudert, M.; et al., “Modification of thermogelling poly(2-oxazoline)-based hydrogels with cell adhesion peptides for their use In biofabrication.” Poster at the Controlled Release Society Local Chapter Germany **2019**.

Beudert, M.; et al., “Development & Translation of Bioresponsive Drug Delivery Systems & Medical Devices.” Poster at Galenus Workshop **2018**.

Beudert, M.; et al., “Biofunctionalization of thermogelling poly(2-oxazoline)-based hydrogels by Diels Alder chemistry.” Poster at the International Conference on Biofabrication **2018**.

Abbreviations

Abbreviations from the individual chapters 1-4 are explained in their respective part and are not listed here.

AA	Amino Acid
AM	Additive manufacturing
API	Active pharmaceutical ingredient
BMP-2	Bone morphogenic protein 2
CHO	Chinese hamster ovary
DBCO	Dibenzocyclooctyne
ECM	Extracellular matrix
Fbg	Fibrinogen
U.S.FDA	United States Food and Drug Administration
IGF-I	Insulin-like growth factor I
MMP	Matrix metalloproteinase
NHS	<i>N</i> -hydroxysuccinimide
PEG	Polyethylene glycol
PLGA	Poly-lactic-glycolic-acid
POx	poly(2-substituted-oxazoline)
POzi	poly(2-oxazine)
RGD	Arginine-glycine-aspartate
TE	Tissue engineering
TG	Transglutaminase
TGF- β 1	Transforming growth factor-beta 1
UV	Ultraviolet
3D	Three-dimensional

1. Introduction

Since time immemorial, materials have been used by humans to fix physical infirmities (e.g., burns, bruises, fractures, bleeding) or ease the burden that often comes with them. In the beginning, dating back to the antique, mostly natural materials were used in the attempt to substitute parts of the body that have been lost due to injuries or diseases. Back then, the selection of materials was highly limited to natural resources like wood or nacre due to their availability.^{1,2} Some of the earliest recordings of the use of biomaterials are the application of linen sutures for wound closure by the early Egyptians or the nacre dental implants by the Mayan people around 600 AD.² The emergence of new synthetic alternatives like polymers or ceramics paved the way for a much more versatile and efficient usage of materials that led to various groundbreaking products such as stents or contact lenses that have revolutionized the biomaterial and biomedical sector.^{1,3,4}

In these early stages of this new wave of biomaterials, the main focus lay on bioinert materials that minimized host tissue interaction and thereby potential rejections or side effects.^{3,5} This is also reflected in the first widely accepted definition for biomaterials that was established at the sixth “Annual International Biomaterial Symposium” in Clemson, South Carolina (USA) in 1974: “A biomaterial is a systematically, pharmacologically inert substance designed for implantation within or incorporation with a living system”.^{5,6} However, starting with the molecular biology evolution and the rise of biosciences, the field of biomaterials gained momentum and changed drastically.^{1,7} Due to new technologies and insights into the molecular processes of the body, the role of life sciences tremendously increased over the years. Nowadays, nature is increasingly used as a model and inspiration, resulting in biomaterials that are designed to mimic properties of native tissues in order to produce tailored biomaterials for specific applications.⁸ New advances enable the integration of spatiotemporal distribution of biochemical moieties⁹ as well as stimulated changes to the materials that can impact cell behaviour.^{10,11}

1.1 The Extracellular Matrix as a Role Model for Biomaterials

The human body consists of a multitude of different tissues. Daily life is a constant interplay and remodeling both in healthy tissues due to adaptations as well as during diseases, e.g., in tumor growth or invasion.¹²⁻¹⁴ It has been established for years, that the microenvironment of the cells can determine cell fate and behavior.¹⁵ Therefore, one of the main interests for biomaterials has been the recreation of target microenvironments. In all tissues, the extracellular matrix (ECM) is surrounding the cells and provides structural support as well as a dynamic interplay of physical and chemical signals needed for vital processes like cell adhesion, migration, or stimulation.^{16,17}

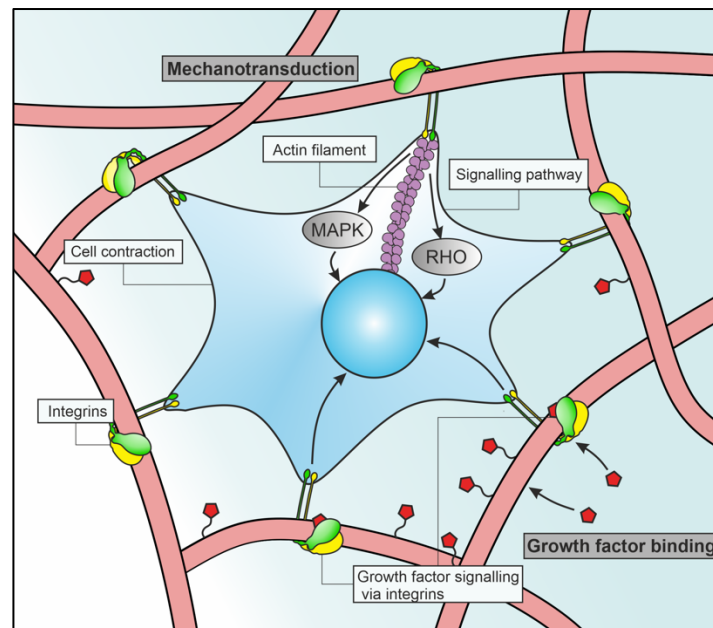


Figure 1: Schematic overview of the natural ECM and the triggered growth factor signalling and mechanotransduction (adapted and modified from ¹⁸).

The ECM is a dynamic three-dimensional (3D) network that consists of a multitude of different macromolecules, including fibrous proteins (e.g., collagen), glycoproteins (e.g., fibronectin) and proteoglycans (e.g., aggrecan).^{19, 20} The ECM network (fiber diameter range from 10 nm to 300 μm) forms a hydrogel-like structure *in vivo* that builds both a foundation and structural framework for cells and can influence cell behavior, e.g., by mechanotransduction (Fig. 1).^{14, 18, 20} Different components of the ECM contain specific AA sequences that facilitate important properties of native tissues. One of the most studied sequences is the so-called arginine-glycine-aspartate-(RGD-)motif which is found in different ECM proteins including fibronectin or fibrinogen (Fbg). This sequence facilitates cell adhesion via integrin binding and is therefore essential for a multitude of cellular processes such as cell migration or differentiation ^{21, 22} Another important mechanism in tissues is the dynamic balance between ECM maintenance and remodeling. Cells, e.g., secrete proteases such as matrix metalloproteases (MMP) that recognize and cleave specific peptide sequences in ECM proteins. This enables ECM turnover and regeneration during important process such as tissue healing.²³ Furthermore, the ECM contains and presents a wide array of different biomolecules (e.g., growth factors or cytokines) that are essential for cellular processes and signalling.²⁴ Because of these unique properties, the development and use of hydrogels has become increasingly important in order to mimic these exceptional properties of ECM.

1.2 Hydrogels – Design and Application in Biomedicine

For decades, hydrogels have been developed as biomaterials for their use in biomedicine. Even though the term hydrogel was already mentioned at the end of the 19th century as a description for colloidal gels²⁵, the earliest hydrogels, according to the current use of the term, were developed by the 1950s and 60s.^{3, 26, 27} In general, hydrogels are defined as highly water-absorbable 3D networks.²⁷⁻²⁹ In the early stages, hydrogel technologies were mainly developed for their application in/on human bodies such as contact lenses.²⁷ However, due to the high-water content, porosity, adaptability and in general favorable properties that resemble human tissue, hydrogels have emerged as a powerful platform for a multitude of biomedical applications such as tissue engineering (TE).^{28, 30, 31}

There is a vast variety of different design criteria that must be considered before choosing a hydrogel for specific applications in biomedicine such as – (I) biocompatibility (II) polymer source (III) crosslinking mechanism and (IV) printability. (I) One of the most important criteria in this regard is the ability of biomaterials body without harming surrounding tissue or even enhance the performance and interaction of the material with native tissue. This is generally referred to as biocompatibility.³² (II) Another popular criterion is the choice of the material depending on its origin. In general, you can distinguish between natural and synthetic polymers which can be used either in pure form or as hybrid formulation (Fig. 2). Both classes have been extensively studied over the years and have different advantages and disadvantages that need to be considered before using them as biomaterials.

Natural polymers are polymers that are derived from a natural source. This group comprises a huge variety of different materials and has several properties that make them promising biomaterials, including biocompatibility and biodegradability.³³ However, there are also limitations such as weaker mechanical properties or batch-to-batch variations.^{34, 35} Synthetic polymers are designed and synthesized from monomers and can be customized, e.g., regarding their molecular weight as well as their mechanical properties for different applications and are reproducible.^{36, 37} Yet, synthetic polymers are most of the time bioinert and can show more cytotoxicity than their natural counterpart.^{38, 39} (III) A different important property is the type of crosslinking mechanism used for the gel formation. Hydrogels can be formed either by chemical crosslinking (covalent conjugation, see paragraph on covalent hydrogel crosslinking) or physical crosslinking.²⁷ The latter are reversible and mostly based on physical interactions such as pi-pi-stacking⁴⁰, ionic⁴¹ and hydrophobic interactions⁴², or hydrogen bonds⁴³. Independent of the type of crosslinking, gel formation can be induced through a multitude of different stimuli such as pH-value⁴⁴, temperature⁴⁵, or ultraviolet (UV)-light⁴⁶.

Different criteria can also be applied regarding specific properties needed for target applications. (IV) Hydrogels can, e.g., be classified into printable and non-printable materials which is important to create more complex structures, e.g., in field of biofabrication.

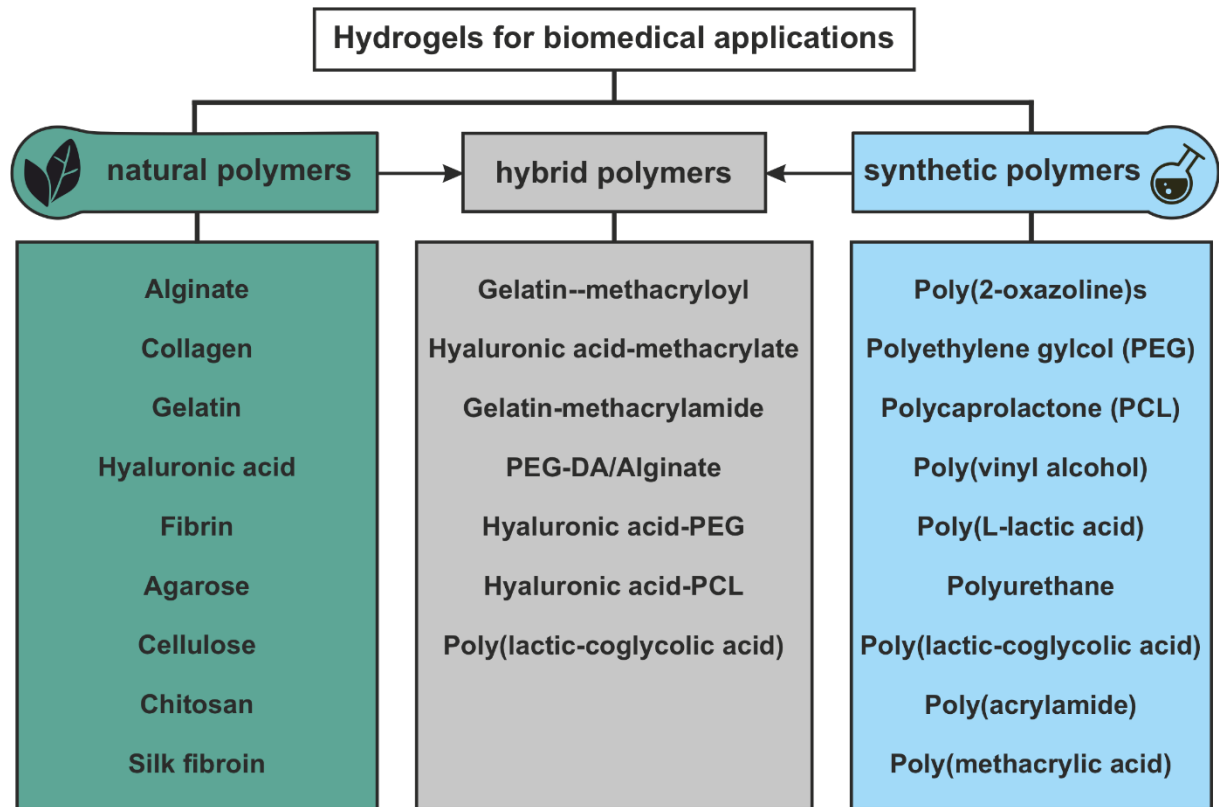


Figure 2: Overview and classification of polymers that have been used for biomedical applications according to their origin (adapted and modified from ⁴⁷)

1.3. Hydrogel Conjugation Strategies

The role and design of biomaterials drastically changed over time towards mimicking native tissues both in form and functionality (vide supra). To facilitate, enhance or tune hydrogel properties, e.g., for hydrogel formation or the conjugation of different moieties, chemical modifications are often needed. There is a multitude of different modification and conjugation strategies that have been deployed over the years. Due to their application in biomedicine, the approaches of interest should be non-cytotoxic and performed under physiological condition.⁴⁸

1.3.1. Covalent Hydrogel Crosslinking

As previously mentioned, many hydrogels are formed due to physical interactions. However, for many applications, such as 3D cell culture, a covalent network is needed to facilitate long-term stability and shape fidelity in aqueous environments.⁴⁹ For this purpose, several crosslinking strategies have been used over the years.

One of the most commonly used covalent crosslinking approaches is photo-activated free radical polymerization. For this, both acrylates and methacrylates can be incorporated into the polymer during synthesis and used for crosslinking of hydrogels or the introduction of other chemical moieties using irradiation.^{46, 50} This approach offers the opportunity to control the modification degree or providing spatial and temporal control over crosslinking or conjugation processes.^{46, 51, 52} Due to the increasing attention that this approach received in biomedical applications, over the years different cytocompatible photoinitiators such as Irgacure 2959 (2-Hydroxy-4'-(2-hydroxyethoxy)-2-methylpropiophenone)⁵³, one of the most frequently used ones, or Irgacure 819 (Phenylbis(2,4,6-trimethylbenzoyl)phosphine oxide)⁵⁴ have been designed and used, e.g., for the controlled post-printing maturation of 3D printed constructs in biofabrication.⁴⁹ However, there are also some drawbacks regarding this approach, such as a low curing depth due to the weak light penetration⁵⁵ or the exposure to UV light that can lead to deoxyribonucleic acid damages in cells.⁵⁶

Another frequently applied conjugation strategy is the use of Diels-Alder chemistry. In this reaction, a [4 + 2] cycloaddition of a conjugated diene and a dienophile leads to the formation of a cycloadduct.^{57, 58} Diels-Alder chemistry has been widely applied for hydrogel crosslinking for different reasons such as absence of side products or initiators that potentially can affect the cytocompatibility of the biomaterial.⁵⁹ Furthermore, the cycloaddition can be applied at physiological conditions and polymerization kinetics can be controlled by adjusting temperature or pH values.⁶⁰⁻⁶² Even though multiple Diels-Alder combinations are being used, the most widely applied system uses furan as diene and the dienophile maleimide.⁵⁸

In addition to the crosslinking mechanisms mentioned above, there is a wide range of other chemical crosslinking strategies that have been applied for hydrogel formation and maturation over the years including Michael-addition⁶³ or imine (e.g., Schiff-base)⁶⁴ and hydrazone⁶⁵ formation, among others.

1.3.2. Bioconjugation Strategies

To enhance functionality of biomaterials and mimic native tissues in fields such as TE, biofabrication or drug delivery, scientists are trying to leverage multiple disciplines including chemistry, material sciences as well biology. An integral part in creating biomaterials that interact with native tissues and stimulate cellular processes is the incorporation of biochemical cues.⁶⁶ Biomolecules such as proteins or peptides can be made accessible with spatial and temporal control using conjugation techniques.^{67, 68} However, there are different challenges that need to be considered depending on the biomolecule and the application. Most importantly, the 3D structure of biomolecules plays a pivotal role for their function. Especially proteins are susceptible to denaturation or aggregation. Therefore, mild reaction conditions

need to be chosen for the conjugation of biomolecules. Over the years, a multitude of different conjugation techniques have been developed and successfully applied (Fig. 3).

One of the most frequently used approaches for the conjugation of different moieties to proteins is *N*-hydroxysuccinimide (NHS) ester-mediated chemistry. This technique is based on the reaction of NHS esters with primary amino groups, more specific the ϵ -amino groups of lysine residues and N-terminus, for the conjugation of biomolecules. However, NHS ester chemistry can lead to an unspecific binding with different stoichiometries thereby impacting protein function.^{69, 70}

This is the reason why site-specific conjugation strategies have gained more attention over time. One requirement for site-specific conjugation is the presence of highly selective and unique chemical residue inside the protein/peptide. One of the most applied chemoselective conjugation strategies is the use of click-chemistry. Leveraging the presence of a single free thiol groups (cysteine residues) on the surface of the target structure is one possible approach. In this case, coupling of the protein or peptide of interest to the target polymer can be achieved, e.g., via thiol-maleimide click chemistry.⁷¹ Another approach is the incorporation of new selective chemical residues. They can be introduced in peptides via solid-phase peptide synthesis or in proteins via genetic engineering. This enables the introduction of unique functional groups. Characteristic functional groups can be proteinogenic AAs, such as a free cysteine, or an introduced unnatural AA containing a bioorthogonal group.⁷²⁻⁷⁴ Another advantage is that these additional AAs can be incorporated at different sites allowing site-directed conjugation, e.g., in the case of proteins, to prevent negative impacts on protein activity due to uncontrolled polymer conjugations as described before for NHS esters.⁷⁰ A click reaction that has been studied frequently in this regard is the strain-promoted alkyne-azide cycloaddition that results in stable 1,2,3-triazoles with the absence of toxic side products or catalysts.⁷⁵ This approach was recently used for the site-specific conjugation of different polymers to interferon α 2a to increase its half-life.⁷³

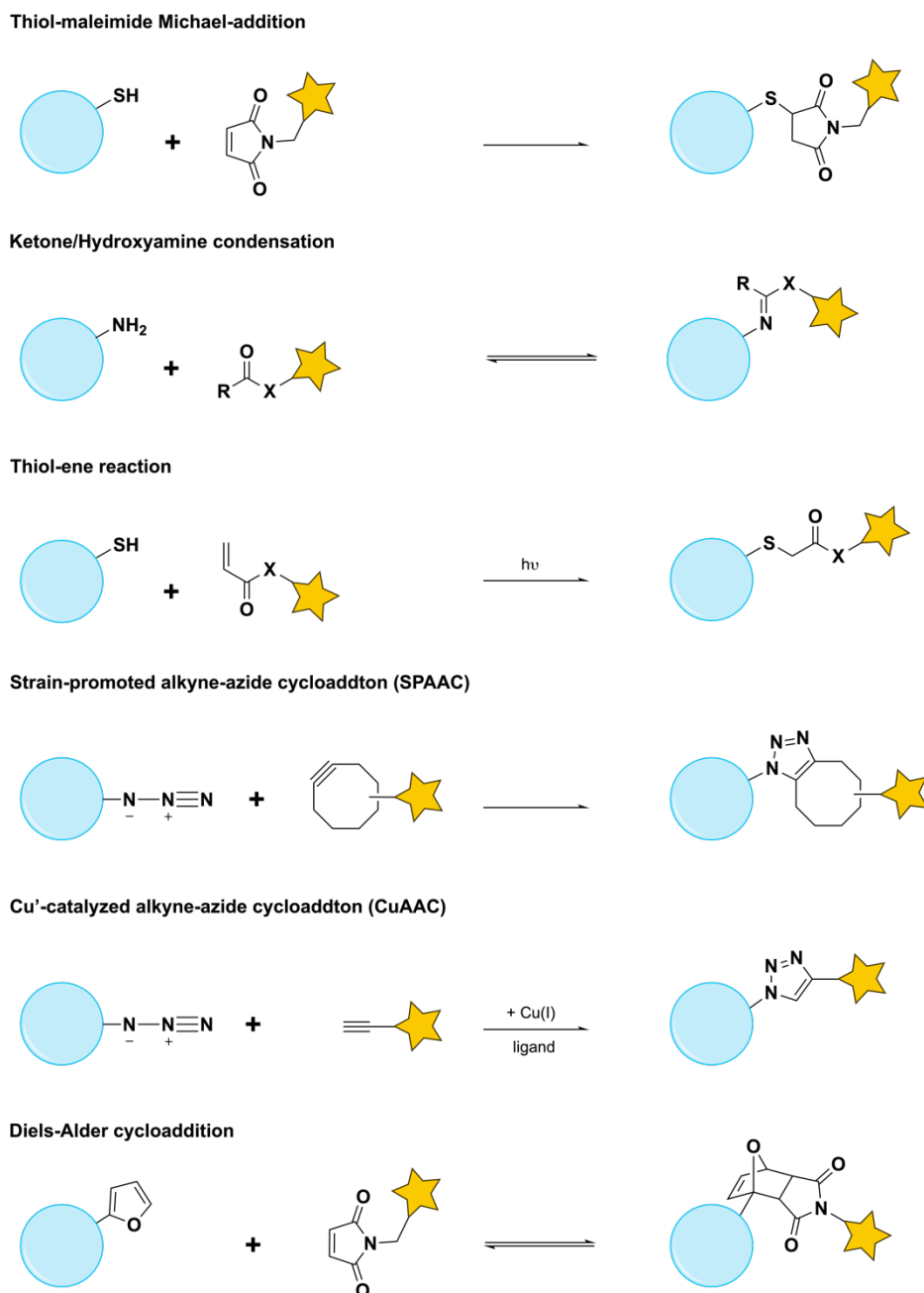


Figure 3: Overview over different bioorthogonal conjugation methods.

Lastly, enzyme-mediated ligation can be deployed for the coupling of biomolecules. To perform this conjugation method, specific enzyme recognition sites have to be available in the target structure. There is a multitude of different enzymes that catalyze ligation reactions in nature including tyrosinases or sortases.^{76, 77} One of the most studied class of enzymes in this context are the so-called transglutaminases (TG). This class of enzymes facilitates a transamidation reaction that leads to the formation of N^ε-(γ-glutamyl)-lysine isopeptide bonds.^{78, 79} The enzyme recognition sites can either be introduced via genetic engineering⁸⁰, as already mentioned above, or intrinsic recognition sites, e.g., insulin-like growth factor I (IGF-I) whose intrinsic TG recognition site was used for the site-specific conjugation of polyethylene glycole (PEG) via an MMP-sensitive peptide.⁸¹

1.4. Applications

Due to the vast progress and developments of hydrogels in science, the role and potential of hydrogels for biomedical application has drastically changed over the decades. Today, there is a huge variety of different biological and medical applications of hydrogels that have or can have an impact on life in the future ranging from contact lenses or device coatings to delivering drugs.^{82, 83} The focus of the following section will therefore be on biomedical applications that are relevant for the hydrogels used in this study.

1.4.1. Hydrogels as Wound Sealants

One of the most studied biomedical applications of hydrogels is their use in hemostatic control. Hundreds of million surgeries are performed every year.⁸⁴ One major drawback of these medical procedures is the possibility of severe bleeding which can lead to elevated morbidity and mortality.⁸⁵ Over the last decades tissue sealants, hemostats and adhesives have been developed as alternative technologies to staples, sutures and clips to tackle challenges like application time or bacterial infections.^{86, 87} There are several requirements for biomaterials to be used as wound sealants that must be considered, including safety, manufacturable, applicability as well as biocompatibility. In addition, they should be applicable to a wide range of wounds and stop blood loss at the surgical site.^{88, 89} One of the best studied groups of biomaterials for wound closure that are used in clinics are hydrogels, because of their similarities with native tissues (*vide supra*).

In general, hydrogels as wound sealants can also be divided into two different classes – natural and synthetic materials (*vide supra*).

There are different synthetic hydrogel-based materials that can be used as tissue sealant, which already have been approved by the U.S. FDA.⁸⁷ Cyanoacrylates are promising candidates because of their fast polymerization kinetics as well as their mechanical strength.^{87, 90} They are used for different surgeries including neurologic⁹¹, cardiac⁹², or ophthalmologic procedures⁹³. However, the use of cyanoacrylates is still restricted due to concerns about cytotoxicity of by-products, the adverse effects of the exothermic polymerization reaction or the lack of interaction with wet tissue.⁸⁷ Another class of polymers that has already been approved by the U.S. FDA is PEG.^{94, 95} Yet, there are still shortcomings like the high swelling-degrees that limit their usage.⁸⁷

Another sealant and probably the most important commercially available product so far is a natural wound sealant, the so-called fibrin sealant. Fibrin sealant was first approved by the U.S. FDA in 1998.⁹⁶ The importance of fibrin as a medical product is further underlined by the fact that it is the only material to date that is approved by the U.S. FDA as a hemostat, tissue sealant and wound adhesive.^{96, 97} Fbg and thrombin are the main components of the sealant. In nature, the protein Fbg plays a pivotal role in the final step of the blood coagulation cascade

and forms the fibrin clot after exposure to the enzyme thrombin, thereby facilitating wound closure. The network is further strengthened by chemical crosslinking between Fbg via factor XIII. In most of the commercially available fibrin sealants, Fbg and thrombin are stored in two different chambers and are mixed directly at the site of action inducing fibrin polymerization and subsequently wound closure. Due to its origin and biocompatibility, fibrin sealants are often the preferred solution in clinical applications. However, there are still shortcomings associated with these sealants such as fast *in vivo* resorption and future potential developments which are described in more detail in **chapter 3 and 4** of this work.^{98, 99}

As a result of an ageing population and an increasing number of surgeries, the demand for more advanced and effective wound sealants will only increase in the future. Therefore, the development of novel hydrogel systems with improved properties or the incorporation of biological cues is and will be highly relevant in the years to come.

1.4.2. Hydrogels in Biofabrication

Another application that has led to and benefited from the development of novel hydrogels is TE. This research field aims for the regeneration of damaged tissues by using constructs that mimic their native biological counterpart or help restore their full functionality. These artificial constructs mainly consist of 3 different components – scaffold, cells and biological entities such as growth factors.¹⁰⁰ However, it has become evident that the hierarchy, organizational structure and architecture are essential for the formation of fully functional tissues. Because of that, the field of biofabrication has emerged within the last decade.^{101, 102} In biofabrication, additive manufacturing (AM) techniques are used to develop three-dimensional (3D) scaffolds to reproduce the structural hierarchy of native tissues.¹⁰⁰ This process is highly interdisciplinary and requires both AM technologies and the development of novel materials, so-called bioinks.^{100, 103, 104}

There are different AM methods that have been used for bioprinting approaches: laser-induced forward transfer¹⁰⁵, inkjet printing^{106, 107} and extrusion printing (robotic dispensing)¹⁰⁸ (Fig. 4). The probably most used method among these three is the extrusion bioprinting. During this process, a cell-laden hydrogel is transferred to a syringe. Next, the hydrogel is dispensed from the syringe pneumatically, by a piston or a screw.¹⁰⁰ In contrast to other techniques such as inkjet printing, hydrogels are dispensed as strand in a layer-by-layer form by using pressurized gas resulting in 3D constructs with a resolution off around 200 - 100 μm .^{109, 110} Precise control over the applied pressure, printing speed as well as the hardware such as nozzle diameter enables the use of different bioinks and the printing of 3D scaffolds using computer-aided design.¹⁰⁰

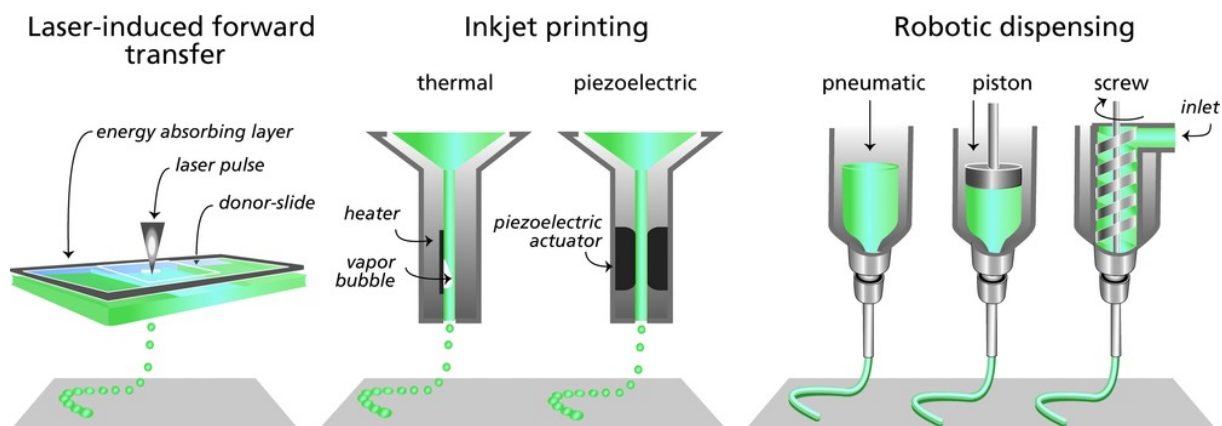


Figure 4: Schematic overview over the different bioprinting technologies. Reprinted with permission from reference ¹⁰⁰.

The other component needed for biofabrication is the bioink. Bioinks were recently defined as a “formulation of cells that is suitable to be processed by an automated biofabrication technology.”¹⁰³ There are several key characteristics that need to be analyzed before using a bioink. The printability of the hydrogels is one of the most important characteristics and is strongly influenced by the rheological properties.^{111, 112} Shear thinning behavior enables the extrusion during the printing process and the stabilization of the construct afterwards due to the viscoelastic solid-like character.^{45, 113} In addition, other properties such as shape fidelity of the hydrogel as well as pore size are important.^{114, 115} Furthermore, it is beneficial for a bioink to show long-term stability, e.g., via photo crosslinking.^{49, 116} In general, bioinks should be biocompatible and not negatively impact cell survival or proliferation.¹¹⁷ On the contrary, the hydrogel should contribute or even enhance the biological performance of cells and mimic native tissues (*vide supra*).

Classes of polymers that have gained interest over the last decades in this regard are poly(2-oxazoline)s (POx) and poly(2-oxazines) (POzi), polyamides, or polymeric amides that were first reported in 1966 and 1967.¹¹⁸⁻¹²² Besides their good cytocompatibility^{45, 123, 124}, one of the main reasons for the increasing interest in POx/POzi systems is their chemical versatility.¹²⁵ By varying different substituents of the monomers, diverse side chain functionalities can be introduced to the polymer. This gives the opportunity to adapt or control the polymer properties thereby enabling, e.g., thermoresponsive behaviour⁴⁵ as well as chemical¹²⁶ or photo-crosslinking⁴⁶ to form POx hydrogels. Furthermore, functional groups can be introduced at the α - or Ω -position which can be used for labelling or site-directed protein conjugation.^{71, 127}

In recent years, the focus in the field of biofabrication has shifted towards better integration of biological aspects into bioprinting (*vide supra*). To achieve this, developments from molecular biology and biotechnology have to be used in unison with advances in material science to get closer to mimicking the natural cellular environment.¹⁰¹ Especially, the availability of biochemical cues has accelerated the development of engineered hydrogels with enhanced

cell-material interaction. Most frequently, protein and peptide sequences are used to stimulate different cellular processes including cell-receptor interaction or differentiation. One of the best studied approaches is the introduction of cell-adhesive sequences to bioinert hydrogels. These sequences are most of the time derived from naturally occurring adhesive sequences from parts of the ECM.⁶⁶ The arguably most studied sequence is the RGD-motif (*vide supra*). This short peptide sequence has shown to facilitate cell adhesion of cells which is also part of **Chapter 1**. However, different parameters such as peptide architecture or the amount of peptide can influence the cellular response to the peptide.^{46, 128}

Over the years the influence of RGD on cellular behavior has been studied extensively. Studies show that the impact of RGD-peptides is strongly dependent on variables such as topography and density.^{129, 130} Furthermore, the spacing of RGD-peptides on the surface can have a big influence on morphology and differentiation of cells.¹³¹ The importance of facilitate adhesion has also led to the development of different and novel adhesive sequences, e.g., the development of RGD-mimetic poly(amidoamine) oligomer based scaffolds for adipose tissue engineering among others.¹³²⁻¹³⁴ Even though the understanding of cell adhesion peptides has increased over the years, there is still a long way to go in order to fully understand and mimic the natural tissue environment. Lately, especially the spatial-temporal control of the presentation of adhesive sites has gained a lot of attention to further understand the importance of the dynamic character of natural microenvironments.¹³⁵

Another important part of the microenvironment is the availability of soluble biochemical cues such as growth factors or other ECM associated proteins (*vide supra*). Cell surface receptors can interact with these cues and influence different cellular responses and processes such as cell growth.¹³⁶ That is why the incorporation of different biomolecules has been often used in to enhance the biological performance of biomaterials.⁶⁶

However, this approach has not only been crucial for the progress and advances in the previously mentioned research fields, but it also gained attention in the field of controlled drug delivery, lately. Current advances in hydrogel protein conjugation techniques can be used in both areas of research and therefore cannot be discussed separately. Hence, conjugation techniques for the research fields will be analyzed jointly in the next paragraph on the application of hydrogel for controlled drug delivery.

1.4.3. Hydrogels in Controlled Drug Delivery

Over last decades the market for novel peptide and protein-based pharmaceuticals has drastically increased.¹³⁷ However, conventional dosing such as oral delivery are highly limited due to poor bioavailability. Furthermore, biologics have a short half-life, e.g., due to proteolytic degradation, and the transport to the site of action is often impaired by physiological barriers such as skin or mucus.¹³⁸ In order to overcome these challenges, there has been an increasing

interest in advanced drug delivery platforms. There are several different approaches that have been studied over the years such as hydrogels, liposomes, or nanoparticles.¹³⁹⁻¹⁴²

Hydrogels have been extensively investigated and used for drug delivery due to their favorable properties. As already mentioned before, most hydrogels are networks that are biocompatible and mimic native tissues. Due to their hydrophilic character and high water content, proteins or peptide can easily be incorporated into the hydrogel and are less susceptible to aggregation or denaturation.¹⁴³

One of the most important design criteria for hydrogels in drug delivery is their structure and pore size. Incorporated drugs diffuse through the mesh depending on the pore size of the hydrogels, thereby facilitating, and determining sustained release over a longer period of time.¹⁴³ Furthermore, the release can be influenced by the physical and chemical interactions between drug and hydrogel. There is a huge variety of different modifications that can be introduced into the polymer backbone. Active pharmaceutical ingredients (API) can interact with the polymer, e.g., via electrostatic interactions or be covalently linked to the polymer leading to enhanced and controlled drug release profiles (Fig. 5).^{143, 144}

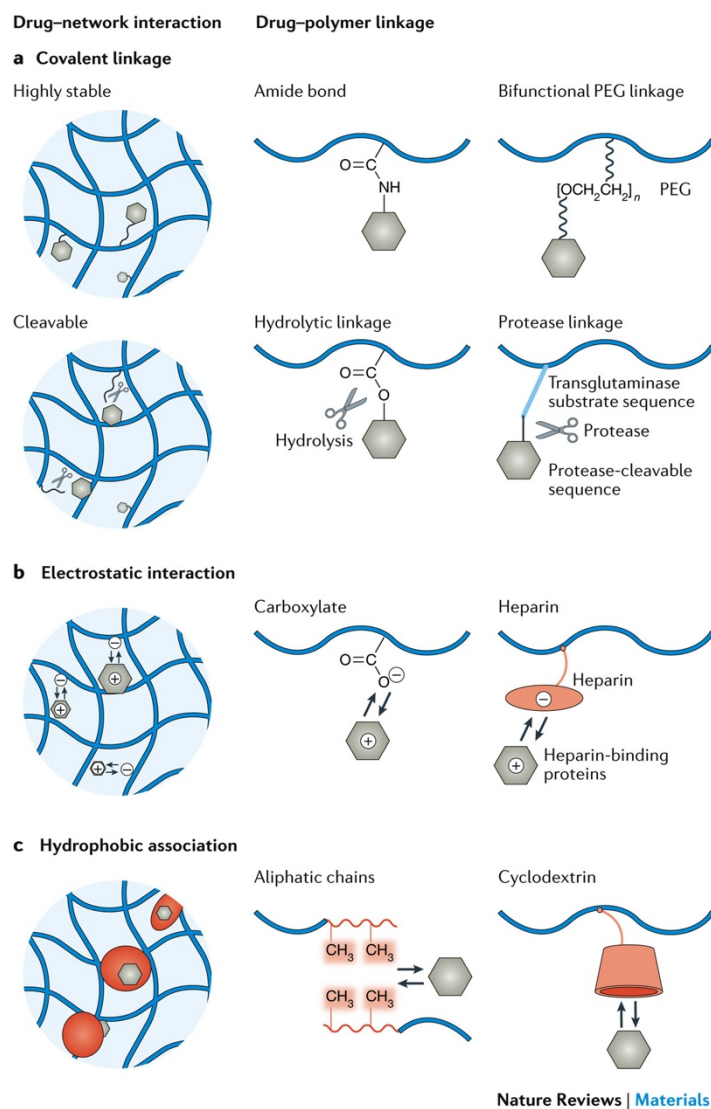


Figure 5: Overview of different chemical interactions to facilitate drug release. A. Stable and cleavable covalent linkages. B. Drug-polymer coupling by using electrostatic interactions. C. Hydrophobic interactions between drug and polymer. Reprinted with permission from reference ¹⁴³.

In addition to that, currently, there is a paradigm shift in the pharmaceutical industry away from traditional dosing forms and towards personalized medicine. The use of 3D printing methods for the manufacturing of drugs could transform the field of drug delivery in the future for both small molecules and biologics and already led to the approval a first 3D-printed pharmaceutical approved by the U.S. FDA in Spritam (Aprelia Pharmaceuticals).^{145, 146} Additive manufacturing allows the on-demand production of medicines directly on-site thereby reducing costs and waste during the manufacturing process.¹⁴⁷⁻¹⁴⁹ Furthermore, it allows personalized drug dosing and can lead to enhanced drug release profiles by taking advantage of size or complex 3D structures of scaffolds or spatial control over the drug distribution (also discussed in **Chapter 2**).^{150, 151} In one study, transforming growth factor-beta 1 (TGF- β 1) was attached to printable hyaluronic acid-based bioink using Michael-addition. After 3D printing, the protein-modified

bioink showed enhanced mesenchymal stromal cells chondrogenesis compared to the hydrogel containing soluble

TGF- β 1 highlighting a potential application for cartilage regeneration in the future.¹⁵² Another approach is the targeted drug release. With this, APIs can be released directly at the site action by an ex- or internal stimulus such as pH value, temperature, or enzymatic activity, preventing off target effects of systemic administrations.^{143, 153-155} By using, e.g., multiple growth factor containing bioinks, spatiotemporal patterns can be created to control the distribution inside the 3D scaffold thereby enhancing the performance of hydrogels.¹⁵⁶

Due to the aforementioned favorable properties and novel approaches, hydrogels are promising candidates to extending the current toolbox of personalized drug dosing and targeted drug delivery.

2. Summary

Over the years, hydrogels have been developed and used for a huge variety of different applications ranging from drug delivery devices to medical products. In this thesis, a poly(2-methyl-2-oxazoline) (POx) / poly(2-*n*-propyl-2-oxazine) (POzi) bioink was modified and analyzed for the use in biofabrication and targeted drug delivery. In addition, the protein fibrinogen (Fbg) was genetically modified for an increased stability towards plasmin degradation for its use as wound sealant.

In **Chapter 1**, a thermogelling, printable POx/POzi-based hydrogel was modified with furan and maleimide moieties in the hydrophilic polymer backbone facilitating post-printing maturation of the constructs via Diels-Alder chemistry. The modification enabled long-term stability of the hydrogel scaffolds in aqueous solutions which is necessary for applications in biofabrication or tissue engineering. Furthermore, we incorporated RGD-peptides into the hydrogel which led to cell adhesion and elongated morphology of fibroblast cells seeded on top of the scaffolds. Additional printing experiments demonstrate that the presented POx/POzi system is a promising platform for the use as a bioink in biofabrication.

Chapter 2 highlights the versatility of the POx/POzi hydrogels by adapting the system to a use in targeted drug delivery. We used a bioinspired approach for a bioorthogonal conjugation of insulin-like growth factor I (IGF-I) to the polymer using an omega-chain-end dibenzocyclooctyne (DBCO) modification and a matrix metalloprotease-sensitive peptide linker. This approach enabled a bioresponsive release of IGF-I from hydrogels as well as spatial control over the protein distribution in 3D printed constructs which makes the system a candidate for the use in personalized medicine.

Chapter 3 gives a general overview over the necessity of wound sealants and the current generations of fibrin sealants on the market including advantages and challenges. Furthermore, it highlights trends and potential new strategies to tackle current problems and broadens the toolbox for future generations of fibrin sealants.

Chapter 4 applies the concepts of recombinant protein expression and molecular engineering to a novel generation of fibrin sealants. In a proof-of-concept study, we developed a new recombinant fibrinogen (rFbg) expression protocol and a Fbg mutant that is less susceptible to plasmin degradation. Targeted lysine of plasmin cleavage sites in Fbg were exchanged with alanine or histidine in different parts of the molecule. The protein was recombinantly produced and restricted plasmin digest was analyzed using high resolution mass spectrometry. In

addition to that, we developed a novel time resolved screening protocol for the detection of new potential plasmin cleavage sites for further amino acid exchanges in the fibrin sealant.

3. Zusammenfassung

Hydrogele wurden im Laufe der Jahre für eine Vielzahl von Anwendungen, von der Verabreichung von Medikamenten bis hin zu medizinischen Produkten, entwickelt und eingesetzt. In dieser Arbeit wurde eine Poly(2-methyl-2-oxazolin) (POx) / Poly(2-n-propyl-2-oxazolin) (POzi) Biotinte modifiziert und für den Einsatz in der Biofabrikation und für die gezielte Verabreichung von Medikamenten analysiert. Außerdem wurde das Protein Fibrinogen (Fbg) gentechnisch verändert, um seine Stabilität gegenüber dem Plasminabbau in seiner Funktion als Wundkleber zu erhöhen

In **Kapitel 1** wurde ein thermogelierendes, druckbares Hydrogel auf POx/POzi-Basis mit Furan- und Maleimid-Funktionen im hydrophilen Polymerrückgrat modifiziert, was die Reifung der Konstrukte nach dem Druck durch Diels-Alder-Chemie bewirkt. Die Modifizierung ermöglichte eine langfristige Stabilität der Hydrogele in wässrigen Lösungen, was für Anwendungen im Bereich der Biofabrikation oder im Tissue Engineering erforderlich ist. Darüber hinaus haben wir RGD-Peptide in das Hydrogel integriert, was zur Zelladhäsion und einer verlängerten Morphologie von Fibroblasten, die auf den Gelen ausgesät wurden, führte. Weitere Druckexperimente zeigen außerdem, dass das POx/POzi-System eine vielversprechende Plattform für den Einsatz als Biotinte in der Biofabrikation ist.

Kapitel 2 unterstreicht die Vielseitigkeit der POx/POzi-Hydrogele, indem das System für die gezielte Abgabe von Medikamenten angepasst wird. Wir verwendeten einen von der Natur inspirierten Ansatz für eine biorthogonale Konjugation vom Insuline-like Growth Factor I (IGF-I) an das Polymer unter Verwendung einer Dibenzocyclooctin-Modifikation des Polymers am Ende der Omega-Kette und eines Matrix-Metalloproteasen-empfindlichen Peptid-Linkers. Dieser Ansatz ermöglichte eine bioresponsive Freisetzung von IGF-I aus Hydrogelen sowie eine räumliche Kontrolle über die Proteinverteilung in 3D-gedruckten Konstrukten, was das System zu einem Kandidaten für den Einsatz in der personalisierten Medizin macht.

Kapitel 3 gibt einen allgemeinen Überblick über die Notwendigkeit von Wundversiegelungsmitteln und die derzeit auf dem Markt befindlichen Generationen von Fibrinklebern einschließlich der Vorteile und Herausforderungen. Darüber hinaus werden Trends und potenzielle neue Strategien zur Lösung aktueller Probleme und zur Erweiterung der Toolbox für künftige Generationen von Fibrinklebern aufgezeigt.

In **Kapitel 4** werden die Konzepte der rekombinanten Proteinexpression und des Molecular Engineering auf eine neue Generation von Fibrin Wundklebern angewandt. In einer Proof-of-

Concept-Studie haben wir ein neues rekombinantes Fbg Expressionsprotokoll und eine Fbg Mutante entwickelt, die weniger anfällig für einen Abbau durch Plasmin ist. Gezielte Lysine in Plasmin-Schnittstellen in Fbg wurde entweder durch Alanin oder Histidin in unterschiedlichen Teilen des Moleküls ausgetauscht. Das Protein wurde rekombinant hergestellt und eine verminderte Schnittrate wurde mittels hochauflösender Massenspektrometrie gezeigt. Zusätzlich haben wir ein neues zeitaufgelöstes Screening-Protokoll entwickelt, mit dem sich neue potenzielle Plasmin-Spaltstellen für weitere Aminosäureaustausche in Fibrin-Klebern auflösen lassen.

4. Chapter 1: From Thermogelling Hydrogel towards Functional Bioinks: Controlled Modification and Cytocompatible Crosslinking

Lukas Hahn^{†1}, Matthias Beudert^{‡2}, Marcus Gutmann², Larissa Keßler¹, Philipp Stahlhut³, Lena Fischer⁴, Emine Karakaya⁵, Thomas Lorson², Ingo Thievensen⁴, Rainer Detsch⁵, Tessa Lühmann², Robert Luxenhofer^{1,6}

¹Institute of Pharmacy and Food Chemistry, Julius-Maximilians-University Würzburg, Am Hubland, 97074 Würzburg, Germany

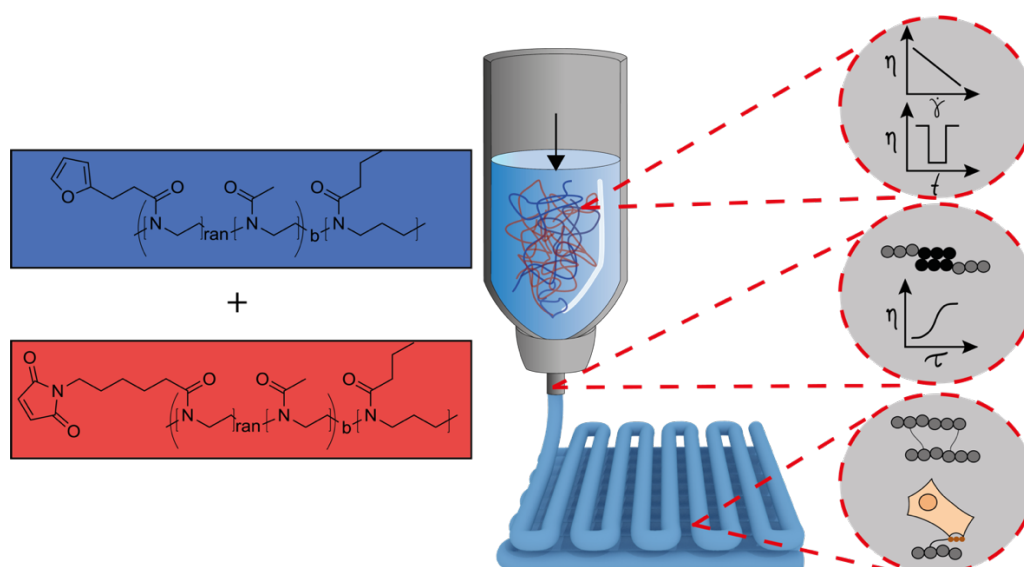
²Functional Polymer Materials, Chair for Advanced Materials Synthesis, Institute for Functional Materials and Biofabrication, Department of Chemistry and Pharmacy and Bavarian Polymer Institute, Julius-Maximilians-University Würzburg, Röntgenring 11, 97070 Würzburg, Germany

³Department for Functional Materials in Medicine and Dentistry, University of Würzburg, Pleicherwall 2, 97070 Würzburg, Germany

⁴Center for Medical Physics and Technology, Biophysics Group, Friedrich-Alexander-University of Erlangen-Nuremberg, Henkestrasse 91, 91052 Erlangen, Germany

⁵Institute of Biomaterials, University of Erlangen-Nürnberg, Cauerstr. 6, 91058, Erlangen, Germany

⁶Soft Matter Chemistry, Department of Chemistry and Helsinki Institute of Sustainability Science, Faculty of Science, University of Helsinki, P.O. Box 55, FIN-00014, Helsinki, Finland



The following open access article was published in *Macromolecular Bioscience*, Hahn, L.; Beudert, M.; Gutmann, M.; Keßler, L.; Stahlhut, P.; Fischer, L.; Karakaya, E.; Lorson, T.; Thievensen, I.; Detsch, R.; Lühmann, T.; Luxenhofer, R., From Thermogelling Hydrogels toward Functional Bioinks: Controlled Modification and Cytocompatible Crosslinking, 2021, e2100122, DOI: <https://doi.org/10.1002/mabi.202100122>, With permission of John Wiley and Sons, License number: 5446590767260, © 2021 The Authors. *Macromolecular Bioscience* published by Wiley-VCH GmbH.

RESEARCH ARTICLE

From Thermogelling Hydrogels toward Functional Bioinks: Controlled Modification and Cytocompatible Crosslinking

Lukas Hahn, Matthias Beudert, Marcus Gutmann, Larissa Keßler, Philipp Stahlhut, Lena Fischer, Emine Karakaya, Thomas Lorson, Ingo Thievessen, Rainer Detsch, Tessa Lühmann,* and Robert Luxenhofer*

Hydrogels are key components in bioink formulations to ensure printability and stability in biofabrication. In this study, a well-known Diels-Alder two-step post-polymerization modification approach is introduced into thermogelling diblock copolymers, comprising poly(2-methyl-2-oxazoline) and thermoresponsive poly(2-*n*-propyl-2-oxazine). The diblock copolymers are partially hydrolyzed and subsequently modified by acid/amine coupling with furan and maleimide moieties. While the thermogelling and shear-thinning properties allow excellent printability, trigger-less cell-friendly Diels-Alder click-chemistry yields long-term shape-fidelity. The introduced platform enables easy incorporation of cell-binding moieties (RGD-peptide) for cellular interaction. The hydrogel is functionalized with RGD-peptides using thiol-maleimide chemistry and cell proliferation as well as morphology of fibroblasts seeded on top of the hydrogels confirm the cell adhesion facilitated by the peptides. Finally, bioink formulations are tested for biocompatibility by incorporating fibroblasts homogeneously inside the polymer solution pre-printing. After the printing and crosslinking process good cytocompatibility is confirmed. The established bioink system combines a two-step approach by physical precursor gelation followed by an additional chemical stabilization, offering a broad versatility for further biomechanical adaptation or bioresponsive peptide modification.

1. Introduction

In the field of biofabrication, researchers try to create functional tissue models by using an additive manufacturing technique. Especially in bioprinting, advances strongly rely on the availability of suitable bioinks.^[1–3] These materials, in turn, are mostly based on polymers—either of synthetic or natural origin—and contain living cells, the required growth factors, as well as nutrition to be processed by an automated biofabrication technology.^[4,5] In most cases, direct ink-writing of a hydrogel is used, allowing the production of clinically relevant designs with respect to time and size.^[6] Bioinks have to be printable at cell friendly conditions, and allow maturation of the printed construct for several weeks. Several key characteristics can be associated with an ideal hydrogel bioink. First, a pronounced shear thinning character of the precursor hydrogel during extrusion facilitates 3D-printing and concurrently the viscoelastic solid like character prevents cell sedimentation in the barrel.^[7] Second, it

L. Hahn, L. Keßler, R. Luxenhofer
 Functional Polymer Materials, Chair for Advanced Materials Synthesis,
 Institute for Functional Materials and Biofabrication, Department of
 Chemistry and Pharmacy and Bavarian Polymer Institute
 Julius-Maximilians-University Würzburg
 Röntgenring 11, Würzburg 97070, Germany
 E-mail: robert.luxenhofer@helsinki.fi


M. Beudert, M. Gutmann, T. Lorson, T. Lühmann
 Institute of Pharmacy and Food Chemistry
 Julius-Maximilians-University Würzburg
 Am Hubland, Würzburg 97074, Germany
 E-mail: tessa.luehmann@uni-wuerzburg.de

P. Stahlhut
 Department for Functional Materials in Medicine and Dentistry
 University of Würzburg
 Pleicherwall 2, Würzburg 97070, Germany

L. Fischer, I. Thievessen
 Center for Medical Physics and Technology, Biophysics Group
 Friedrich-Alexander-University of Erlangen-Nuremberg
 Henkestrasse 91, Erlangen 91052, Germany

E. Karakaya, R. Detsch
 Institute of Biomaterials
 University of Erlangen-Nürnberg
 Cauerstr. 6, Erlangen 91058, Germany

R. Luxenhofer
 Soft Matter Chemistry, Department of Chemistry and Helsinki Institute
 of Sustainability Science, Faculty of Science
 University of Helsinki
 P.O. Box 55, Helsinki FIN-00014, Finland

 The ORCID identification number(s) for the author(s) of this article can be found under <https://doi.org/10.1002/mabi.202100122>

© 2021 The Authors. Macromolecular Bioscience published by Wiley-VCH GmbH. This is an open access article under the terms of the Creative Commons Attribution-NonCommercial-NoDerivs License, which permits use and distribution in any medium, provided the original work is properly cited, the use is non-commercial and no modifications or adaptations are made.

DOI: 10.1002/mabi.202100122

should ideally allow for sufficient and fast stabilization after the printing process. The former, that is, the formation of a precursor hydrogel, can be ensured by a wide variety of approaches, such as specific chemical pre-crosslinking,^[8] pH,^[9] or temperature switch,^[10] as described, for example, for alginate, collagen, and gelatine. The defined control of these approaches to provide a cytocompatible printing process is an ongoing challenge.

Thermogelling polymer solutions that undergo fast gelation are promising candidates for bioinks. A well-known example is the polymer Pluronic F127, also known as Poloxamer 407. This triblock copolymer based on polypropylene glycol as thermoresponsive central block, flanked by two hydrophilic polyethylene glycol (PEG) blocks, forms a physical hydrogel at room temperature. Since Pluronic F127 gels represent excellent printability,^[11] they are used in many applications as a support material and sacrificial structure.^[12] One possible alternative for PEG-based systems is the family of polymers known as poly(2-oxazoline)s (POx) and their close relative poly(2-substituted-5,6-dihydro-4H-1,3-oxazine)s (poly(2-oxazine)s, POzi), which serve as a diverse biomaterials platform for different applications due to good cytocompatibility and chemical versatility.^[13–17]

In the context of biofabrication, only few reports can be found describing POx/POzi based structures used in bioprinting. Lorson et al. reported a thermogelling diblock copolymer comprising hydrophilic poly(2-methyl-2-oxazoline) (PMeOx) and thermoresponsive poly(2-*n*-propyl-2-oxazine) (P*n*PrOzi) moieties.^[18] In first bioprinting experiments excellent cytocompatibility was confirmed. The printability and shape fidelity could be significantly improved by the addition of Laponite XLG.^[19] However, this thermoresponsive hydrogel does not allow for long-term cell culture experiments, as it dissolves upon addition of an excess of cell culture medium. More recently, Trachsel et al. investigated a multi-material approach with enzymatically stabilized hydrophilic poly(2-ethyl-2-oxazoline) hydrogels via sortase linkage.^[20] To use this system in a bioink formulation, alginate was needed to stabilize the constructs after printing by Ca²⁺. Furthermore, cellulose nanofibrils were added to improve printability.^[21]

In recent years, several approaches—mainly based on irradiation with UV-light—have been described to introduce covalent crosslinking after printing,^[22–24] fueling ongoing and controversial discussions about the potential negative effect of UV irradiation on cell viability.^[24,25] More recently, crosslinking using visible light has gained attention. Irrespective of the wavelength used, photoinitiators are typically needed for crosslinking which may affect cells either immediately or during the maturation.^[24] Accordingly, alternative approaches of in situ chemical crosslinking of hydrophilic polymers by the reaction of complementary functional groups, to obtain hydrogels, remain actively investigated. One such alternative is the Diels-Alder chemistry, already introduced for hydrogel synthesis by Chujo et al. a few decades ago^[26] besides other crosslinking strategies^[27,28] and recently studied again by Shoichet et al.^[29–32] as well as Nahm et al.,^[33] among others. Chujo et al. used the hydrophilic PMeOx functionalized with maleimide and furan groups in the polymer side chain. However, these hydrogel precursors would be unlikely candidates for dispense plotting, due to their hydrophilic nature and expected rheological properties.

In this work, we established a double-crosslinked bioink platform obtained by one starting block copolymer and its modifications, combining thermoresponsive precursor gelation together with temperature-controlled Diels-Alder crosslinking, in order to employ the benefits of both crosslinking mechanisms for creating a functional and adaptable bioink platform. Therefore, a previously described diblock copolymer comprising a hydrophilic PMeOx block and a thermoresponsive P*n*PrOzi block (PMeOx-*b*-P*n*PrOzi = P0),^[18] which showed pronounced physical thermogelation in aqueous solutions, was modified with furan and maleimide moieties.^[26] The fast physical sol/gel transition was used to obtain a homogenous cell distribution throughout the construct, in combination with good printability. After the extrusion, the cytocompatible in situ Diels-Alder crosslinking stabilized the construct and offered the possibility to introduce bioinstructive peptides. Beside the two functionalized polymers, no further compound such as crosslinker, initiators or viscosity modulators were used in order to obtain both a physically and chemically crosslinked hydrogel.

2. Results and Discussion

The presented bioink concept builds on two independent crosslinking mechanisms. At first, thermoreversible hydrophobic interactions offer excellent handling and printing properties. Second, a slow but essentially irreversible Diels-Alder crosslinking post-processing provides long-term stability and maturation.

In addition, Diels-Alder functionalities enable the conjugation of bioactive components (Figure 1A).^[34–36] In order to introduce the corresponding functionalities, the thermogelling diblock copolymer P0, with a similar degree of polymerization as described previously,^[18] was partially hydrolyzed, yielding secondary amines, which are subsequently coupled with carboxylic acids (Figure 1B). Doing so, it is critical that the thermogelling properties of the polymer P0 (Figure S1, Supporting Information) are retained after modification and that the crosslinking occurs in a time period suitable for bioprinting. The first step was a carefully controlled partial hydrolysis of the polymer yielding ethyleneimine (EI) moieties in the hydrophilic part of the polymer. We expected that the MeOx repeat units are hydrolyzed significantly faster than the *n*PrOzi units.^[37,38] ¹H-Nuclear magnetic resonance (NMR) spectroscopy confirmed that backbone and sidechain signals attributed to MeOx repeat units decreased significantly with increasing reaction time (Figures S2, S3A, B, Supporting Information), while the signals attributed to *n*PrOzi repeat units remained preserved. The degree of hydrolysis has a significant impact on the thermogelling properties (Figure S3C, Supporting Information). Here, the polymers with a hydrolysis degree of 10% of the PMeOx block were further investigated ((P(MeOx_{90-co}-EI₁₀)-*b*-P*n*PrOzi₁₀₀ = P1). The thermogelling properties of three different P1 polymer batches performed similar like the unmodified polymers described by Lorson et al. (Table S1, Supporting Information),^[18] indicating the reproducibility of the approach.^[39] Modification of P1 with furan or maleimide moieties resulted in the final functionalized polymers P(MeOx_{90-co}-Fu₁₀)-*b*-P*n*PrOzi₁₀₀ (P-Fu) and P(MeOx_{90-co}-Ma₁₀)-*b*-P*n*PrOzi₁₀₀ (P-Ma). The successful and complete modification was verified by ¹H-NMR spectroscopy (Figure S4, Supporting Information) and

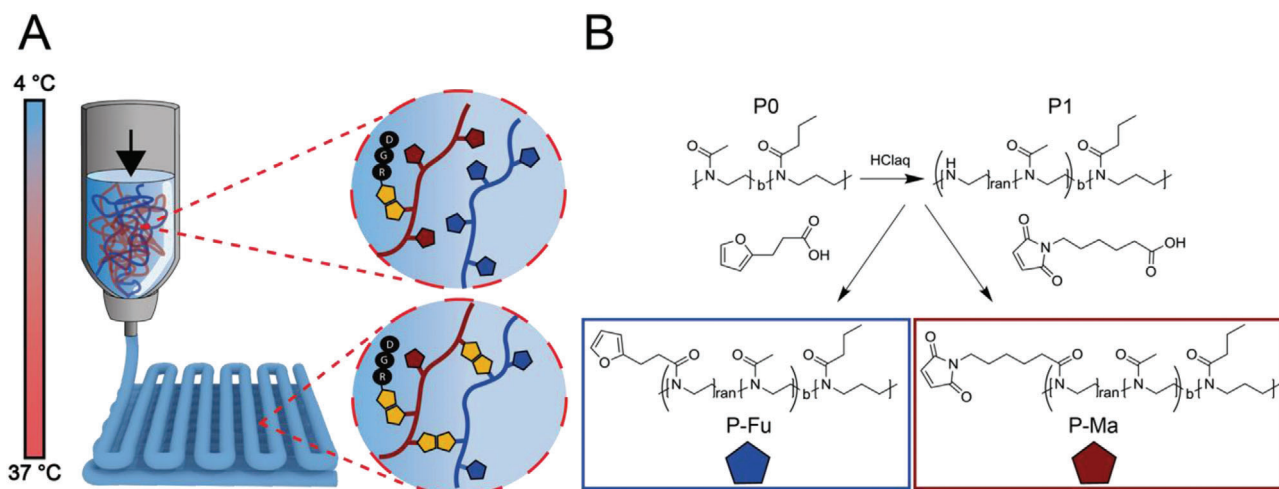


Figure 1. Investigated strategy for functional bioink formulations. A) Schematic illustration of the bioink strategy. At 5 °C the polymer solutions P-Fu and P-Ma are present as low viscous liquids, which can be easily mixed with cells and peptide motifs (e.g., RGD). Increasing the temperature to 37 °C leads to a rapid physical gelation of both P-Fu and P-Ma preventing cell sedimentation and ensuring good printability. After printing, the chemical crosslinking takes place at 37 °C generating stable and biofunctionalized constructs. B) Synthesis route to establish the thermogelling polymers P-Fu and P-Ma: Partial acidic hydrolysis of the thermogelling diblock copolymer P0 followed by the introduction of furan and maleimide moieties by amide coupling (P-Fu and P-Ma).

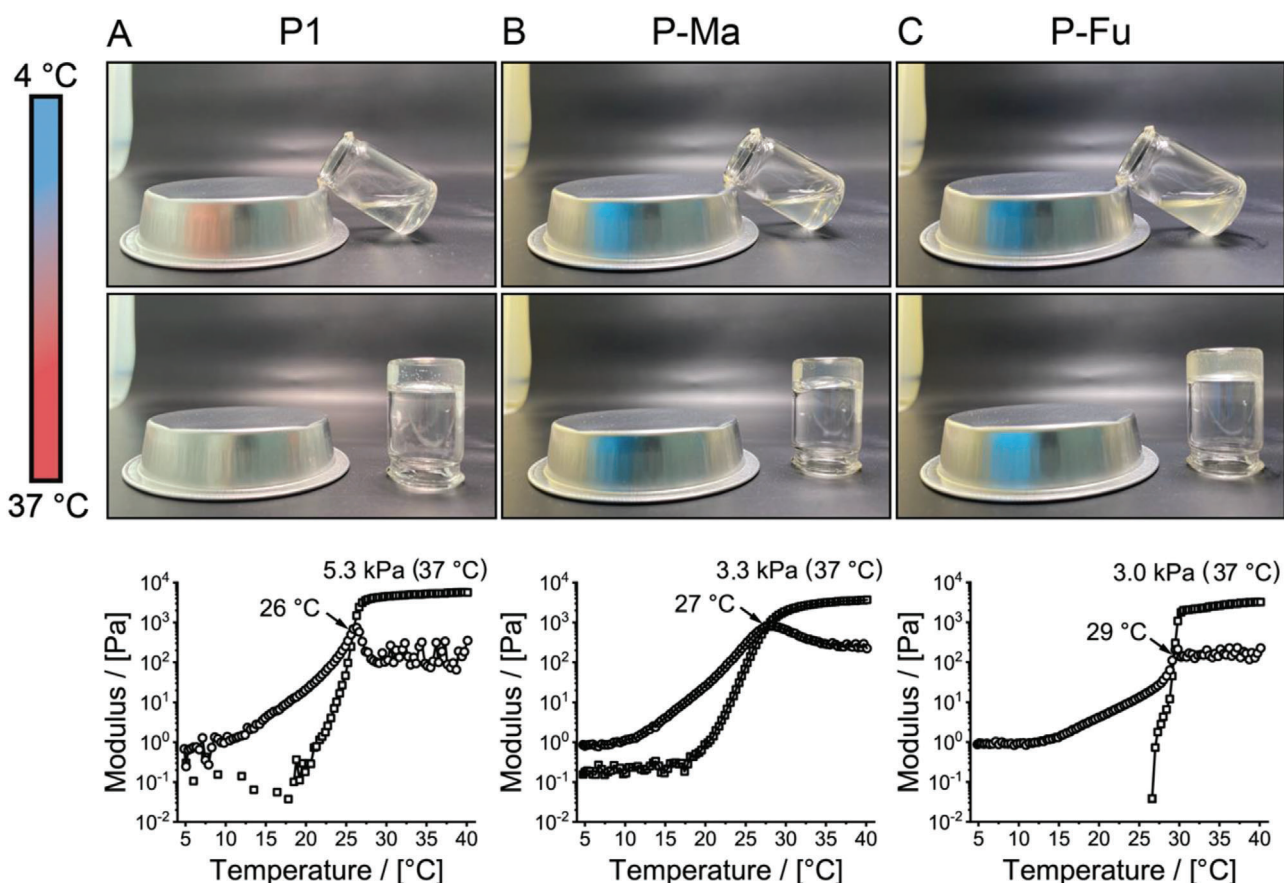


Figure 2. Thermogelling properties of the different modified polymers. A) P1, B) P-Ma, and C) P-Fu in the temperature range of 5–37 °C (heat rate: 0.05 °C s⁻¹) and at 20 wt% aqueous solutions (□: Storage modulus G' , ○: Loss modulus G''). Images were taken at 5 and 37 °C following the described temperature scale.

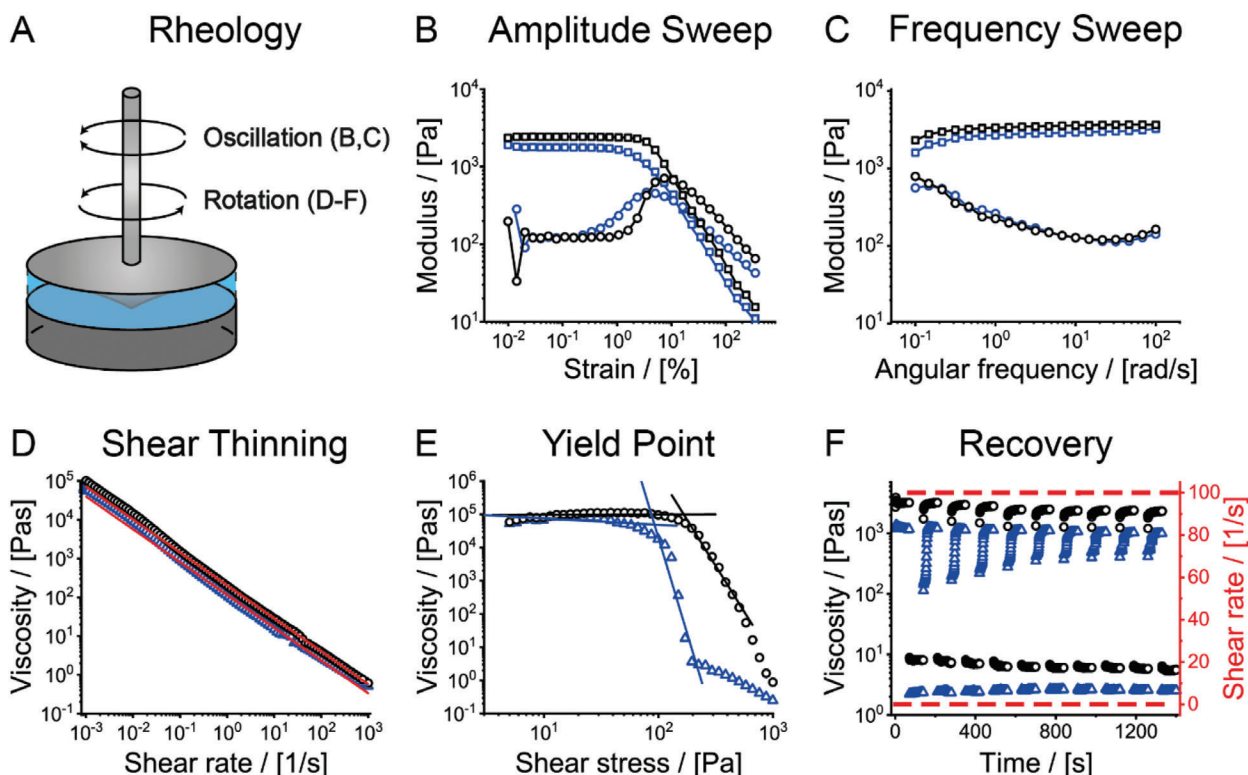


Figure 3. Determination of important rheological properties. A) Rheological properties for direct ink-writing of P-Fu (blue) and P-Ma (black) at a concentration of 20 wt% and 37 °C. B) Amplitude sweep (\square : Storage modulus G' , \circ : Loss modulus G'') and C) frequency sweep. D) Shear thinning properties: Viscosity in dependence of the applied shear rate. Red line: data fitted with a power law function. E) Yield point determination: Viscosity as a function of applied shear stress. The onset of viscosity decrease designates the yield point τ . F) Structure-recovery properties: Alternated high and low-shear regimes.

all relevant signals could be attributed. It is important to note that the signals attributed to EI repeat units completely disappeared. Furthermore, complete modification of all secondary amines (EI units) was confirmed via titration (Figure S4, Supporting Information).

The polymers P1, P-Fu and P-Ma exhibited pronounced thermogelling properties in the temperature range of 5–40 °C (5 °C low viscous liquid, 40 °C stable hydrogel, Figure 2) with sol/gel transitions between 26 and 29 °C (Figure 2). Compared to the precursor polymer P0 the transition temperature increased, which simplifies handling at room temperature (T_{gel} (P0) = 21 °C, Figure S1, Supporting Information). Notably, the storage modulus G' at 37 °C increased from 3.8 kPa for P0 to 5.3 kPa for P1 (Figure 2A). In contrast, the addition of furan and maleimide moieties resulted to a reversal of G' to 3.3 and 3.0 kPa, respectively (Figure 2B,C). Clearly, modifications of the hydrophilic block affect the polymer self-assembly, presumably by affecting the compatibility between the blocks. The physical hydrogels P-Fu and P-Ma at 37 °C and a concentration of 20 wt% were further characterized individually via oscillatory and rotational shear rheology to investigate whether their rheological parameters would be favorable for 3D printing (Figure 3).

Both samples showed a pronounced linear viscoelastic region in the amplitude sweep (Figure 3B). Slightly higher G' values are obtained for the polymer P-Ma, which is in agreement with the values obtained during the temperature sweep (Figure 2). In the

investigated frequency region both polymers exhibited viscoelastic solid-like character throughout (Figure 3C). The pronounced shear-thinning (Figure 3D) with flow indices of $n = 0.15$ for P-Fu and P-Ma, well-defined yield-points (Figure 3E; τ (P-Fu) = 92 Pa and τ (P-Ma) = 166 Pa), high viscosity at low shear stress (≈ 100 kPa s) and fast structure recovery (Figure 3F) suggests good printability for both hydrogels. This rheological profile allows the low viscosity polymer sols to be mixed with cells at ≤ 10 °C, and subsequently printed at 37 °C on a preheated printing dish, where the crosslinking Diels-Alder reaction takes place, subsequently (Figure 4A).

Accordingly, we mixed 20 wt% aqueous solutions of both polymers (1/1, v/v) at 10 °C and followed G' and G'' at 10, 20, and 37 °C over time (Figure 4B). Over the investigated time of 2 h no hydrogel formation was observed at 10 °C and the sample remained a low viscous liquid, ideal for sample preparation, cell distribution, and transfer into a printing syringe. Only a minor increase in viscosity is observed after ≈ 1 h. With a temperature-controlled printing setup, this allows for prolonged printability, if needed. In contrast, at 25 °C, which is below T_{gel} hydrogel, a sol/gel transition is observed after 65 min and must be attributed to the Diels-Alder crosslinking. At 37 °C the mixture thermogelled immediately, followed by additional Diels-Alder crosslinking, as evidenced by an increase of G' and G'' . After less than 50 min a plateau value of more than 10 kPa was reached. Accordingly, printing the bioink at room temperature onto a preheated

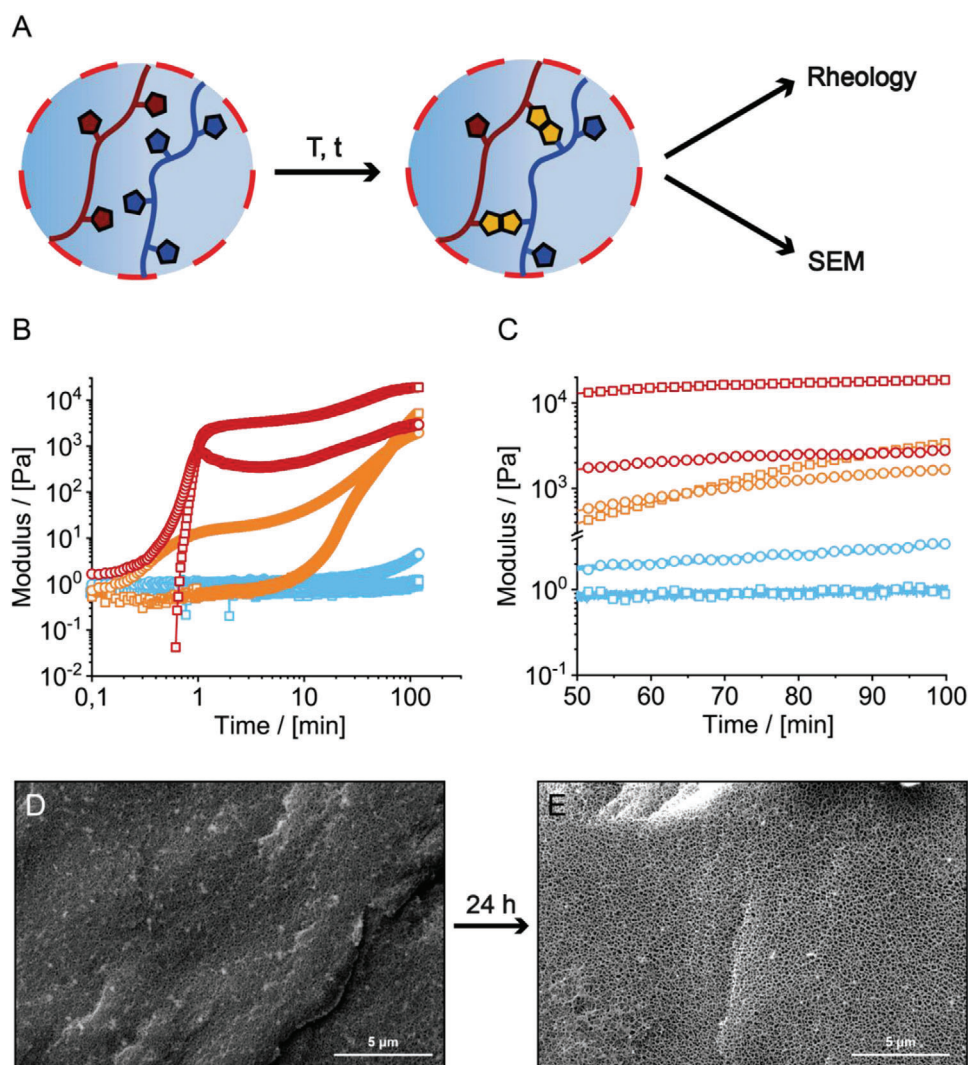


Figure 4. Chemical crosslinking of mixed P-Fu and P-Ma hydrogels. A) Workflow for crosslinking analysis (B–C) Crosslinking kinetics of P-Fu and P-Ma mixtures (1:1) at different temperatures (blue: 10 °C, orange: 20 °C, and red: 37 °C) and 20 wt% concentration (\square : Storage modulus G' , \circ : Loss modulus G''): B) Time scans of 120 min with a fixed amplitude of 0.5 % and an angular frequency of 10 rad s^{-1} with a C) detailed view for 50–100 min which we deem critical for preparing and conducting a typical print. Cryogenic scanning electron microscopy (SEM) investigations to visualize the porous structure of the bioink: Samples were recorded after D) crosslinking of 24 h and E) additional swelling for 24 h.

dish should ensure rapid crosslinking and stability of the printed construct.

Due to the nature of the chemical crosslinked synthetic hydrogel, a highly porous network with features in the range of a few dozen nm was obtained (Figure 4D). Swelling for 24 h led to a significant increase in pore size into the lower 100 nm range (Figure 4E). Although the pore size is sufficiently large for diffusion of nutrients, cells will not be able to migrate through the generated network. Compared to the physical hydrogel of P0 (Figure S1B, Supporting Information) the pore size decreased significantly after chemical crosslinking, due to the formation of a more compact three-dimensional covalent network. In order to highlight the adaptability of the platform in terms of stiffness, the concentration of precursor solutions of P-Fu and P-Ma was decreased by dilution with water leading to softer hydrogels with slower crosslinking kinetics (Figure S5, Supporting Information). Ad-

ditionally, the nature of the crosslinker can be adapted to specific applications. To demonstrate this, we used PEG₆₀₀-bismaleimide as a model crosslinker. The P-Fu-PEG mixtures showed a slower crosslinking and resulted in softer and less dense networks as characterized by rheology and cryogenic scanning electron microscopy, respectively (Figure S6, Supporting Information). Not surprising, this led to a more pronounced swelling of the hydrogels compared to the P-Fu/P-Ma crosslinking.

Based on the favorable rheological properties of the precursor hydrogels and the controlled crosslinking kinetics, first 3D printing experiments were performed. At 5 °C, P-Fu and P-Ma solutions were homogeneously mixed and transferred into a printing cartridge (held at 5 °C) followed by printing onto a preheated (37 °C) printing bed (Figure 5A–C). After 1 h of in situ chemical crosslinking at 37 °C, the constructs were immersed in fresh cell culture medium and incubated for 14 days at 37 °C. The

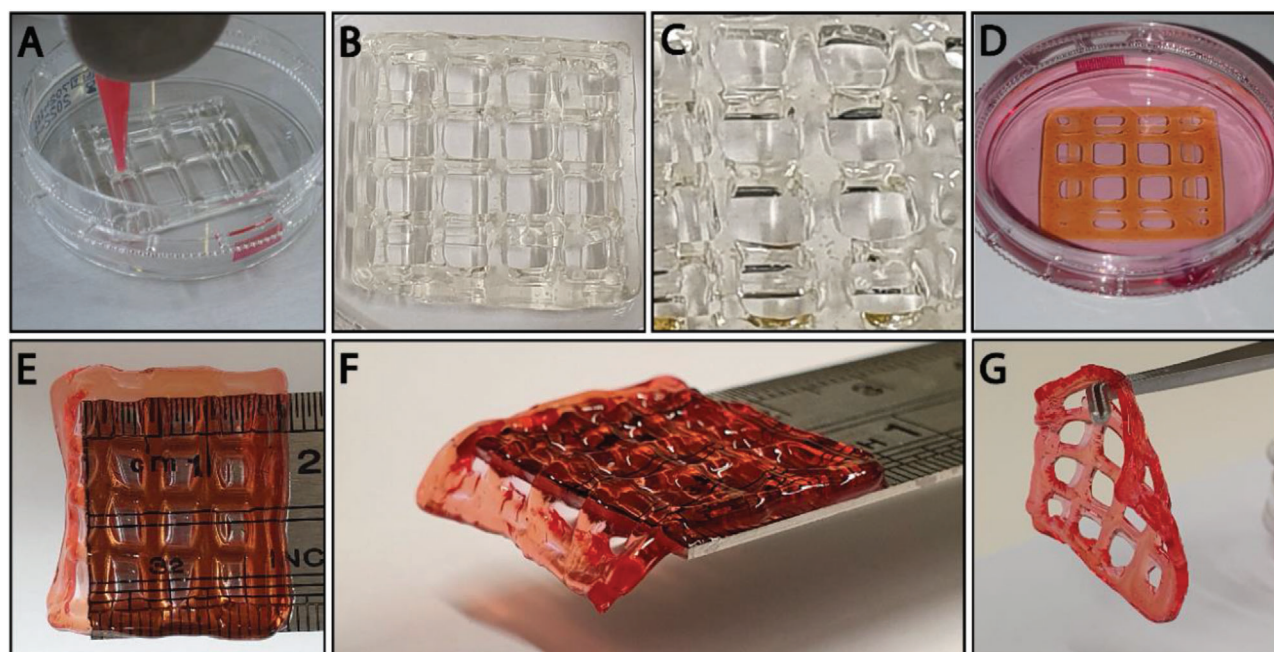


Figure 5. Printing of P-Fu and P-Ma crosslinking hydrogels. A) Image of the printed scaffold during the printing process. B,C) Illustration of the printed scaffold immediately after printing. D) Printed scaffolds after incubation in culture medium for 14 days. E–G) Handling and transfer of P-Fu and P-Ma crosslinked hydrogels after 14 days in culture medium.

constructs remained stable with good structural integrity (Figure 5D). However, fusion of stacked layers with direct contact can be seen. During incubation, swelling increases the contact between individual layers, which can then cross-link with each other. In the end, this leads to a homogeneous construct with relatively low stackability. Even though the hydrogels are soft, as analyzed by rheology and shown above, they were easily handled and transferred while retaining their printed shape (Figure 5D–G).

Furthermore, we analyzed the swelling of the crosslinked P-Fu and P-Ma hydrogels (20 wt%, ratio P-Fu/P-Ma 1:1). Only little swelling was observed (Figure S10A, Supporting Information), which is explained by the combination of physical and chemical crosslinking with several crosslinking functionalities at every polymer molecule. Interestingly, a significant increase of swelling was observed at 5 °C (Figure S10C,D, Supporting Information). Below the lower critical solution temperature of the nPrOzi block the swelling of the hydrogel increased significantly due to an increased solubility of the thermoresponsive nPrOzi block and the removal of physical crosslinks upon cooling. In addition, the stability was further confirmed by mechanical testing. Elastic moduli of approximately 3000–4000 kPa were obtained for the crosslinked hydrogels after 14 days (Figure S10B, Supporting Information).

As mentioned above, it has been shown that different POx-based hydrogels show no cytotoxic effects on cells and therefore present a promising platform for bioinks.^[40–44] However, applicability in biomedicine requires the adhesive functionalization of POx-based hydrogels, as the material per se does not support cell adhesion. To test, whether adhesive functionalization of our hydrogels supports cell adhesion, we functionalized them with integrin-ligating RGD-peptide. We further generated lentivirally transduced, NIH/3T3-based morphology reporter cells, stably ex-

pressing farnesylated tdTomato red-fluorescent protein, to label the plasma membrane and compared the morphology of our reporter cells cultured on top of RGD-functionalized and non-functionalized POx hydrogels. Epifluorescence microscopy analysis after 3 and 4 days of cultivation revealed that cells on non-functionalized POx hydrogels were low in number and showed a rounded morphology (Figure 6A,C), whereas cells on RGD-functionalized hydrogels displayed a well spread fibroblastoid morphology (Figure 6B) and even increased in number over time (Figure 6D). These data demonstrate that adhesive functionalization of our POx hydrogels supports cell adhesion, spreading and proliferation.

To further study cell viability within the gel (3D), NIH3T3 cells were embedded in the hydrogel pre-printing. After the printing process and cross-linking of the hydrogels, the cell viability of the encapsulated cells in the scaffold was analyzed. Cells were pre-stained with Hoechst 33342 prior to the printing process. This was necessary as preliminary work showed that fluorescein diacetate (FDA) was not able to penetrate the gels in a sufficient manner. Dead cells were visualized using propidium iodide (PI) (here no incompatibilities with in-gel penetration were observed) staining after 1 and 2 days. After optimizing the polymer purification process (Figure S8, Supporting Information) as well as the printing protocol, cell viability staining showed no cytotoxic effect of the hydrogel. No difference between the unmodified and RGD-functionalized constructs was observed. The majority of dead cells that were visible, scanning the entire printed hydrogel construct, could be accounted to drying-off effects at the outer layers, which was reported for other hydrogel systems before (Figure S9, Supporting Information).^[45,46] Despite the RGD-functionalization, the cells showed a rounded morphology after the encapsulation in the hydrogel (Figure 7). It

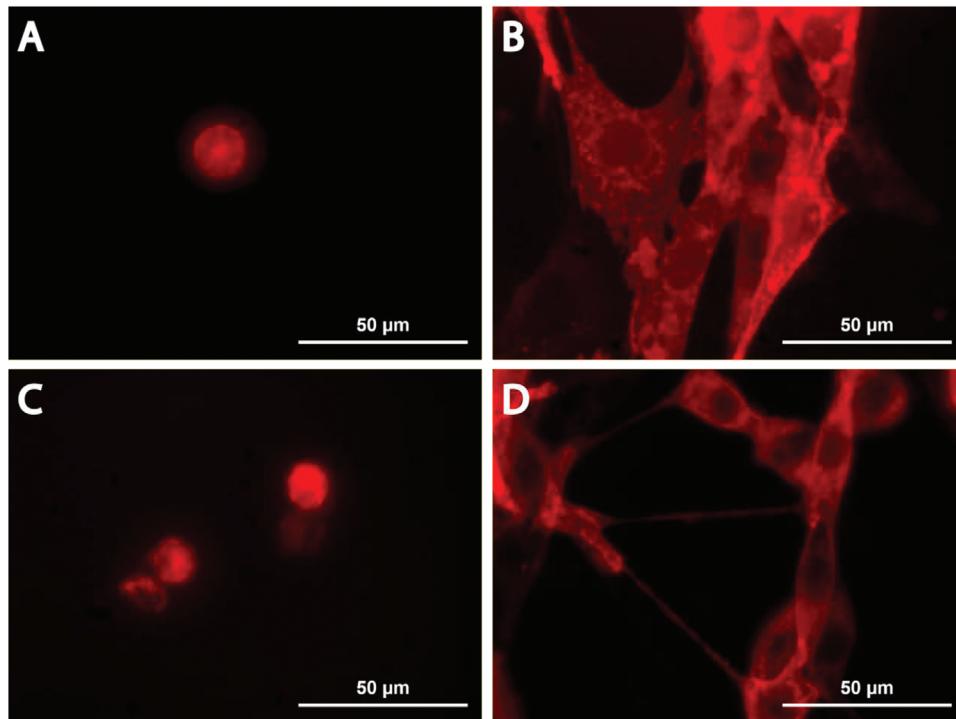


Figure 6. Cell adhesion on the surface of P-Fu and P-Ma crosslinking hydrogels. POx hydrogel without RGD-modification does not allow for good cell adhesion and spreading after A) 3 and C) 4 days. In contrast, cell adhesion and spreading were observed on POx hydrogel with RGD-modification after B) 3 days of and D) 4 days of cultivation.

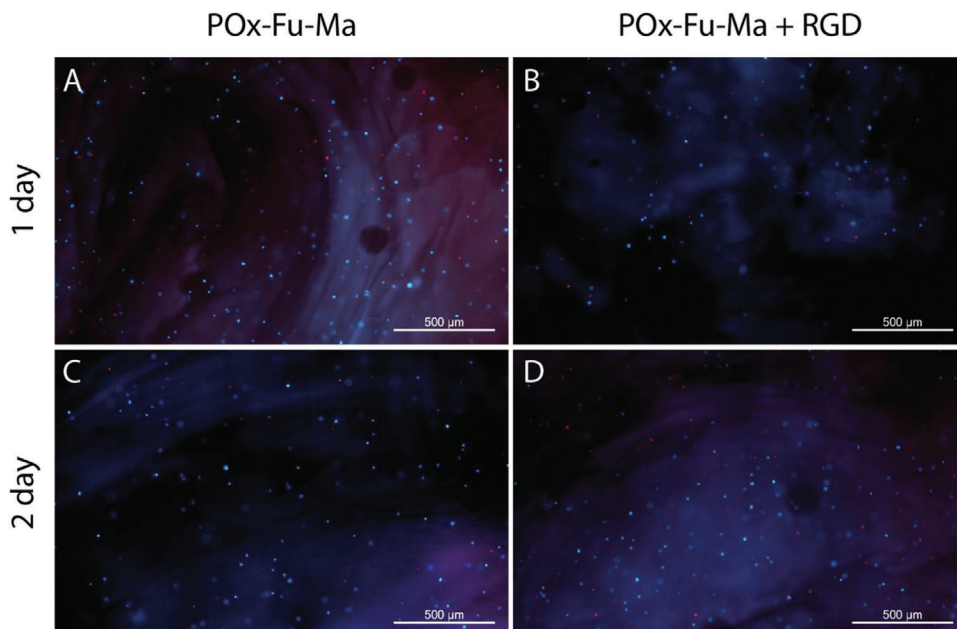


Figure 7. Cell viability of fibroblasts in P-Fu/P-Ma-bioinks after deposition of a bioink drop by extrusion printing. NIH3T3 cells were pre-stained with Hoechst 33 342 (blue) and incorporated, printed, and cultivated in POx-based hydrogels (20 wt%) B,D) with and A,C) without RGD-peptide. Dead cells were assessed by staining with PI (red).

has been previously described that POx hydrogels with moduli of around of around 3.5–4.5 kPa are too stiff for the migration of the cells.^[47,48] Furthermore, small pore sizes, as described above for this system, have been shown to prevent cell spreading and migration.^[49,50] With G' of around 10 kPa and submicron pore size, the hydrogel system, as shown in this study, clearly does not allow the migration and therefore the spreading of the cells.

In an effort to address cell adhesion and migration, we aim at incorporating matrix metalloprotease (MMP) cleavable linkers into the hydrogel network, to ensure cleavage by secreted MMPs and therefore a loosening of the network as demonstrated before.^[51–53] The sequence of the linker (GPQGIAGQ) is derived from collagen. It has been shown to be responsive to MMP cleavage and has already been used in different applications.^[54–57] The linker can be flanked with either thiol or maleimide groups for the cross-linking of both P-Fu and P-Ma and is part of the ongoing research.

3. Conclusion

In this study, favorable thermogelation and shear-thinning properties were combined with cell friendly post-printing chemical crosslinking via Diels-Alder chemistry. The post-polymerization modification preserved the nature of physical crosslinked hydrogels. The crosslinking kinetics and density could be fine-tuned with different temperatures and crosslinking degrees. The second crosslinking step ensured stability of printed constructs over at least two weeks. Biofunctionality was introduced via the attachment of RGD binding motives and NIH 3T3 cells showed cell adhesion and an elongated morphology, when seeded on top of the hydrogels for a couple of days. First bioprinting experiments highlighted the optimized printing setup, the biocompatibility and the functionality of the investigated bioink formulation. With this study, we demonstrate a dual-gelling system based on the versatile and cytocompatible polymer classes of POx and POzi that was used to develop a functional bioinks. Furthermore, the platform can be conveniently decorated with biofunctionalities, which makes it adaptable for many specific applications.

Supporting Information

Supporting Information is available from the Wiley Online Library or from the author.

Acknowledgements

L.H. and M.B. contributed equally to this work. The authors would like to gratefully acknowledge support by the Deutsche Forschungsgemeinschaft (DFG, German Research Foundation)-project number 326998133-TRR225 (subprojects A03, B06). Furthermore, the authors thank the Deutsche Forschungsgemeinschaft for funding the crossbeam scanning electron microscope Zeiss CB 340 (INST 105022/58-1 FUGG) within the DFG State Major Instrumentation Programme.

Open access funding enabled and organized by Projekt DEAL.

Conflict of Interest

The authors declare no conflict of interest.

Data Availability Statement

The data that support the findings of this study are available from the corresponding author upon reasonable request.

Keywords

biofabrication, bioprinting, chemical crosslinking, hydrogels

Received: March 25, 2021

Revised: June 20, 2021

Published online: July 22, 2021

- [1] L. Moroni, T. Boland, J. A. Burdick, C. De Maria, B. Derby, G. Forgacs, J. Groll, Q. Li, J. Malda, V. A. Mironov, C. Mota, M. Nakamura, W. Shu, S. Takeuchi, T. B. F. Woodfield, T. Xu, J. J. Yoo, G. Vozzi, *Trends Biotechnol.* **2018**, *36*, 384.
- [2] D. Chimene, K. K. Lennox, R. R. Kaunas, A. K. Gaharwar, *Ann. Biomed. Eng.* **2016**, *44*, 2090.
- [3] L. Valot, J. Martinez, A. Mehdi, G. Subra, *Chem. Soc. Rev.* **2019**, *48*, 4049.
- [4] J. Groll, J. A. Burdick, D. - W. Cho, B. Derby, M. Gelinsky, S. C. Heilshorn, T. Jüngst, J. Malda, V. A. Mironov, K. Nakayama, A. Ovsianikov, W. Sun, S. Takeuchi, J. J. Yoo, T. B. F. Woodfield, *Biofabrication* **2018**, *11*, 013001.
- [5] J. Groll, T. Boland, T. Blunk, J. A. Burdick, D.-W. Cho, P. D. Dalton, B. Derby, G. Forgacs, Q. Li, V. A. Mironov, L. Moroni, M. Nakamura, W. Shu, S. Takeuchi, G. Vozzi, T. B. F. Woodfield, T. Xu, J. J. Yoo, J. Malda, *Biofabrication* **2016**, *8*, 013001.
- [6] D. Chimene, R. Kaunas, A. K. Gaharwar, *Adv. Mater.* **2020**, *32*, 1902026.
- [7] T. Jungst, W. Smolan, K. Schacht, T. Scheibel, J. Groll, *Chem. Rev.* **2016**, *116*, 1496.
- [8] J. Hazur, R. Detsch, E. Karakaya, J. Kaschta, J. Teßmar, D. Schneider, O. Friedrich, D. W. Schubert, A. R. Boccaccini, *Biofabrication* **2020**, *12*, 045004.
- [9] E. O. Osidak, V. I. Kozhukhov, M. S. Osidak, S. P. Domogatsky, *Int. J. Bioprint.* **2020**, *6*, 270.
- [10] L. Ouyang, R. Yao, Y. Zhao, W. Sun, *Biofabrication* **2016**, *8*, 035020.
- [11] M. Müller, J. Becher, M. Schnabelrauch, M. Zenobi-Wong, *Biofabrication* **2015**, *7*, 035006.
- [12] D. B. Kolesky, R. L. Truby, A. S. Gladman, T. A. Busbee, K. A. Homan, J. A. Lewis, *Adv. Mater.* **2014**, *26*, 3124.
- [13] T. Lorson, M. M. Lübtow, E. Wegener, M. S. Haider, S. Borova, D. Nahm, R. Jordan, M. Sokolski-Papkov, A. V. Kabanov, R. Luxenhofer, *Biomaterials* **2018**, *178*, 204.
- [14] J. - R. Park, E. C. L. Bolle, A. D. Santos Cavalcanti, A. Podevyn, J. F. R. Van Guyse, A. Forget, R. Hoogenboom, T. R. Dargaville, *Biointerphases* **2021**, *16*, 011001.
- [15] M. M. Lübtow, T. Lorson, T. Finger, F. - K. Gröber-Becker, R. Luxenhofer, *Macromol. Chem. Phys.* **2020**, *221*, 1900341.
- [16] M. M. Lübtow, S. Oerter, S. Quader, E. Jeanclos, A. Cubukova, M. Krafft, M. S. Haider, C. Schulte, L. Meier, M. Rist, O. Sampetean, H. Kinoh, A. Gohla, K. Kataoka, A. Appelt-Menzel, R. Luxenhofer, *Mol. Pharmaceutics* **2020**, *17*, 1835.
- [17] J. Humphries, D. Pizzi, S. E. Sonderegger, N. L. Fletcher, Z. H. Houston, C. A. Bell, K. Kempe, K. J. Thurecht, *Biomacromolecules* **2020**, *21*, 3318.
- [18] T. Lorson, S. Jaksch, M. M. Lübtow, T. Jüngst, J. Groll, T. Lühmann, R. Luxenhofer, *Biomacromolecules* **2017**, *18*, 2161.
- [19] C. Hu, L. Hahn, M. Yang, A. Altmann, P. Stahlhut, J. Groll, R. Luxenhofer, *J. Mater. Sci.* **2021**, *56*, 691.

- [20] L. Trachsel, N. Broguiere, J. - G. Rosenboom, M. Zenobi-Wong, E. M. Benetti, *J. Mater. Chem. B* **2018**, *6*, 7568.
- [21] L. Trachsel, C. Johnbosco, T. Lang, E. M. Benetti, M. Zenobi-Wong, *Biomacromolecules* **2019**, *20*, 4502.
- [22] S. Stichler, T. Jungst, M. Schamel, I. Zilkowski, M. Kuhlmann, T. Böck, T. Blunk, J. Teßmar, J. Groll, *Ann. Biomed. Eng.* **2017**, *45*, 273.
- [23] S. Bertlein, G. Brown, K. S. Lim, T. Jungst, T. Boeck, T. Blunk, J. Tessmar, G. J. Hooper, T. B. F. Woodfield, J. Groll, *Adv. Mater.* **2017**, *29*, 1703404.
- [24] K. S. Lim, B. S. Schon, N. V. Mekhileri, G. C. J. Brown, C. M. Chia, S. Prabakar, G. J. Hooper, T. B. F. Woodfield, *ACS Biomater. Sci. Eng.* **2016**, *2*, 1752.
- [25] W. T. Han, T. Jang, S. Chen, L. S. H. Chong, H.-D.o Jung, J. Song, *Biomater. Sci.* **2020**, *8*, 450.
- [26] Y. Chujo, K. Sada, T. Saegusa, *Macromolecules* **1990**, *23*, 2636.
- [27] Y. Chujo, K. Sada, T. Saegusa, *Macromolecules* **1990**, *23*, 2693.
- [28] Y. Chujo, K. Sada, T. Saegusa, *Polymer Journal* **1993**, *25*, 599.
- [29] C. M. Nimmo, S. C. Owen, M. S. Shoichet, *Biomacromolecules* **2011**, *12*, 824.
- [30] A. E. G. Baker, R. Y. Tam, M. S. Shoichet, *Biomacromolecules* **2017**, *18*, 4373.
- [31] L. J. Smith, S. M. Taimoory, R. Y. Tam, A. E. G. Baker, N. Binth Mohammad, J. F. Trant, M. S. Shoichet, *Biomacromolecules* **2018**, *19*, 926.
- [32] V. Delplace, P. E. B. Nickerson, A. Ortin-Martinez, A. E. G. Baker, V. A. Wallace, M. S. Shoichet, *Adv. Funct. Mater.* **2020**, *30*, 1903978.
- [33] D. Nahm, F. Weigl, N. Schaefer, A. Sancho, A. Frank, J. Groll, C. Villmann, H. - W. Schmidt, P. D. Dalton, R. Luxenhofer, *Mater. Horiz.* **2020**, *7*, 928.
- [34] A. C. Braun, M. Gutmann, T. Lühmann, L. Meinel, *J. Controlled Release* **2018**, *273*, 68.
- [35] A. H. St. Amant, D. Lemen, S. Florinas, S. Mao, C. Fazenbaker, H. Zhong, H. Wu, C. Gao, R. J. Christie, J. Read De Alaniz, *Bioconjugate Chem.* **2018**, *29*, 2406.
- [36] A. H. St. Amant, F. Huang, J. Lin, D. Lemen, C. Chakiath, S. Mao, C. Fazenbaker, H. Zhong, J. Harper, W. Xu, N. Patel, L. Adams, B. Vijayakrishnan, P. W. Howard, M. Marelli, H. Wu, C. Gao, J. Read De Alaniz, R. J. Christie, *Bioconjugate Chem.* **2019**, *30*, 2340.
- [37] M. Mees, E. Haladjova, D. Momekova, G. Momekov, P. S. Sheshtakova, C. B. Tsvetanov, R. Hoogenboom, S. Rangelov, *Biomacromolecules* **2016**, *17*, 3580.
- [38] M. A. Mees, R. Hoogenboom, *Polym. Chem.* **2018**, *9*, 4968.
- [39] R. Luxenhofer, *Nanomedicine* **2015**, *10*, 3109.
- [40] R. Luxenhofer, G. Sahay, A. Schulz, D. Alakhova, T. K. Bronich, R. Jordan, A. V. Kabanov, *J. Controlled Release* **2011**, *153*, 73.
- [41] F. C. Gaertner, R. Luxenhofer, B. Blechert, R. Jordan, M. Essler, *J. Controlled Release* **2007**, *119*, 291.
- [42] L. Hahn, M. Maier, P. Stahlhut, M. Beudert, V. Flegler, S. Forster, A. Altmann, F. Töppke, K. Fischer, S. Seiffert, B. Böttcher, T. Lühmann, R. Luxenhofer, *ACS Appl. Mater. Interfaces* **2020**, *12*, 12445.
- [43] Lübtow, Mrlik, Hahn, Altmann, Beudert, Lühmann, Luxenhofer, *J. Funct. Biomater.* **2019**, *10*, 36.
- [44] M. Bauer, S. Schroeder, L. Tauhardt, K. Kempe, U. S. Schubert, D. Fischer, *J. Polym. Sci., Part A: Polym. Chem.* **2013**, *51*, 1816.
- [45] Y. Yu, Y. Zhang, J. A. Martin, I. T. Ozbolat, *J. Biomech. Eng.* **2013**, *135*, 91011.
- [46] J. Hauptstein, T. Böck, M. Bartolf-Kopp, L. Forster, P. Stahlhut, A. Nadernezhad, G. Blahetek, A. Zernecke-Madsen, R. Detsch, T. Jüngst, J. Groll, J. Teßmar, T. Blunk, *Adv. Healthcare Mater.* **2020**, *9*, 2000737.
- [47] B. L. Farrugia, K. Kempe, U. S. Schubert, R. Hoogenboom, T. R. Dargaville, *Biomacromolecules* **2013**, *14*, 2724.
- [48] K. Bott, Z. Upton, K. Schrobback, M. Ehrbar, J. A. Hubbell, M. P. Lutolf, S. C. Rizzi, *Biomaterials* **2010**, *31*, 8454.
- [49] C. M. Murphy, F. J. O'brien, *Cell Adhes. Migr.* **2010**, *4*, 377.
- [50] F. Geiger, D. Rüdiger, S. Zahler, H. Engelke, *PLoS One* **2019**, *14*, e0225215.
- [51] M. R. Arkenberg, D. M. Moore, C.-C. Lin, *Acta Biomater.* **2019**, *83*, 83.
- [52] D. Seliktar, A. H. Zisch, M. P. Lutolf, J. L. Wrana, J. A. Hubbell, *J. Biomed. Mater. Res. A* **2004**, *68A*, 704.
- [53] H. P. Wurst, K. Larbi, M. Herrmann, US20130052736, **2013**.
- [54] J. Ritzer, T. Lühmann, C. Rode, M. Pein-Hackelbusch, I. Immohr, U. Schedler, T. Thiele, S. Stübinger, B. V. Rechenberg, J. Waser-Althaus, F. Schlottig, M. Merli, H. Dawe, M. Karpišek, R. Wyrwa, M. Schnabelrauch, L. Meinel, *Nat. Commun.* **2017**, *8*, 264.
- [55] A. C. Braun, M. Gutmann, T. D. Mueller, T. Lühmann, L. Meinel, *J. Controlled Release* **2018**, *279*, 17.
- [56] A. C. Braun, M. Gutmann, R. Ebert, F. Jakob, H. Gieseler, T. Lühmann, L. Meinel, *Pharm. Res.* **2017**, *34*, 58.
- [57] K. Dodt, S. Lamer, M. Driefßen, S. Bölch, A. Schlosser, T. Lühmann, L. Meinel, *ACS Biomater. Sci. Eng.* **2020**, *6*, 5240.

Supporting Information

From Thermogelling Hydrogels Towards Functional Bioinks: Controlled Modification and Cytocompatible Crosslinking

Lukas Hahn^{1*}, Matthias Beudert^{2*}, Marcus Gutmann², Larissa Keßler¹, Philipp Stahlhut³,
Lena Fischer⁴, Emine Karakaya⁵, Thomas Lorson², Ingo Thievessen⁴, Rainer Detsch⁵, Tessa
Lühmann^{2,*} and Robert Luxenhofer^{1,6,*}

¹*Functional Polymer Materials, Chair for Advanced Materials Synthesis, Institute for Functional Materials and Biofabrication, Department of Chemistry and Pharmacy and Bavarian Polymer Institute, Julius-Maximilians-University Würzburg, Röntgenring 11, 97070 Würzburg, Germany*

²*Institute of Pharmacy and Food Chemistry, Julius-Maximilians-University Würzburg, Am Hubland, 97074 Würzburg, Germany*

³*Department for Functional Materials in Medicine and Dentistry, University of Würzburg, Pleicherwall 2, 97070 Würzburg, Germany*

⁴*Center for Medical Physics and Technology, Biophysics Group, Friedrich-Alexander-University of Erlangen-Nuremberg, Henkestrasse 91, 91052 Erlangen, Germany*

⁵*Institute of Biomaterials, University of Erlangen-Nürnberg, Cauerstr. 6, 91058, Erlangen, Germany*

⁶*Soft Matter Chemistry, Department of Chemistry and Helsinki Institute of Sustainability Science, Faculty of Science, University of Helsinki, P.O. Box 55, FIN-00014, Helsinki, Finland*

*Contributed equally

Corresponding authors: tessa.luehmann@uni-wuerzburg.de, robert.luxenhofer@helsinki.fi

Materials and Methods

All substances and reagents for the monomere synthesis, polymerization and post-polymerization modification were purchased from Sigma-Aldrich (Steinheim, Germany), TCI-chemicals (Tokyo, Japan) or Thermo Fisher Scientific (Waltham, USA) and were used as received unless otherwise stated. Deuterated solvents for NMR analysis were obtained from Deutero GmbH (Kastellaun, Germany). 3-(2-Furyl)propionic acid was freshly sublimated prior of usage in polymer modification. Maleimidohexanoic acid was recrystallized using hexane as solvent. The RGD-peptide (Acetyl-Cys-Doa-Doa-GRGDSP-NH₂; Doa: 8-amino-3,6-dioxaoctanoic acid) was purchased from Cellendes (Reutlingen, Germany)

Nuclear Magnetic Resonance (NMR):

For ¹H-NMR analysis of polymers and kinetic studies spectra were recorded on a Bruker Fourier 300 (¹H 300.12 MHz) spectrometer at 298 K from Bruker BioSpin (Rheinstetten, Germany) and calibrated using the solvent signals.

Gel Permeation Chromatography (GPC):

Experiments were performed on a Polymer Standard Service PSS (Mainz, Germany) like described in previous studies.[1]

Rheology:

Experiments were performed on an Anton Paar (Ostfildern, Germany) Physica MCR 301 system utilizing a plate-plate geometry (25 mm diameter) and a solvent trap and a Peltier element. The temperature-sweep measurements were performed from 5 to 40 °C (heating-rate: 0.05 °C) by a fixed amplitude of 0.5 % and angular frequency of 10 rad/s. The crosslinking kinetics were monitored for 2 h at different temperatures in oscillatory mode (angular frequency: 10 rad/s, amplitude: 0.5 %). The samples were prepared at 10 °C and placed on the precooled rheometer plate prior to measurement. For the investigation of printing preconditions an amplitude-, frequency-, shear-rate- and shear-stress-sweep and

structure recovery testing was conducted at 37 °C like described previously.[1] For steady shear experiments, the control shear rate mode was used. The data were fitted using the power-law expression established by Ostwald-de Waele. To evaluate the yield point of the systems, steady stress sweeps were performed from 5 to 1000 Pa shear stress. The onset of viscosity decrease is recommended as the yield point. To investigate structure recovery the shear rate was alternated from 0.1 1/s to 100 1/s several times at 37 °C.

Cryo Scanning Electron Microscopy (SEM):

The crosslinking was performed at 37 °C for 24 h. In addition, the swelling was conducted in an excess of water at 37 °C over night. The sample preparation and imaging using a Crossbeam 340 field emission scanning electron microscope (Carl Zeiss Microscopy, Oberkochen, Germany) was adapted as described previously.[1]

Cell Culture:

Mouse embryonic fibroblast NIH3T3 cells were cultured in growth medium (DMEM 10 % FCS, 100 U/mL penicillin G and 100 µg/mL streptomycin) on 25 cm² culture flasks at 37 °C and 5 % CO₂.

Distribution of NIH-3T3 cells:

25 wt% aqueous solutions of both furan- and maleimide-modified polymer were prepared at 4 °C. Both polymer solutions were mixed in a ratio of 2:3 respective to the furan-modified polymer. RGD-maleimide (0.5 µmol) of was added to the polymer solution to a final concentration of 10 µM and 22.5 wt%. The gels were casted and incubated at 37 °C for 1 h. Afterwards the hydrogels were overlaid with an RGD-solution (5 µM) and incubated at 37 °C for 1 h. After washing the gel with PBS for 3 times 2×10^4 in NIH3T3 tdTomato-Farnesyl-5 reporter cells were seeded on top of the hydrogels. After 1 h of incubation at 37 °C and 5 % CO₂ the construct was overlaid with growth medium (DMEM 10 % FCS, 100 U/mL penicillin G and 100 µg/mL streptomycin, 3 µg/ml puromycin).

Direct ink-writing:

For the printing of hydrogel scaffolds an extrusion-based bench-top 3D bioprinter (Bio X, Cellink, Sweden) was used. 23 wt% aqueous solutions of both furan- and maleimide-modified polymer were prepared at 4 °C and printed at room temperature. Both polymers were mixed in a ratio of 2:3 with respect to furan-modified polymer and transferred immediately to the nozzle. The printer was equipped with a 25 GA (Cellink, #4116) diameter precision nozzle. A pressure ranging from 30 to 80 kPa was applied and the printing speed was set to 10 mm/s. For the visualization of the printed letters (TRR225) 5 % of Alexa Fluor™ 488 azide [5 mg/ml] (ThermoFisher Scientific, #2146855) was added to constructs to a final concentration 23 wt% of the bioink. After printing, the constructs were incubated at 37 °C and 5 % CO₂. After 1 h the constructs were overlaid with growth medium (DMEM 10 % FCS, 100 U/mL penicillin G and 100 µg/mL streptomycin) or ddH₂O.

Swelling:

After dissolving the polymers P-Fu and P-Ma (20 wt%) at 5 °C in DPBS (Gibco™, Sigma Aldrich), both solutions were mixed in a ratio of 1:1 and 200 µL of the final mixture were transferred into a stench with holes of a diameter of 10 mm. Crosslinking took place at 37 °C for 1 h yielding stable hydrogel films (n=5). These discs were weighted (m₀) and transferred to a well plate with 4 mL HBSS (Gibco™, Sigma Aldrich) and incubated over 14 days at 37 °C, 95 % humidity and 5 % CO₂ in an incubator. Further, the medium was changed every 3 days. After certain time points, all samples were dried using a paper wipe and weighted directly after incubation (m_s) using a precision balance (GX-600, A&D Instruments, United Kingdom), respectively. After 14 days all hydrogel discs were additionally incubated in the fridge (5 °C) for 2 h and were dried as well as weighted subsequently. The ratio of swelling was calculated by the following equation:

$$\text{Eq. (1): } \%Swelling = \frac{m_s}{m_0} * 100$$

Mechanical characterization:

Using a puncher, round shaped discs with a diameter of 3 mm and a height of 2 mm were fabricated. The modulus of elasticity of these samples was analyzed using a microtester (Cellscale, Canada). The Elastic modulus was determined from the load-displacement relations operating a square shaped beam clamp (6x6 mm) and a beam with a diameter of 1.016 mm at room temperature. A displacement of 15 % was set for recording 3 cycles of all films (n=3), respectively.

Cell viability staining:

NIH 3T3 fibroblasts (CRL-1658; ATCC, Manassas, VA) were maintained in treated surface area 75 cm² culture flasks in growth medium (DMEM containing heat-inactivated FCS (10 %), penicillin G (100 U/mL) and streptomycin (100 µg/µL) at 37 °C under 5 % CO₂. Prior to use, the cells were washed with PBS and detached by trypsin (0.005 %) with EDTA (0.025 %). Trypsin/EDTA activity was stopped by the addition of growth medium and the cells were washed once with growth medium. After one washing step including centrifugation (214x g, 5 min) and aspiration, the cells were resuspended in adjusted growth medium (DMEM containing heat-inactivated FCS (20 %), penicillin G (100 U/mL) and streptomycin (100 µg/µL) and stained with Hoechst 33342 Solution [20 mM] (1 µL/mL – 20 µM) for 15 min at 37 °C under 5 % CO₂. Subsequently, the cells were washed twice with adjusted growth medium and resuspended to a concentration of 2.000.000 cells/mL. 25 wt% solutions of both P-Fu and P-Fu were prepared with growth medium (without FCS) at 4 °C. P-Fu and P-Fu solutions were mixed in a ration of 7:3 (P-Fu:P-Ma) at 4 °C and FCS (10 %), RGD-peptide (5 µM) was added to a final concentration of 20 wt%. 1 x 10⁶ cells/ml were incorporated into the gel and printed as described above. The prepared POx-gels were removed from the cell

culture at the respective times (t_{0h} , t_{4h} , t_{24h} and t_{48h}) and stained with 1 $\mu\text{g}/\text{mL}$ Propidium iodide [2mg/mL] for 2 min at 37 °C under 5 % CO_2 .

Generation of NIH3T3 morphology reporter cells

The cDNA of farnesylated tdTomato fluorescent protein was amplified from tdTomato-farnesyl-5 plasmid (Addgene, # 58092) with a 5' primer encoding a *Bam*HI site and a 3' primer encoding a *Not*I site and used to replace the AcGFP cDNA in pLVX-AcGFP-N1 (Clontech, # 632154). The PCR product was purified, digested with BamHI and NotI, and inserted into equally digested pLVX-AcGFP-N1 lentiviral vector. Plasmid DNA was purified using the NucleoBond Xtra Maxi Kit (Macherey-Nagel, # 740414.50) and verified by DNA sequencing (Eurofins Genomics Germany GmbH, Ebersberg, Germany). Infectious lentivirus was generated by co-transfection of the lentiviral transfer plasmid with packaging plasmid psPAX.2 (Addgene, # 8454) and envelope plasmid VSV-G (Addgene, # 12260) into LentiX 293 T cells (Takara, # 632180) using Lipofectamine 2000 (ThermoFisher Scientific, # 11668019). Lentivirus containing supernatant was harvested 48 h after transfection, briefly centrifuged and concentrated (10x) using the LentiX concentrator (Takara, #631232). The concentrated virus was used for subsequent transduction of NIH3T3 cells which were seeded 24 h prior to transduction at a density of 100,000 cells per 9.6 cm^2 . 10 $\mu\text{g}/\text{ml}$ polybrene was added during infection. Successfully transduced NIH3T3 cells were selected with puromycin (5 $\mu\text{g}/\text{ml}$) and sorted for high fluorescence intensity by fluorescence-activated cell sorting (FACS) to obtain cell lines with homogeneous expression levels.

Fluorescence microscopy

Cell Adhesion as well as cell viability was analyzed using an Axio Observer.Z7 microscope equipped with an A-Plan 10x/0.25 Ph1 objective (Zeiss). The images were recorded with a 90 HE LED multispectral reflector module ($\lambda_{\text{ex}} = 385/30 \text{ nm}$ $\lambda_{\text{em}} = 425/30 \text{ nm}$; $\lambda_{\text{ex}} = 469/38 \text{ nm}$ $\lambda_{\text{em}} = 514/30 \text{ nm}$; $\lambda_{\text{ex}} = 555/30 \text{ nm}$ $\lambda_{\text{em}} = 592/25 \text{ nm}$; $\lambda_{\text{ex}} = 631/33 \text{ nm}$ $\lambda_{\text{em}} = 709/100 \text{ nm}$) with a Colibri 7 LED lamp. Image processing was performed in ImageJ (<http://imagej.nih.gov/ij/>).

Polymer Synthesis:

The polymer P0 (Me-PMeOx₁₀₀-b-PnPrOzi₁₀₀-EIP) was synthesized following the description of Lorson et al.[2]. Figure S1 shows the thermogelling properties and microstructure of P0 investigated via rheology and cryoSEM.

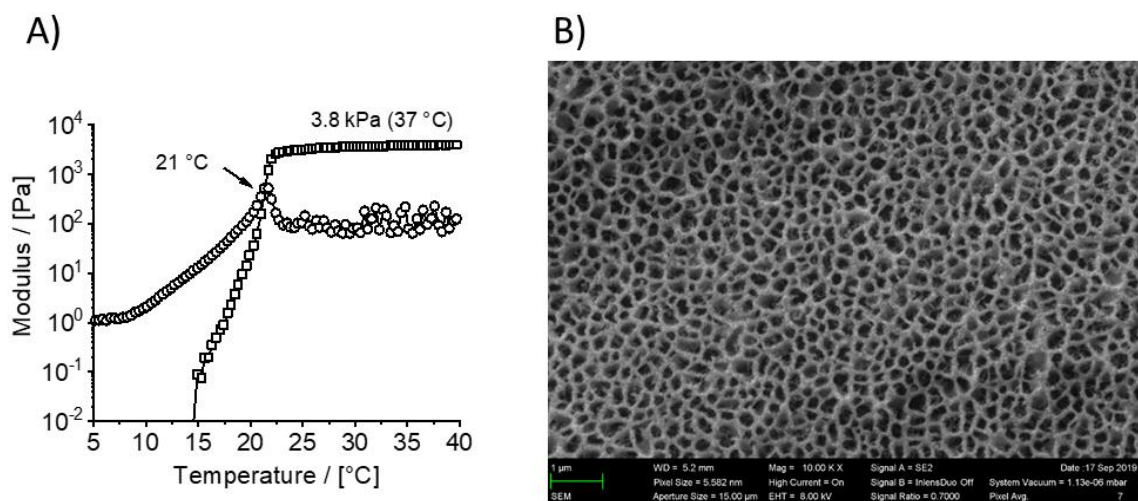


Figure S1. A) Thermogelling properties of a 20 wt% aqueous sample of P0. B) CryoSEM image of the physical hydrogel of P0.

Partial hydrolysis of P0 to obtain polyethyleneimine (PEI) moieties in PMeOx-b-PnPrOzi polymers

For the partial hydrolysis, the procedure first described by Nahm et al. was adapted.[3] In principle the polymer was dissolved in Millipore water and heated up to 90 °C inner temperature. After reaching a constant temperature of 90 °C and equilibration for 10 min concentrated HCl (t=0 min) was added to obtain a total amide concentration of 0.48 M. To investigate hydrolysis kinetics samples were taken at different time intervals and quenched immediately with 20 wt% aqueous NaOH solution at 0 °C.

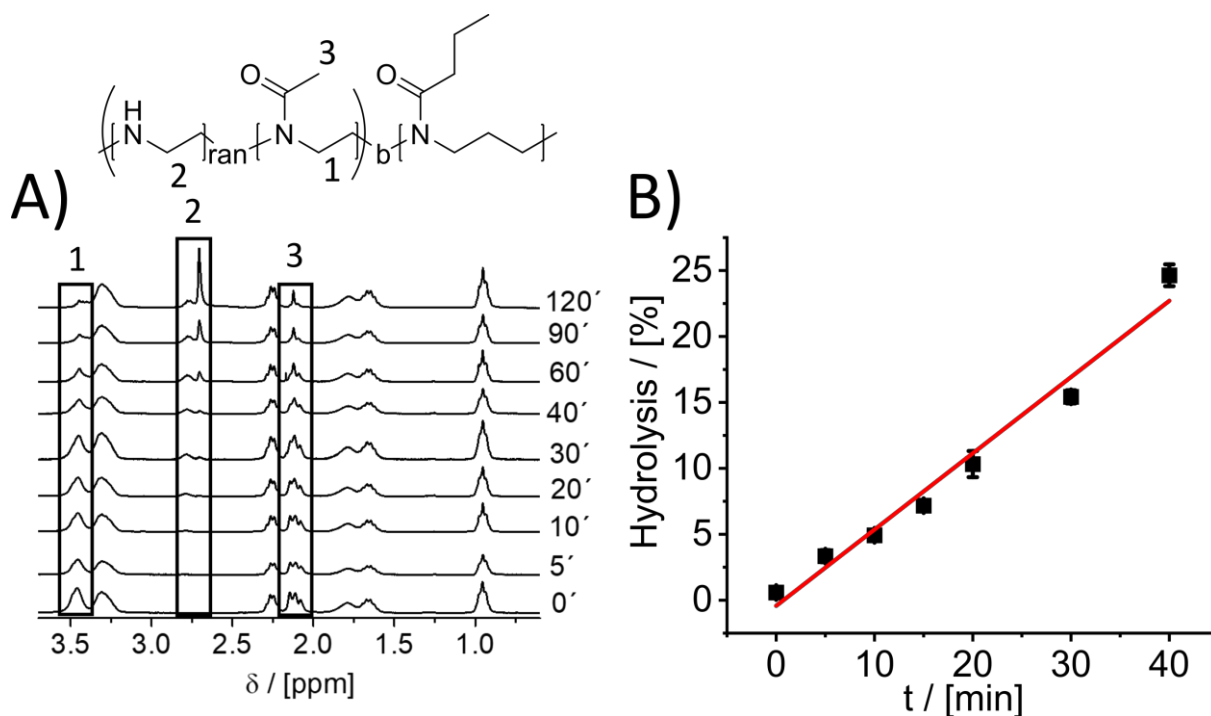


Figure S2. Analysis of acidic hydrolysis via $^1\text{H-NMR}$ experiments. A) Mainly the PMeOx block (signals 1, 2 and 3) is affected during acidic hydrolysis. No change of the PnPrOzi block signals (all other peaks) were observed. The signals 2 and 3 decrease and the signal 1 increased as a function of the reaction time. B) For the kinetic investigations the reactions were done in triplicates in the time range of 0→40 minutes. Data were fitted with linear fit function and used to calculate reaction time for the polymers P1.1-P1.3 and P1(5)-P1(20) (P1 = P(MeOx_{90-co}-EI₁₀)-b-PnPrOzi₁₀₀).

For example, to yield a hydrolysis degree of 10 % of PMeOx units the reaction time was set to 18 min following the results investigated by the kinetic studies. After the calculated time the reaction mixture was quenched using a 20 wt% aqueous NaOH solution at 0 °C to reach pH~9. After removal of water, the polymer was dissolved in MeOH and the remaining solid NaCl was filtered. After removal of MeOH the polymer was dissolved in water and dialyzed (1 kD MWCO) over night and lyophilized to obtain the Polymer P(MeOx_{90-co}-EI₁₀)-b-PnPrOzi₁₀₀ (P1) as white powder. The structures were characterized via $^1\text{H-NMR}$ and GPC. The degree of hydrolysis H_{degree} was calculated using following equation and the characteristic signals in the $^1\text{H-NMR}$ spectrum:

$$H_{\text{degree}} [\%] = \frac{I(\text{PEI } bb)}{I(\text{PMeOx } bb) + I(\text{PEI } bb)} \cdot 100$$

With I (PEI bb): Intensity of PEI backbone signal, I (PMeOx bb): Intensity of the PMeOx backbone signal.

P1.1: *Me-(PMeOx₉₀-ran-PEI₁₀)-b-PnPrOzi₁₀₀*

m(P0): 7.7 g,

reaction time: 18 min,

Hydrolysis of PMeOx-block: 9 % (obtained via ¹H-NMR)

Đ: 1.29 (obtained via GPC)

Yield: 6.8 g (0.32 mmol, 90 %).

P1.2: *Me-(PMeOx₉₀-ran-PEI₁₀)-b-PnPrOzi₁₀₀*

m(P0): 7.7 g,

reaction time: 18 min,

Hydrolysis of PMeOx-block: 11 % (obtained via ¹H-NMR)

Đ: 1.25 (obtained via GPC)

Yield: 5.7 g (0.27 mmol, 75 %).

P1.3: *Me-(PMeOx₉₀-ran-PEI₁₀)-b-PnPrOzi₁₀₀*

m(P0): 7.7 g,

reaction time: 18 min,

Hydrolysis of PMeOx-block: 12 % (obtained via ¹H-NMR)

Đ: 1.31 (obtained via GPC)

Yield: 6.8 g (0.33 mmol, 92 %).

Table S1. Summary of thermogelling properties of P1.1-P1.3 investigated via temperature scan using rheology in oscillation mode. The storage modulus at 37 °C and the onset of significant gelation ($G' \gg G''$ onset) was highlighted.

Polymer	$G'_{37^\circ\text{C}}$ [kPa]	$G' \gg G''$ (onset) [°C]
P1.1	4.6	24.0
P1.2	4.3	24.9
P1.3	5.6	26.4

Other hydrolysis degrees were obtained by the variation of reaction times (Figure S3 A, B). In figure S3 C the thermogelling properties as a function of the degree of hydrolysis were investigated. The increase of viscosity in comparison to P1(10) is shifted towards higher temperatures for the polymers P1(5), P1(15) and P1(20). In the investigated temperature range (5-40 °C) for the polymer P1(20) no plateau value was reached. The plateau values for the polymers P1(5)-P1(15) were similar. Based on that the polymer P1(10) was used for further modifications.

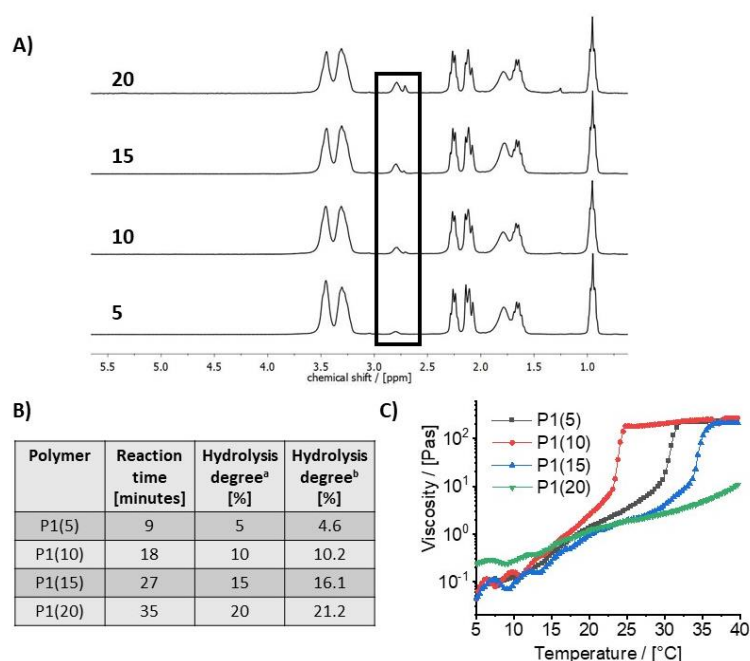


Figure S3. Thermogelation of polymers with different degrees of hydrolysis A) ^1H NMR spectra of polymers with different degrees of hydrolysis (5-20 % hydrolysis of PMeOx units). B) Table of different hydrolysis degrees obtained by changing the reaction time. ^aHydrolysis degree theoretical,

^bHydrolysis degree determined using ¹H NMR signal integration. C) Temperature sweeps (shear rate 0.5 1/s, heat-rate 0.05 °C/s) of polymers with different hydrolysis degrees (20 wt% aqueous samples).

The synthesis of furan- and maleimide-functionalized polymers P(MeOx_{90-co}-Fu₁₀)-*b*-PnPrOzi₁₀ (P-Fu) and P(MeOx_{90-co}-Ma₁₀)-*b*-PnPrOzi₁₀₀ (P-Ma) was performed as described in detail by Nahm et al.[3] To purify the polymer several dialysis steps in water/ethanol (9:1) mixtures were necessary to prevent cytotoxicity.

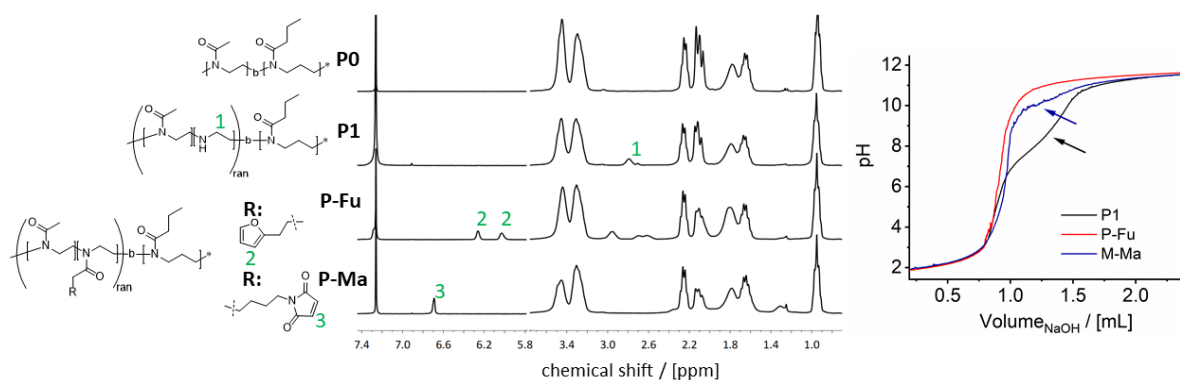


Figure S4. Following the post polymerization modification via ¹H-NMR experiments. Specific signal assignment of P1 (Signal 1), P-Fu (Signals 2) and P-Ma (Signal 3) structures after modification of P0. Additionally, titration curves for the polymers P1, P-Fu and P-Ma are shown. P1 (black) exhibited a pronounced buffer effect in the alkaline region (pH=9, black arrow) originated by secondary amines. P-Fu (red) showed only one defined pH-switch corresponding to the HCl/NaOH titration and no buffer effect of the polymer was detected confirming complete modification of all secondary amines. P-Ma showed a buffer effect at ca. pH=10 (blue arrow), which can be attributed to the hydrolysis of maleimide functionality during titration.

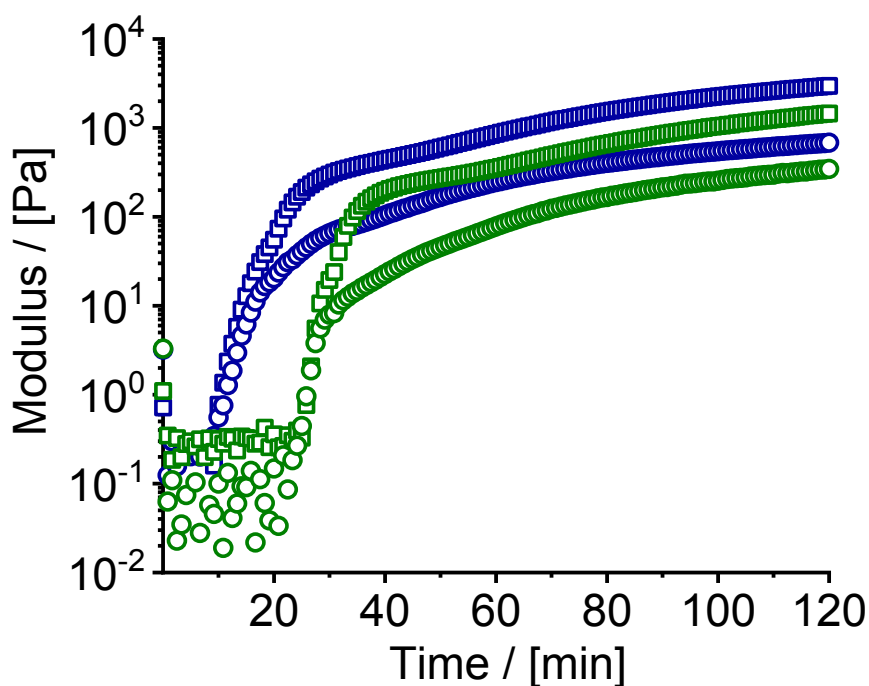


Figure S5. Different degrees of chemical crosslinking of P-Fu-P-Ma hydrogels. Crosslinking of P-Fu and P-Ma at 37 °C and an angular frequency of 10 rad/s and amplitude of 0.5 % at different concentrations (\square : Storage modulus G' , \circ : Loss modulus G''). 20 wt% samples of P-Fu/P-Ma (1:1) were mixed at 5 °C with H₂O at a ratio of 1:1 (10 wt%) (blue) and 1:2 (6.7 wt%) (green).

Using polyethylene glycol (PEG)₆₀₀-Bismaleimide as crosslinker:

P-Fu was cross-linked by an adapted procedure of the polymer analogous modification using Diels-Alder reaction.[4] As crosslinker a PEG-bismaleimide with a molecular weight of 600 g/mol (Creative PEGworks, Chapel Hill, NC, USA) was used. Both cross-linker and polymer stock solution (22 wt%) were dissolved in ddH₂O and mixed at 4 °C to get a final polymer concentration of 20 wt%. Analysis of the crosslinking reaction was performed using an Anton Paar (Ostfildern, Germany) Physica MCR302, equipped with peltier elements (P-PTD200/Air & H-PTD200) and a plate-plate geometry (diameter 25 mm) at 37 °C by mounting the sample on top of a preheated rheometer plate (Figure S5 A). Data were processed using RheoCompass software version 1.23.378 (Anton Paar, Graz, Austria). In addition to that, the degree of crosslinking was varied and the crosslinked samples were analyzed after 24 h of crosslinking at room temperature (50 % (low), 80 % (medium) and 100 % (high) crosslinking with respect to the furan moieties) (Figure S5 B).

Additionally, a PEG-bismaleimide crosslinked sample was analyzed via *cryoSEM* after 24 h (Figure S5 C i) of crosslinking and swelling for 24 h (Figure S6 C ii).

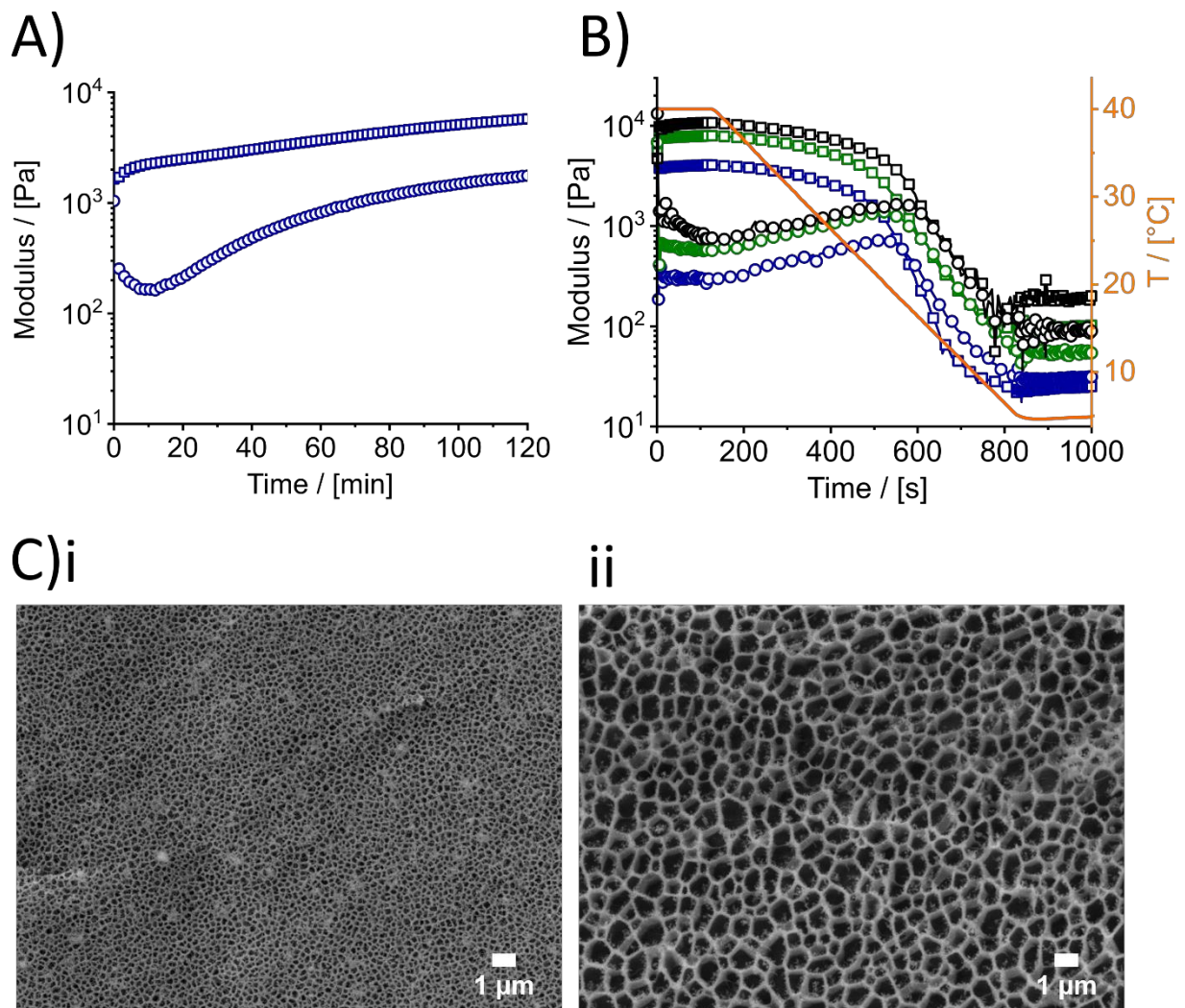


Figure S6. Chemical crosslinking of P-Fu hydrogels with PEG-linker A) Crosslinking of P-Fu using PEG bismaleimide at 37 °C and a polymer concentration of 20 wt% (\square : Storage modulus G' , \circ : Loss modulus G''). B) Influence of crosslinking degree (blue: low (50 %), green: middle (80 %) and black: high (100 %) with respect to the furan moieties). C) *CryoSEM* analysis of a PEG-crosslinked hydrogel after crosslinking for 24 h (i) and swelling for 24 h (ii) in aqueous solution at 37 °C.

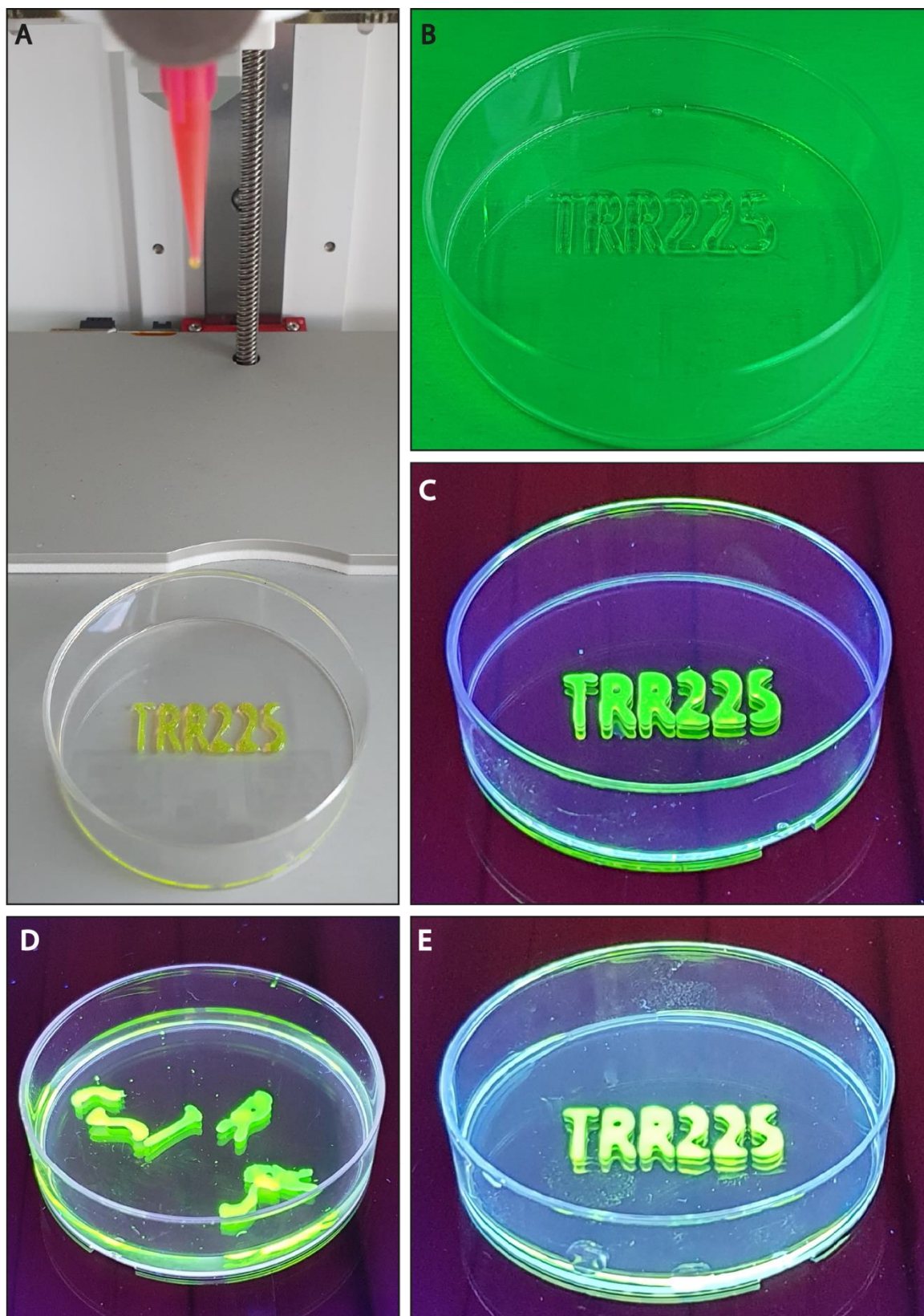


Figure S7. Printing of P-Fu and P-Ma crosslinking hydrogels. A) Image of the printed fluorescent scaffold during the printing process. B) Image of the printed fluorescent scaffold immediately after printing. C) Image of printed fluorescent scaffold with irradiation at 488 nm. D) Image of printed fluorescent construct detached from the surface with irradiation at 488 nm after 24 h of incubation in

H₂O at 37 °C. E) Image of printed scaffold with irradiation at 488 nm after 24 h incubation in H₂O at 37 °C.

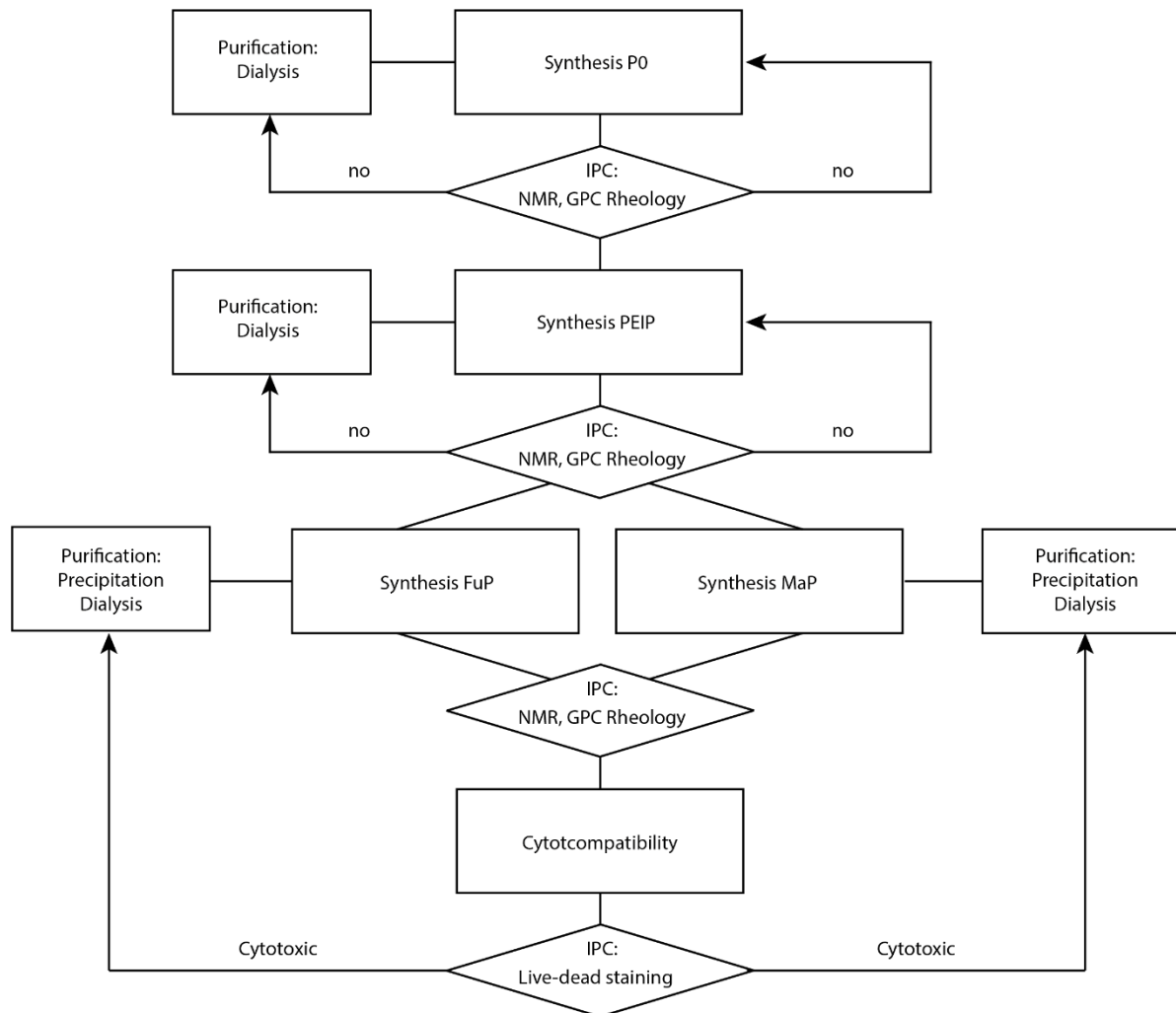


Figure S8. Workflow and process control of bioink development.

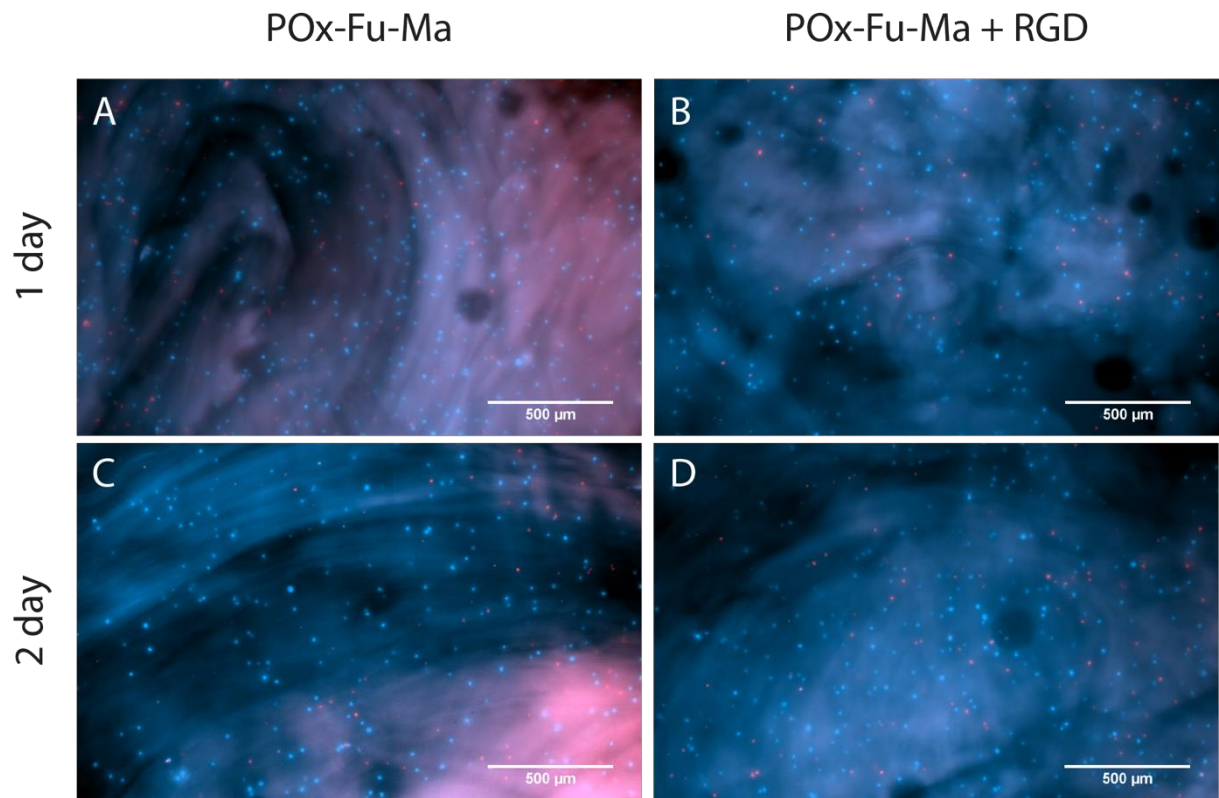


Figure S9. Bioprinting of fibroblasts in P-Fu-P-Ma-hydrogels. Z-stack of the POx-based hydrogels (20 wt%) with (B and D) and without RGD-peptide (A and C) with NIH3T3 cells incorporated, printed and cultivated for 1 or 2 days.

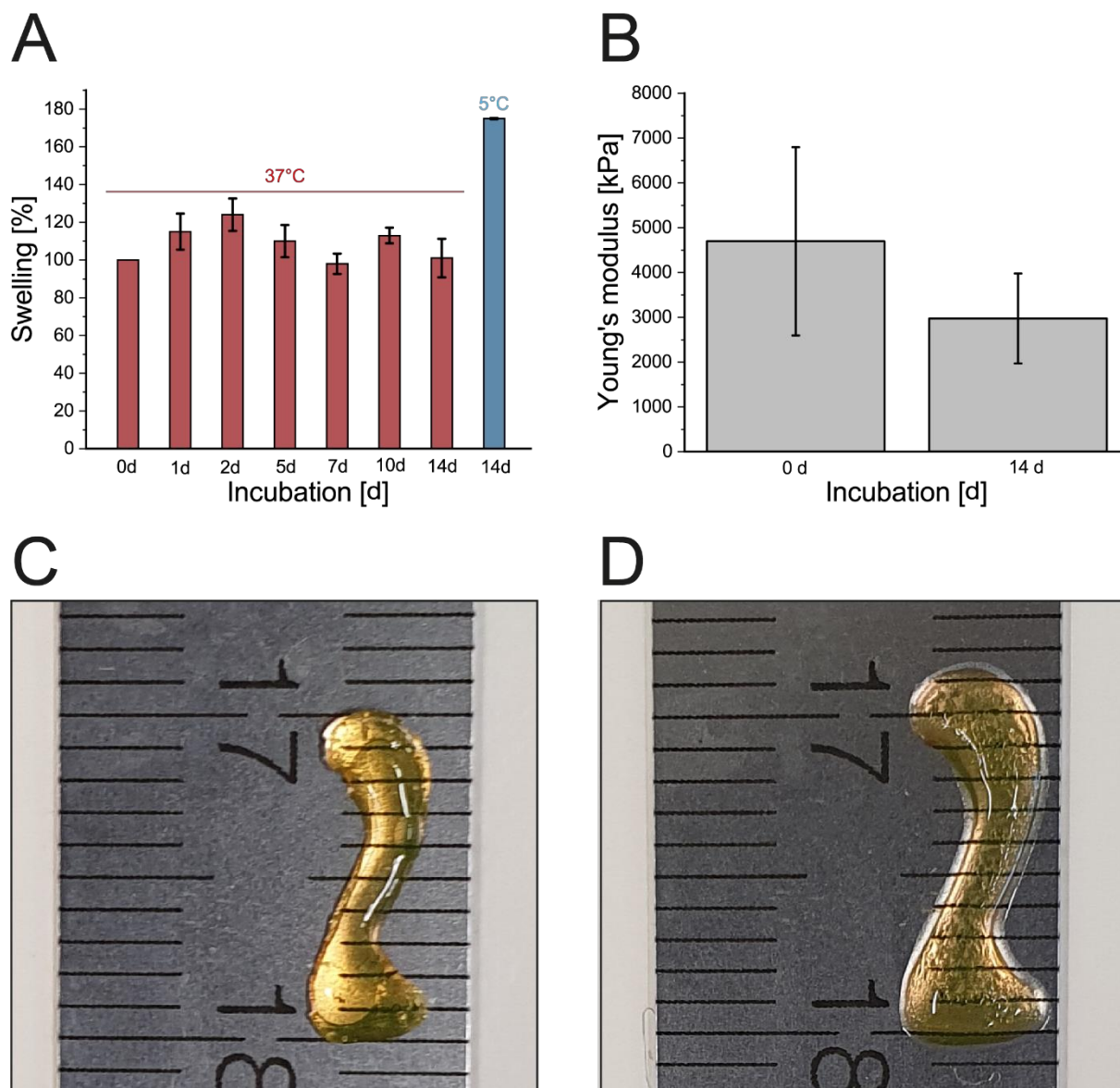


Figure S10. Swelling behaviour and mechanical testing of P-Fu/P-Ma hydrogels. A) Swelling study for 14 days at 37 °C. At day 14 the thermoresponsive character of the poly(2-*n*-propyl-2-oxazine) block was demonstrated by an increased swelling at 5 °C. B) Elastic modulus of the hydrogels after crosslinking and incubation for 14 days at 37 °C. C) Image of printed number after incubation in ddH₂O for 24 h at 37 °C. D) Image of printed number after incubation in ddH₂O for 24 h at 4 °C.

References

1. Hahn, L., et al., *Inverse Thermogelation of Aqueous Triblock Copolymer Solutions into Macroporous Shear-Thinning 3D Printable Inks*. ACS Appl Mater Interfaces, 2020. **12**(11): p. 12445-12456.
2. Lorson, T., et al., *A Thermogelling Supramolecular Hydrogel with Sponge-Like Morphology as a Cytocompatible Bioink*. Biomacromolecules, 2017. **18**(7): p. 2161-2171.
3. Nahm, D., et al., *A versatile biomaterial ink platform for the melt electrowriting of chemically-crosslinked hydrogels*. Materials Horizons, 2020. **7**(3): p. 928-933.
4. Chujo, Y., K. Sada, and T. Saegusa, *Reversible gelation of polyoxazoline by means of Diels-Alder reaction*. Macromolecules, 1990. **23**(10): p. 2636-2641.

5. Chapter 2: Merging Bioresponsive Release of Insulin-like Growth Factor I with 3D Printable Thermogelling Hydrogels

Matthias Beudert^{†1}, Lukas Hahn^{1,2}, Anselm H.C. Horn^{3,4}, Niklas Hauptstein¹, Heinrich Sticht^{3,4}, Lorenz Meinel^{1,5}, Robert Luxenhofer^{2,6}, Marcus Gutmann^{*1}, Tessa Lühmann^{*1}

¹Institute of Pharmacy and Food Chemistry, Julius-Maximilians-University Würzburg, Am Hubland, 97074 Würzburg, Germany

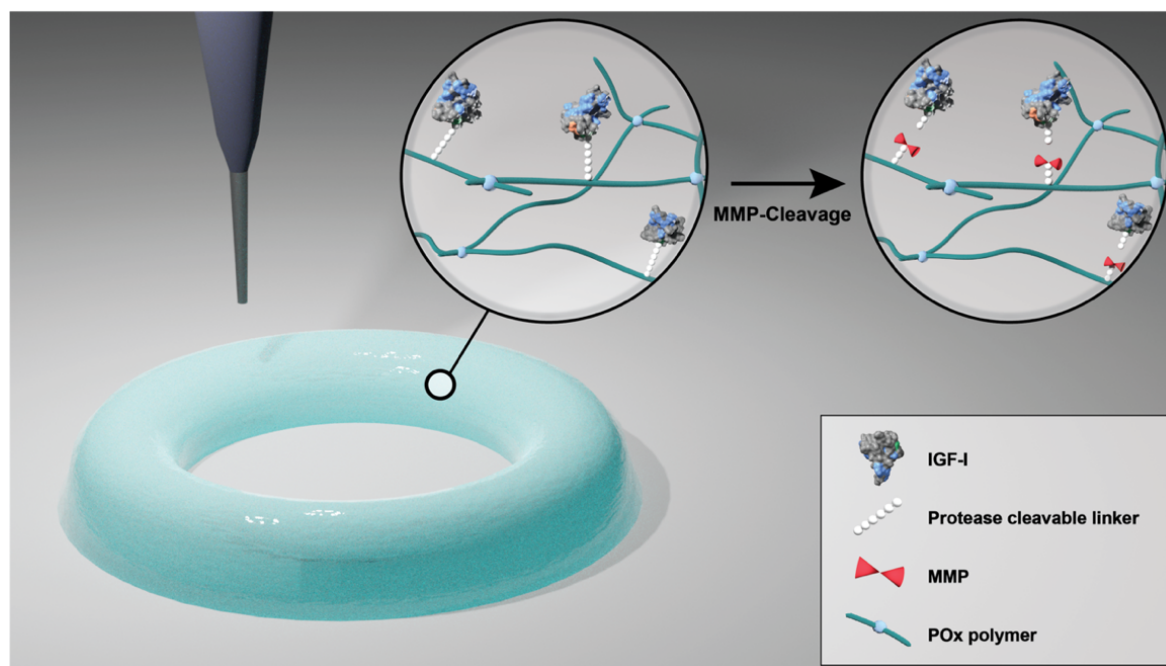
²Functional Polymer Materials, Chair for Advanced Materials Synthesis, Institute for Functional Materials and Biofabrication, Department of Chemistry and Pharmacy and Bavarian Polymer Institute, Julius-Maximilians-University Würzburg, Röntgenring 11, 97070 Würzburg, Germany

³Bioinformatics, Institute of Biochemistry, Friedrich-Alexander-Universität Erlangen-Nürnberg, Fahrstraße 17, DE-91054 Erlangen, Germany

⁴Erlangen National High Performance Computing Center (NHR@FAU), Friedrich-Alexander-University Erlangen-Nürnberg, Martensstraße 1, DE-91058 Erlangen, Germany

⁵Helmholtz Institute for RNA-based Infection Research, Josef-Schneider-Straße 2, DE-97080 Würzburg, Germany

⁶Soft Matter Chemistry, Department of Chemistry and Helsinki Institute of Sustainability Science, Faculty of Science, University of Helsinki, P.O. Box 55, FIN-00014, Helsinki, Finland



This article was published in *Journal of Controlled Release*, vol. 347, Beudert, M.; Hahn, L.; Horn, A. H. C.; Hauptstein, N.; Sticht, H.; Meinel, L.; Luxenhofer, R.; Gutmann, M.; Lühmann, T., Merging bioresponsive release of insulin-like growth factor I with 3D printable thermogelling hydrogels, pp. 115-126, Copyright © Elsevier (2022).



Contents lists available at ScienceDirect

Journal of Controlled Release

journal homepage: www.elsevier.com/locate/jconrel

Merging bioresponsive release of insulin-like growth factor I with 3D printable thermogelling hydrogels

Matthias Beudert^a, Lukas Hahn^{a,b}, Anselm H.C. Horn^{c,d}, Niklas Hauptstein^a, Heinrich Sticht^{c,d}, Lorenz Meinel^{a,e}, Robert Luxenhofer^{b,f}, Marcus Gutmann^{a,*}, Tessa Lühmann^{a,*}

^a Institute for Pharmacy and Food Chemistry, University of Würzburg, DE-97074 Würzburg, Germany

^b Functional Polymer Materials, Chair for Advanced Materials Synthesis, Institute for Functional Materials and Biofabrication, Department of Chemistry and Pharmacy, Julius-Maximilians-University Würzburg, Röntgenring 11, DE-97070 Würzburg, Germany

^c Bioinformatics, Institute of Biochemistry, Friedrich-Alexander-Universität Erlangen-Nürnberg, Fahrstraße 17, DE-91054 Erlangen, Germany

^d Erlangen National High Performance Computing Center (NHR@FAU), Friedrich-Alexander-Universität Erlangen-Nürnberg, Martensstraße 1, DE-91058 Erlangen, Germany

^e Helmholtz Institute for RNA-based Infection Research, Josef-Schneider-Straße 2, DE-97080 Würzburg, Germany

^f Soft Matter Chemistry, Department of Chemistry and Helsinki Institute of Sustainability Science, Faculty of Science, University of Helsinki, P.O. Box 55, 00014 Helsinki, Finland

ARTICLE INFO

Keywords:

Matrix metalloproteinase
IGF-I
POx
Poly(2-methyl-2-oxazoline)-b-poly(2-propyl-2-oxazoline)
Biofabrication
3D printing
Transglutaminase

ABSTRACT

3D printing of biomaterials enables spatial control of drug incorporation during automated manufacturing. This study links bioresponsive release of the anabolic biologic, insulin-like growth factor-I (IGF-I) in response to matrix metalloproteinases (MMP) to 3D printing using the block copolymer of poly(2-methyl-2-oxazoline) and thermoresponsive poly(2-n-propyl-2-oxazine) (POx-b-POzi). For that, a chemo-enzymatic synthesis was deployed, ligating IGF-I enzymatically to a protease sensitive linker (PSL), which was conjugated to a POx-b-POzi copolymer. The product was blended with the plain thermogelling POx-b-POzi hydrogel. MMP exposure of the resulting hydrogel triggered bioactive IGF-I release. The bioresponsive IGF-I containing POx-b-POzi hydrogel system was further detailed for shape control and localized incorporation of IGF-I via extrusion 3D printing for future applications in biomedicine and biofabrication.

1. Introduction

3D printing holds the potential of spatial arrangement of biomaterials, living cells, and drug molecules, enabled by automated manufacturing procedures [1]. Thereby, the modulation of the spatial distribution or separation of drug molecules in line with their release kinetics may yield into individualized constructs for biomedical application [2]. One key component for 3D bioprinting is the biomaterial based bioink. Biomaterial inks are composed of hydrogels/polymers that may contain further biologically active additives while bioinks are defined by the incorporation of cells to the formulation [3]. Often, these inks are handled as sol before and are crosslinked immediately during the printing process [3,4]. This can be achieved via chemical cross-linking of complementary functional groups, ionic crosslinking or after being exposed to an external impulse like UV-light for photopolymerization, among others [5–8]. Alternatively, highly shear-

thinning hydrogels can liquify during the printing process and solidify immediately after exiting the nozzle. As UV radiation during cross-linking may influence drug stability and biocompatibility [8,9], responsive polymers (e.g. pH-sensitive, temperature-sensitive, ion-sensitive) have been brought lately to the spotlight [10,11]. Especially thermogelling and shear-thinning hydrogels have gained attention due to their thermoresponsive properties as bioink material [12,13]. This type of hydrogel may be a sol at a certain temperature and gels at another. Typically, formation of a hydrogel occurs by physical interaction. Besides biological thermogelling polymers including methylcellulose [14] or agarose [15], synthetic polymers show thermoresponsive behavior with several advantages over natural polymers such as high versatility in chemical functionalization, rapid gelation and comparably easy modification of gelling behavior [16,17]. Among synthetic thermogels, block copolymers and in particular poloxamers (in particular Pluronic® F127) are established systems [18–21]. An alternative class of

* Corresponding authors.

E-mail addresses: marcus.gutmann@uni-wuerzburg.de (M. Gutmann), tessa.luehmann@uni-wuerzburg.de (T. Lühmann).

<https://doi.org/10.1016/j.jconrel.2022.04.028>

Received 30 November 2021; Received in revised form 31 March 2022; Accepted 16 April 2022

Available online 6 May 2022

0168-3659/© 2022 Elsevier B.V. All rights reserved.

thermoresponsive polymers that has been intensively studied is based on poly(2-substituted-2-oxazoline)s (POx) and more recently also poly(2-substituted-5,6-dihydro-4H-1,3-oxazine)s (poly(2-oxazine)s (POzi) [22–25]. These two closely related polymer families have previously been used as non-fouling materials and for drug formulations with good cytocompatibility [25–31]. Some members of this family have shown excellent biocompatibility in several species, including one particular POx-drug conjugate that already has advanced into clinical trials [32,33]. Furthermore, amphiphilic poly(2-oxazolines) are able to improve cellular and neuronal uptake of conjugated proteins [34,35]. Besides several inverse thermogelling hydrogels [36], an AB-type diblock copolymer consisting of a hydrophilic poly(2-methyl-2-oxazoline) A block and a thermo-responsive poly(2-*n*-propyl-2-oxazine) (*n*PrOzi) B block showed physical thermogelling at room temperature. Moreover, this POx-*b*-POzi based hydrogel displayed rapid and complete recovery after application of shear stress rendering it a promising material for biofabrication [37]. We recently showed that introduction of different chemical functionalities (furan-, maleimide-moieties) to POx-*b*-POzi allowed for defined chemical functionalization without affecting the rheological properties before and during the printing process, enabling chemical crosslinking via Diels-Alder chemistry thereafter [38].

The addition of recombinant therapeutic proteins and peptides into biomaterial- and bioinks becomes more and more important for therapeutic use [39]. Up to date, model proteins and growth factors have been physically loaded into printable hydrogel systems with the aim to direct cellular function with sustained drug release profiles [40,41]. In order to link drug release to disease patterns, collagenases such as matrix metalloproteinases (MMPs) are frequently used [42,43]. We recently showed that a bioconjugate of IGF-I and polyethylene glycol (PEG) linked by a protease sensitive linker (PSL) was effective in releasing IGF-I in response to MMPs [44–46].

IGF-I (7.5 kDa) [47] is therapeutically used for the treatment of dwarfism [48–50]. In tissue injury, locally synthesized IGF-I critically impacts trophic tissue repair [51,52]. IGF-I plays a critical role in a number of biological processes, including proliferation and protection against apoptosis, which positively influences tissue growth, repair and regeneration of many cell types [53–55]. Despite its outstanding effects, adequate therapies with IGF-I remain difficult due to its short half-life and potential side effects after systemic administration (mainly hypoglycaemia) [48–50,56,57], which has sparked interest in local depot/administration and controlled release systems to overcome these limitations [58–65].

In this study, we synthesized a novel copolymer POx-*b*-POzi-DBCO for modification of IGF-I using enzymatic and bioorthogonal bioconjugation strategies. The IGF-I bioconjugate was designed for physical incorporation into the thermogelling POx-*b*-POzi hydrogel system without changing its physicochemical properties during bioprinting and for bioresponsive release of IGF-I in response to MMP. By combination of the bioconjugate with the thermogelling POx-*b*-POzi hydrogel system, a 3D-printable construct with spatial control of IGF-I function was achieved, which preserved IGF-I activity as prerequisite for future biomedical applications.

2. Materials and methods

2.1. Materials

All substances and reagents for the monomer and polymer synthesis were purchased from Sigma-Aldrich (Steinheim, Germany) and were used as received unless otherwise stated. Deuterated solvents for NMR analysis were obtained from Deutero GmbH (Kastellaun, Germany). For polymerization, methyl trifluoromethylsulfonate (MeOTf), 2-methyl-2-oxazoline (MeOx) and 2-*n*-propyl-2-oxazine (*n*PrOzi) were refluxed over CaH₂ for several hours and distilled prior to usage. The solvent benzonitrile (PhCN) was dried over phosphorus pentoxide.

The monomers MeOx and *n*PrOzi were synthesized by the Witte and Seeliger [66] method like described several times [36,67].

Recombinant human insulin-like growth factor I (IGF-I; Mecermin; Increlex®) was purchased from Ipsen Group (Paris, France). Fibrogammin® was purchased from CSL Behring (Marburg, Germany). Protected L-amino acids used for peptide synthesis as well as acetonitrile (HPLC grade), trifluoroacetic acid (HPLC grade) were purchased from VWR (Ismaning, Germany). Fmoc-PEG(3)-COOH, Fmoc-PEG(6)-COOH, Fmoc-L-Azidohomoalanine as well as Fmoc-Rink-Amide Resin were obtained from Iris Biotech GmbH (Marktredwitz, Germany). Human neutrophil matrix metalloproteinase 9 (MMP-9) was purchased from Merck KGaA (Darmstadt, Germany). Quantikine® ELISA Human IGF1/IGF-1 was from R&D Systems (Abingdon, England) Tissue culture polystyrene (TCPS) cell culture flasks (75 cm²) were from Nunc (Thermo Fisher Scientific, Schwerte, Germany) and 96 well plates from Greiner Bio One (Frickenhausen, Germany). WST-1 was purchased from Roche (Basel, Switzerland). Fetal bovine serum (FBS) was from Gibco (Darmstadt, Germany). Penicillin G and streptomycin solution was purchased from Biochrom AG (Berlin, Germany). Dulbecco Modified Eagle Medium was from Sigma-Aldrich (Steinheim, Germany). All other chemicals used were at least of pharmaceutical grade. Phospho-p44/42 MAPK (Erk1/2) (Thr202/Tyr204) Antibody #9101, p44/42 MAPK (Erk1/2) Antibody #9102, Phospho-Akt (Ser473) (D9E) XP® Rabbit mAb #4060, Akt (pan) (C67E7) Rabbit mAb #4691 and Anti-rabbit IgG, HRP-linked Antibody #7074 were from Cell Signaling (Hitchin, UK).

2.2. Polymer synthesis

The AB diblock copolymer Me-(poly-*n*PrOzi)₅₀-*b*-(poly-MeOx)₅₀-DBCO (POx-*b*-POzi-DBCO) was synthesized using a general procedure based on previous reports (Fig. S2 A) [37]. In brief, under dry and inert conditions, 11 mg (0.07 mmol, 1 eq.) of MeOTf and 440 mg (3.46 mmol, 49 eq.) of *n*PrOzi were added to 1.5 mL of PhCN and stirred for 4 h at 130 °C. Full monomer conversion was monitored by ¹H NMR spectroscopy. The second block 300 mg MeOx (3.52 mmol, 50 eq.) was added, and the reaction mixture was stirred for 2 h at 110 °C. After completion of the second block, termination was carried out overnight using 93 mg of 11,12-Didehydro- ϵ -oxodibenz[*b,f*]azocine-5(6H)-hexanoic acid (DBCO-acid) (0.28 mmol, 4 eq.) and 36 mg of dried diisopropylethylamine (0.28 mmol, 4 eq.) at 60 °C. The reaction mixture was poured into ice-cold diethyl ether. The precipitate was dissolved in deionized water, dialyzed overnight using a regenerated cellulose membrane with a MWCO of 1 kDa, and freeze dried (yield: 51.4%, 400 mg, 0.036 mmol). The polymer structure was confirmed using ¹H NMR end group analysis (Fig. S2 C, D). The number average molar mass M_n and the dispersity \bar{D} were determined via GPC analysis (Fig. S2 B). A reasonably narrow molar mass size distribution and an increase of the number average molar mass during the polymerization reaction (M_n (1st block): 2.3 kg/mol, \bar{D} (1st block): 1.25; M_n (2nd block): 3.8 kg/mol, \bar{D} (2nd block): 1.30; M_n (purified polymer): 4.6 kg/mol, \bar{D} (purified polymer): 1.36), indicative of the living polymerization, was confirmed. Please note, absolute values for M_n were not accessible via GPC due to the used calibration.

2.3. Nuclear magnetic resonance (NMR)

NMR was performed on a Bruker Fourier 300 (¹H: 300.12 MHz) spectrometer at 298 K from Bruker BioSpin (Rheinstetten, Germany) and calibrated using the solvent signals.

2.4. Gel permeation chromatography (GPC)

GPC experiments were performed on a Polymer Standard Service PSS (Mainz, Germany) system with following specifications: pump mod. 1260 infinity, MDS RI-detector mod. 1260 infinity (Agilent Technologies, Santa Clara, California, USA), precolumn: 50 × 8 mm PSS PFG

linear M; 2 columns: 300 × 8 mm PSS PFG linear M (particle size 7 µm; pore size 0.1–1.000 kg/mol) with hexafluoroisopropanol (HFIP, containing 3 g/L potassium trifluoroacetate (KTFA)) as eluent calibrated against PEG standards with molar masses from 0.1 kg/mol to 1000 kg/mol. The columns were held at 40 °C and the flow rate was set to 0.7 mL/min. Prior to each measurement, samples were dissolved in eluent and filtered through 0.2 µm PTFE filters (Rotilabo, Karlsruhe, Germany) to remove particles, if any.

2.5. Peptide synthesis and purification of the protease-sensitive linker (PSL)

The protease-sensitive linker (PSL) with the sequence Ac-GNQEQVSP-PEG(3)-GPQGIAGQ-PEG(6)-A(N₃) was synthesized by solid-phase fmoc-peptide synthesis using a microwave peptide synthesizer (Initiator+, Biotage, USA). Shortly, fmoc-rink-amid resin was loaded into a 15 mL reaction vessel with a glass frit in the bottom. Deprotection was done using 10% piperidine in DMF (v/v) at 75 °C for 3 min. Subsequently, a 5-fold molar excess of the amino acid compared to the functional group was dissolved in DMF and mixed with 0.5 M 1-hydroxybenzotriazole (HOBt) (v/v) as well as diisopropylethylamine (DIPEA) and N,N'-diisopropylcarbodiimid (DIC). Coupling was performed for 3 h at 25 °C. After cleavage from the resin using 92,5% trifluoroacetic acid (TFA), 2,5% H₂O, 2,5% 3,6-dioxa-1,8-octanedithiol (DOT) and 2,5% triisopropylsilane (TIPS), the peptide was purified by reversed-phase chromatography using an FPLC system (GE Healthcare Äkta Explorer, Life sciences, Freiburg, Germany) with a Luna C18 100A column (21.2 mm × 250 mm, Phenomenex Inc., Torrance, CA). Successful peptide synthesis was analyzed using high performance liquid chromatography (HPLC) and liquid chromatography-mass spectrometry (LC-MS).

2.6. Liquid chromatography-mass spectrometry (LC-MS)

Successful synthesis of PSL was determined using a LC-MS system (Shimadzu, Duisburg, Germany) equipped with a DGU-20A3R degassing unit, an LC-20AB liquid chromatograph, a SPD-20A UV/Vis detector. UV-spectra were monitored at 214 nm and mass spectra were recorded with an LCMS-2020 device (Shimadzu, Duisburg, Germany) [68]. A Synergi 4 µm fusion-RP column (140 × 4.6 mm) (Phenomenex Inc., Torrance, CA) was utilized as stationary phase with a gradient of Eluant A (water, 0.1% formic acid (v/v)) and Eluent B (methanol, 0.1% formic acid (v/v)) as mobile phase. Gradient: 5 to 90% of eluent B in 8 min followed by 5 min of 90% Eluent B; 90 to 5% eluent B in 5 min with subsequent equilibration of the column with 5% of eluent B (4 min). Peptides were detected in a range from 500 to 2000 (m/z). Electrospray ionization (ESI) spectra were measured with a microTOF-focus at a capillary temperature of 210 °C and 3.5 kV voltage with the carrier gas N₂.

2.7. Matrix-assisted laser desorption/ionization (MALDI)

A solution of 20 µL (1 mg/mL) of the sample protein was desalted using Zip Tip® C 18 resin (Merck Millipore, Billerica, USA) following manufacturer instructions. One µL of the desalted protein was emended in a matrix, consisting of 3,5-Dimethoxy-4-hydroxycinnamic acid in TA-solvent (30:70 (v/v) acetonitrile (ACN)/0.1% trifluoroacetic acid (TFA) in water). MALDI mass spectra were acquired in the linear positive mode with a 337 nm nitrogen laser using an Autoflex II LFR instrument (Bruker Daltonics Inc., Billerica, USA). Protein Standard I (Bruker Daltonics Inc., Billerica, USA) was used for calibration. Theoretical masses of proteins were calculated (https://web.expasy.org/peptide_mass/).

2.8. Coupling of PSL-peptide with IGF-I

Factor XIIIa (FXIIIa, 250 U/mL, Fibrogammin®, CSL Behring) was

activated according to the manufacturer's protocol and stored at –80 °C until further use.

Recombinant human IGF-I (Increlex®, Ipsen Pharma GmbH) was purified by cation-exchange chromatography (CIEX) using an FPLC system (GE Healthcare Äkta Explorer, Life sciences, Freiburg, Germany) with a HiTrap SP-HP column (Cytiva, Freiburg, Germany). After buffer exchange (10 mM Tris/HCL, 150 mM NaCl, 2.5 mM CaCl₂, pH 7.6) IGF-I was incubated with 5-fold molar excess of PSL and 10 U/mL FXIIIa at 37 °C for 20 min. The reaction was monitored over the course of time using HPLC with a Zorbax® 300SB-CN (4.6 × 150 mm) column. Samples were taken at different time points and the reaction was stopped by the addition of EDTA (10 mM). The protein-peptide conjugate was purified using CIEX using an FPLC system (GE Healthcare Äkta Explorer, Life sciences, Freiburg, Germany) with a HiTrap SP-HP column (Cytiva, Freiburg, Germany) and the reaction products were analyzed using SDS-PAGE.

2.9. Site-specific conjugation with POx-b-POzi -DBCO

Purified IGF-PSL construct was dialyzed against PBS, mixed with 20-fold molar excess of POx-b-POzi-DBCO at pH 7.4 and incubated for 72 h at 4 °C while stirring gently. IGF-PSL-POx-b-POzi was purified using purified by CIEX using an FPLC system (GE Healthcare Äkta Explorer, Life sciences, Freiburg, Germany) with a HiTrap SP-HP column (Cytiva, Freiburg, Germany). The polymer conjugate was eluted with 50 mM sodium acetate, 1 M NaCl buffer at pH 4.3. Successful coupling was verified by SDS-PAGE as well as western blot. The concentration of the purified construct was determined by BCA protein assay and was stored at –20 °C until further use.

2.10. Cleavage of IGF-PSL-POx-b-POzi by MMP-9

Pro-MMP-9 was activated with 4-aminophenylmercuric acetate (APMA) according to manufacturer's instructions. IGF-PSL-POx-b-POzi was dialyzed against MMP-buffer (50 mM Tris, 150 mM NaCl, 1 µM ZnCl₂, 10 mM CaCl₂, 0.05% Brij 35, pH 6.8) and 3 µg of the conjugate were incubated with 8 nM of MMP-9 at 37 °C and 450 rpm. After different time points, samples were taken, and protease activity was stopped by the addition of 50 mM EDTA and heating at 95 °C for 10 min. The cleavage of IGF-PSL-POx-b-POzi over time was monitored using HPLC with a Zorbax® 300SB-CN (4.6 × 150 mm) column. Samples were analyzed after 0, 2, 6, and 24 h of exposure to MMP-9, respectively.

2.11. SDS-PAGE

Purified proteins and conjugates were analyzed using Tris-glycine SDS-PAGE as described before [58]. Gels were stained with Coomassie Brilliant Blue G250 Merck KGaA (Darmstadt, Germany) and documented using FluorChem FC2 imaging system (Protein Simple, Santa Clara, USA).

2.12. pAKT/AKT and pERK/ERK signaling

Extracellular signaling of IGF-I variants in respect to human IGF-I was conducted by pAKT/AKT and pERK/ERK assay. C2C12 myoblasts were seeded in a 96-well plate (1 × 10³ cells/mL, 125 µL per well) in growth medium overnight at 37 °C under 5% CO₂. The medium was changed to assay medium (DMEM high-glucose 0.5% FCS, 100 U/mL penicillin G and 100 µg/mL streptomycin) and cells were grown for 24 h. Cells were stimulated with a dilution series of each IGF-I variant as well as IGF-I ranging from 0.02 to 200 nM and incubated for 30 min at 37 °C. After stimulation, the cells were placed on ice, washed with ice cold PBS and proteins were extracted using mammalian extraction buffer (M-PER™ Mammalian Protein Extraction Reagent, Thermo Scientific). After extraction, proteins were immediately shock frozen using liquid nitrogen. The concentration of each condition was determined by

BCA assay following manufacturer instructions. 1 µg total protein of each condition was loaded on a 12% SDS-Page gel and processed using standard SDS-PAGE and Western blotting procedures. Prior to phosphorylated AKT/ERK analysis, Ponceau red staining was performed. For detection of phosphorylated AKT, a Phospho-Akt (Ser473) (D9E) XP® Rabbit mAb (1:1000) in Tris buffered saline (TBS), containing 0.1% (w/w) Tween-20 (TBST) and for phosphorylated ERK, a Phospho-p44/42 MAPK (Erk1/2) (Thr202/Tyr204) antibody was used overnight at 4 °C, respectively. After incubation with the first antibody, the blot was washed and incubated with an Anti-rabbit IgG, HRP-linked Antibody (1:2000 in TBST). Signals were detected using SuperSignal™ West Pico PLUS Chemiluminescent Substrate and were subsequently monitored by a FluorChem FC 2 imaging system (Protein Simple, Santa Clara, USA). After detection of the phosphorylated AKT/ERK, the blot was stripped with 2-Mercaptoethanol-Buffer (50 mM Tris-HCl, 2% (w/w) SDS and 0.8% 2-mercaptoethanol-buffer, pH 6.8) for 45 min at 56 °C and was washed under rinsing water for 1 h. For the detection of AKT, an Akt (pan) (C67E7) Rabbit mAb (1:1000 in TBST) and for the detection of ERK a p44/42 MAPK (Erk1/2) antibody as well as Anti-rabbit IgG (1:2000 in TBST), HRP-linked antibody was used with identical steps, respectively.

2.13. Cell culture

Immortalized mouse myoblast C2C12 cells (ATCC CRL-1772) were cultured in growth medium (DMEM high-glucose 10% FCS, 100 U/mL penicillin G and 100 µg/mL streptomycin) on 75 cm² culture flasks at 37 °C and 5% CO₂.

2.14. WST-1 proliferation assay

Bioactivity of IGF-I variants compared to human IGF-I was conducted by formazan assay. In brief, C2C12 myoblasts were seeded in a 96-well plate (2 × 10³ cells/mL, 125 µL per well) in growth medium overnight at 37 °C under 5% CO₂. The medium was changed to assay medium (DMEM high-glucose 0.5% FCS, 100 U/mL penicillin G and 100 µg/mL streptomycin) and cells were grown for 24 h. Dilution series of each IGF-I variant as well as IGF-I ranging from 0.01 nmol to 200 nmol were prepared in assay medium and added (1:1 (v/v)) to the cells. Cells were stimulated for 24 h at 37 °C and 5% CO₂. After stimulation, 10 µL WST-1 reagent were added to each well and cells were incubated for 4 h at 37 °C according to manufacturer instructions. Every 30 min, cells were analyzed and the absorbance of the soluble formazan product at 450 nm as well as background noise at 630 nm were determined using an Infinite 200Pro (Tecan, Männedorf, Switzerland).

2.15. Bioresponsive release from POx hydrogels

25 wt% solutions of P(MeOx_{90-co}-Fu₁₀)-b-PnPrOzi₁₀₀ (P-Fu) and P(MeOx_{90-co}-Ma₁₀)-b-PnPrOzi₁₀₀ (P-Ma) were prepared in MMP-buffer (50 mM Tris, 150 mM NaCl, 1 µM ZnCl₂, 10 mM CaCl₂, pH 7.4) at 4 °C. P-Fu and P-Ma were mixed in ratio of 1:4 (P-Fu:P-Ma) and IGF or IGF-PSL-POx-b-POzi (final concentration 10 µg/mL) were added to the mixture. 20 µL gels were casted in 96 well plate. After 45 min of incubation at 37 °C the hydrogels were overlaid with 180 µL MMP-buffer. MMP-9 was added to a final concentration of 8 nm. Gels were incubated at 37 °C and 100 rpm. Samples were taken after 0, 2, 4 and 6 h and instantly frozen in liquid nitrogen. The release of IGF-I as well as its bioactivity were monitored using WST-1 proliferation assay.

2.16. Enzyme-linked immunosorbent assay (ELISA)

IGF-I (Increlex®) and IGF-PSL-POx-b-POzi were analyzed using standard sandwich ELISA, following manufacturer's instructions. In brief, IGF-I and IGF-PSL-POx-b-POzi were diluted in Calibrator RD5–18 ranging from 40 ng/mL to 0.125 ng/mL, respectively. The microplate

was washed initially as well as after each following step with 300 µL Assay Diluent RD1–99 and incubated for 3 h at 4 °C. 200 µL Human IGF-I conjugate was added to each well for 1 h at room temperature. For detection, 200 µL Substrate AB solution was added to each well and incubated for 30 min. The reaction was stopped by adding 50 µL Stop Solution and absorption was measured at 450 nm and 630 nm with a microplate reader (Infinite® F200, Tecan, Meannedorf, Switzerland), respectively.

2.17. NHS-labelling

IGF-PSL-POx-b-POzi was incubated with a 20-fold molar excess of Atto 488-NHS-ester (Sigma-Aldrich, Steinheim, Germany) in bicarbonate buffer (100 mM) for at least 1 h. Unattached Atto 488-NHS-ester was removed from the solution via spin column (Vivaspin™, Sartorius, Göttingen, Germany).

2.18. Rheology

Experiments were performed on an Anton Paar (Ostfildern, Germany) Physica MCR302, equipped with peltier elements (P-PTD200/Air & H-PTD200) and a solvent trap as described previously [69]. Briefly, the pre-cooled samples (final polymer concentration: 25 wt%; IGF-PSL-POx-b-POzi: 25 µg/mL) were placed on the cooled rheometer (5 °C). First, to simulate the printing workflow, G' and G'' were recorded for 10 min at 5 °C and a fixed amplitude of 0.5% and angular frequency of 10 rad/s. Subsequently, a temperature sweep from 5 to 37 °C was conducted. The crosslinking kinetics were monitored for 2 h at 37 °C (angular frequency: 10 rad/s, amplitude: 0.5%). To highlight the covalent crosslinks further experiments were performed. After crosslinking for several minutes at 37 °C the crosslinked samples were cooled to 5 °C recording G' and G''. In the end, experiments were performed to evaluate all aspects of the printing process:

- 1) Sample equilibration (5 °C, shear rate: 0.01 1/s, 1 min)
- 2) Temperature sweep (5 °C - 37 °C, shear rate: 0.01 1/s, 0.1 °C/s, approx. 5 min)
- 3) Shear response (37 °C, shear rate: 0.01–100 1/s)
- 4) Recovery and crosslinking (37 °C, shear rate: 0.01 1/s)

2.19. Circular dichroism (CD) spectroscopy

Samples were dialyzed against 10 mM NaOAc (pH 4.3), or 20 mM NaH₂PO₄ (pH 7.5) for 2 days at 4 °C. The identical buffers were used for blank measurements. CD spectra were recorded at the indicated temperature in a 1 mm path length cell on a spectropolarimeter and 5 scans were averaged (J715 spectropolarimeter, equipped with a Jasco peltier element, Jasco Labor- and Datentechnik GmbH, Groß-Umstadt, Germany). The following parameters were used: 100 mdeg sensitivity, 0.1 nm step resolution, 50 nm min⁻¹ scan speed from 260 to 190 nm, 2 s time constant. Protein solutions had a concentration of 0.16–0.2 mg/mL. Heated samples were heated at a rate of 2 °C per min. Raw data were processed with Graphpad Prism 6 (GraphPad Software, La Jolla California USA, www.graphpad.com) and smoothing was performed using 10 neighbouring points on each side.

2.20. Direct ink-writing

For the printing of hydrogel scaffolds an extrusion-based bench-top 3D bioprinter (Bio X, Cellink, Sweden) was used. 25 wt% aqueous solutions of both furan- and maleimide-modified polymer were prepared and mixed at 4 °C and subsequently printed at room temperature. Both polymers were mixed in a ratio of 6:10 with respect to furan-modified polymer and transferred immediately to the nozzle. The printer was equipped with a 22 GA (Cellink, #30047) diameter precision nozzle. A pressure ranging from 120 to 180 kPa was applied and the printing

speed was set to 3 mm/s. The print bed was preheated to 40 °C. For the visualization of the printed constructs, Texas Red™ C₂ Maleimide (0.1 mg/mL) (ThermoFisher Scientific) or IGF-PSL-POx-b-POzi-Atto 488 were added to the precursor solutions to a final concentration around 23 wt% of the biomaterial ink. After printing, the constructs were incubated at 37 °C and 5% CO₂. After incubation of at least 30 min the constructs were overlaid with ddH₂O and incubated at 37 °C and 5% CO₂.

2.21. Fluorescence microscopy

Distribution of IGF-PSL-POx-b-POzi in the 3D construct after printing was analyzed using an Axio Observer.Z1 microscope equipped with an A-Plan 10×/0.25 Ph1 objective (Zeiss), 38 HE Green Fluorescent Protein ($\lambda_{\text{ex}} = 450\text{--}490\text{ nm}$ $\lambda_{\text{em}} = 500\text{--}550\text{ nm}$), 43 DsRed Reflector ($\lambda_{\text{ex}} = 538\text{--}562\text{ nm}$ $\lambda_{\text{em}} = 570\text{--}640\text{ nm}$) and a mercury vapor short-arc lamp. Image processing was performed in ImageJ (<http://imagej.nih.gov/ij/>).

2.22. Molecular dynamics simulations

Simulations started from the solution structure of IGF-I (PDB code 2GF1 [70]) with the protease sensitive linker (PSL) attached via an isopeptide bond. For the parametrization of the PEG spacers within the PSL, atomic charges were derived using the R.E.D. server [71]. The parm14SB force field [72] was used for the amino acids of PSL and IGF-I, and TIP3P [73] for water. Four starting conformations were generated: two contained the linker peptide in extended conformation and in the other two the initial linker peptide conformation was selected from a previous short MD simulation of the isolated PSL. All systems were placed in truncated octahedral water boxes containing one Na⁺ counter ion for electrical neutralization and ~ 22,000 water molecules, thus ensuring that even the most extended system was solvated with at least 12 Å distance to the border of the periodic boundary box. Simulations were performed with AMBER20 [74] using the GPU-accelerated version of pmemd [75,76] on A100 Nvidia cards. The four independent simulations (1 μs each) were run as NPT ensemble at 310 K and 1 bar with a time step of 2 fs using SHAKE to constrain hydrogen atoms [77,78],

following a previously established simulation protocol [79]. Structural analysis and visualization were done with the program VMD [80].

2.23. Statistics

All data were reported as mean \pm standard deviation unless specified otherwise. Statistical significance was calculated by Tukey's one-way analysis of variance (OriginLab, Northampton, USA; GraphPad Software, La Jolla, CA). *P*-values less than 0.05 were considered statistically significant.

3. Results and discussion

The IGF-PSL-POx-b-POzi conjugate was designed to enable physical anchoring and bioresponsive release of IGF-I by MMPs from the thermogelling POx-b-POzi hydrogel system [38]. Here, the conjugate was obtained by transglutaminase-mediated coupling of IGF-I to a PSL using lysine (K) at position 68, following published procedures (Fig. 1A, B) [46]. This approach has the advantage of controlled site-specific conjugation of IGF-I compared to unspecific chemical conjugation methods such as 1-ethyl-3-(3-dimethylaminopropyl)carbodiimide chemistry, which may impair protein's active sites, potentially affecting biological performances as well as leading to high batch to batch variations during the production process [81,82]. Furthermore, K68 is part of the D domain of IGF-I which is not involved in receptor binding and therefore does not affect the IGF-I's bioactivity (Fig. 1A) [83–85]. To this end, a transglutaminase donor peptide -NQEQVSPL-, derived from alpha-2 plasmin inhibitor (α 2PI) [86], was added at the N-terminus of the MMP-sensitive sequence (GPQGIAGQ; derived from type I collagen [87,88]) as well as an azide functionalization located at the C-terminus (Fig. 1A). Using the extended termini at the C-terminus, the PSL was coupled (1) to IGF-I via the N-terminal transglutaminase donor peptide and (2) to the polymer POx-b-POzi-DBCO via the C-terminal azide function using strain-promoted azide-alkyne cycloaddition (SPAAC).

For IGF-I bioconjugation, a POx-b-POzi-DBCO diblock copolymer

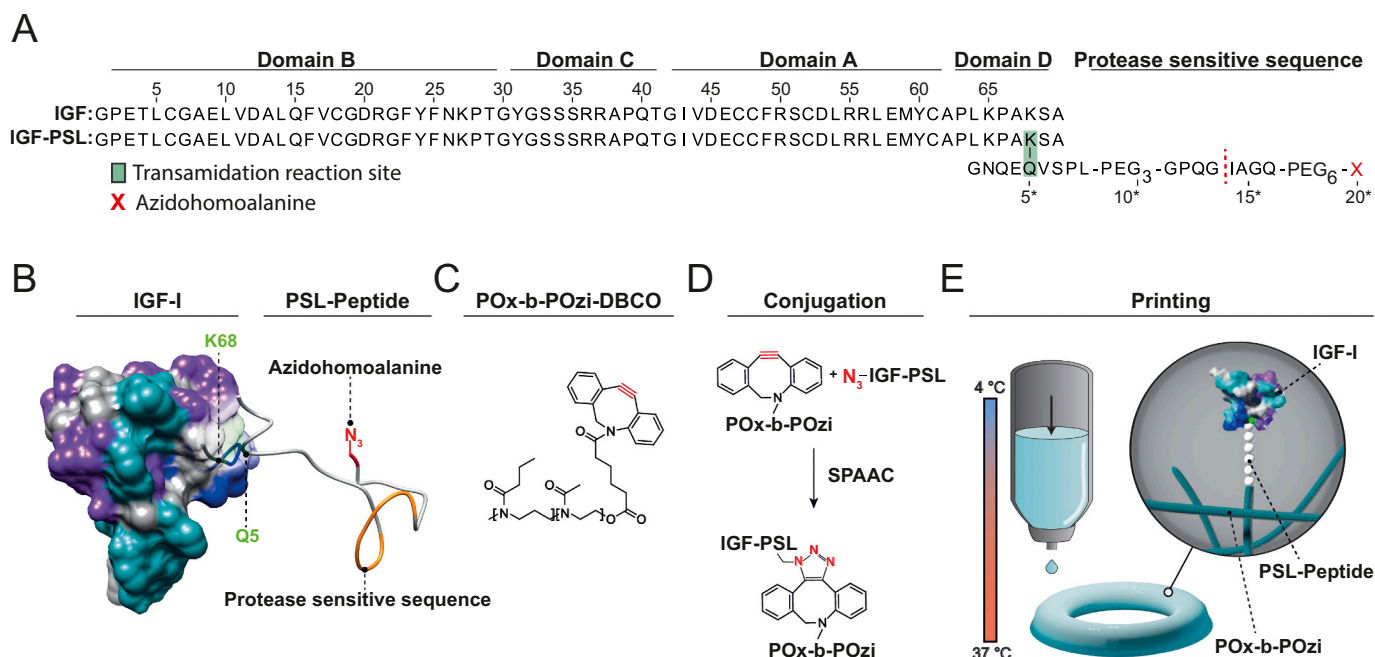


Fig. 1. Bioinspired site-directed IGF-polymer conjugation. (A) Alignment of amino acid sequence of human IGF-I and IGF-PSL. The sequence alignment was created with Jalview 2.11.1.4 [89]. (B) 3D structure of human IGF-I (PDB code 2GF1 [70]) and PSL (depicted structure is an approximation created by using Pep-Fold3 Best-Model prediction). (C) Structure of Me-PnPrOzi₅₀-b-PMeOx-DBCO (POx-b-POzi-DBCO) (D) POxylation of IGF-PSL using SPAAC. Molecular structures were created using UCSF Chimera 1.15 [90]. (E) Scheme of the printing process of IGF-PSL-POx-b-POzi.

comprising a hydrophilic PMeOx block and a thermoresponsive PnPrOzi block (POx-b-POzi) with a DBCO functionalization was developed. The design of the polymer was not intended to be used for half-life extension as frequently used for systemically applied therapeutic proteins [43,91–92] but for anchoring of IGF-I into the thermogelling POx-b-POzi hydrogel system (Fig. 1B).

Prior to the synthesis of the polymer and peptide, we used molecular dynamics (MD) simulations to assess the properties of the PSL with respect to the formation of intramolecular interactions that might hamper receptor binding. Based on four independent 1- μ s MD simulations, the interactions between the PSL and IGF-I were monitored (Fig. 2B; S1). The dynamics of simulation run 1 is available as supplementary movie (Video S1) and representative snapshots from this simulation are shown in Fig. 2A. All simulations showed that the PSL fused to the C-terminus of IGF-I is highly dynamic and only formed transient interactions. These results indicate that the IGF-PSL interaction is weak and will not critically affect receptor binding affinity.

Afterwards, the PSL-peptide was synthesized using solid-phase fmoc-peptide synthesis and analyzed by ESI-MS and RP-HPLC (Fig. S3). Assembly of the IGF-PSL construct was achieved by coupling IGF-I with PSL using the transglutaminase factor XIIIa (vide supra). The successful coupling of IGF-I and PSL was confirmed using RP-HPLC (Fig. 3A), SDS-PAGE (Fig. 3B), and MALDI-MS analysis (Fig. S4). RP-HPLC analysis revealed that the enzymatic protein-peptide conjugation is rapid with around 60% conversion after 20 min (Fig. 3C). The final IGF-PSL was purified using cation-exchange chromatography (CIEX) with a purity >95%.

The thermoresponsive polymer Me-PnPrOzi₅₀-b-PMeOx-DBCO (POx-b-POzi-DBCO; Fig. 1C, Fig. S2 A) was synthesized by living cationic ring opening polymerization. The DBCO functionality at the omega-chain-end was introduced via termination reaction of deprotonated DBCO-acid as nucleophile after complete monomer consumption. The polymerization was monitored via ¹H NMR and GPC analysis

(Fig. S2 B-D) and the polymer structure was confirmed via ¹H NMR end group analysis (Fig. S2 C, D). An increase in the number average molar mass during sequential polymerization was confirmed via GPC and the purified polymer exhibited a reasonably narrow molar mass size distribution ($\mathcal{D} = 1.36$; Fig. S2 B).

The conjugate IGF-PSL-POx-b-POzi was prepared by coupling the POx-b-POzi-DBCO to the C-terminal azide function of the PSL-peptide within the IGF-PSL sequence using SPAAC (Fig. 1D). After 48 h of incubation, IGF-PSL-POx-b-POzi was purified using CIEX leading to a protein-polymer conjugate with a purity >95% (Fig. 3 A, B).

The high coupling efficiency and the homogeneous product enabled by transglutaminase and subsequent SPAAC chemistry highlight the versatility of this approach and demonstrate that bioconjugation of IGF-I to a thermoresponsive diblock copolymer originated from POx and POzi is successful. Especially in view of the increasing interest in PEG substitutes, both POx and POzi (and their combinations) represent excellent PEG alternatives due to the high flexibility in chemical synthesis and good cytocompatibility [91].

The different conjugation steps starting with IGF-I (7.6 kDa) and resulting in IGF-PSL (10 kDa) (Fig. S4) and IGF-PSL-POx-b-POzi (25 kDa) were followed and confirmed by SDS-PAGE. Also, reversal of the POxylation via MMP-9 mediated cleavage of IGF-PSL-POx-b-POzi was successful as shown by the appearance of the band of unconjugated IGF-I (below 15 kDa) (Fig. 3B). RP-HPLC analysis showed 62% of cleaved IGF-I from IGF-PSL-POx-b-POzi over 24 h (Fig. 3D, S5). While the polymer conjugate showed a broader distribution in both RP-HPLC and SDS-PAGE, the cleaved IGF-I product displayed narrower signals, in line with the removal of the disperse polymer (Fig. 3B).

Successful cleavage of the protein-polymer conjugate IGF-PSL-POx-b-POzi was achieved at 8 nM of activated MMP-9. This MMP concentration was chosen as it represents the range of upregulated enzyme levels of proteolytically active MMP-9 during the course of inflammation in diseased tissues such as in rheumatoid arthritis [93]. Our results

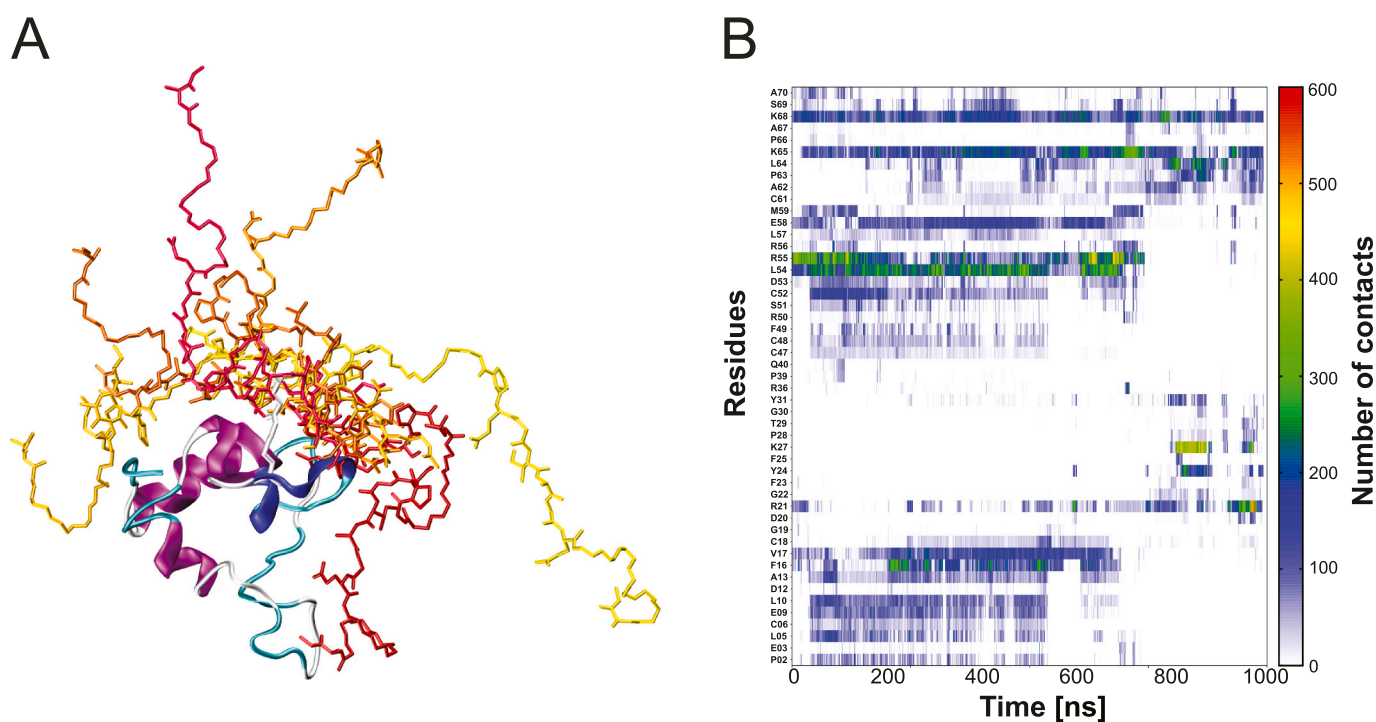


Fig. 2. Molecular dynamics simulation of IGF-PSL (A) Structure of PSL-bound IGF-I. For PSL, snapshots from different time points of the molecular dynamics simulation are overlaid. IGF-I is shown in ribbon presentation (colored according to the secondary structure) and PSL is shown in stick presentation (colors from yellow to dark red correspond to progressing time points of the simulation). (B) Number of contacts between PSL and IGF-I over the simulation time (run 1). The simulation time is shown as horizontal axis and the interacting IGF-I residues on the vertical axis. The number of IGF-PSL contacts is colour coded (see vertical scale bar on the right). (For interpretation of the references to colour in this figure legend, the reader is referred to the web version of this article.)

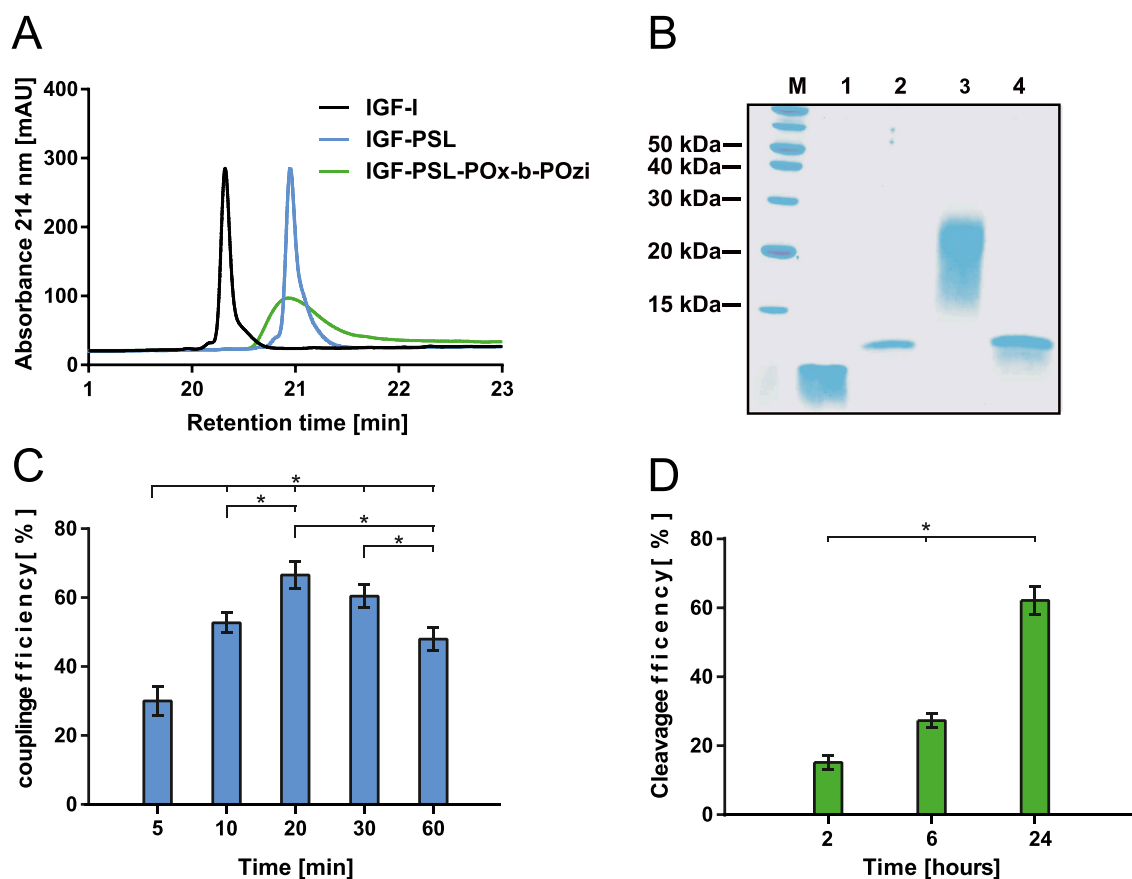


Fig. 3. Characterization of IGF-PSL-POx-b-POzi conjugate. (A) RP-HPLC analysis of IGF-I, IGF-PSL and IGF-PSL-POx-b-POzi. (B) SDS-PAGE of IGF-I (1), IGF-PSL (2), IGF-PSL-POx-b-POzi (3) and cleaved IGF-PSL-POx-b-POzi (4). (C) Efficiency of the TG-catalyzed IGF-PSL coupling. (D) Cleavage efficiency of IGF-PSL-POx-b-POzi with MMP-9. Mean \pm SD, $n \geq 5$, one-way ANOVA followed by Tukey's Multiple Comparison Test; $p \leq 0.05$ was considered statistically significant and highlighted by asterisks.

demonstrate that the integrated MMP-sensitive sequence within the IGF-PSL-POx-b-POzi is accessible for the enzyme MMP-9 and full-length IGF-I is released from its bioconjugate as previously monitored for PEGylated IGF-I [46].

CD analysis revealed that all tested proteins and conjugates remained α -helical as described before for IGF-I [94], indicating that peptide and polymer conjugation does not affect secondary structure (Fig. 4A). Moreover, enzymatic conjugation to the PSL did not alter thermal stability of IGF-I (Fig. S6).

Bioactivity of the different IGF-conjugates were analyzed by WST-1 proliferation assay (Fig. 4B, S7) and ERK and AKT phosphorylation, respectively (Fig. 4C, S8).

IGF-PSL-POx-b-POzi (EC_{50} : 4.3 nM; 95% CI: 3.5–5.1 nM) stimulated the growth of C2C12 cells as potent as the commercially available IGF-I (EC_{50} : 4.6 nM; 95% CI: 4.0–5.4 nM). The analyzed downstream signaling of ERK phosphorylation as well as AKT phosphorylation on C2C12 cells showed a concentration dependent induction of ERK and AKT phosphorylation, confirming that the receptor binding sites of IGF-I were not jeopardized during coupling of the PSL and by the amphiphilic POx-b-POzi polymer.

As POx-b-POzi-DBCO forms only transient (shear-thinning and dilution sensitive) hydrogels due to reversible physical interactions, we combined the previously described furan-modified variant (P(MeOx₉₀-co-Fu₁₀)-b-PnPrOzi₁₀₀; P-Fu) and the maleimide-modified variant (P(MeOx₉₀-co-Ma₁₀)-b-PnPrOzi₁₀₀; P-Ma) of the POx polymer (Fig. S9) for covalent cross-linking via Diels-Alder chemistry [8]. IGF-I or IGF-PSL-POx-b-POzi (25 μ g/mL) were added to the polymer solution (P-Fu/P-Ma) prior to thermogelation, followed by chemical Diels-Alder mediated cross-linking. To monitor biological performances of IGF-I and its

bioconjugate in the presence and absence of MMP-9 (8 nM), supernatant samples were collected after 2, 4, and 6 h and subsequently analyzed. Direct enzyme-linked immunosorbent assay (ELISA) readout of released IGF-I and IGF-PSL-POx-b-POzi from the hydrogel was not possible as the different constructs with equivalent concentrations displayed strongly differing signals (Fig. S10). Therefore, bioactivity of the released construct in comparison to unconjugated IGF-I was performed by WST-1 cell proliferation assay. MMP-9 treated supernatants significantly impacted the stimulation of C2C12 cells for 4 h compared to cells, which were treated with supernatants, lacking MMP-9 treatment (Fig. 5, S11).

These results indicate that without the presence of MMP-9, the bioconjugate IGF-PSL-POx-b-POzi is retained due to the physical interactions of the POx-b-POzi polymer within the POx-b-POzi hydrogel network. In the presence of MMP-9, hydrogel pores, with pore sizes in the lower 100 nm range (determined by cryo scanning electron microscopy) [69] allow MMP-9 diffusion (Stokes-Einstein radius of MMP-9: 4.5 nm [95]), cleavage of IGF-PSL-POx-b-POzi and the diffusion of cleaved IGF-I (Stokes-Einstein radius of IGF-I: 1.54 nm [96]) out of the hydrogel. However, since the IGF-PSL-POx-b-POzi is “only” weakly bound to the hydrogel by physical (hydrophobic) interactions, part of the conjugate is still released due to swelling of the hydrogel and diffusion effects. This aspect may be addressed by introducing chemical crosslinking moieties (furan / maleimide) to the POx-b-POzi-DBCO polymer to enable covalent cross-linking within the hydrogel network.

Due to the limited stability of IGF-I at physiological pH values (buffer for MMP-activity according to manufacturer's manual, Merck KGaA), IGF release was restricted to 6 h in this study [97]. However, conjugation of IGF-I to hydrophilic polymers such as PEG resulted into prolonged serum stability of IGF-I [46]. This behavior might also apply for

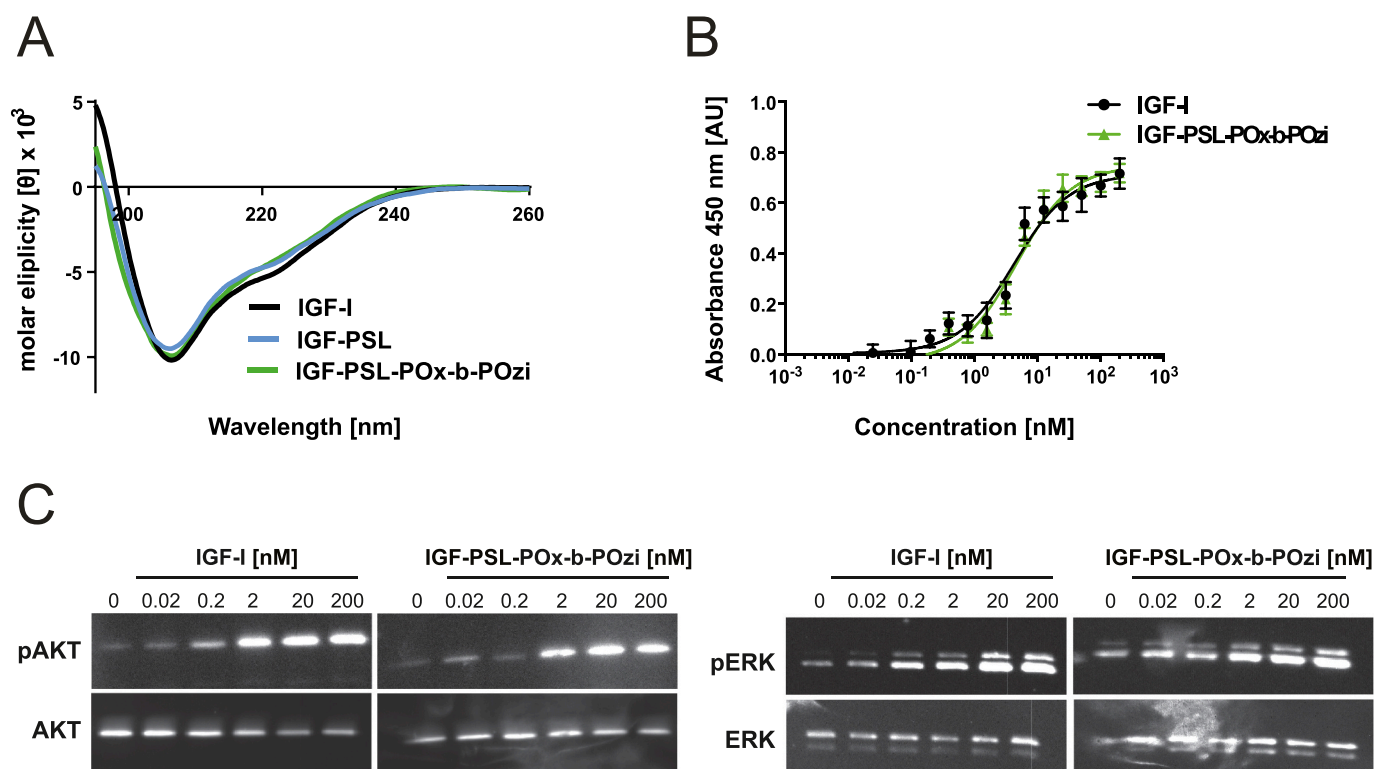


Fig. 4. Structural and functional analysis of IGF-PSL-POx-b-POzi conjugate. (A) CD spectra of IGF-I, IGF-PSL, IGF-PSL-POx-b-POzi. (B) C2C12 myoblast proliferation assay with IGF-I, IGF-PSL-POx-b-POzi ($n = 3$ biological replicates and $n = 3$ technical replicates) (C) Western blot analysis of AKT and ERK phosphorylation in C2C12 myoblasts after exposure to IGF-I and IGF-PSL-POx-b-POzi.

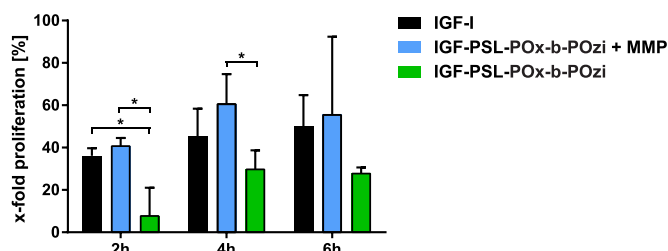


Fig. 5. Bioresponsive release of IGF-PSL-POx-b-POzi. C2C12 myoblast proliferation assay with IGF-I, IGF-PSL-POx-b-POzi after release from POx-b-POzi-hydrogels via MMP-9 after different time-points. The asterisk shows statistical significance between the different groups ($p < 0.05$).

conjugation with POx within the POx-b-POzi hydrogel network and should be investigated in future studies.

To assess the influence of IGF-PSL-POx-b-POzi on the printability and crosslinking kinetics, preliminary rheological experiments were performed. All the investigated samples remained liquid at 5 °C. Increased temperature to 37 °C induced the rapid thermogelation followed by Diels-Alder crosslinking for the samples containing both crosslinking polymers (P-Fu/P-Ma). The incorporation of IGF-PSL-POx-b-POzi did not affect either the thermogelation, shear thinning and recovery after printing or the crosslinking reaction as assessed by rheological analysis (Fig. 6A, S13, S14).

To illustrate the performances of the described POx-b-POzi thermogelling hydrogel system for 3D bioprinting application, we labeled IGF-PSL-POx-b-POzi with the fluorescent dye Atto 488, using amine-reactive linker chemistry for visualization within the P-Fu/P-Ma solution. A second P-Fu/P-Ma solution was modified with Texas Red™ C₂ maleimide using Diels-Alder chemistry. As proof of concept, we printed two separate rings consisting of the two hydrogel batches using an

extrusion 3D printing setup (Fig. 6B, C, Fig. S12A, B). Only one of the compartments contained the IGF-PSL-POx-b-POzi conjugate. Both types of hydrogels were successfully printed and were stored at least 5 h in buffer (PBS, pH 7.5) solution. The distribution of the IGF-PSL-POx-b-POzi as well as Texas Red™ was qualitatively analyzed using fluorescence microscopy. After 5 h of incubation, the printed structures showed good shape fidelity and both IGF-PSL-POx-b-POzi and Texas Red™ were located and visible in their respective printed POx-b-POzi hydrogel compartment (Fig. 6D, E and S12C, D). This result indicates that IGF-I can be easily printed in a defined 3D construct with spatial control within the hydrogel structure. Furthermore, it shows that the addition of IGF-PSL-POx-b-POzi does not interfere with the physical characteristics as well as the chemical cross-linking (Diels-Alder) of the hydrogel platform.

Our IGF-I based POx-b-POzi hydrogel system principally enables individualized, and patient-specific manufacturing within a predefined IGF-I location within the construct architecture (Fig. 6).

In the future the bioresponsive IGF-I modified biomaterial/bioink platform may be used to create more complex drug-release profiles customized for the formation of bulk or surface gradients or co-application of different growth factors due to the printing of sophisticated 3D structures and/or spatially separated compartments. Bio-responsive IGF-I release (and combination thereof) may be further tailored with the use of various PSLs to induce spatially definitive cellular responses in generating tissues.

Potential therapeutic applications of such a hydrogel system are within the area of bioresponsive wound sealants that enable the targeted growth factor release at the incision site due to an excess of MMPs [98–100]. Another potential application is the use of the POx-b-POzi hydrogel system for the regeneration of cartilage tissue. Cellular approaches such as the administration of chondrocytes or stem cells remain challenging and often need to be supported by external growth factors [101]. Thus, encapsulation of IGF-I has been frequently

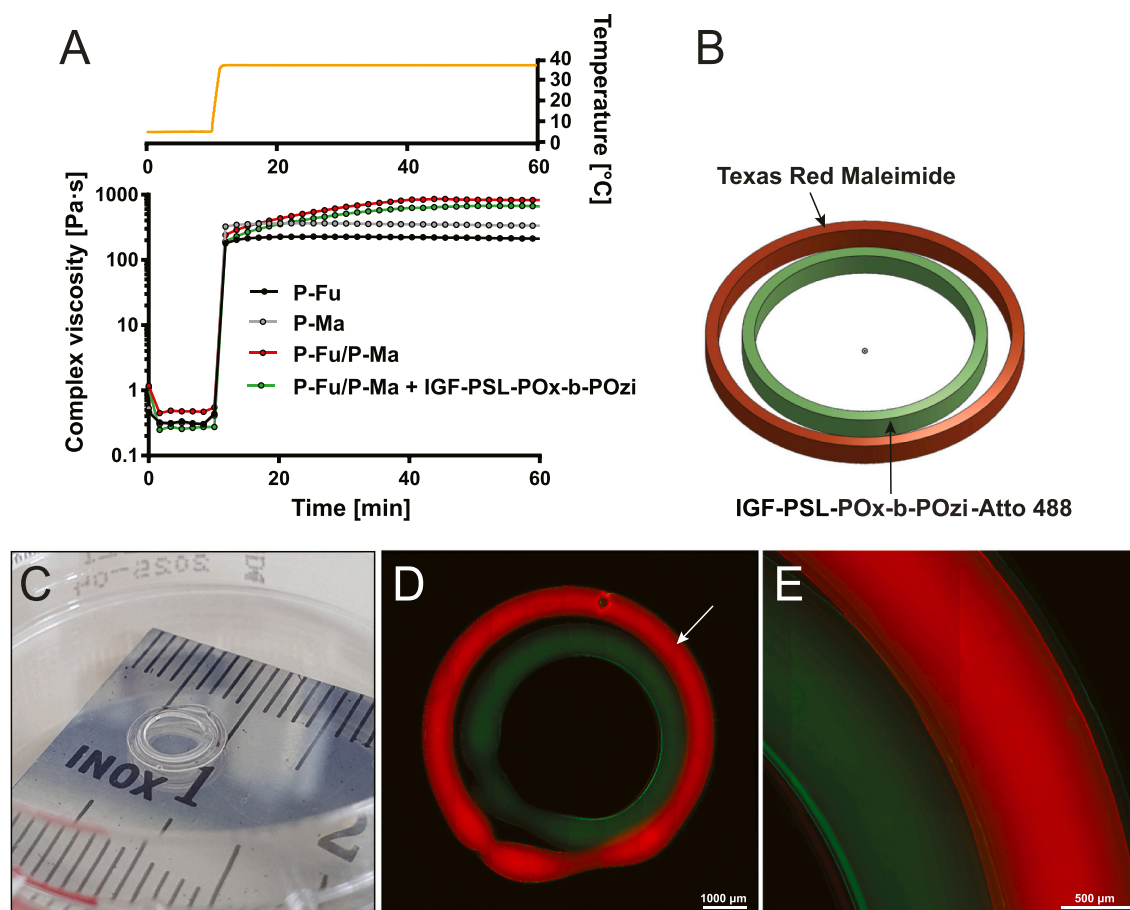


Fig. 6. 3D printing of IGF-PSL-POx-b-POzi (A) Crosslinking of hydrogels in oscillatory mode (complex viscosity as a function of time) for 10 min at 5 °C followed by 60 min at 37 °C (amplitude: 0.5%, angular frequency: 10 rad/s, polymer concentration: 25 wt% and IGF-PSL-POx-b-POzi: 25 µg/mL). (B) 3D model of the printed construct. The model was created by onshape® (Boston, MA 02210) (C) Image of printed POx hydrogel construct. (D-E) Fluorescence images of printed POx constructs after 5 h in PBS. Incorporated IGF-PSL-POx-b-POzi (green) was visualized via NHS-labelling with NHS Alexa Fluor™ 488. For the visualization of the outer ring P-Fu was functionalized with Texas Red C2 Maleimide™ (red) prior to printing. (For interpretation of the references to colour in this figure legend, the reader is referred to the web version of this article.)

performed in hydrogel systems to stimulate chondral repair [63,102,103] A localized and bioresponsive delivery of IGF-I in personalized bioprinted construct may be thus suitable to enhance IGF-I biological performances for cartilage formation.

In an effort to address cell adhesion and migration within the POx-b-POzi hydrogel system, incorporation of MMP cleavable linkers and RGD sequences for maturation of cells within the hydrogel matrix and in vivo characterization of bioresponsive IGF-I release is part of ongoing research.

4. Conclusion

3D printing has emerged as a promising tool to deposit materials with high shape control. In this study, we developed a 3D bioprintable hydrogel system for the bioresponsive release of the anabolic growth factor IGF-I by combining enzymatic and biorthogonal conjugation techniques. The coupling of the thermoresponsive POx-b-POzi polymer to IGF-I did not impair its bioactivity. Incorporation of the protein conjugate into POx-b-POzi hydrogels enabled bioresponsive release of IGF-I after the addition of MMP-9 as an external stimulus, did not impair the rheological properties of the hydrogel system and showed high shape fidelity after 3D-printing.

In general, the herein presented POx-b-POzi hydrogel platform provides a high degree of flexibility through the exchange of individual or multiple components (e. g. therapeutic protein, protease sensitive

sequence) and enables future manufacture of complex 3D architectures with release of the bioactive molecule linked to the activity of matrix metalloproteinases in tissue engineering applications including wound healing and cartilage repair.

Credit author statement

M.B.: Methodology, Visualization, Validation, Data analysis, Investigation, Writing – Original Draft. **L.H.** Methodology, Visualization, Validation, Data analysis, Investigation, Writing – Original Draft.

A.H.C.H.: Methodology, Visualization, Data analysis, Investigation, Writing – Editing.

N.H.: Methodology, Visualization, Validation, Data analysis, Investigation, Writing – Editing.

H.S. Validation, Conceptualization, Writing – Reviewing & Editing.

L.M.: Validation, Project administration, Resources, Visualization, Conceptualization, Writing -Reviewing & Editing, Supervision, Funding acquisition.

R.L.: Validation, Resources, Conceptualization, Writing -Reviewing & Editing, Funding acquisition.

M.G. Project administration, Methodology, Visualization, Validation, Data analysis, Investigation, Writing – Original Draft.

T.L.: Validation, Project administration, Resources, Visualization, Conceptualization, Writing – Original Draft, Writing -Reviewing & Editing, Supervision, Funding acquisition.

Declaration of Competing Interest

The authors declare no conflict of interest.

Acknowledgement

We thank Dr. Juliane Adelman for MALDI-MS analysis. The authors would like to gratefully acknowledge support by the Deutsche Forschungsgemeinschaft (DFG, German Research Foundation)-project number 326998133-TRR225 (subprojectA03).

Appendix A. Supplementary data

Supplementary data to this article can be found online at <https://doi.org/10.1016/j.jconrel.2022.04.028>.

References

- [1] A.A. Konta, M. García-Piña, D.R. Serrano, Personalised 3D printed medicines: which techniques and polymers are more successful? *Bioengineering* 4 (4) (2017) 79.
- [2] I. Bayindir-Buchhalter, U. Göbel, L. Stimson, Biofabrication, biomedical devices, nanomedicine, and tissue engineering – advanced materials in healthcare, *Adv. Healthc. Mater.* 7 (1) (2018) 1701399.
- [3] J. Groll, J.A. Burdick, D.W. Cho, B. Derby, M. Gelinsky, S.C. Heilshorn, T. Jüngst, J. Malda, V.A. Mironov, K. Nakayama, A. Ovsianikov, W. Sun, S. Takeuchi, J. J. Yoo, T.B.F. Woodfield, A definition of bioinks and their distinction from biomaterial inks, *Biofabrication* 11 (1) (2018), 013001.
- [4] R. Levato, T. Jüngst, R.G. Scheuring, T. Blunk, J. Groll, J. Malda, From shape to function: the next step in bioprinting, *Adv. Mater.* 32 (12) (2020) 1906423.
- [5] S. Stiehler, T. Jüngst, M. Schamel, I. Zilkowski, M. Kuhlmann, T. Böck, T. Blunk, J. Teßmar, J. Groll, Thiol-ene clickable poly(glycidol) hydrogels for biofabrication, *Ann. Biomed. Eng.* 45 (1) (2017) 273–285.
- [6] S. Bertlein, G. Brown, K.S. Lim, T. Jungst, T. Boeck, T. Blunk, J. Tessmar, G. J. Hooper, T.B.F. Woodfield, J. Groll, Thiol-Ene clickable gelatin: a platform bioink for multiple 3D biofabrication technologies, *Adv. Mater.* 29 (44) (2017).
- [7] B.L. Farrugia, K. Kempe, U.S. Schubert, R. Hoogenboom, T.R. Dargaville, Poly(2-oxazoline) hydrogels for controlled fibroblast attachment, *Biomacromolecules* 14 (8) (2013) 2724–2732.
- [8] F. Abasalizadeh, S.V. Moghaddam, E. Alizadeh, E. Akbari, E. Kashani, S.M. B. Fazljou, M. Torbati, A. Akbarzadeh, Alginate-based hydrogels as drug delivery vehicles in cancer treatment and their applications in wound dressing and 3D bioprinting, *J. Biol. Eng.* 14 (1) (2020) 8.
- [9] K.S. Lim, B.S. Schon, N.V. Mekhileri, G.C.J. Brown, C.M. Chia, S. Prabakar, G. J. Hooper, T.B.F. Woodfield, New visible-light photoinitiating system for improved print fidelity in gelatin-based bioinks, *ACS Biomater. Sci. Eng.* 2 (10) (2016) 1752–1762.
- [10] M.A. Ward, T.K. Georgiou, Thermoresponsive polymers for biomedical applications, *Polymers* 3 (3) (2011) 1215–1242.
- [11] M. Liu, X. Zeng, C. Ma, H. Yi, Z. Ali, X. Mou, S. Li, Y. Deng, N. He, Injectable hydrogels for cartilage and bone tissue engineering, *Bone Res.* 5 (1) (2017) 17014.
- [12] S. Chatterjee, P.C.-L. Hui, C.-W. Kan, Thermoresponsive hydrogels and their biomedical applications: special insight into their applications in textile based transdermal therapy, *Polymers* 10 (5) (2018) 480.
- [13] L. Klouda, Thermoresponsive hydrogels in biomedical applications: a seven-year update, *Eur. J. Pharm. Biopharm.* 97 (2015) 338–349.
- [14] N. Contessi, L. Altomare, A. Filippini, S. Farè, Thermo-responsive properties of methylcellulose hydrogels for cell sheet engineering, *Mater. Lett.* 207 (2017) 157–160.
- [15] S.P. Miguel, M.P. Ribeiro, H. Brancal, P. Coutinho, L.J. Correia, Thermoresponsive chitosan–agarose hydrogel for skin regeneration, *Carbohydr. Polym.* 111 (2014) 366–373.
- [16] R. Khoeini, H. Nosrati, A. Akbarzadeh, A. Eftekhari, T. Kavetskiy, R. Khalilov, E. Ahmadian, A. Nasibova, P. Datta, L. Roshangar, D.C. Deluca, S. Davaran, M. Cucchiari, I.T. Ozbolat, Natural and synthetic bioinks for 3D bioprinting, *Adv. NanoBiomed Res.* 1 (8) (2021) 2000097.
- [17] F.L.C. Morgan, L. Moroni, M.B. Baker, Dynamic bioinks to advance bioprinting, *Adv. Healthc. Mater.* 9 (15) (2020) 1901798.
- [18] A. Pitto-Barry, N.P.E. Barry, Pluronic® block-copolymers in medicine: from chemical and biological versatility to rationalisation and clinical advances, *Polym. Chem.* 5 (10) (2014) 3291–3297.
- [19] E.V. Batrakova, A.V. Kabanov, Pluronic block copolymers: evolution of drug delivery concept from inert nanocarriers to biological response modifiers, *J. Control. Release* 130 (2) (2008) 98–106.
- [20] I.R. Schmolka, A review of block polymer surfactants, *J. Am. Oil Chem. Soc.* 54 (3) (1977) 110–116.
- [21] A.M. Bodratti, P. Alexandridis, Formulation of poloxamers for drug delivery, *J. Funct. Biomater.* 9 (1) (2018) 11.
- [22] H. Schlaad, C. Diehl, A. Gress, M. Meyer, A.L. Demirel, Y. Nur, A. Bertin, Poly(2-oxazoline)s as smart bioinspired polymers, *Macromol. Rapid Commun.* 31 (6) (2010) 511–525.
- [23] Z. Varanaraja, J. Kim, C.R. Becer, Poly(2-oxazine)s: a comprehensive overview of the polymer structures, physical properties and applications, *Eur. Polym. J.* 147 (2021), 110299.
- [24] M.M. Bloksma, R.M. Paulus, H.P.C. van Kuringen, F. van der Woerd, H.M. L. Lambermont-Thijs, U.S. Schubert, R. Hoogenboom, Thermoresponsive poly(2-oxazine)s, *Macromol. Rapid Commun.* 33 (1) (2012) 92–96.
- [25] T. Lorson, M.M. Lübtow, E. Wegener, M.S. Haider, S. Borova, D. Nahm, R. Jordan, M. Sokolski-Papkov, A.V. Kabanov, R. Luxenhofer, Poly(2-oxazine)s based biomaterials: a comprehensive and critical update, *Biomaterials* 178 (2018) 204–280.
- [26] M.M. Lübtow, L. Hahn, M.S. Haider, R. Luxenhofer, Drug specificity, synergy and antagonism in ultrahigh capacity poly(2-oxazoline)/poly(2-oxazine) based formulations, *J. Am. Chem. Soc.* 139 (32) (2017) 10980–10983.
- [27] M.M. Lübtow, M.S. Haider, M. Kirsch, S. Klisch, R. Luxenhofer, Like dissolves like? A comprehensive evaluation of partial solubility parameters to predict polymer–drug compatibility in ultrahigh drug-loaded polymer micelles, *Biomacromolecules* 20 (8) (2019) 3041–3056.
- [28] M.M. Lübtow, L.C. Nelke, J. Seifert, J. Kühnemundt, G. Sahay, G. Dandekar, S. L. Nietzer, R. Luxenhofer, Drug induced micellization into ultra-high capacity and stable curcumin nanoformulations: Physico-chemical characterization and evaluation in 2D and 3D in vitro models, *J. Control. Release* 303 (2019) 162–180.
- [29] Hahn, D.; Sonntag, J. M.; Lück, S.; Maitz, M. F.; Freudenberg, U.; Jordan, R.; Werner, C., Poly(2-alkyl-2-oxazoline)-heparin hydrogels—expanding the physicochemical parameter space of biohybrid materials. *Adv. Healthc. Mater.* n/a (n/a), 2101327.
- [30] Z. He, X. Wan, A. Schulz, H. Bludau, M.A. Dobrovolskaia, S.T. Stern, S. A. Montgomery, H. Yuan, Z. Li, D. Alakhova, M. Sokolsky, D.B. Darr, C.M. Perou, R. Jordan, R. Luxenhofer, A.V. Kabanov, A high capacity polymeric micelle of paclitaxel: implication of high dose drug therapy to safety and in vivo anti-cancer activity, *Biomaterials* 101 (2016) 296–309.
- [31] D. Hwang, N. Vinod, S.L. Skoczen, J.D. Ramsey, K.S. Snapp, S.A. Montgomery, M. Wang, C. Lim, J.E. Frank, M. Sokolsky-Papkov, Z. Li, H. Yuan, S.T. Stern, A. V. Kabanov, Bioequivalence assessment of high-capacity polymeric micelle nanoformulation of paclitaxel and Abraxane® in rodent and non-human primate models using a stable isotope tracer assay, *Biomaterials* 278 (2021), 121140.
- [32] R.W. Moreadith, T.X. Viegas, M.D. Bentley, J.M. Harris, Z. Fang, K. Yoon, B. Dizman, R. Weimer, B.P. Rae, X. Li, C. Rader, D. Standaert, W. Olanow, Clinical development of a poly(2-oxazoline) (POZ) polymer therapeutic for the treatment of Parkinson’s disease – proof of concept of POZ as a versatile polymer platform for drug development in multiple therapeutic indications, *Eur. Polym. J.* 88 (2017) 524–552.
- [33] C.W. Olanow, D.G. Standaert, K. Kiebert, T.X. Viegas, R. Moreadith, Once-weekly subcutaneous delivery of polymer-linked rotigotine (SER-214) provides continuous plasma levels in Parkinson’s disease patients, *Mov. Disord.* 35 (6) (2020) 1055–1061.
- [34] J. Tong, R. Luxenhofer, X. Yi, R. Jordan, A.V. Kabanov, Protein modification with amphiphilic block copoly(2-oxazoline)s as a new platform for enhanced cellular delivery, *Mol. Pharm.* 7 (4) (2010) 984–992.
- [35] J. Tong, X. Yi, R. Luxenhofer, W.A. Banks, R. Jordan, M.C. Zimmerman, A. V. Kabanov, Conjugates of superoxide dismutase 1 with amphiphilic poly(2-oxazoline) block copolymers for enhanced brain delivery: synthesis, characterization and evaluation in vitro and in vivo, *Mol. Pharm.* 10 (1) (2013) 360–377.
- [36] L. Hahn, E. Karakaya, T. Zorn, B. Sochor, M. Maier, P. Stahlhut, S. Forster, K. Fischer, S. Seiffert, A.-C. Pöppler, R. Detsch, R. Luxenhofer, An inverse thermogelling bioink based on an ABA-type poly(2-oxazoline) amphiphile, *Biomacromolecules* 22 (7) (2021) 3017–3027.
- [37] T. Lorson, S. Jaksch, M.M. Lübtow, T. Jüngst, J. Groll, T. Lühmann, R. Luxenhofer, A Thermogelling supramolecular hydrogel with sponge-like morphology as a cytocompatible bioink, *Biomacromolecules* 18 (7) (2017) 2161–2171.
- [38] L. Hahn, M. Beudert, M. Gutmann, L. Keßler, P. Stahlhut, L. Fischer, E. Karakaya, T. Lorson, I. Thievensen, R. Detsch, T. Lühmann, R. Luxenhofer, From thermogelling hydrogels toward functional bioinks: controlled modification and cytocompatible crosslinking, *Macromol. Biosci.* 21 (10) (2021), e2100122.
- [39] G.L. Koons, A.G. Mikos, Progress in three-dimensional printing with growth factors, *J. Control. Release* 295 (2019) 50–59.
- [40] C.W. Peak, K.A. Singh, M.A. Adlouni, J. Chen, A.K. Gaharwar, Printing therapeutic proteins in 3D using nanoengineered bioink to control and direct cell migration, *Adv. Healthc. Mater.* 8 (11) (2019) 1801553.
- [41] R. Luxenhofer, Y. Han, A. Schulz, J. Tong, Z. He, A.V. Kabanov, R. Jordan, Poly(2-oxazoline)s as polymer therapeutics, *Macromol. Rapid Commun.* 33 (19) (2012) 1613–1631.
- [42] A.C. Braun, M. Gutmann, R. Ebert, F. Jakob, H. Gieseler, T. Lühmann, L. Meinel, Matrix metalloproteinase responsive delivery of myostatin inhibitors, *Pharm. Res.* 34 (1) (2017) 58–72.
- [43] A.C. Braun, M. Gutmann, T.D. Mueller, T. Lühmann, L. Meinel, Bioresponsive release of insulin-like growth factor-I from its PEGylated conjugate, *J. Control. Release* 279 (2018) 17–28.
- [44] S.N.S. Alconcel, A.S. Baas, H.D. Maynard, FDA-approved poly(ethylene glycol)–protein conjugate drugs, *Polym. Chem.* 2 (7) (2011) 1442–1448.

- [45] A. Kolate, D. Baradia, S. Patil, I. Vhora, G. Kore, A. Misra, PEG — a versatile conjugating ligand for drugs and drug delivery systems, *J. Control. Release* 192 (2014) 67–81.
- [46] A.C. Braun, M. Gutmann, T.D. Mueller, T. Lühmann, L. Meinel, Bioresponsive release of insulin-like growth factor-I from its PEGylated conjugate, *J. Control. Release* 279 (2018) 17–28.
- [47] E. Rinderknecht, R.E. Humbel, The amino acid sequence of human insulin-like growth factor I and its structural homology with proinsulin, *J. Biol. Chem.* 253 (8) (1978) 2769–2776.
- [48] T. Breil, C. Kneppo, M. Bettendorf, German IGF-I Deficiency Study Group, H. L. Muller, K. Kapelari, D. Schnabel, J. Woelfle, Sequential measurements of IGF-I serum concentrations in adolescents with Laron syndrome treated with recombinant human IGF-I (rhIGF-I), *J. Pediatr. Endocrinol. Metab.* 31 (8) (2018) 895–902.
- [49] H. Boro, S.H. Rahman, S. Khatiwada, S. Alam, R. Khadgawat, Laron syndrome: an experience of treatment of two cases, *J. Clin. Translat. Endocrinol. Case Rep.* 19 (2021), 100076.
- [50] S.D. Chernausek, P.F. Backeljauw, J. Frane, J. Kuntze, L.E. Underwood, Long-term treatment with recombinant insulin-like growth factor (IGF)-I in children with severe IGF-I deficiency due to growth hormone insensitivity, *J. Clin. Endocrinol. Metabol.* 92 (3) (2007) 902–910.
- [51] H.A. Hansson, L.B. Dahlin, N. Danielsen, L. Fryklund, A.K. Nachemson, P. Polleryd, B. Rozell, A. Skottner, S. Stemme, G. Lundborg, Evidence indicating trophic importance of IGF-I in regenerating peripheral nerves, *Acta Physiol. Scand.* 126 (4) (1986) 609–614.
- [52] H.A. Hansson, L.B. Dahlin, N. Danielsen, L. Fryklund, A.K. Nachemson, P. Polleryd, B. Rozell, A. Skottner, S. Stemme, G. Lundborg, Evidence indicating trophic importance of IGF-I in regenerating peripheral nerves, *Acta Physiol. Scand.* 126 (4) (1986) 609–614.
- [53] E. Osher, V.M. Macaulay, Therapeutic targeting of the IGF axis, *Cells* 8 (8) (2019) 895.
- [54] J.I. Jones, D.R. Clemmons, Insulin-like growth factors and their binding proteins: biological actions*, *Endocr. Rev.* 16 (1) (1995) 3–34.
- [55] C.D. Stiles, G.T. Capone, C.D. Scher, H.N. Antoniades, J.J. Van Wyk, W.J. Pledger, Dual control of cell growth by somatomedins and platelet-derived growth factor, *Proc. Natl. Acad. Sci.* 76 (3) (1979) 1279–1283.
- [56] A. Cittadini, M.G. Monti, V. Petrillo, G. Esposito, G. Imparato, A. Luciani, F. Urciuolo, E. Bobbio, C.F. Natale, L. Saccà, P.A. Netti, Complementary therapeutic effects of dual delivery of insulin-like growth factor-I and vascular endothelial growth factor by gelatin microspheres in experimental heart failure, *Eur. J. Heart Fail.* 13 (12) (2011) 1264–1274.
- [57] R.G. Rosenfeld, IGF-I therapy in growth disorders, *Eur. J. Endocrinol.* 157 (Suppl. 1) (2007). S57–60.
- [58] O. Germershaus, I. Schultz, T. Lühmann, M. Beck-Broichsitter, P. Högger, L. Meinel, Insulin-like growth factor-I aerosol formulations for pulmonary delivery, *Eur. J. Pharm. Biopharm.* 85 (1) (2013) 61–68.
- [59] V. Luginbuehl, E. Wenk, A. Koch, B. Gander, H.P. Merkle, L. Meinel, Insulin-like growth factor I-releasing alginate-tricalciumphosphate composites for bone regeneration, *Pharm. Res.* 22 (6) (2005) 940–950.
- [60] V. Luginbuehl, E. Zoidis, L. Meinel, B. von Rechenberg, B. Gander, H.P. Merkle, Impact of IGF-I release kinetics on bone healing: a preliminary study in sheep, *Eur. J. Pharm. Biopharm.* 85 (1) (2013) 99–106.
- [61] L. Meinel, O.E. Illi, J. Zapf, M. Malfanti, H. Peter Merkle, B. Gander, Stabilizing insulin-like growth factor-I in poly(D,L-lactide-co-glycolide) microspheres, *J. Control. Release* 70 (1–2) (2001) 193–202.
- [62] L. Meinel, E. Zoidis, J. Zapf, P. Hassa, M.O. Hottiger, J.A. Auer, R. Schneider, B. Gander, V. Luginbuehl, R. Bettschart-Wolfberger, O.E. Illi, H.P. Merkle, B. von Rechenberg, Localized insulin-like growth factor I delivery to enhance new bone formation, *Bone* 33 (4) (2003) 660–672.
- [63] L. Uebersax, H.P. Merkle, L. Meinel, Insulin-like growth factor I releasing silk fibroin scaffolds induce chondrogenic differentiation of human mesenchymal stem cells, *J. Control. Release* 127 (1) (2008) 12–21.
- [64] E. Wenk, A.J. Wandrey, H.P. Merkle, L. Meinel, Silk fibroin spheres as a platform for controlled drug delivery, *J. Control. Release* 132 (1) (2008) 26–34.
- [65] J. Feng, Y. Wu, W. Chen, J. Li, X. Wang, Y. Chen, Y. Yu, Z. Shen, Y. Zhang, Sustained release of bioactive IGF-I from a silk fibroin microsphere-based injectable alginate hydrogel for the treatment of myocardial infarction, *J. Mater. Chem. B* 8 (2) (2020) 308–315.
- [66] H. Witte, W. Seeliger, Simple synthesis of 2-substituted 2-oxazolines and 5,6-dihydro-4H-1,3-oxazines, *Angew. Chem. Int. Ed. Eng.* 11 (4) (1972) 287–288.
- [67] L. Hahn, M.M. Lübtow, T. Lorson, F. Schmitt, A. Appelt-Menzel, R. Schobert, R. Luxenhofer, Investigating the influence of aromatic moieties on the formulation of hydrophobic natural products and drugs in poly(2-oxazoline)-based amphiphiles, *Biomacromolecules* 19 (7) (2018) 3119–3128.
- [68] J. Hofmann, S. Favez, M. Scheiner, M. Hoffmann, S. Oerter, A. Appelt-Menzel, P. Maher, T. Maurice, G. Bringmann, M. Decker, Sterubin: enantioresolution and configurational stability, enantiomeric purity in nature, and neuroprotective activity in vitro and in vivo, *Chemistry* 26 (32) (2020) 7299–7308.
- [69] Hahn, L.; Beudert, M.; Gutmann, M.; Keßler, L.; Stahlhut, P.; Fischer, L.; Karakaya, E.; Lorson, T.; Thievsen, I.; Detsch, R.; Lühmann, T.; Luxenhofer, R., From thermogelling hydrogels toward functional bioinks: controlled modification and cytocompatible crosslinking. *Macromol. Biosci. n/a* (n/a), 2100122.
- [70] R.M. Cooke, T.S. Harvey, I.D. Campbell, Solution structure of human insulin-like growth factor 1: a nuclear magnetic resonance and restrained molecular dynamics study, *Biochemistry* 30 (22) (1991) 5484–5491.
- [71] E. Vanquelef, S. Simon, G. Marquant, E. Garcia, G. Klimerak, J.C. Delepine, P. Cieplak, F.Y. Dupradeau, R.E.D. Server: a web service for deriving RESP and ESP charges and building force field libraries for new molecules and molecular fragments, *Nucleic Acids Res.* 39 (Web Server issue) (2011). W511–7.
- [72] J.A. Maier, C. Martinez, K. Kasavajhala, L. Wickstrom, K.E. Hauser, C. Simmerling, ff14SB: improving the accuracy of protein side chain and backbone parameters from ff99SB, *J. Chem. Theory Comput.* 11 (8) (2015) 3696–3713.
- [73] W.L. Jorgensen, J. Chandrasekhar, J.D. Madura, R.W. Impey, M.L. Klein, Comparison of simple potential functions for simulating liquid water, *J. Chem. Phys.* 79 (2) (1983) 926–935.
- [74] D.A. Case, T.A. Darden, T.E. Cheatham 3rd, C. Simmerling, J. Wang, R.E. Duke, R. Luo, M. Crowley, R.C. Walker, W. Zhang, K.M. Merz, B. Wang, S. Hayik, A. Roitberg, G. Seabra, I. Kolossvary, K.F. Wong, F. Paesani, J. Vanicek, X. Wu, S. R. Brozell, T. Steinbrecher, H. Gohlke, L. Yang, C. Tan, J. Mongan, V. Hornak, G. Cui, D.H. Mathews, M.G. Seetin, C. Sagui, V. Babin, J.W. Kollman, Amber20, University of California, San Francisco, 2020.
- [75] R. Salomon-Ferrer, A.W. Götz, D. Poole, S. Le Grand, R. Walker, C., routine microsecond molecular dynamics simulations with AMBER on GPUs. 2. Explicit solvent particle mesh Ewald, *J. Chem. Theory Comput.* 9 (9) (2013) 3878–3888.
- [76] A.W. Götz, M.J. Williamson, D. Xu, D. Poole, S. Le Grand, R.C. Walker, Routine microsecond molecular dynamics simulations with AMBER on GPUs. 1. Generalized born, *J. Chem. Theory Comput.* 8 (5) (2012) 1542–1555.
- [77] J.-P. Ryckaert, G. Ciccotti, H.J.C. Berendsen, Numerical integration of the cartesian equations of motion of a system with constraints: molecular dynamics of n-alkanes, *J. Comput. Phys.* 23 (3) (1977) 327–341.
- [78] S. Miyamoto, P.A. Kollman, Settle: an analytical version of the SHAKE and RATTLE algorithm for rigid water models, *J. Comput. Chem.* 13 (8) (1992) 952–962.
- [79] C.A. Söldner, H. Sticht, A.H.C. Horn, Role of the N-terminus for the stability of an amyloid- β fibril with three-fold symmetry, *PLoS One* 12 (10) (2017), e0186347.
- [80] W. Humphrey, A. Dalke, K. Schulten, VMD: Visual molecular dynamics, *J. Mol. Graph.* 14 (1) (1996) 33–38.
- [81] H. Lee, T.G. Park, Preparation and characterization of mono-PEGylated epidermal growth factor: evaluation of in vitro biologic activity, *Pharm. Res.* 19 (6) (2002) 845–851.
- [82] J.K. Dozier, M.D. Distefano, Site-specific PEGylation of therapeutic proteins, *Int. J. Mol. Sci.* 16 (10) (2015) 25831–25864.
- [83] M.A. Cascieri, G.G. Chicchi, J. Applebaum, N.S. Hayes, B.G. Green, M.L. Bayne, Mutants of human insulin-like growth factor I with reduced affinity for the type 1 insulin-like growth factor receptor, *Biochemistry* 27 (9) (1988) 3229–3233.
- [84] T. Sitar, G.M. Popowicz, I. Siwanowicz, R. Huber, T.A. Holak, Structural basis for the inhibition of insulin-like growth factors by insulin-like growth factor-binding proteins, *Proc. Natl. Acad. Sci.* 103 (35) (2006) 13028–13033.
- [85] M.L. Bayne, J. Applebaum, D. Underwood, G.G. Chicchi, B.G. Green, N.S. Hayes, M.A. Cascieri, The C region of human insulin-like growth factor (IGF) I is required for high affinity binding to the type 1 IGF receptor, *J. Biol. Chem.* 264 (19) (1989) 11004–11008.
- [86] J.C. Schense, J.A. Hubbell, Cross-linking exogenous bifunctional peptides into fibrin gels with factor XIIIa, *Bioconjug. Chem.* 10 (1) (1999) 75–81.
- [87] J. Ritzter, T. Lühmann, C. Rode, M. Pein-Hackelbusch, I. Immoher, U. Schedler, T. Thiele, S. Stübinger, B.V. Rechenberg, J. Waser-Althaus, F. Schlottig, M. Merli, H. Dawe, M. Karpfsek, R. Wyrwa, M. Schnabelrauch, L. Meinel, Diagnosing peri-implant disease using the tongue as a 24/7 detector, *Nat. Commun.* 8 (1) (2017) 264.
- [88] H. Nagase, G.B. Fields, Human matrix metalloproteinase specificity studies using collagen sequence-based synthetic peptides, *Biopolymers* 40 (4) (1996) 399–416.
- [89] A.M. Waterhouse, J.B. Procter, D.M.A. Martin, M. Clamp, G.J. Barton, Jalview version 2—a multiple sequence alignment editor and analysis workbench, *Bioinformatics* 25 (9) (2009) 1189–1191.
- [90] E.F. Pettersen, T.D. Goddard, C.C. Huang, G.S. Couch, D.M. Greenblatt, E. C. Meng, T.E. Ferrin, UCSF chimera—a visualization system for exploratory research and analysis, *J. Comput. Chem.* 25 (13) (2004) 1605–1612.
- [91] T. Lühmann, M. Schmidt, M.N. Leiske, V. Spieler, T.C. Majdanski, M. Grube, M. Hartlieb, I. Nischang, S. Schubert, U.S. Schubert, L. Meinel, Site-specific POxylation of interleukin-4, *ACS Biomater. Sci. Eng.* 3 (3) (2017) 304–312.
- [92] N. Hauptstein, P. Pouyan, J. Kehrein, M. Dirauf, M.D. Driessen, M. Raschig, K. Licha, M. Gottschaldt, U.S. Schubert, R. Haag, L. Meinel, C. Sottriffer, T. Lühmann, Molecular insights into site-specific interferon- α 2a bioconjugates originated from PEG, LPG, and PetOx, *Biomacromolecules* 22 (11) (2021) 4521–4534.
- [93] D. Ahrens, A.E. Koch, R.M. Pope, M. Stein-Picarella, M.J. Niedbala, Expression of matrix metalloproteinase 9 (96-kd gelatinase B) in human rheumatoid arthritis, *Arthritis Rheum.* 39 (9) (1996) 1576–1587.
- [94] L. Gauguin, C. Delaine, C.L. Alvino, K.A. McNeil, J.C. Wallace, B.E. Forbes, P. De Meyts, Alanine scanning of a putative receptor binding surface of insulin-like growth factor-I*, *J. Biol. Chem.* 283 (30) (2008) 20821–20829.
- [95] G. Rosenblum, P.E. Van den Steen, S.R. Cohen, J.G. Grossmann, J. Frenkel, R. Sertchook, N. Slack, R.W. Strange, G. Opendakker, I. Sagi, Insights into the structure and domain flexibility of full-length pro-matrix metalloproteinase-9/gelatinase B, *Structure* 15 (10) (2007) 1227–1236.
- [96] J.V. Nauman, P.G. Campbell, F. Lanni, J.L. Anderson, Diffusion of insulin-like growth factor-I and ribonuclease through fibrin gels, *Biophys. J.* 92 (12) (2007) 4444–4450.

- [97] O. Germershaus, I. Schultz, T. Lühmann, M. Beck-Broichsitter, P. Högger, L. Meinel, Insulin-like growth factor-I aerosol formulations for pulmonary delivery, *Eur. J. Pharm. Biopharm.* 85 (1) (2013) 61–68.
- [98] J.P. Jee, R. Pangei, S.K. Jha, Y. Byun, J.W. Park, Preparation and in vivo evaluation of a topical hydrogel system incorporating highly skin-permeable growth factors, quercetin, and oxygen carriers for enhanced diabetic wound-healing therapy, *Int. J. Nanomedicine* 14 (2019) 5449–5475.
- [99] M.P. Caley, V.L.C. Martins, E.A. O'Toole, Metalloproteinases and wound healing, *Adv. Wound Care (New Rochelle)* 4 (4) (2015) 225–234.
- [100] Z. Garoufalia, A. Papadopetraki, E. Karatza, D. Vardakostas, A. Philippou, G. Kouraklis, D. Mantas, Insulin-like growth factor-I and wound healing, a potential answer to non-healing wounds: a systematic review of the literature and future perspectives, *Biomed Rep* 15 (2) (2021) 66.
- [101] H. Cho, J. Kim, S. Kim, Y.C. Jung, Y. Wang, B.-J. Kang, K. Kim, Dual delivery of stem cells and insulin-like growth factor-1 in coacervate-embedded composite hydrogels for enhanced cartilage regeneration in osteochondral defects, *J. Control. Release* 327 (2020) 284–295.
- [102] J. Elisseeff, W. McIntosh, K. Fu, T. Blunk, R. Langer, Controlled-release of IGF-1 and TGF- β 1 in a photopolymerizing hydrogel for cartilage tissue engineering, *J. Orthop. Res.* 19 (6) (2001) 1098–1104.
- [103] L.M. Mullen, S.M. Best, S. Ghose, J. Wardale, N. Rushton, R.E. Cameron, Bioactive IGF-1 release from collagen-GAG scaffold to enhance cartilage repair in vitro, *J. Mater. Sci. Mater. Med.* 26 (1) (2015) 5325.

Supporting Information

Merging bioresponsive release of insulin-like growth factor I with 3D printable thermogelling hydrogels

Matthias Beudert¹, Lukas Hahn^{1,2}, Anselm H.C. Horn^{3,4}, Niklas Hauptstein¹, Heinrich Sticht^{3,4}, Lorenz Meinel^{1,5}, Robert Luxenhofer^{2,6}, Marcus Gutmann^{1*}, Tessa Lühmann^{1*}

¹ University of Würzburg, Institute for Pharmacy and Food Chemistry, 97074 Würzburg, Germany

² Functional Polymer Materials, Chair for Advanced Materials Synthesis, Institute for Functional Materials and Biofabrication, Department of Chemistry and Pharmacy, Julius-Maximilians-University Würzburg, Röntgenring 11, 97070 Würzburg, Germany

³ Bioinformatics, Institute of Biochemistry, Friedrich-Alexander-Universität Erlangen-Nürnberg, Fahrstraße 17, 91054 Erlangen, Germany

⁴ Erlangen National High Performance Computing Center (NHR@FAU), Friedrich-Alexander-Universität Erlangen-Nürnberg, Martensstraße 1, 91058 Erlangen, Germany

⁵ Helmholtz Institute for RNA-based Infection Research, Josef-Schneider-Straße 2, DE-97080 Würzburg, Germany.

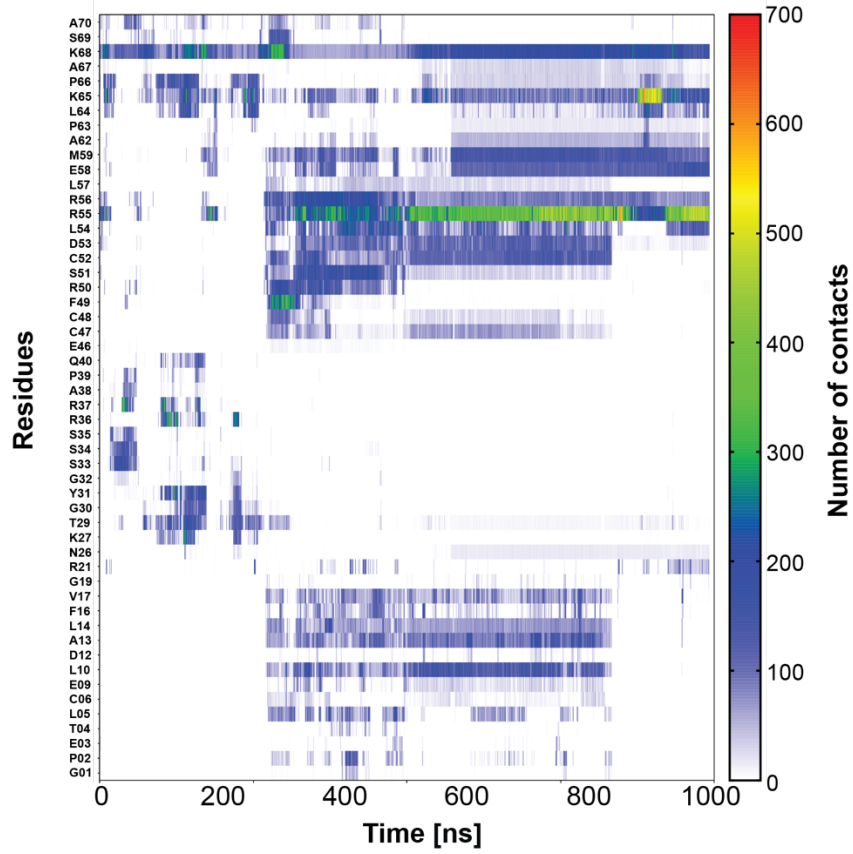
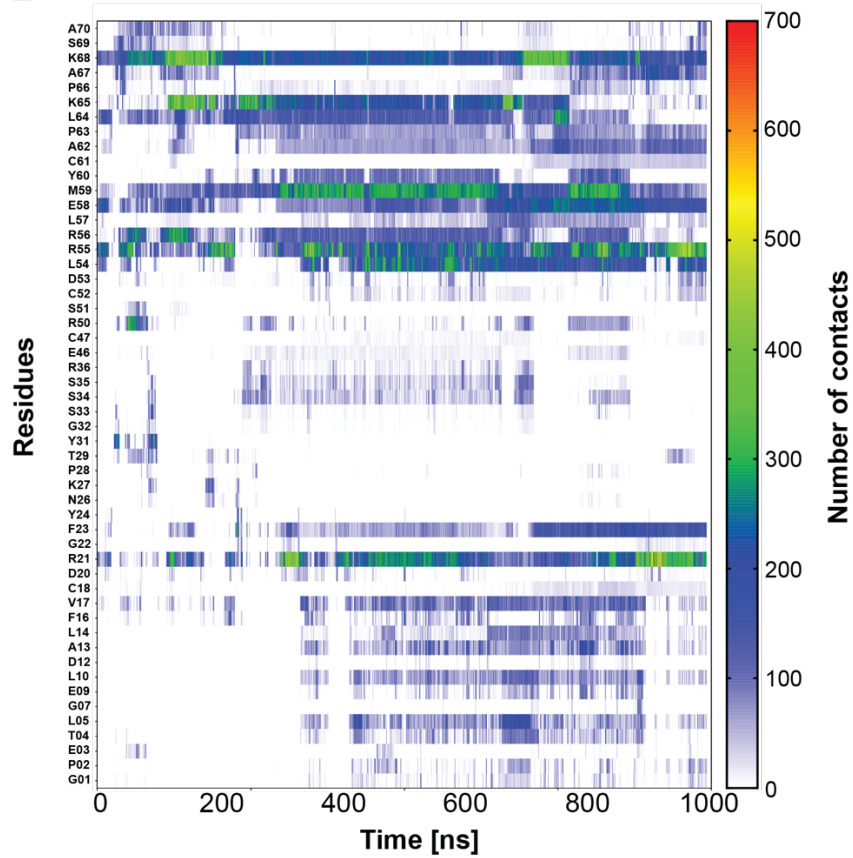
⁶ Soft Matter Chemistry, Department of Chemistry and Helsinki Institute of Sustainability Science, Faculty of Science, University of Helsinki, P.O. Box 55, 00014 Helsinki, Finland

Number of pages: S1–S14

Number of figures: S1–S14

Number of videos: S1

Number of tables: None

A**B**

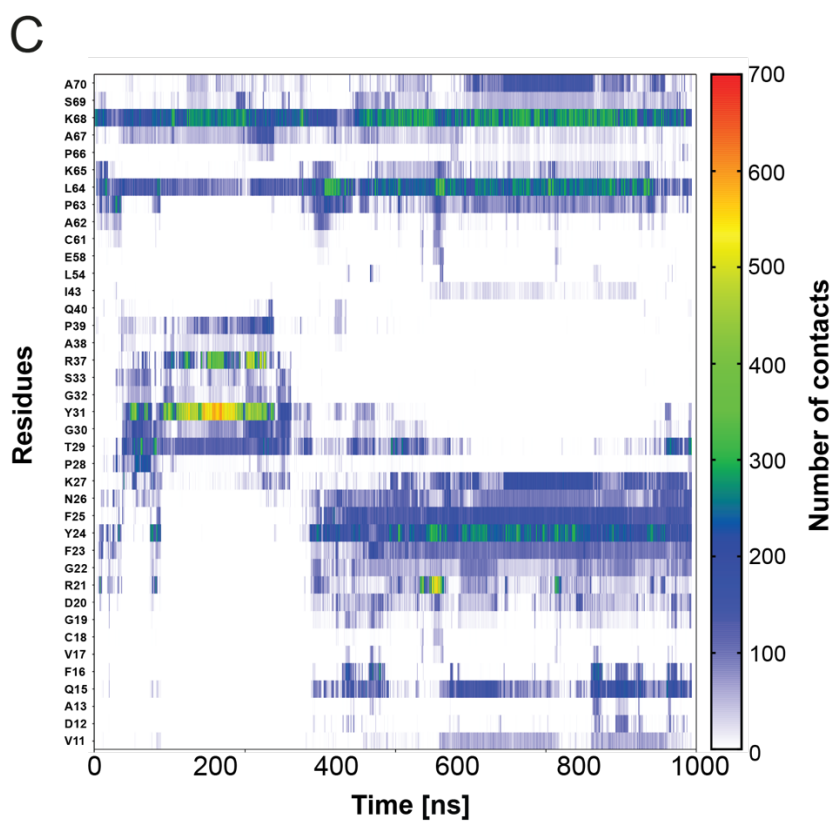


Figure S1: (A) Number of contacts between PSL and IGF-I over the simulation time (run 2). The simulation time is shown as horizontal axis and the interacting IGF-I residues on the vertical axis. (B) Number of contacts between PSL and IGF-I over the simulation time (run 3). (C) Number of contacts between PSL and IGF-I over the simulation time (run 4). The simulation time is shown as horizontal axis and the interacting IGF-I residues on the vertical axis. The number of IGF-PSL contacts is color coded (see vertical scale bar on the right).

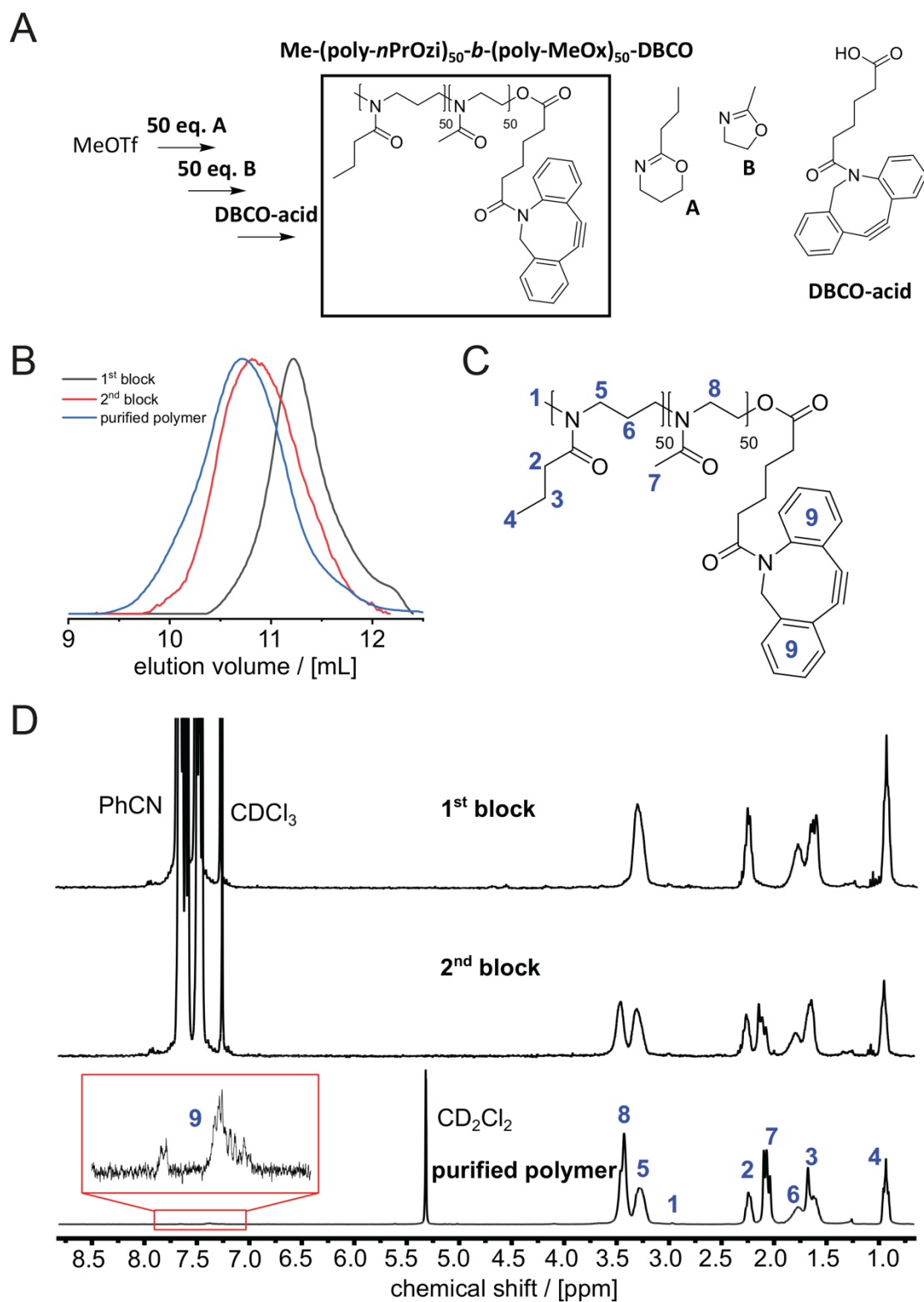


Figure S2: Synthesis and characterization of POx-b-POzi-DBCO (A) Schematic description of the synthesis of a thermoresponsive AB diblock copolymer (degree of polymerization: 100, block ratio: 1:1) comprising the thermoresponsive A block (poly-*n*PrOzi), the hydrophilic B block (poly-MeOx) and a DBCO omega functionality. (B) Following the reaction process via GPC. (C) Chemical structure of the AB diblock copolymer with the assignment of all relevant peaks in ¹H NMR experiments. (D) ¹H NMR spectra after the 1st, 2nd block and the purified polymer.

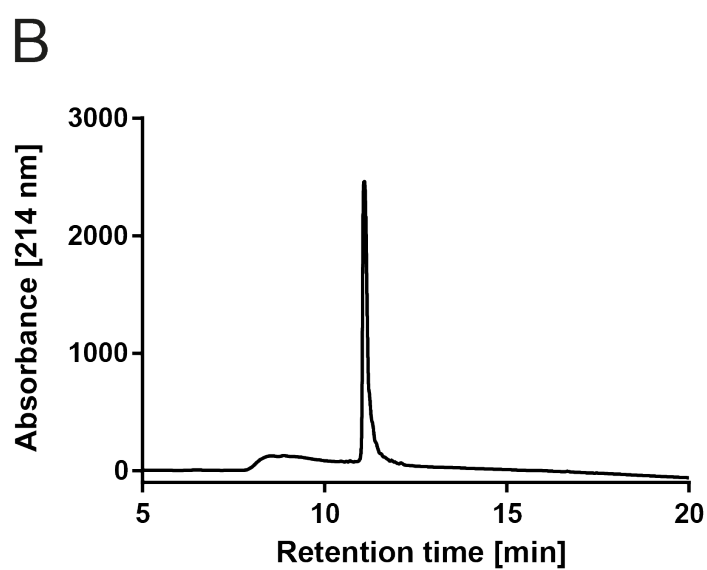
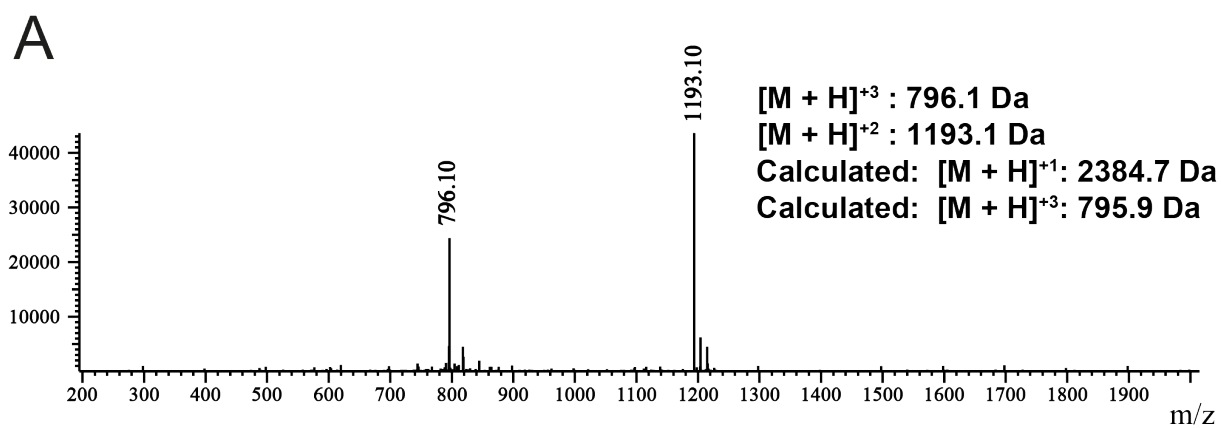


Figure S3: Characterization of PSL peptide. (A) ESI-MS analysis. (B) Purity of the peptide analyzed by HPLC.

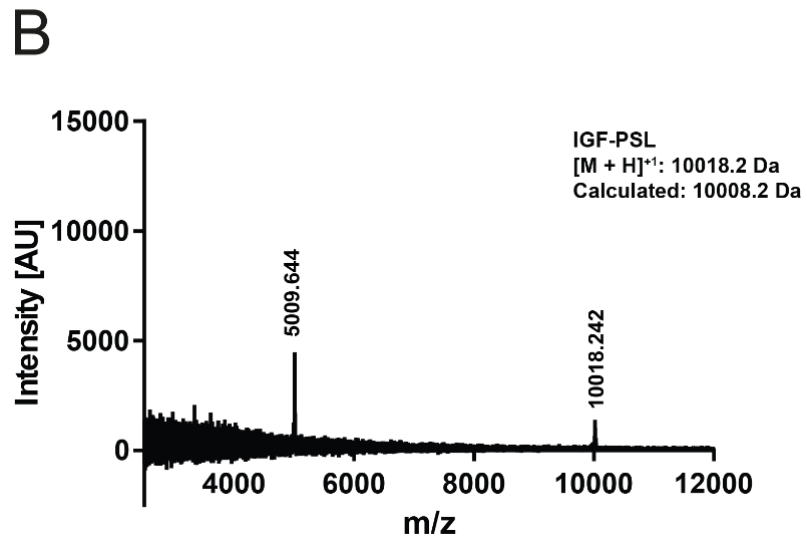
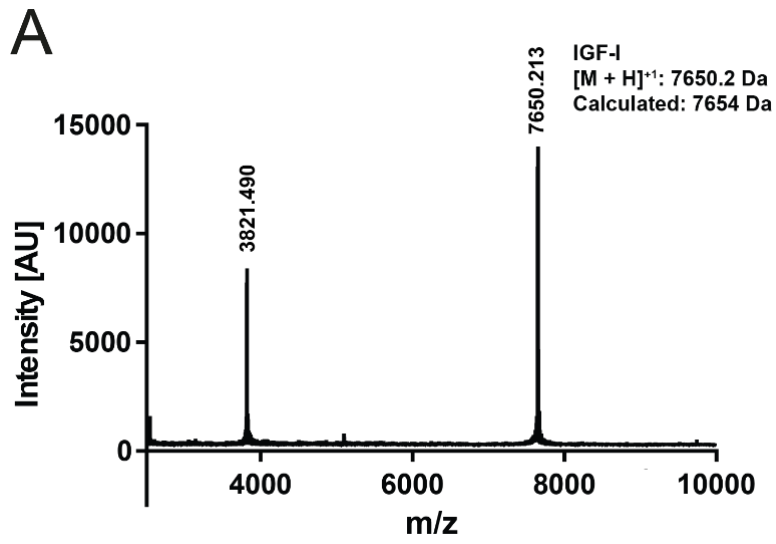


Figure S4: MALDI-MS analysis of (A) IGF-I and (B) IGF-PSL.

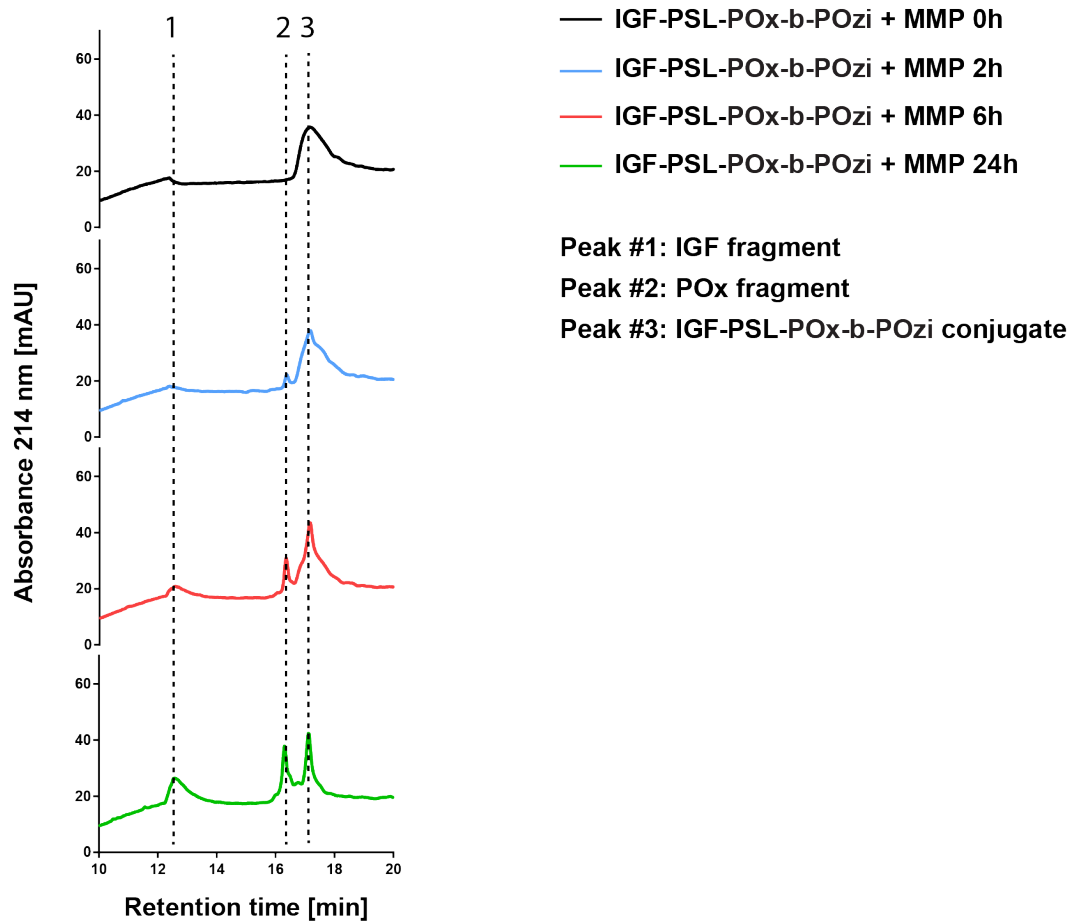


Figure S5: HPLC chromatograms of IGF-PSL-POx-b-POzi incubated with 8 nm MMP-9 at different time points.

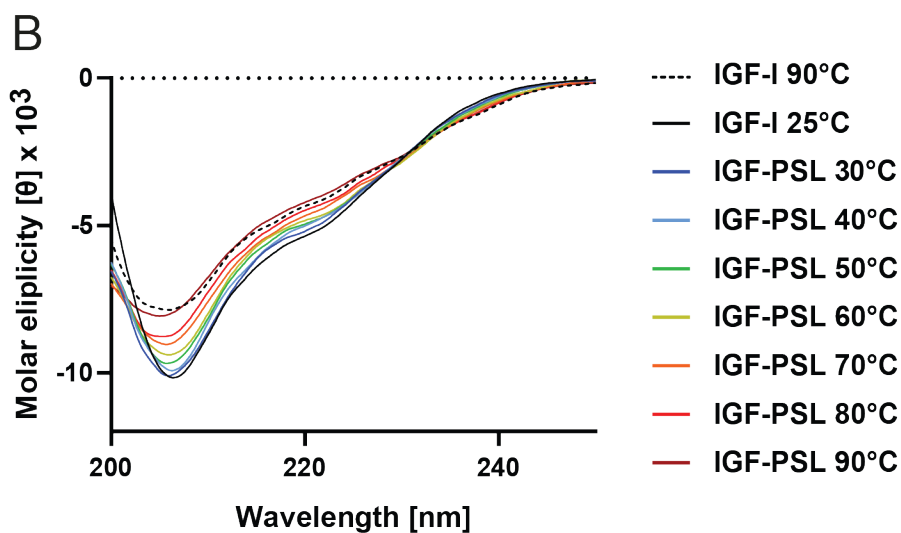


Figure S6: CD spectra of IGF-I (25 °C and 90 °C) and IGF-PSL at different temperatures ranging from 30 to 90 °C.

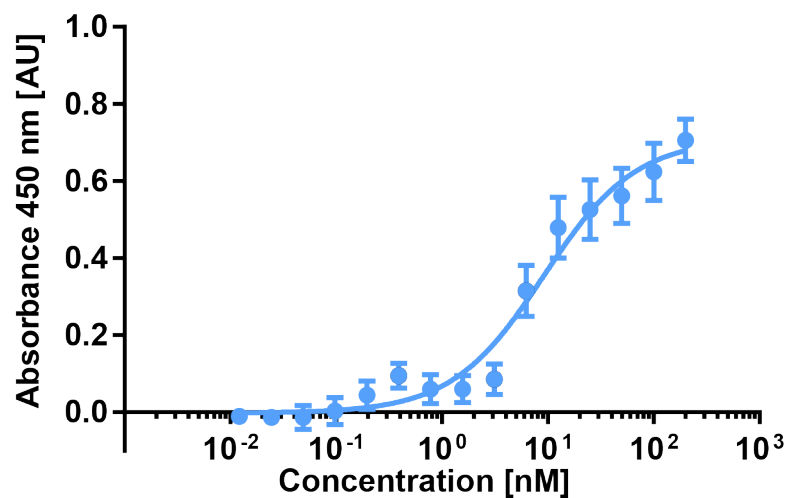


Figure S7: C2C12 myoblast proliferation assay with IGF-PSL (n=3 biological replicates and n=3 technical replicates).

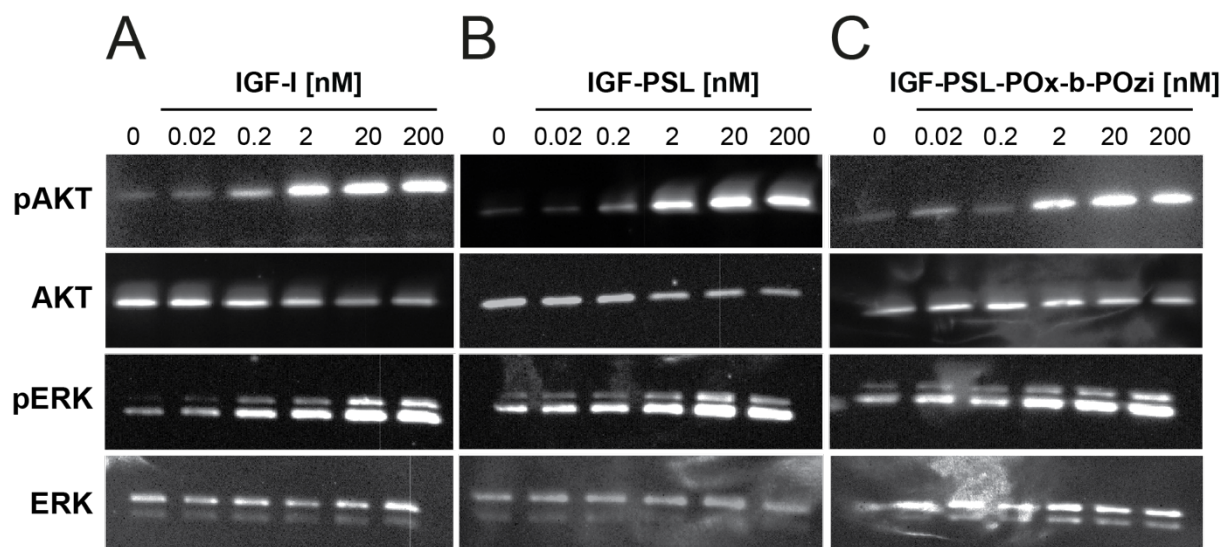


Figure S8: Bioactivity of IGF variants using western blot analysis of AKT and ERK phosphorylation in C2C12 myoblasts after exposure to (A) IGF-I, (B) IGF-PSL and (C) IGF-PSL-POx-b-POzi.

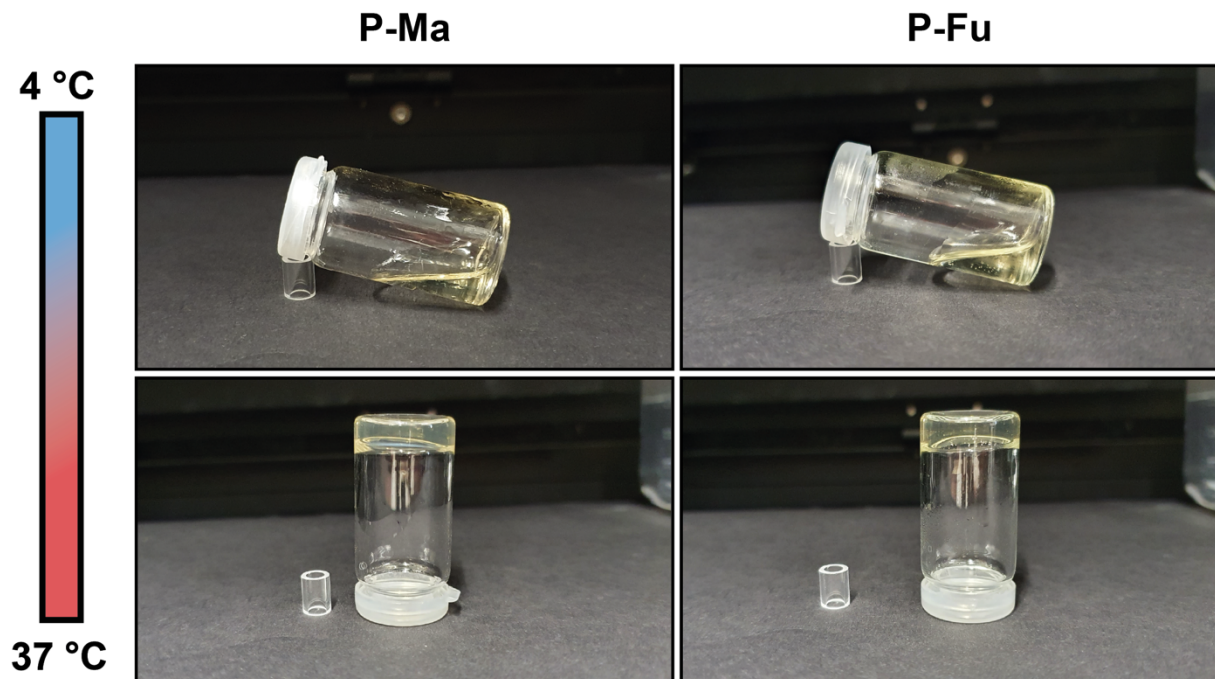


Figure S9: Thermogelling properties of the different modified polymers. P-Ma and P-Fu at 4 °C and RT.

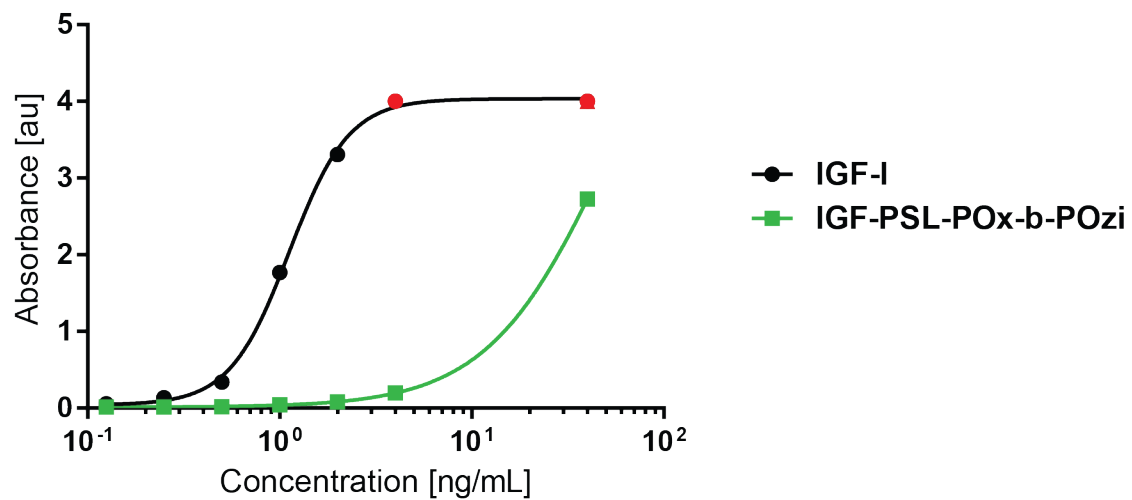
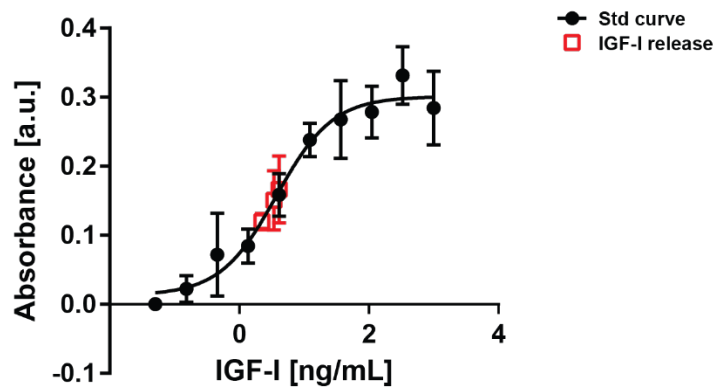
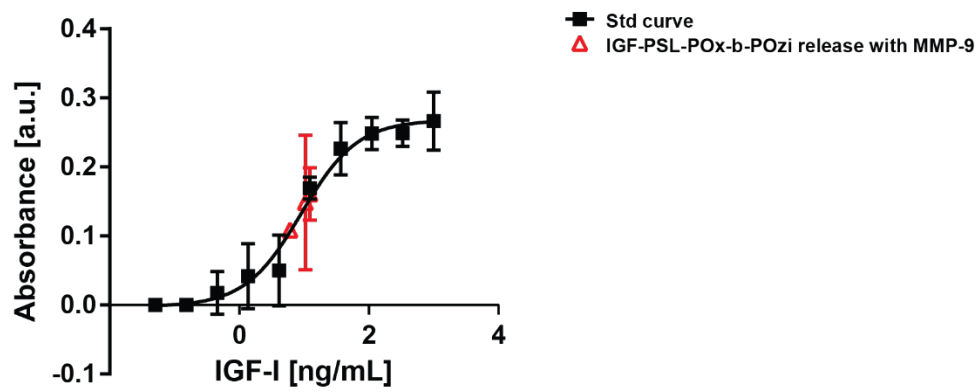


Figure S10: IGF-I ELISA standard curve for Increlex[®] (IGF-I) and IGF-PSL-POx-b-POzi. Red dots were not measurable and set to maximal possible measurable value.

A



B



C

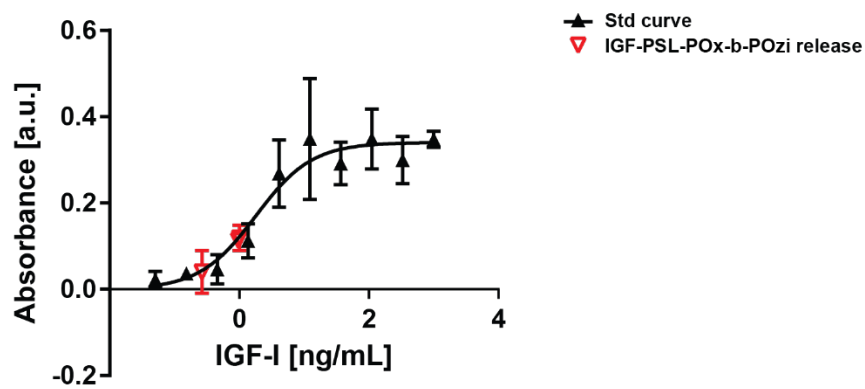


Figure S11: WST-1 standard curve of IGF-I (n=3).

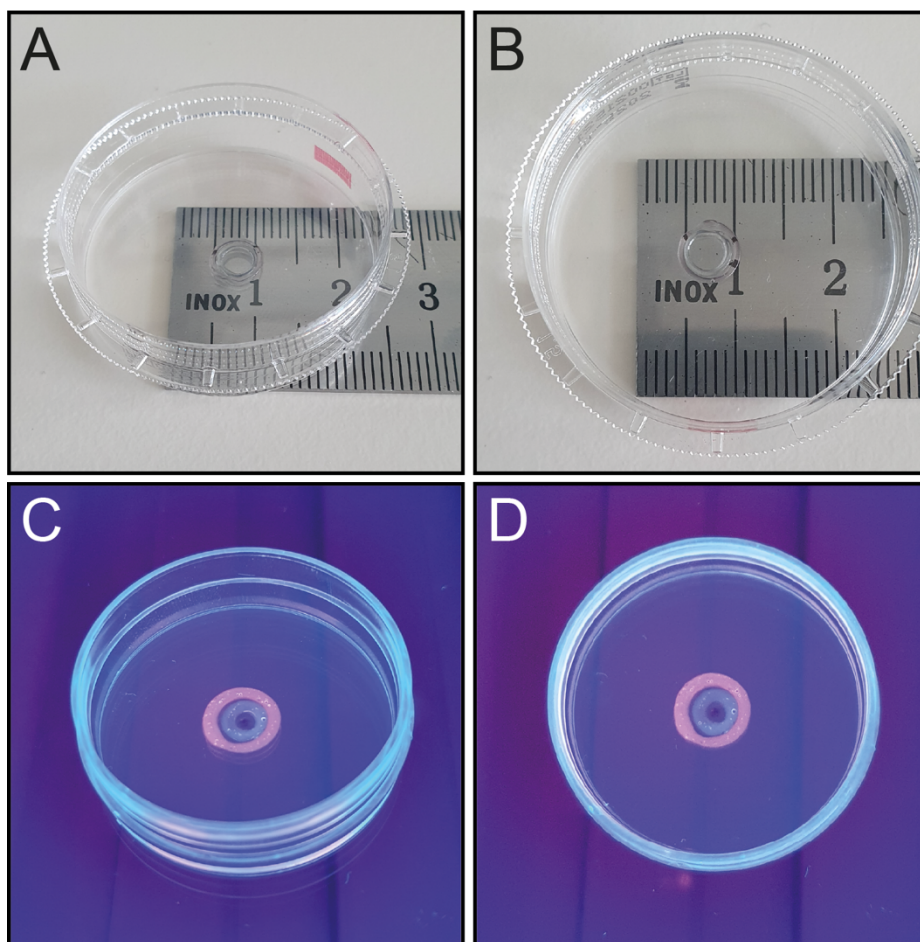


Figure S12: (A-B) 3D printed construct with IGF-PSL-POx-b-POzi. (C-D) 3D printed construct with IGF-PSL-POx-b-POzi (green) visualized via NHS-labelling with NHS Alexa Fluor™ 488 and Texas Red C2 Maleimide™ (red; P-Fu modified via Diels-Alder chemistry)

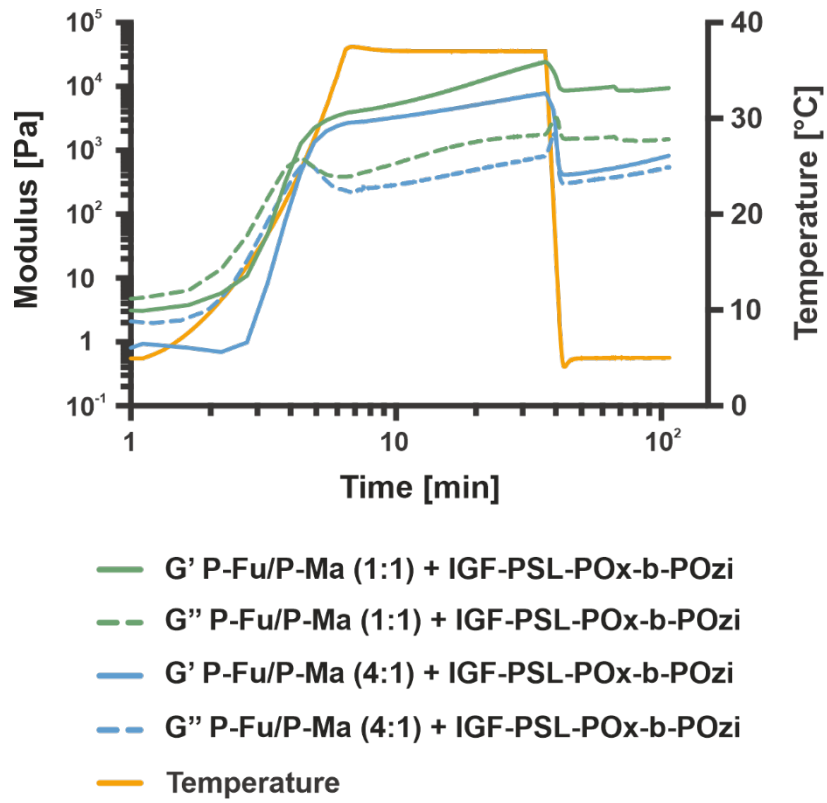


Figure S13: Chemical cross-linking of POx-b-POzi hydrogels with IGF-PSL-POx-b-POzi in the temperature range of 5 to 37 °C at 25 wt.% aqueous solutions.

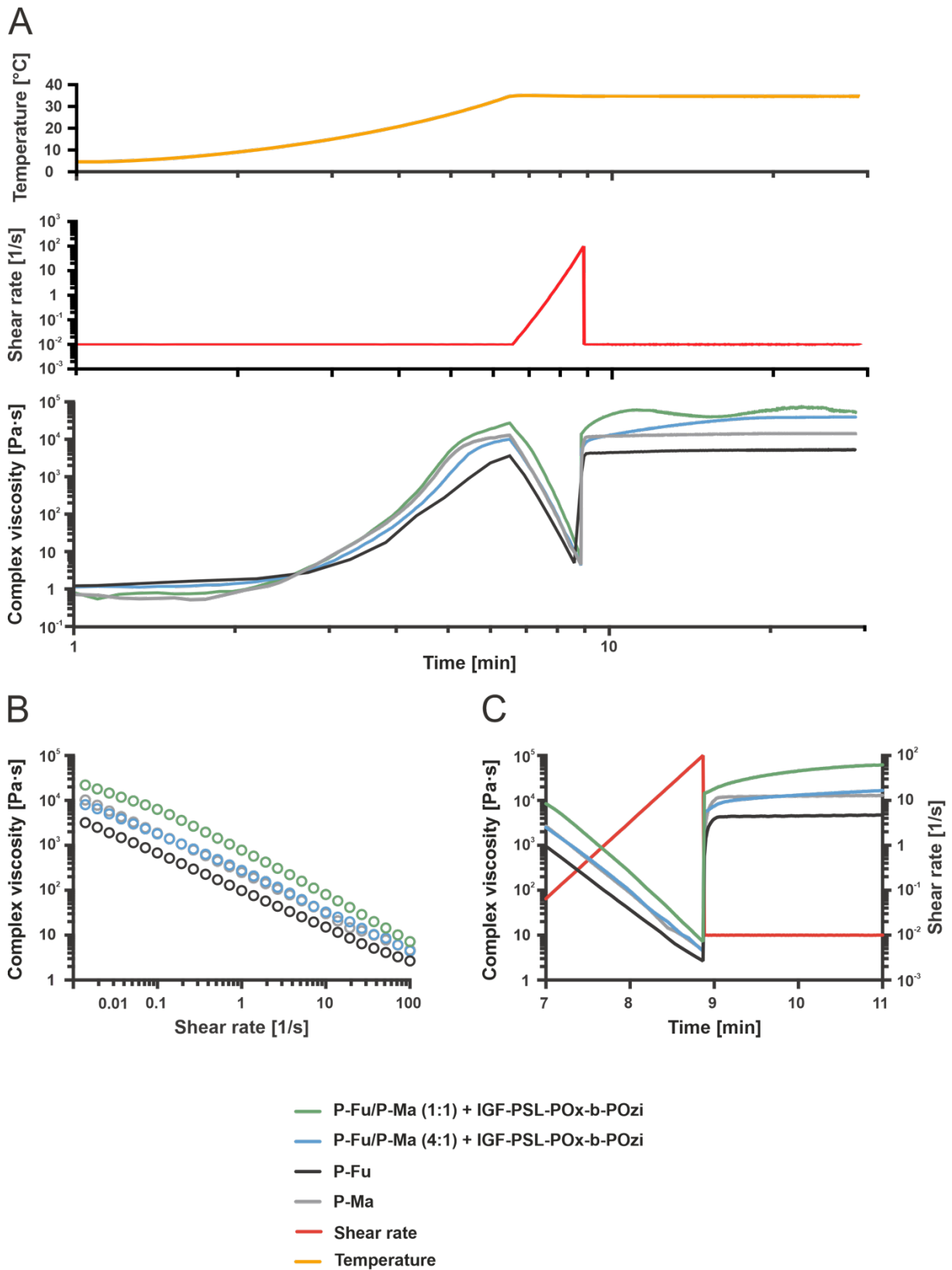
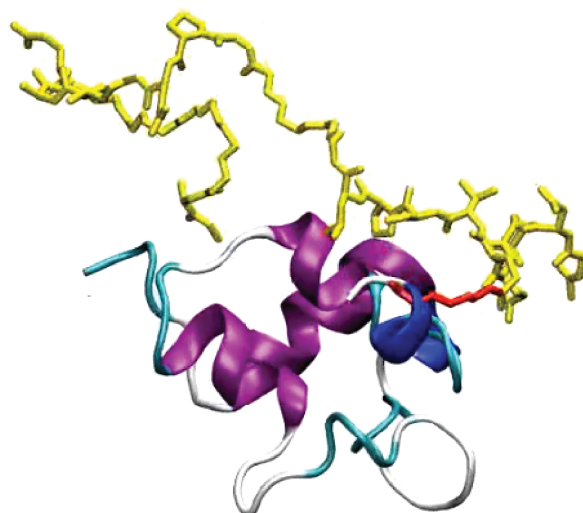


Figure S14: Rheological measurements of POx-b-POzi hydrogels simulating a printing process with and without the addition of IGF-PSL-POx-b-POzi. (A) Overview over the whole process. (B) Shear thinning behaviour of the the POx-b-POzi hydrogels. (C) Recovery of POx-b-POzi hydrogels.



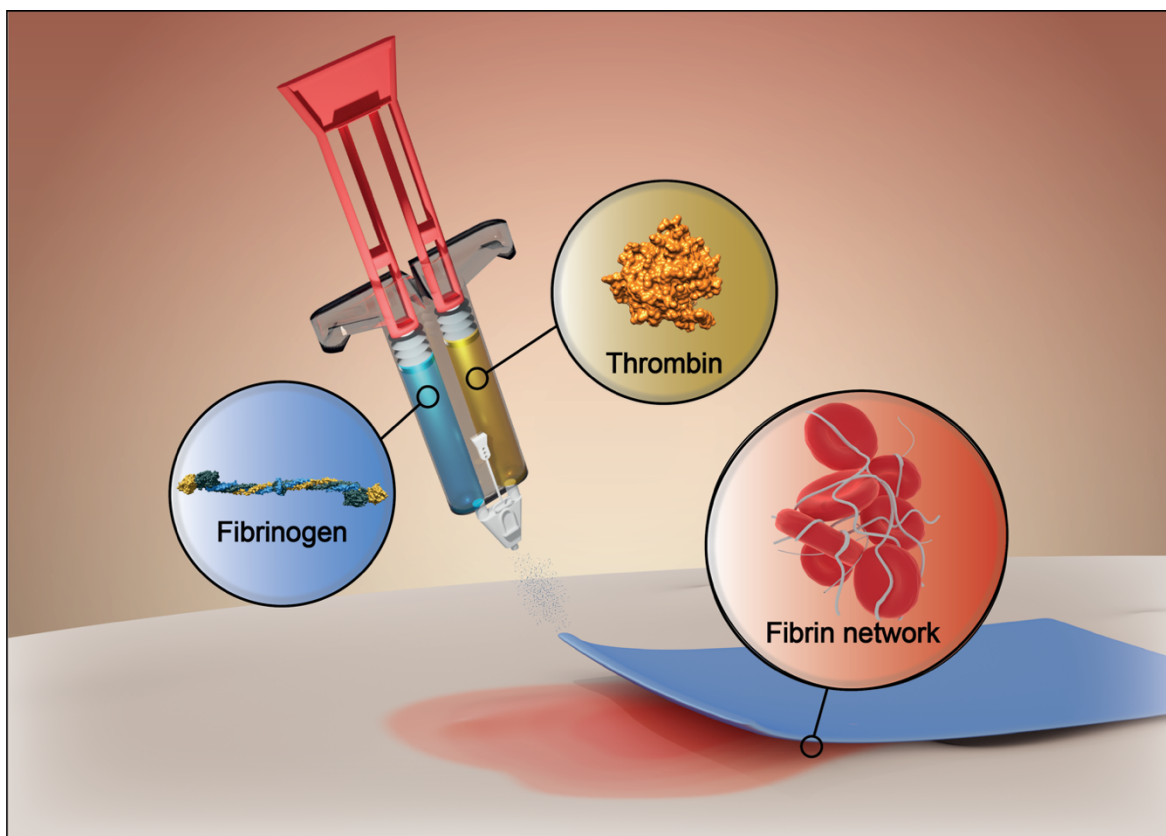
Video S1: Dynamics of PSL-bound IGF-I. IGF-I is shown in ribbon presentation (colored according to the initial secondary structure), the PSL is shown in yellow stick presentation, and the isopeptide bond in red. The data corresponds to 1 μ s simulation time from simulation run 1. Motions of the protein are smoothed over 5 time frames to improve visual impression.

6. Chapter 3: Fibrin Sealants – Today and Tomorrow

Matthias Beudert¹, Marcus Gutmann¹, Tessa Lühmann¹, Lorenz Meinel^{1,2}

¹Institute of Pharmacy and Food Chemistry, Julius-Maximilians-University Würzburg, Am Hubland, 97074 Würzburg, Germany

²Helmholtz Institute for RNA-based Infection Research, Josef-Schneider-Straße 2, DE-97080 Würzburg, Germany



This following article was reprinted with permission from ACS Biomaterials Science & Engineering, 2022, 8 (6), 2220-2231 DOI: 10.1021/acsbomaterials.1c01437. Copyright © 2022 American Chemical Society.

Fibrin Sealants: Challenges and Solutions

Matthias Beudert, Marcus Gutmann, Tessa Lühmann, and Lorenz Meinel*

Cite This: *ACS Biomater. Sci. Eng.* 2022, 8, 2220–2231

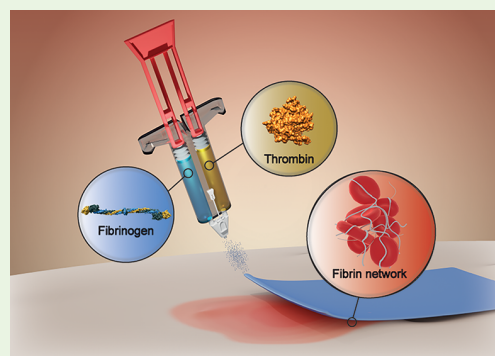
Read Online

ACCESS |

Metrics & More

Article Recommendations

ABSTRACT: Intraoperative bleeding and postoperative bleeding are major surgical complications. Tissue sealants, hemostats, and adhesives provide the armamentarium for establishing hemostatic balance, including the tissue sealant fibrin. Fibrin sealants combine advantages including instantaneous effect, biocompatibility, and biodegradability. However, several challenges remain. This review summarizes current fibrin product generations and highlights new trends and potential strategies for future improvement.



KEYWORDS: fibrin, fibrinogen, sealant, glue, hemostasis, medical device, surgery

INTRODUCTION

An estimated 313 million surgeries are performed globally every year.¹ The risk of bleeding during surgery contributes to elevated morbidity and mortality,² leading up to 20%, e.g., in elective vascular surgeries,^{3,4} following hepatotectomy,^{5–8} or during cardiac surgery.⁹ As a result, bleeding or hemorrhage is a major driver of societal health burden and healthcare costs.^{9–11} Bleeding is controlled by different medical devices, including sutures, clips, and staples, with estimated annual sales of up to \$15 billion by 2024.¹² However, in spite of their general use, challenges remain, including increased application times, accuracy, cosmetic aspects, and bacterial colonization.^{12–15}

Furthermore, tissue sealants, adhesives, and hemostats are available to prevent drainage from wounds, connect tissue ends, or support blood hemostasis. Proper material selection among these options is critical for adequate wound healing.^{16,17} The emerging importance of adhesives and sealants is reflected by a market volume with a value of \$10.3 billion in 2020 and a projected compound annual growth rate of 5.6%.¹⁸ In contrast to sutures, staples, etc., success with these materials and particularly for hemostats is jeopardized by the remaining mobility of the wound and resulting instability risks.¹² Even though more and more new approaches are being developed,^{19,20} the translation to the clinic has been a major problem limiting treatment options to a handful of clinically approved adhesives today.^{21–29} Reflecting missing alternatives, the gold standard, and last resort, is blood transfusion.²⁰

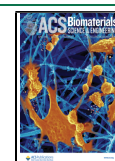
HEMOSTASIS

Limiting blood loss after injury, hemostasis is essential for survival. Hemostasis (i) enables rapid closure of blood vessels while (ii) maintaining blood flow in the circulation and finally (iii) removal of the clot after vessel repair.^{30,31} Hemostasis was previously categorized as primary (platelet activation) and secondary (coagulation), but it is a simultaneous interplay between platelet responses, coagulation proteins, and components of the vessel wall.^{30,32–34} Nowadays, a cell-based model is frequently cited, consisting of three different and overlapping phases (initiation phase, amplification phase, and propagation phase; Figure 1).^{33,35–39} After injury of a vessel wall, platelet adhesion and aggregation occur at the damaged site through interactions of platelet receptors with extracellular ligands and soluble proteins (primary hemostasis).^{40–42} Simultaneously, exposure of subendothelial tissue factors (TFs) at the injury site results in the activation of coagulation factors leading to activation, adhesion, and aggregation of both preexisting and circulating platelets (secondary hemostasis).^{40,42,43} Repetitive loops in the coagulation system and platelet activation produce large amounts of fibrin that stabilize previously formed platelet thrombi.⁴⁴ One of the major players in hemostasis is factor XIII, which catalyzes the formation of covalent cross-links

Received: November 12, 2021

Accepted: May 13, 2022

Published: May 24, 2022



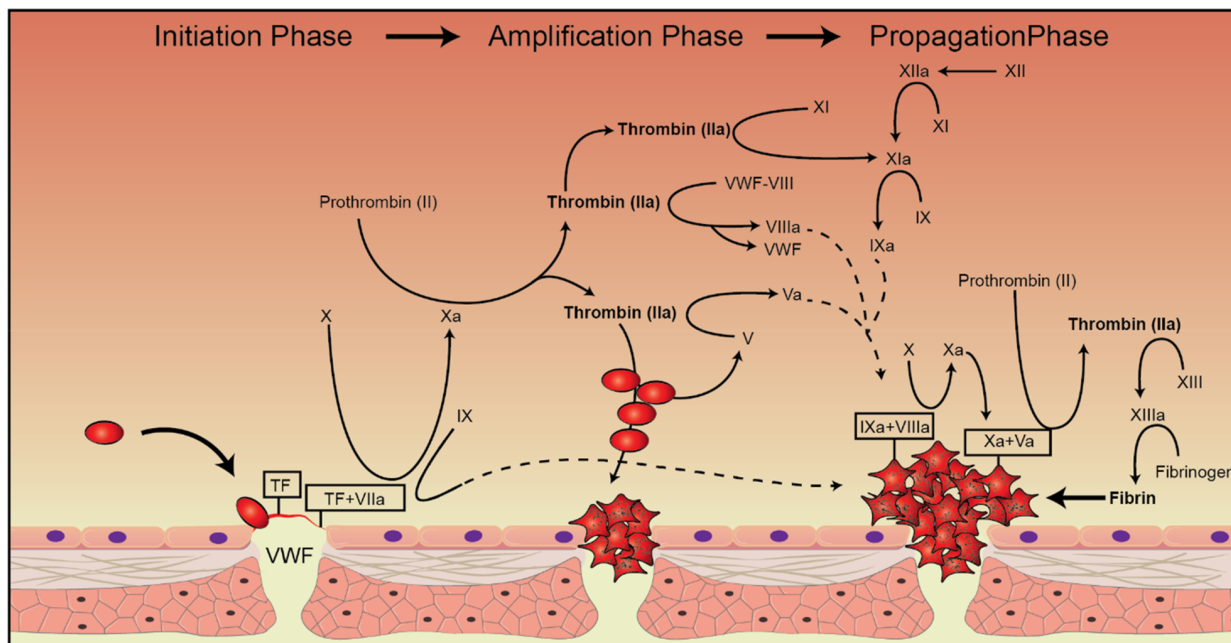


Figure 1. Scheme of cell surface based hemostasis. In the initiation phase, tissue factor (TF) expressing cells are exposed to the coagulation factors and initiate thrombosis by recruiting platelets to the site. The simultaneously formed TF–factor VIIa (FVIIa) complex activates coagulation factor (FIX and FX) generating a small amount of thrombin. In the amplification phase, thrombin acts as a signal for further platelet activation and aggregation as well as a signal for VWF, FVIII, and FXI activation. In the propagation phase the FIX–FVIII complex is formed on the platelet surface, activating FX–FV complex, accelerating thrombin activation and the activation of fibrinogen to fibrin.^{30,33,40}

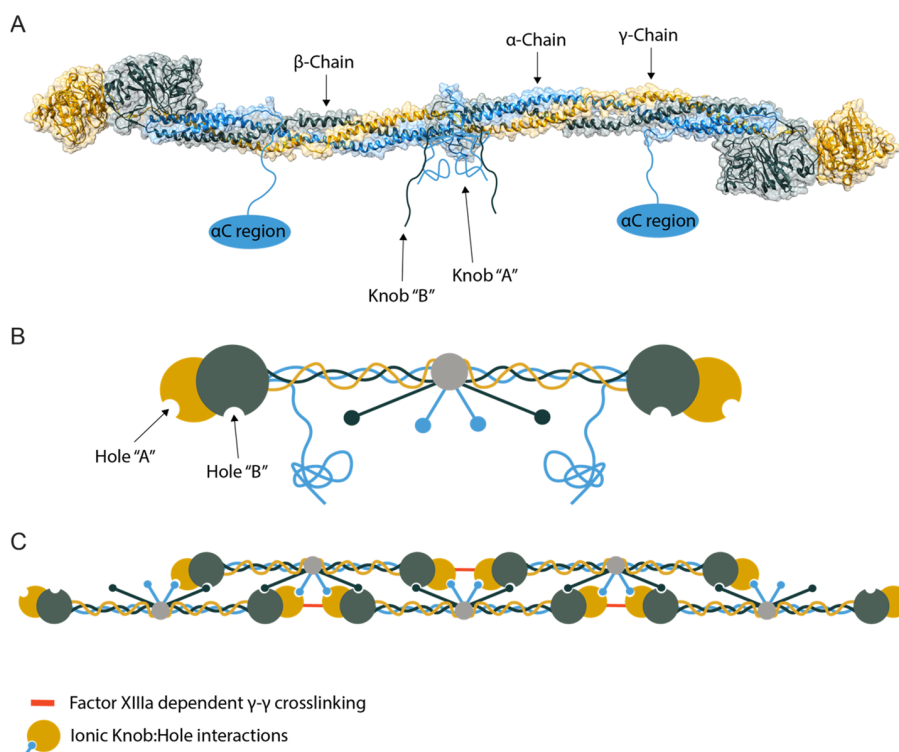


Figure 2. Overview of the polymerization of fibrinogen to fibrin fibers. (A) Crystal structure of human fibrinogen (PDB 3GHG) with the addition of the C- and N-terminal regions of the α -chain and the N-terminal regions of the β -chain that are missing in the crystal structure. (B) Abstraction of fibrinogen from its crystal structure. (C) Fibrin polymerization: In the beginning the α C-region is cleaved by plasmin and the so-called fragment X is formed. After the cleavage of both FpA and FpB by thrombin, knobs A and B are exposed and form knob:hole bonds through ionic interactions. Simultaneously, covalent γ – γ interactions are formed stimulated by factor XIIIa leading to the formation of a fibrin network. (C) From ref 66. CC BY 4.0.

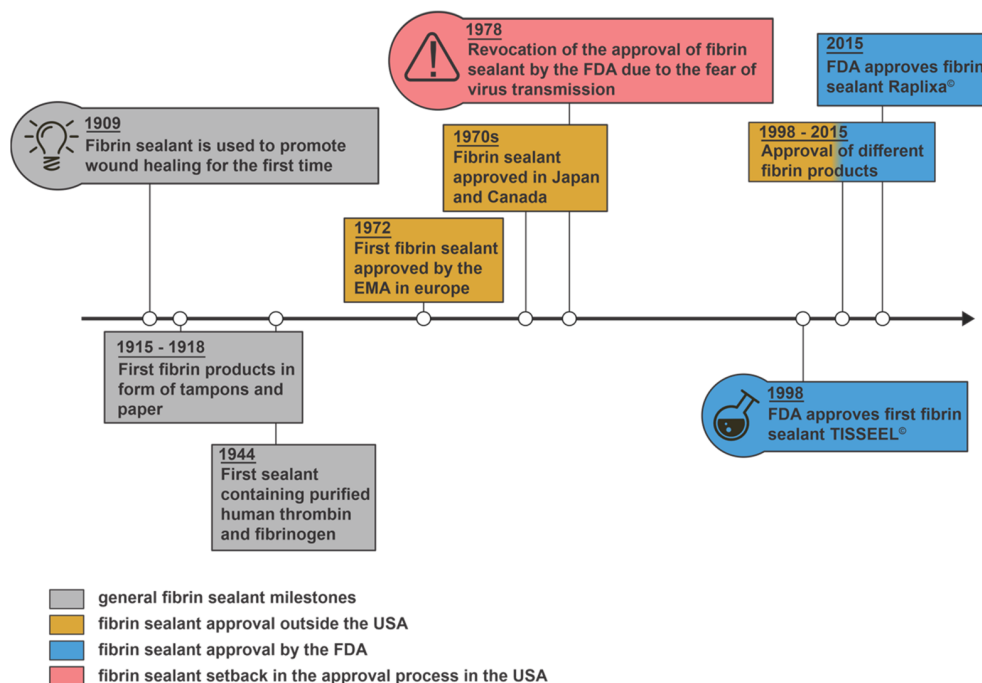


Figure 3. Timeline with milestones in the history of fibrin-based sealants, adhesives, and hemostats.^{28,72–77}

between soluble fibrinogen, to form a fibrinogen network, and plasmin, which acts as an opposing player to factor XIII to degrade the fibrinogen network.^{45,46}

■ FIBRINOGEN AND ITS ROLE IN NATURE

Efficient hemostasis is vital for all vertebrates sharing the basic mechanism that leads to blood coagulation. All important factors in the mammalian hemostasis originate from the reduplication and differentiation of a vitamin K dependent serine protease comprised of either the (i) Gla-EGF1-EGF2-SP or (ii) A1-A2-B-A3-C1-C2 domain, including thrombin.^{47,48} Strategies for balancing blood coagulation, including prothrombin and fibrinogen, are similar within the phylum Chordata.^{47,49–52} For example, the homology of full-length prothrombin is 69% between humans and zebrafish and around 50% between humans and hagfish, with homology being defined as at least 30% identical sequence. In comparison, cytochrome *c* oxidase, a key player in ATP synthesis, shows a sequence similarity of around 50% between different organisms and is seen as homologous among species.^{47,53,54} Fibrinogen has also been purified from the plasma of lamprey.^{55–57} Structural analysis of the isolated D-fragment of lamprey fibrinogen showed structural conservation compared to human fibrinogen.⁵⁸ The cDNA sequence analysis revealed that the α -chain showed 37% similarity and the β - and γ -chains are highly conserved with 67% similarity.⁴⁷

The conversion of fibrinogen to fibrin is key to blood coagulation (Figure 2). Fibrinogen is an α -helical protein with three subunits: $\alpha\alpha$ -, $\beta\beta$ -, and γ -chains. In the native form, the protein is a hexamer consisting of two units of each of the described chains, bound together by five disulfide bridges at the N-terminus with an overall molecular weight of around 340 kDa.^{59–61} Exposure of the protein to thrombin, the final step of hemostasis, leads to the elimination of fibrinopeptide A (FpA) in the N-terminus of the $\alpha\alpha$ -chain and fibrinopeptide B (FpB) in the $\beta\beta$ -chain. The elimination converts fibrinogen to

insoluble, clot-forming fibrin, which is additionally cross-linked by factor XIII.^{45,62–64} The coagulation of fibrin and its impact on wound closure and hemostasis were reviewed before.⁶⁵

■ FIBRIN SEALANT

Fibrin sealant was first approved by the FDA as a medical product in 1998. It is the only material licensed as a hemostat, tissue sealant, and wound adhesive (Figure 3).^{28,67,68} Fibrinogen and thrombin are the functional components of the sealant, resulting in the formation of hemostatic fibrin after administration. Marketed products (Table 1) are often based on these two components. Still, they differ in fibrinogen and thrombin concentrations to accommodate for mechanical strength requirements or to modulate the polymerization dynamics of the sealants.⁶⁹

There are various fibrinogen concentrations in the different products ranging from 18 to 106 mg/mL (Table 2). The concentration of fibrinogen directly influences the mechanical properties of the network, with higher concentrations resulting in higher mechanical strength. Furthermore, the addition of factor XIII affects mechanical properties by introducing covalent cross-links between fibrinogen molecules and greater tensile strength.⁷⁰ In contrast, the thrombin concentration has a big impact on the polymerization rate. Both commercially available products from Baxter—Tisseel and Artiss—share the same components in the formulation. However, Artiss contains only around 4 IU/mL thrombin in contrast to about 500 IU/mL for Tisseel. Consequently, prolonged clotting times are established by Artiss as compared to Tisseel.⁷¹

The fast fibrin clotting kinetics resulting from thorough mixing of thrombin and fibrinogen, and subsequent application to the injury site must be controlled by application devices to deposit homogeneous and reproducibly formed fibrin clots.⁷⁸ These challenges fueled the development of different application devices.

Table 1. Fibrin Sealants Currently Approved by the FDA and EMA^{a,b}

name	manufacturer	components	indication	accessories	authorization	issued	ref
Tisseel	Baxter Healthcare Corp.	HF, HT, aprotinin, CaCl ₂	hemostat	spray set	1998: cardiopulmonary bypass, splenic injuries 2012: general surgeries 1998: colonic anastomosis 1998	FDA	99
Beriplast P	CSL Behring GmbH	HF, HT, factor XIII, aprotinin, CaCl ₂	sealant hemostat	Pantajet		EMA	100
Evicel	Omnix Biopharmaceutical Ltd.	HF, HT	hemostat	Catheject spray tip spray or syringe ¹⁰¹	2017 2003: liver surgery	FDA FDA	65 102
TachoSil	Nycomed Danmark ApS (as of 2019 Ethicon)	HF, HT	hemostat	patch ¹⁰⁶	2007: vascular surgery 2008: general surgery 2008: vascular surgery 2004: cardiovascular surgery	EMA EMA EMA EMA	103 104 105 107
Cryoseal	ThermoGenesis	autologous fibrinogen	hemostat, sealant	device to produce fibrinogen and thrombin from human plasma; spray and drop tips for application	2016: neurological surgery 2010: cardiovascular surgery 2007: adjunct to hemostasis during liver resection	EMA FDA FDA	108 109 110, 111
Artiss	Baxter Healthcare Corp.	HF, HT, aprotinin, CaCl ₂	adhesive	spray set ¹¹²	2008: autologous skin grafts	FDA	113
RiaSTAP	CSL Behring GmbH	HF	face-lift hemostat	lyophilizate	2011: facial rhytidectomy surgery 2009: acute bleeding episodes in patients with congenital fibrinogen deficiency	FDA	114 115
Fibryna/Fibryga	Octapharma Pharm. Prod.	HF	hemostat	lyophilizate	2017: treatment of acute bleeding episodes in adults and adolescents with congenital fibrinogen deficiency	FDA	116–118
Vivostat	Vivostat A/S	autologous fibrinogen	hemostat, sealant	spray			65
Evarrest	Ethicon	HF, HT	hemostat	patch	2012: retroperitoneal, intra-abdominal, pelvic and noncardiac thoracic surgeries 2015: adult liver surgery 2015: general surgery ⁷⁸	FDA FDA	119 120 77, 121, 122
Raplixa	The Medicines Co.	HF, HT	hemostasis	spray	2017: vascular surgery	EMA	123, 124
VeraSeal/Vistaseal	Instituto Grifols/Ethicon	HF, HT	hemostasis	spray, syringe ¹²³			

^aFrom ref 65. CC BY 4.0. ^bHF, human fibrinogen; HT, human thrombin.

Table 2. Components of Fibrin Sealants Currently Approved by the FDA and EMA^{65,70,79,101,106,112,122,123,125–128}

name	fibrinogen	thrombin	factor XIII	plasmin inhibitor	excipients
Tisseel	67–106 mg/mL	400–625 IU/mL	0.6–5 IU/mL	aprotinin, 2250–3750 KIU/mL	histidine; human albumin; NaCl; niacinamide; polysorbate 80; trisodium citrate
Artiss	67–106 mg/mL	2.5–6.5 IU/mL	0.6–5 IU/mL	aprotinin, 2250–3750 KIU/mL	histidine; human albumin; NaCl; niacinamide; polysorbate 80; trisodium citrate
Evicel	55–85 mg/mL	800–1200 IU/mL	9 IU/mL ^a		arginine HCl, CaCl ₂ ; glycine; human albumin; NaCl; mannitol; sodium acetate; sodium citrate
Raplix	79 mg/g	699 IU/g			CaCl ₂ ; human albumin, L-arginine HCl; NaCl; sodium citrate; trehalose
VistaSeal/VeraSeal	80 mg/mL	500 IU/mL			arginine; CaCl ₂ ; glutamic acid monosodium; glycine; human albumin; isoleucine; NaCl; sodium citrate dihydrate
Berioplast P	90 mg/mL	500 IU/mL	60 U/mL (40–80)	aprotinin, 1000 KIU/mL	human albumin; L-arginine HCl; L-isoleucine; NaCl; sodium citrate dihydrate; sodium L-glutamate monohydrate
Fibryna/Fibryga	20 mg/mL				L-arginine HCl; glycine; NaCl; sodium citrate dihydrate
RiaSTAP	18–26 mg/mL				albumin; arginine, hydrochloride; NaCl; sodium citrate; sodium hydroxide
Evarrest	8.6 mg/cm ²	37.5 U cm ²			arginine hydrochloride; CaCl ₂ ; glycine; human albumin; mannitol; sodium acetate; NaCl; sodium citrate
TachoSil	3.6–7.4 mg/cm ²	1.3–2.7 U/cm ²			human albumin; equine collagen; L-arginine hydrochloride; NaCl; riboflavin (E101); sodium citrate
Cryoseal	N/A				
Vivostat	N/A				

^aFactor XIII is not listed as a component by Omrix Biopharmaceuticals Ltd. Value taken from the literature.⁷⁰

A frequently used system is a dual-syringe applicator system in which thrombin and fibrinogen are separated in two different chambers during storage (Tisseel, Baxter). The device was further developed by integrating a gas connection for carbon dioxide insufflation of the abdomen for laparoscopic procedures.^{79–81} Other devices combine the collection of autologous blood components and their application.⁸² For example, the Vivostat system facilitates the preparation of autologous fibrin sealants. It combines the preparation of a fibrin sealant from whole blood and an electromechanical applicator unit delivering a liquid spray under sensor control for exact dosing of the individual sealant components. Furthermore, this system was used for the coadministration of drug substances such as fibroblast growth factor 2 to stimulate fibroblast proliferation during tissue regeneration.^{83–85} Raplix applies both fibrinogen and thrombin as a powder spray, driven by a gas flow generator with an agitator by which the components are directly deposited onto the injury site.^{86–88} This powder approach has advantages compared to liquid fibrin glues in that the components are stable at room temperature (Figure 4).^{89,90} Another recently approved product is a fibrin patch for wound sutures called Evarrest (Ethicon, Inc.). It combines bioresorbable suture components (Vicryl and poly(lactide-co-glycolide)) with a cellulose matrix being coated with both human fibrinogen and human thrombin.^{91–93} Upon contact with wound fluids, the forming fibrin clot integrates the patch into the wound. For detailed reviews of the clinical applications and the performances of the different fibrin sealants, we direct the reader to excellent articles.^{67,68,94–98}

■ CURRENT CHALLENGES AND SOLUTIONS

When fibrin adhesives are used, several drug risks and warnings must be taken into account. In addition to the adverse effects observed in clinical studies, there are also some warnings and instructions for the application of fibrin glues.^{129,130} The warnings and instructions for use include, above all, the risk of

thrombosis in the case of intravascular administration, hypersensitivity reactions, and gas or air embolism in the use of spray devices.¹³¹ For discussion on the pricing critique of vendors, we refer to previous contributions.^{28,132} Fibrinogen obtained from human plasma has a risk of disease transmission.^{76,132,133} Viral contamination is expected in only about 1 vial in 10¹⁵ for viruses such as human immunodeficiency virus (HIV) or hepatitis B virus (HBC) and higher for parvovirus (HPV) B19 with 1 contaminated vial in 500 000.¹³⁴ Studies linked such contamination to increased infection rates seen in patients receiving fibrin glues compared to naive subjects.¹³⁵ This viral risk can be met by recombinant production. Unfortunately, biotechnological production is quite challenging, as fibrinogen is large and has a complex structure with 29 inter- and intrachain disulfide bridges and a complex glycosylation pattern.^{136–139} Consequently, *Escherichia coli* is a nonideal vector to meet these demands.¹³⁹ Functional recombinant fibrinogen was collected from the milk of transgenic mice and cows.^{140–142} In spite of its success, this approach was discussed regarding zoonotic risks and ethical concerns.^{143,144} Large-scale production of recombinant fibrinogen in mammalian cell based protein expression systems is also challenging. One difficulty is the stability of the α -chain during cell culture.¹⁴⁵ One expression system containing all three chains— α -, β -, and γ -chains—on one vector was developed as a stable cell line, and a reasonable yield of up to 1.3 g/L was reported.¹⁴³ In addition to that contribution,¹⁴³ many patents/patent applications provide essential information on recombinant fibrinogen production (Table 3), also highlighting one crucial aspect, which is the protection of the α -chain from proteolysis during culture.¹⁴⁶

Typically, fibrin adhesives rapidly degrade *in vivo* through plasmin proteolysis, at least partially catalyzed by plasminogen. Furthermore, plasminogen is a common byproduct in current fibrin glues derived from human material and may contribute to rapid breakdown.^{159–162} To meet these challenges, the 6.5 kDa serine protease inhibitor aprotinin was incorporated into

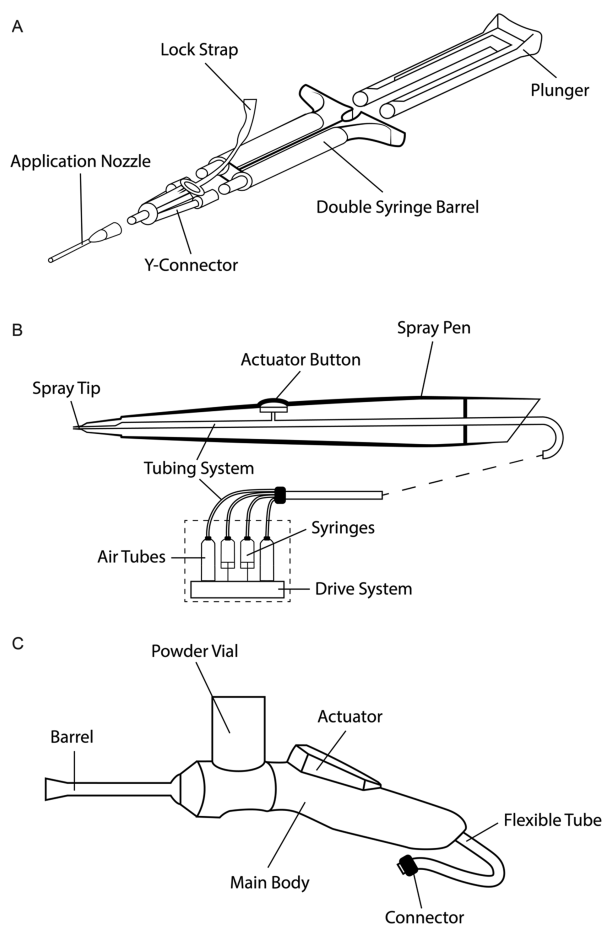


Figure 4. Designs of different fibrin sealant applicators. (A) Dual-syringe system DUO SET by Baxter. Adapted with permission from ref 79. Copyright 2013 Baxter Healthcare Corp. (B) Vivo Spraypen and electromechanical applicator drive system Vivostat developed by Vivostat A/S. Adapted with permission from ref 83. Copyright 2001 Garbasch et al. (C) Design of RaplixaSpray by Ethicon.⁸⁷ Adapted with permission from ref 87. Copyright 2010 Greenhalgh et al.

the formulation (e.g., Baxter's Tisseel) delaying fibrinolysis (Tables 1 and 2).^{163–165} Aprotinin has reported rare side effects, including allergic or anaphylactic reactions.^{166–169} The control of early fibrinolysis by aprotinin is further limited in tissues with high fibrinolytic activity. Recently, it has been shown that the addition of elastin inhibitors effectively hampers early fibrinolysis even without aprotinin.¹⁷⁰ Furthermore, the delaying impact of inhibitors on fibrinolysis is limited by rapid diffusion from the fibrin glue.¹⁷¹ One study successfully addressed this challenge by localizing aprotinin or tranexamic acid (TA), another plasmin inhibitor, within biodegradable microspheres supplemented into the fibrin glue and from which the inhibitors were released in a sustained manner.¹⁷² Another successful strategy was the covalent decoration of fibrinogen with aprotinin,¹⁷³ which was further refined by presenting aprotinin bound to a transglutaminase-responsive peptide sequence. This aprotinin-containing peptide sequence was bound to fibrin in the clot, catalyzed by transglutaminases present in the fibrin clot.^{159,174,175} A different strategy for delaying the diffusion of aprotinin was the covalent attachment to fibronectin and mixing of the conjugate with fibrinogen prior to gelation.¹⁷⁶

Table 3. Selected Patents/Patent Applications Covering the Recombinant Production of Fibrinogen

organism	patent number	title	date	description	ref
yeast	WO 1996007728 A1	production and secretion of recombinant fibrinogen by yeast	1996	production of recombinant fibrinogen, variants, and subunits	147
	JP 2004016055 A	method for producing recombinant fibrinogen	2004	production of fibrinogen in <i>Pichia</i> yeast	148
transgenic animal	CA 2347579 A1	transgenic fibrinogen	1995	production of fibrinogen, modified fibrinogen, or fibrinogen fusion proteins in lactating transgenic animal	149
	US 20060174357 A1	transgenic fibrinogen	2006	production of recombinant fibrinogen or modified fibrinogen variants in mammalian glands	150
silkworm	EP 0744891 B1	transgenic fibrinogen	2007	nonhuman mammalian animal with stable expression of human fibrinogen	151
	US 20130345401 A1	fibrinogen-producing transgenic silkworm	2013	production of fibrinogen at low cost with coagulation activity	152
mammalian cells	US 6037457 A	method for recombinant fibrinogen production	2000	production of recombinant fibrinogen in a long-term mammalian cell culture system	153
	US 6083902 A	recombinant fibrin chains, fibrin, and fibrin homologues	2000	production of fibrin, fibrin homologues, and fibrinogen analogues	154
	US 10208101 B2	recombinant fibrinogen high-production line and method for producing the same	2019	recombinant production of fibrinogen by coexpressing fibrinogen and α 2-plasmin inhibitor and/or plasminogen activator inhibitor-2	155
human embryonic kidney 293 cell line	US 20100151522 A1	process for producing recombinant fibrinogen highly producing cell and highly producing cell	2010	highly producing cell line for recombinant fibrinogen due to alterations in subunit ratio and use of baculovirus P3S gene	156
	US 20100159512 A1	method for preparation of recombinant human thrombin and fibrinogen	2010	production and novel preparation of recombinant fibrinogen and thrombin for increased safety	157
Chinese hamster ovary (CHO) cells	US 20170037108 A1	recombinant fibrinogen	2017	optimized nucleotide sequences for expression of fibrinogen in eukaryotic cell culture systems	145
Chinese hamster ovary (CHO) cells	WO 2018161135 A1	fibrin glue of recombinant origin	2018	high production of recombinant fibrinogen by coexpression of ERp57	158

Another possibility is the use of bivalent modulating hemostasis and thrombosis.¹⁷⁷ Zn²⁺ reduces plasminogen activation by tPA and fibrin degradation by plasmin.¹⁷⁸

Furthermore, enhancing fibrin fibrils' structure by adding polyphosphates (PolyP) increases the stability of fibrin clots toward plasmin degradation.¹⁷⁹

Even though clinical studies have shown the benefits of fibrin sealants, these products are still used more selectively than routinely in the clinics. One future strategy to further improve and increase the use of fibrin sealants could build on targeted incorporation of biological cues into fibrinogen to adapt and tune the properties of the sealants. One of the advantages of fibrinogen is its ability to bind biomolecules such as growth factors (VEGF or BMP) or drugs either transiently by fibrinogen's heparin-binding domains or covalently by transglutaminase.^{65,180–183} Upon release, these moieties stimulate cells and improve tissue regeneration, which is one of the reasons why this material has also been extensively studied as a biomaterial in tissue engineering.^{184–186} Transglutaminase-responsive sequences could be used for site specific fibrinogen decoration with other polymers to modulate the mechanical properties of fibrin gels, depending on the applications. However, this approach of covalent coupling to fibrinogen is restricted to specific sites within the protein for transglutaminase-catalyzed binding. To expand from this site to other sites, one strategy is the recombinant, site-directed integration of unnatural amino acids by using an expanded genetic code expansion during recombinant protein expression.^{187–191} The great potential of such approaches is the batch-to-batch reproducibility of homogeneous bioconjugates, with quality and analytical advantages.

CONCLUSION

Fibrin glues have been used for decades with enormous needs, as reflected by an estimated compound annual growth rate exceeding 6.6%.¹⁹² Building on the initial FDA approval in 1998, many successful adaptations have been introduced, integrating progress in device development or fibrinolysis modulators to accommodate for both surgical challenges and improperly fast degradation, respectively. However, several challenges remain including bioburden and rapid mechanical stability loss. These challenges are met by research activities as reflected by a lasting intellectual property stream pointing toward promising new products in the future.

AUTHOR INFORMATION

Corresponding Author

Lorenz Meinel – Institute of Pharmacy and Food Chemistry, Julius-Maximilians-University Würzburg, 97074 Würzburg, Germany; Helmholtz Institute for RNA-based Infection Research, 97080 Würzburg, Germany; orcid.org/0000-0002-7549-7627; Email: lorenz.meinel@uni-wuerzburg.de

Authors

Matthias Beudert – Institute of Pharmacy and Food Chemistry, Julius-Maximilians-University Würzburg, 97074 Würzburg, Germany; orcid.org/0000-0002-6981-5107

Marcus Gutmann – Institute of Pharmacy and Food Chemistry, Julius-Maximilians-University Würzburg, 97074 Würzburg, Germany; orcid.org/0000-0001-6000-7923

Tessa Lühmann – Institute of Pharmacy and Food Chemistry, Julius-Maximilians-University Würzburg, 97074 Würzburg, Germany; orcid.org/0000-0001-7552-6435

Complete contact information is available at:
<https://pubs.acs.org/10.1021/acsbomaterials.1c01437>

Notes

The authors declare no competing financial interest.

ACKNOWLEDGMENTS

The authors gratefully acknowledge support by the Deutsche Forschungsgemeinschaft (DFG, German Research Foundation), Project No. 326998133-TRR225 (subproject A03).

REFERENCES

- (1) Meara, J. G.; Leather, A. J. M.; Hagander, L.; Alkire, B. C.; Alonso, N.; Ameh, E. A.; Bickler, S. W.; Conteh, L.; Dare, A. J.; Davies, J.; Mérisier, E. D.; El-Halabi, S.; Farmer, P. E.; Gawande, A.; Gillies, R.; Greenberg, S. L. M.; Grimes, C. E.; Gruen, R. L.; Ismail, E. A.; Kamara, T. B.; Lavy, C.; Lundeg, G.; Mkandawire, N. C.; Raykar, N. P.; Riesel, J. N.; Rodas, E.; Rose, J.; Roy, N.; Shrimme, M. G.; Sullivan, R.; Verguet, S.; Watters, D.; Weiser, T. G.; Wilson, I. H.; Yamey, G.; Yip, W. Global Surgery 2030: evidence and solutions for achieving health, welfare, and economic development. *Lancet* **2015**, *386* (9993), 569–624.
- (2) Ramirez, M. G.; Castillo, G. F.; Ramirez, M. A. The Economic Burden of Bleeds and Transfusions in Selected Surgeries: A Retrospective Multi Center Analysis from the US Perspective. *Am. J. Biomed. Sci. Res.* **2019**, DOI: [10.34297/AJBSR.2019.02.000610](https://doi.org/10.34297/AJBSR.2019.02.000610).
- (3) Stokes, M. E.; Ye, X.; Shah, M.; Mercaldi, K.; Reynolds, M. W.; Rupnow, M. F. T.; Hammond, J. Impact of bleeding-related complications and/or blood product transfusions on hospital costs in inpatient surgical patients. *BMC Health Services Research* **2011**, *11* (1), 135.
- (4) Shander, A. Financial and clinical outcomes associated with surgical bleeding complications. *Surgery* **2007**, *142* (4), S20–S25.
- (5) Berrevoet, F.; de Hemptinne, B. Use of Topical Hemostatic Agents during Liver Resection. *Digestive Surgery* **2007**, *24* (4), 288–293.
- (6) Aldrighetti, L.; Pulitanò, C.; Arru, M.; Catena, M.; Finazzi, R.; Ferla, G. "Technological" approach versus clamp crushing technique for hepatic parenchymal transection: a comparative study. *J. Gastrointest Surg* **2006**, *10* (7), 974–9.
- (7) Girardis, M.; Busani, S.; Marietta, M. Severe bleeding in critical care. *Anaesthesia, Pain, Intensive Care and Emergency A.P.I.C.E.*; Gullo, A., Ed.; Springer: Milan, 2006; p 687.
- (8) Doci, R.; Gennari, L.; Bignami, P.; Montalto, F.; Morabito, A.; Bozzetti, F.; Bonalumi, M. G. Morbidity and mortality after hepatic resection of metastases from colorectal cancer. *Br J. Surg* **2005**, *82* (3), 377–81.
- (9) Al-Attar, N.; Johnston, S.; Jamous, N.; Mistry, S.; Ghosh, E.; Gangoli, G.; Danker, W.; Etter, K.; Ammann, E. Impact of bleeding complications on length of stay and critical care utilization in cardiac surgery patients in England. *J. Cardiothorac Surg* **2019**, *14* (1), 64.
- (10) Christensen, M. C.; Krapf, S.; Kempel, A.; von Heymann, C. Costs of excessive postoperative hemorrhage in cardiac surgery. *J. Thorac Cardiovasc Surg* **2009**, *138* (3), 687–93.
- (11) Biancari, F.; Brascia, D.; Onorati, F.; Reichart, D.; Perrotti, A.; Ruggieri, V. G.; Santarpino, G.; Maselli, D.; Mariscalco, G.; Gherli, R.; Rubino, A. S.; De Feo, M.; Gatti, G.; Santini, F.; Dalén, M.; Saccocci, M.; Kinnunen, E. M.; Airaksinen, J. K.; D'Errigo, P.; Rosato, S.; Nicolini, F. Prediction of severe bleeding after coronary surgery: the WILL-BLEED Risk Score. *Thromb Haemostasis* **2017**, *117* (3), 445–456.
- (12) Taboada, G. M.; Yang, K.; Pereira, M. J. N.; Liu, S. S.; Hu, Y.; Karp, J. M.; Artzi, N.; Lee, Y. Overcoming the translational barriers of tissue adhesives. *Nature Reviews Materials* **2020**, *5* (4), 310–329.
- (13) Matz, D.; Teuteberg, S.; Wiencierz, A.; Soysal, S. D.; Heizmann, O. Do antibacterial skin sutures reduce surgical site infections after elective open abdominal surgery? - Study protocol of a prospective, randomized controlled single center trial. *Trials* **2019**, *20* (1), 390.

- (14) Edmiston, C. E.; Krepel, C. J.; Marks, R. M.; Rossi, P. J.; Sanger, J.; Goldblatt, M.; Graham, M. B.; Rothenburger, S.; Collier, J.; Seabrook, G. R. Microbiology of Explanted Suture Segments from Infected and Noninfected Surgical Patients. *Journal of Clinical Microbiology* **2013**, *51* (2), 417.
- (15) Sanders, L.; Nagatomi, J. Clinical applications of surgical adhesives and sealants. *Crit Rev. Biomed Eng.* **2014**, *42* (3–4), 271–292.
- (16) Bhagat, V.; Becker, M. L. Degradable Adhesives for Surgery and Tissue Engineering. *Biomacromolecules* **2017**, *18* (10), 3009–3039.
- (17) Spotnitz, W. D.; Burks, S. State-of-the-art review: Hemostats, sealants, and adhesives II: Update as well as how and when to use the components of the surgical toolbox. *Clin Appl. Thromb Hemost* **2010**, *16* (5), 497–514.
- (18) Global Medical Adhesives and Sealants Industry. *Reportlinker*. https://www.reportlinker.com/p05478477/Global-Medical-Adhesives-and-Sealants-Industry.html?utm_source=GNW (accessed 2021-11-08).
- (19) di Lena, F. Hemostatic polymers: the concept, state of the art and perspectives. *J. Mater. Chem. B* **2014**, *2* (23), 3567–3577.
- (20) Hickman, D. A.; Pawlowski, C. L.; Sekhon, U. D. S.; Marks, J.; Gupta, A. S. Biomaterials and Advanced Technologies for Hemostatic Management of Bleeding. *Adv. Mater.* **2018**, *30* (4), 1700859.
- (21) Ethicon OMNEX Surgical Sealant - FDA Premarket Approval (PMA) P060029. U.S. Food and Drug Administration. <https://fda.report/PMA/P060029> (accessed 2021-11-08).
- (22) Premarket Approval (PMA) Cohera medical TISSUGLU. U.S. Food and Drug Administration. <https://www.accessdata.fda.gov/scripts/cdrh/cfdocs/cfpma/pma.cfm?id=P130023> (accessed 2021-11-08).
- (23) Premarket Approval (PMA) DuraSeal Dural EXACT Sealant System. U.S. Food and Drug Administration. <https://www.accessdata.fda.gov/scripts/cdrh/cfdocs/cfpma/pma.cfm?id=P040034S032> (accessed 2021-11-08).
- (24) Premarket Approval (PMA) FOCAL SEAL-L SYNTHETIC ABSORBABLE SEALANT. U.S. Food and Drug Administration. <https://www.accessdata.fda.gov/scripts/cdrh/cfdocs/cfpma/pma.cfm?id=P990028> (accessed 2021-11-08).
- (25) Premarket Approval (PMA) DERMABOND (A FORMULATION OF 2-OCTYL CYANOACRYLATE). U.S. Food and Drug Administration. <https://www.accessdata.fda.gov/scripts/cdrh/cfdocs/cfpma/pma.cfm?id=p960052> (accessed 2021-11-08).
- (26) Premarket Approval (PMA) Progel Pleural Air Leak Sealant (Progel PALS). U.S. Food and Drug Administration. <https://www.accessdata.fda.gov/scripts/cdrh/cfdocs/cfpma/pma.cfm?id=P010047S064> (accessed 2021-11-08).
- (27) Premarket Approval (PMA) BioGlue Surgical Adhesive. U.S. Food and Drug Administration. <https://www.accessdata.fda.gov/scripts/cdrh/cfdocs/cfpma/pma.cfm?id=P010003S037> (accessed 2021-11-08).
- (28) Mintz, P. D.; Mayers, L.; Avery, N.; Flanagan, H. L.; Burks, S. G.; Spotnitz, W. D. Fibrin sealant: clinical use and the development of the University of Virginia Tissue Adhesive Center. *Ann. Clin. Lab. Sci.* **2001**, *31* (1), 108–118.
- (29) Spotnitz, W. D.; Burks, S. Hemostats, sealants, and adhesives: components of the surgical toolbox. *Transfusion* **2008**, *48* (7), 1502–16.
- (30) Versteeg, H. H.; Heemsker, J. W.; Levi, M.; Reitsma, P. H. New fundamentals in hemostasis. *Physiol Rev.* **2013**, *93* (1), 327–58.
- (31) Ogedegbe, H. O. An Overview of Hemostasis. *Laboratory Medicine* **2002**, *33* (12), 948–953.
- (32) Lippi, G.; Favaloro, E. J. Hemostasis practice: state-of-the-art. *J. Lab. Precis. Med.* **2018**, *3*, 67.
- (33) De Caterina, R.; Husted, S.; Wallentin, L.; Andreotti, F.; Arnesen, H.; Bachmann, F.; Baigent, C.; Huber, K.; Jespersen, J.; Kristensen, S. D.; Lip, G. Y.; Morais, J.; Rasmussen, L. H.; Siegbahn, A.; Verheugt, F. W.; Weitz, J. I. General mechanisms of coagulation and targets of anticoagulants (Section I). Position Paper of the ESC Working Group on Thrombosis–Task Force on Anticoagulants in Heart Disease. *Thromb. Haemost.* **2013**, *109* (04), 569–579.
- (34) Hoffman, M. Remodeling the Blood Coagulation Cascade. *Journal of Thrombosis and Thrombolysis* **2003**, *16* (1), 17–20.
- (35) Bittar, L. F.; De Paula, E. V.; Barnabé, A.; Mazetto, B. M.; Zapponi, K. C. S.; Montalvão, S. A. L.; Colella, M. P.; Orsi, F. A.; Annichino-Bizzacchi, J. M. Plasma Factor VIII Levels as a Biomarker for Venous Thromboembolism. *Biomarkers in Cardiovascular Disease*; Patel, V., Preedy, V., Eds.; Springer: 2015; pp 1–19..
- (36) Monroe, D. M.; Hoffman, M. What does it take to make the perfect clot? *Arterioscler Thromb Vasc Biol.* **2006**, *26* (1), 41–8.
- (37) Roberts, H. R.; Hoffman, M.; Monroe, D. M. A cell-based model of thrombin generation. *Semin Thromb Hemost* **2006**, *32*, 032–038.
- (38) Mann, K. G.; Brummel, K.; Butenas, S. What is all that thrombin for? *J. Thromb Haemost* **2003**, *1* (7), 1504–14.
- (39) Adams, R. L.; Bird, R. J. Review article: Coagulation cascade and therapeutics update: relevance to nephrology. Part I: Overview of coagulation, thrombophilias and history of anticoagulants. *Nephrology (Carlton)* **2009**, *14* (5), 462–70.
- (40) Gale, A. J. Continuing education course #2: current understanding of hemostasis. *Toxicol Pathol* **2011**, *39* (1), 273–80.
- (41) Ghoshal, K.; Bhattacharyya, M. Overview of platelet physiology: its hemostatic and nonhemostatic role in disease pathogenesis. *Scientific World Journal* **2014**, *2014*, 781857.
- (42) Kuharsky, A. L.; Fogelson, A. L. Surface-Mediated Control of Blood Coagulation: The Role of Binding Site Densities and Platelet Deposition. *Biophys. J.* **2001**, *80* (3), 1050–1074.
- (43) Mackman, N. Role of tissue factor in hemostasis, thrombosis, and vascular development. *Arterioscler Thromb Vasc Biol.* **2004**, *24* (6), 1015–22.
- (44) Winter, W. E.; Flax, S. D.; Harris, N. S. Coagulation Testing in the Core Laboratory. *Laboratory Medicine* **2017**, *48* (4), 295–313.
- (45) Ariens, R. A.; Lai, T. S.; Weisel, J. W.; Greenberg, C. S.; Grant, P. J. Role of factor XIII in fibrin clot formation and effects of genetic polymorphisms. *Blood* **2002**, *100* (3), 743–54.
- (46) Chapin, J. C.; Hajjar, K. A. Fibrinolysis and the control of blood coagulation. *Blood Rev.* **2015**, *29* (1), 17–24.
- (47) Davidson, C. J.; Tuddenham, E. G.; McVey, J. H. 450 million years of hemostasis. *J. Thromb Haemost* **2003**, *1* (7), 1487–94.
- (48) Kim, S.; Carrillo, M.; Kulkarni, V.; Jagadeeswaran, P. Evolution of primary hemostasis in early vertebrates. *PLoS One* **2009**, *4* (12), e8403.
- (49) Doolittle, R. F.; Oncley, J. L.; Surgenor, D. M. Species differences in the interaction of thrombin and fibrinogen. *J. Biol. Chem.* **1962**, *237*, 3123–7.
- (50) Doolittle, R. F. Differences in the clotting of lamprey fibrinogen by lamprey and bovine thrombins. *Biochem. J.* **1965**, *94* (3), 735–41.
- (51) Jagadeeswaran, P.; Gregory, M.; Zhou, Y.; Zon, L.; Padmanabhan, K.; Hanumanthaiah, R. Characterization of Zebrafish Full-Length Prothrombin cDNA and Linkage Group Mapping. *Blood Cells, Molecules, and Diseases* **2000**, *26* (5), 479–489.
- (52) Banfield, D. K.; Irwin, D. M.; Walz, D. A.; MacGillivray, R. T. Evolution of prothrombin: isolation and characterization of the cDNAs encoding chicken and hagfish prothrombin. *J. Mol. Evol* **1994**, *38* (2), 177–87.
- (53) Popovic, D. M.; Leontyev, I. V.; Beech, D. G.; Stuchebrukhov, A. A. Similarity of cytochrome c oxidases in different organisms. *Proteins: Struct., Funct., Bioinf.* **2010**, *78* (12), 2691–2698.
- (54) Pearson, W. R. An introduction to sequence similarity (“homology”) searching. *Curr. Protoc. Bioinf.* **2013**, *42*, 3.1.1.
- (55) Wang, Y. Z.; Patterson, J.; Gray, J. E.; Yu, C.; Cottrell, B. A.; Shimizu, A.; Graham, D.; Riley, M.; Doolittle, R. F. Complete sequence of the lamprey fibrinogen alpha chain. *Biochemistry* **1989**, *28* (25), 9801–6.
- (56) Bohonus, V. L.; Doolittle, R. F.; Pontes, M.; Strong, D. D. Complementary DNA sequence of lamprey fibrinogen beta chain. *Biochemistry* **1986**, *25* (21), 6512–6.

- (57) Strong, D. D.; Moore, M.; Cottrell, B. A.; Bohonus, V. L.; Pontes, M.; Evans, B.; Riley, M.; Doolittle, R. F. Lamprey fibrinogen gamma chain: cloning, cDNA sequencing, and general characterization. *Biochemistry* **1985**, *24* (1), 92–101.
- (58) Yang, Z.; Spraggon, G.; Pandi, L.; Everse, S. J.; Riley, M.; Doolittle, R. F. Crystal Structure of Fragment D from Lamprey Fibrinogen Complexed with the Peptide Gly-His-Arg-Pro-amide. *Biochemistry* **2002**, *41* (32), 10218–10224.
- (59) Mosesson, M. W. Fibrinogen and fibrin structure and functions. *J. Thromb Haemost* **2005**, *3* (8), 1894–904.
- (60) Matsuda, M.; Sugo, T. Structure and function of human fibrinogen inferred from dysfibrinogens. *International Journal of Hematology* **2002**, *76* (1), 352–360.
- (61) Kollman, J. M.; Pandi, L.; Sawaya, M. R.; Riley, M.; Doolittle, R. F. Crystal Structure of Human Fibrinogen. *Biochemistry* **2009**, *48* (18), 3877–3886.
- (62) Greenberg, C. S.; Miraglia, C. C.; Rickles, F. R.; Shuman, M. A. Cleavage of blood coagulation factor XIII and fibrinogen by thrombin during in vitro clotting. *J. Clin Invest* **1985**, *75* (5), 1463–70.
- (63) Pechik, I.; Madrazo, J.; Mosesson, M. W.; Hernandez, I.; Gilliland, G. L.; Medved, L. Crystal structure of the complex between thrombin and the central "E" region of fibrin. *Proc. Natl. Acad. Sci. U. S. A.* **2004**, *101* (9), 2718–23.
- (64) Riedel, T.; Suttner, J.; Brynda, E.; Houska, M.; Medved, L.; Dyr, J. E. Fibrinopeptides A and B release in the process of surface fibrin formation. *Blood* **2011**, *117* (5), 1700–1706.
- (65) Roberts, I. V.; Bukhary, D.; Valdivieso, C. Y. L.; Tirelli, N. Fibrin Matrices as (Injectable) Biomaterials: Formation, Clinical Use, and Molecular Engineering. *Macromol. Biosci.* **2020**, *20* (1), 1900283.
- (66) Hudson, N. E. Biophysical Mechanisms Mediating Fibrin Fiber Lysis. *Biomed Res. Int.* **2017**, *2017*, 2748340.
- (67) Spotnitz, W. D. Fibrin Sealant: Past, Present, and Future: A Brief Review. *World Journal of Surgery* **2010**, *34* (4), 632–634.
- (68) Spotnitz, W. D. Fibrin Sealant: The Only Approved Hemostat, Sealant, and Adhesive—a Laboratory and Clinical Perspective. *ISRN Surg* **2014**, *2014*, 203943.
- (69) Alving, B. M.; Weinstein, M. J.; Finlayson, J. S.; Menitove, J. E.; Fratantoni, J. C. Fibrin sealant: summary of a conference on characteristics and clinical uses. *Transfusion* **1995**, *35* (9), 783–790.
- (70) Hickerson, W. L.; Nur, I.; Meidler, R. A comparison of the mechanical, kinetic, and biochemical properties of fibrin clots formed with two different fibrin sealants. *Blood Coagul Fibrinolysis* **2011**, *22* (1), 19–23.
- (71) Australian Public Assessment Report for Fibrin Sealant. Therapeutic Goods Administration, October 2010. <https://www.tga.gov.au/sites/default/files/auspar-artiss.pdf> (accessed 2022-01-24).
- (72) Bergel, S. Ueber Wirkungen des Fibrins. *DMW - Deutsche Medizinische Wochenschrift* **1909**, *35* (15), 663–665.
- (73) Harvey, S. C. Fibrin paper as an haemostatic agent. *Ann. Surg* **1918**, *68* (1), 66–70.
- (74) Cronkite, E. P.; Lozner, E. L.; Deaver, J. M. Use of thrombin and fibrinogen in skin grafting: preliminary report. *Journal of the American Medical Association* **1944**, *124* (14), 976–978.
- (75) Tidrick, R. T.; Warner, E. D. Fibrin fixation of skin transplants. *Surgery* **1944**, *15* (1), 90–95.
- (76) Hile, J. Revocation of fibrinogen licenses. *FDA Drug Bull.* **1978**, *8* (2), 15.
- (77) Malarkey, M. A.; Epstein, J. S. *Approval Letter - RAPLIXA*, 2015. U.S. Food and Drug Administration, April 30, 2015. <http://wayback.archive-it.org/7993/20170723024734/https://www.fda.gov/downloads/BiologicsBloodVaccines/BloodBloodProducts/ApprovedProducts/LicensedProductsBLAs/FractionatedPlasmaProducts/UCM445351.pdf> (accessed 2021-11-08).
- (78) Marx, G. Evolution of fibrin glue applicators. *Transfusion Medicine Reviews* **2003**, *17* (4), 287–298.
- (79) Baxter Healthcare Corp. *Package Insert - TISSEEL*. U.S. Food and Drug Administration, n.d. <https://www.fda.gov/media/71674/download> (accessed 2021-11-08).
- (80) Baxter Deutschland GmbH. *DUPLOSPRAY MIS-Applikator*. Paul-Ehrlich-Institute, 2018. https://www.pei.de/SharedDocs/schulungsmaterial/Tisseel-Schulungsmaterial-Aerzte_Version-1_Kurzanleitung.pdf?__blob=publicationFile&v=2 (accessed 2021-11-08).
- (81) *DUPLOSPRAY Quick Reference Guide (laparoscopic procedures)*. Baxter Healthcare Ltd. https://www.hpra.ie/docs/default-source/3rd-party-documents/educational-materials/tisseel_hcp_duplospray-qrq-v1-07-15.pdf (accessed 2022-05-22).
- (82) Kjaergard, H. K.; Trumbull, H. R. Vivostat system autologous fibrin sealant: preliminary study in elective coronary bypass grafting. *Annals of Thoracic Surgery* **1998**, *66* (2), 482–486.
- (83) Garbasch, A.; Hvid, N.; Cianciolo, D. Applicator and electro-mechanical applicator drive system. US 6234356 B1, May 22, 2001.
- (84) Belboul, A.; Dernevik, L.; Aljassim, O.; Skrbic, B.; Rådberg, G.; Roberts, D. The effect of autologous fibrin sealant (Vivostat) on morbidity after pulmonary lobectomy: a prospective randomised, blinded study. *Eur. J. Cardiothorac Surg* **2004**, *26* (6), 1187–91.
- (85) *Vivostat PRF® - A New Approach to Tissue Regeneration*. Sacomed A/S, n.d. <https://sacomed.com/wp-content/uploads/2019/09/Vivostat-PRF.pdf> (accessed 2021-11-08).
- (86) *Controlling Bleeds during Surgery*. Team Consulting Ltd. <https://www.team-consulting.com/work/controlling-bleeds-during-surgery/> (accessed 2021-11-08).
- (87) Greenhalgh, P.; Grimbergen, J. M.; Harvey, O. Powder Delivery Device. WO 2010070333 A2, June 24, 2010.
- (88) Greenhalgh, P.; Schutte, E. Powder delivery device. US 10010705 B2, March 7, 2018.
- (89) The Medicines Company, Inc. *The Medicines Company: Raplixa Approval is Likely, Manufacturing Risk Is Low*. Seeking Alpha. <https://seekingalpha.com/article/2865416-the-medicines-company-raplixa-approval-is-likely-manufacturing-risk-is-low> (accessed 2021-11-08).
- (90) McKeage, K. Raplixa: A Review in Improving Surgical Haemostasis. *Clinical Drug Investigation* **2015**, *35* (8), 519–524.
- (91) Johnson & Johnson Medical N.V. *Coated VICRYL (polyglactin 910) Suture*. Ethicon. <https://www.jnjmedicaldevices.com/en-EMEA/product/coated-vicryl-polyglactin-910-suture> (accessed 2021-11-08).
- (92) Matonick, J. P.; Hammond, J. Hemostatic Efficacy of EVARREST, Fibrin Sealant Patch vs. TachoSil® in a Heparinized Swine Spleen Incision Model. *Journal of Investigative Surgery* **2014**, *27* (6), 360–365.
- (93) Ethicon, Inc. *Package Insert - EVARREST*. U.S. Food and Drug Administration, 2016. <https://www.fda.gov/media/85265/download> (accessed 2021-11-08).
- (94) Albala, D. M. Fibrin sealants in clinical practice. *Cardiovasc. Surg.* **2003**, *11*, 5–11.
- (95) Daud, A.; Kaur, B.; McClure, G. R.; Belley-Cote, E. P.; Harlock, J.; Crowther, M.; Whitlock, R. P. Fibrin and Thrombin Sealants in Vascular and Cardiac Surgery: A Systematic Review and Meta-analysis. *Eur. J. Vasc Endovasc Surg* **2020**, *60* (3), 469–478.
- (96) Brustia, R.; Granger, B.; Scatton, O. An update on topical haemostatic agents in liver surgery: systematic review and meta analysis. *J. Hepatobiliary Pancreat Sci.* **2016**, *23* (10), 609–621.
- (97) Wells, C. I.; Ratnayake, C. B. B.; Mentor, K.; Sen, G.; Hammond, J. S.; French, J. J.; Wilson, C. H.; Manas, D.; White, S.; Pandanaboyana, S. Haemostatic Efficacy of Topical Agents During Liver Resection: A Network Meta-Analysis of Randomised Trials. *World J. Surg* **2020**, *44* (10), 3461–3469.
- (98) Esposito, F.; Angileri, F. F.; Kruse, P.; Cavallo, L. M.; Solari, D.; Esposito, V.; Tomasello, F.; Cappabianca, P. Fibrin Sealants in Dura Sealing: A Systematic Literature Review. *PloS one* **2016**, *11* (4), e0151533–e0151533.
- (99) Lindsey, K. *Clinical Review - Tisseel STN: 103980/5601*, U.S. Food and Drug Administration, n.d. <https://www.fda.gov/media/83108/download> (accessed 2021-11-08).
- (100) Federal Institute for Drugs and Medical Devices Germany. *Beriplast P Combi-Set 0,5 mL*. Paul-Ehrlich-Institute. <https://www.pei>

de/DE/arzneimittel/blutprodukte/fibrinkleber/fibrinkleber-node.html (accessed 2021-11-08).

(101) Ethicon, Inc. *Package Insert - EVICEL*. U.S. Food and Drug Administration, 2013. <http://wayback.archive-it.org/7993/20170723024815/http://www.fda.gov/downloads/BiologicsBloodVaccines/BloodBloodProducts/ApprovedProducts/LicensedProductsBLAs/FractionatedPlasmaProducts/UCM270787.pdf> (accessed 2021-11-08).

(102) Epstein, J. S.; Masiello, S. A. *March 21, 2003 Approval Letter - EVICEL*. U.S. Food and Drug Administration, February 17, 2017. <http://wayback.archive-it.org/7993/20170723024824/http://www.fda.gov/BiologicsBloodVaccines/BloodBloodProducts/ApprovedProducts/LicensedProductsBLAs/FractionatedPlasmaProducts/ucm114102.htm> (accessed 2021-11-08).

(103) Golding, B. *May 9, 2007 Approval Letter - EVICEL*. U.S. Food and Drug Administration, February 17, 2017. <http://wayback.archive-it.org/7993/20170723024821/http://www.fda.gov/BiologicsBloodVaccines/BloodBloodProducts/ApprovedProducts/LicensedProductsBLAs/FractionatedPlasmaProducts/ucm114096.htm> (accessed 2022-01-24).

(104) Golding, B. *January 2, 2008 Approval Letter - EVICEL*. U.S. Food and Drug Administration. <http://wayback.archive-it.org/7993/20170723024818/http://www.fda.gov/BiologicsBloodVaccines/BloodBloodProducts/ApprovedProducts/LicensedProductsBLAs/FractionatedPlasmaProducts/ucm114083.htm> (accessed 2021-11-08).

(105) *Evicel*. European Medicines Agency. <https://www.ema.europa.eu/en/medicines/human/EPAR/evicel> (accessed 2021-11-08).

(106) Baxter Healthcare Corp. *Package Insert - TachoSil*. U.S. Food and Drug Administration, July 2015. <https://www.fda.gov/media/78698/download> (accessed 2021-11-08).

(107) *TachoSil*. European Medicines Agency. <https://www.ema.europa.eu/en/medicines/human/EPAR/tachosil> (accessed 2021-11-08).

(108) *European Commission Approves Surgical Patch TachoSil® (human thrombin/human fibrogen) for Use in Neurological Surgery*. Takeda Pharmaceutical Co. Ltd. <https://www.takeda.com/newsroom/newsreleases/2016/european-commission-approves-surgical-patch-tachosil-human-thrombinhuman-fibrogen-for-use-in-neurological-surgery/> (accessed 2021-11-08).

(109) Cheng, C. *Statistics Review - TachoSil STN: 125351/172*. U.S. Food and Drug Administration, n.d. <https://www.fda.gov/media/93078/download> (accessed 2021-11-08).

(110) *CryoSeal FS System*. U.S. Food and Drug Administration. <https://www.fda.gov/vaccines-blood-biologics/approved-blood-products/cryoseal-fs-system> (accessed 2021-11-08).

(111) ThermoGenesis Corp. *Package Insert - CryoSeal FS System*. U.S. Food and Drug Administration, n.d. <https://www.fda.gov/media/73860/download> (accessed 2021-11-08).

(112) Baxter Healthcare Corp. *Package Insert - ARTISS*. U.S. Food and Drug Administration, n.d. <http://wayback.archive-it.org/7993/20170722072608/http://www.fda.gov/downloads/BiologicsBloodVaccines/BloodBloodProducts/ApprovedProducts/LicensedProductsBLAs/FractionatedPlasmaProducts/UCM073054.pdf> (accessed 2021-11-08).

(113) Epstein, J. S. *March 21, 2008 Approval Letter - ARTISS*. U.S. Food and Drug Administration, 2008. <http://wayback.archive-it.org/7993/20170723024803/http://www.fda.gov/BiologicsBloodVaccines/BloodBloodProducts/ApprovedProducts/LicensedProductsBLAs/FractionatedPlasmaProducts/ucm073064.htm> (accessed 2021-11-08).

(114) Golding, B. *August 29, 2001 Approval Letter - ARTISS*. U.S. Food and Drug Administration, 2001. <http://wayback.archive-it.org/7993/20170723024801/http://www.fda.gov/BiologicsBloodVaccines/BloodBloodProducts/ApprovedProducts/LicensedProductsBLAs/FractionatedPlasmaProducts/ucm270799.htm> (accessed 2021-11-08).

(115) Epstein, J. S. *January 16, 2009 Approval Letter - RiaSTap*. U.S. Food and Drug Administration, 2009. <http://wayback.archive-it.org/7993/20170723024919/http://www.fda.gov/BiologicsBloodVaccines/BloodBloodProducts/ApprovedProducts/LicensedProductsBLAs/FractionatedPlasmaProducts/ucm094007.htm> (accessed 2021-11-08).

(116) *Fibryga*. U.S. Food and Drug Administration. <https://www.fda.gov/vaccines-blood-biologics/approved-blood-products/fibryga> (accessed 2021-11-08).

(117) Bryan, W. W. *June 7, 2017, Approval Letter - Fibryna*. U.S. Food and Drug Administration, 2017. <https://www.fda.gov/media/105873/download> (accessed 2021-11-08).

(118) Purohit-Sheth, T. *December 23, 2020 Approval Letter - Fibryga*. U.S. Food and Drug Administration, 2020. <https://www.fda.gov/media/144964/download> (accessed 2021-11-08).

(119) Malarkey, M. A.; Epstein, J. S. *December 5, 2012 Approval Letter - EVARREST*. U.S. Food and Drug Administration, 2012. <http://wayback.archive-it.org/7993/20170723024836/http://www.fda.gov/BiologicsBloodVaccines/BloodBloodProducts/ApprovedProducts/LicensedProductsBLAs/FractionatedPlasmaProducts/ucm331137.htm> (accessed 2021-11-08).

(120) Mintz, P. D. *March 26, 2015 Approval Letter - EVARREST*. U.S. Food and Drug Administration, 2015. <http://wayback.archive-it.org/7993/20170723024834/http://www.fda.gov/downloads/BiologicsBloodVaccines/BloodBloodProducts/ApprovedProducts/LicensedProductsBLAs/FractionatedPlasmaProducts/UCM440593.pdf> (accessed 2021-11-08).

(121) *FDA Approves Raplixa to Help Control Bleeding during Surgery*. U.S. Food & Drug Administration, April 30, 2015. <http://wayback.archive-it.org/7993/20170723002533/http://www.fda.gov/NewsEvents/Newsroom/PressAnnouncements/ucm445247.htm> (accessed 2021-11-08).

(122) The Medicines Company, Inc. *Package Insert - Raplixa*. U.S. Food and Drug Administration. <https://www.fda.gov/media/91418/download> (accessed 2022-01-24).

(123) Instituto Grifols, S.A. *VeraSeal - Annex I - Summary of product characteristics*. European Medicines Agency. https://www.ema.europa.eu/en/documents/product-information/veraseal-epar-product-information_en.pdf (accessed 2022-01-24).

(124) *VeraSeal*. European Medicine Agency Web site, n.d. <https://www.ema.europa.eu/en/medicines/human/EPAR/veraseal-0> (accessed 2021-11-08).

(125) CSL Behring GmbH. *Beriplast P Combi-Set*. <https://portal.dimdi.de/amispb/doc/pei/Web/2601182-spcen-20130401.pdf> (accessed 2022-01-24).

(126) Octapharma Pharmazeutika Produktionsgesellschaft mbH. *Package Insert - FIBRYGA*. U.S. Food and Drug Administration, 2020. <https://www.fda.gov/media/105864/download> (accessed 2022-01-24).

(127) *RiaSTAP - New Zealand Data Sheet*. CSL Behring GmbH. <https://www.cslbehring.com.au/-/media/cslb-australia/documents/nz-dss/riastap-nz-ds-800b.pdf> (accessed 2022-01-24).

(128) Ethicon, Inc. *Package Insert - EVARREST*. 2016. U.S. Food and Drug Administration, 2016. <https://www.fda.gov/media/85265/download> (accessed 2021-11-08).

(129) Ethicon. *Rote-Hand-Brief: Evicel (07.12.2012)*. Paul-Ehrlich-Insitute, 2012. https://www.pei.de/SharedDocs/Downloads/DE/newsroom/veroeffentlichungen-arzneimittel/rhb/12-12-07-rhb-evicel.pdf?__blob=publicationFile&v=2 (accessed 2021-11-08).

(130) Johnson & Johnson Wound Management. *Rote-Hand-Brief: Quixil/EVICEL Lösungen für Fibrinkleber (16.08.2010)*. Paul-Ehrlich-Insitute, 2010. https://www.pei.de/SharedDocs/Downloads/DE/newsroom/veroeffentlichungen-arzneimittel/rhb/10-08-16-rhb-quixil-evicel.pdf?__blob=publicationFile&v=2 (accessed 2021-11-08).

(131) Instituto Grifols, S.A. *Package Insert - FIBRIN SEALANT (human)*. U.S. Food and Drug Administration, n.d. <https://www.fda.gov/media/108694/download> (accessed 2021-11-08).

- (132) Mandell, S. P.; Gibran, N. S. Fibrin sealants: surgical hemostat, sealant and adhesive. *Expert Opinion on Biological Therapy* **2014**, *14* (6), 821–830.
- (133) Hino, M.; Ishiko, O.; Honda, K. I.; Yamane, T.; Ohta, K.; Takubo, T.; Tatsumi, N. Transmission of symptomatic parvovirus B19 infection by fibrin sealant used during surgery. *Br. J. Haematol.* **2000**, *108* (1), 194–5.
- (134) Horowitz, B.; Busch, M. Estimating the pathogen safety of manufactured human plasma products: application to fibrin sealants and to thrombin. *Transfusion* **2008**, *48* (8), 1739–53.
- (135) Kawamura, M.; Sawafuji, M.; Watanabe, M.; Horinouchi, H.; Kobayashi, K. Frequency of transmission of human parvovirus B19 infection by fibrin sealant used during thoracic surgery. *Ann. Thorac Surg* **2002**, *73* (4), 1098–1100.
- (136) Zhang, J.-Z.; Redman, C. Fibrinogen Assembly and Secretion: ROLE OF INTRACHAIN DISULFIDE LOOPS*. *J. Biol. Chem.* **1996**, *271* (47), 30083–30088.
- (137) Stewart, E. J.; Aslund, F.; Beckwith, J. Disulfide bond formation in the Escherichia coli cytoplasm: an in vivo role reversal for the thioredoxins. *EMBO journal* **1998**, *17* (19), 5543–5550.
- (138) Gaciazar, A.; Khatrri, N. K.; Velez-Suberbie, M. L.; Saaranen, M. J.; Uchida, Y.; Keshavarz-Moore, E.; Ruddock, L. W. Efficient soluble expression of disulfide bonded proteins in the cytoplasm of Escherichia coli in fed-batch fermentations on chemically defined minimal media. *Microbial Cell Factories* **2017**, *16* (1), 108.
- (139) Francis, D. M.; Page, R. Strategies to optimize protein expression in E. coli. *Curr. Protoc. Protein Sci.* **2010**, *61*, 5.2.41–5.2.429.
- (140) Butler, S. P.; O'Sickey, T. K.; Lord, S. T.; Lubon, H.; Gwazdauskas, F. C.; Velander, W. H. Secretion of recombinant human fibrinogen by the murine mammary gland. *Transgenic research* **2004**, *13* (5), 437–450.
- (141) Prunkard, D.; Cottingham, I.; Garner, I.; Bruce, S.; Dalrymple, M.; Lasser, G.; Bishop, P.; Foster, D. High-level expression of recombinant human fibrinogen in the milk of transgenic mice. *Nat. Biotechnol.* **1996**, *14* (7), 867–871.
- (142) Calcaterra, J.; Van Cott, K. E.; Butler, S. P.; Gil, G. C.; Germano, M.; van Veen, H. A.; Nelson, K.; Forsberg, E. J.; Carlson, M. A.; Velander, W. H. Recombinant Human Fibrinogen That Produces Thick Fibrin Fibers with Increased Wound Adhesion and Clot Density. *Biomacromolecules* **2013**, *14* (1), 169–178.
- (143) Hirashima, M.; Imamura, T.; Yano, K.; Kawamura, R.; Meta, A.; Tokieda, Y.; Nakashima, T. High-level expression and preparation of recombinant human fibrinogen as biopharmaceuticals. *J. Biochem* **2016**, *159* (2), 261–70.
- (144) Tripathi, N. K.; Shrivastava, A. Recent Developments in Bioprocessing of Recombinant Proteins: Expression Hosts and Process Development. *Front. Bioeng. Biotechnol.* **2019**, *7*, No. 420.
- (145) Bout, A.; Grimbergen, J.; Koopman, J. Recombinant fibrinogen. US 20170037108 A1, February 9, 2017.
- (146) Hiller, O.; Lichte, A.; Oberpichler, A.; Kocourek, A.; Tschesche, H. Matrix Metalloproteinases Collagenase-2, Macrophage Elastase, Collagenase-3, and Membrane Type 1-Matrix Metalloproteinase Impair Clotting by Degradation of Fibrinogen and Factor XII*. *J. Biol. Chem.* **2000**, *275* (42), 33008–33013.
- (147) Nath, R. S. Production and secretion of recombinant fibrinogen by yeast. WO 1996007728 A1, March 14, 1996.
- (148) Tojo, N.; Miyagu, I.; Miura, M.; Oi, H. Method for producing recombinant fibrinogen. JP 2004016055 A, January 22, 2004.
- (149) Drohan, W.; Johnson, J. L.; Lord, S. T.; Lubon, H.; Russell, C.; Velander, W. H. Transgenic Fibrinogen. CA 2347579 A1, August 24, 1995.
- (150) Velander, W. H.; Lord, S. T.; Drohan, W.; Lubon, H.; Johnson, J. L.; Russell, C. Transgenic Fibrinogen. US 20060174357 A1, August 3, 2006.
- (151) Velander, W. H.; Lord, S. T.; Drohan, W.; Lubon, H.; Johnson, J. L.; Russell, C. Transgenic Fibrinogen. EP 0744891 B1, December 4, 2007.
- (152) Sekiguchi, S.; Takahisa, M.; Tomita, M. Fibrinogen-producing transgenic silkworm. US 20130345401 A1, December 21, 2013.
- (153) Lord, S. T. Method for recombinant fibrinogen production. US 6037457 A, March 14, 2000.
- (154) Cederholm-Williams, S. A. Recombinant fibrin chains, fibrin and fibrin-homologs. US 6083902 A, July 4, 2000.
- (155) Uno, S.; Otaki, M.; Murakami, K.; Ideno, S. Recombinant fibrinogen high-production line and method for producing same. US 10208101 B2, February 19, 2019.
- (156) Matsuyama, R.; Maeda, H. Process For Producing Recombinant Fibrinogen Highly Producing Cell and Highly Producing Cell. US 20100151522 A1, June 17, 2010.
- (157) Osther, K. Method for the preparation of recombinant human thrombin and fibrinogen. US 20100159512 A1, June 24, 2010.
- (158) Krieger, M. A.; Kessler, R. L.; Preti, H.; Ludwig, A.; Soares, L. R. B.; Su, L. Fibrin glue of recombinant origin. WO 2018161135 A1, September 13, 2018.
- (159) Lorentz, K. M.; Kontos, S.; Frey, P.; Hubbell, J. A. Engineered aprotinin for improved stability of fibrin biomaterials. *Biomaterials* **2011**, *32* (2), 430–8.
- (160) Chapin, J. C.; Hajjar, K. A. Fibrinolysis and the control of blood coagulation. *Blood reviews* **2015**, *29* (1), 17–24.
- (161) Francis, C. W.; Marder, V. J. Concepts of Clot Lysis. *Annual Review of Medicine* **1986**, *37* (1), 187–204.
- (162) DePalma, L.; Criss, V. R.; Luban, N. L. The preparation of fibrinogen concentrate for use as fibrin glue by four different methods. *Transfusion* **1993**, *33* (9), 717–20.
- (163) Kassell, B.; Laskowski, M., Sr. The basic trypsin inhibitor of bovine pancreas. V. The disulfide linkages. *Biochem. Biophys. Res. Commun.* **1965**, *20* (4), 463–8.
- (164) Kang, H. M.; Kalnoski, M. H.; Frederick, M.; Chandler, W. L. The kinetics of plasmin inhibition by aprotinin in vivo. *Thromb Res.* **2005**, *115* (4), 327–40.
- (165) Evans, L. A.; Morey, A. F. Current applications of fibrin sealant in urologic surgery. *Int. Braz. J. Urol.* **2006**, *32* (2), 131–41.
- (166) Scheule, A. M.; Beierlein, W.; Wendel, H. P.; Eckstein, F. S.; Heinemann, M. K.; Ziemer, G. Fibrin sealant, aprotinin, and immune response in children undergoing operations for congenital heart disease. *J. Thorac Cardiovasc Surg* **1998**, *115* (4), 883–9.
- (167) Oswald, A.-M.; Joly, L.-M.; Gury, C.; Disdet, M.; Leduc, V.; Kanny, G. Fatal Intraoperative Anaphylaxis Related to Aprotinin after Local Application of Fibrin Glue. *Anesthesiology* **2003**, *99* (3), 762–763.
- (168) Shirai, T.; Shimota, H.; Chida, K.; Sano, S.; Takeuchi, Y.; Yasueda, H. Anaphylaxis to aprotinin in fibrin sealant. *Intern Med.* **2005**, *44* (10), 1088–9.
- (169) Kon, N. F.; Masumo, H.; Nakajima, S.; Tozawa, R.; Kimura, M.; Maeda, S. Anaphylactic reaction to aprotinin following topical use of biological tissue sealant. *Masui* **1994**, *43* (10), 1606–1610.
- (170) Redl, H.; Schlag, G.; Schlag, I.; Eibl, J. Fibrinogen-based tissue adhesive containing an elastase inhibitor. US 20090041748 A1, February 12, 2009.
- (171) Lorentz, K. M.; Kontos, S.; Frey, P.; Hubbell, J. A. Engineered aprotinin for improved stability of fibrin biomaterials. *Biomaterials* **2011**, *32* (2), 430–438.
- (172) Bordoloi, B. K.; Sarma, N. J.; Eisenberg, R. L. System and method of delivering protease inhibitors. US 10154976 B2, December 18, 2018.
- (173) Smith, J. D.; Chen, A.; Ernst, L. A.; Waggoner, A. S.; Campbell, P. G. Immobilization of aprotinin to fibrinogen as a novel method for controlling degradation of fibrin gels. *Bioconjug Chem.* **2007**, *18* (3), 695–701.
- (174) Sacchi, V.; Mittermayr, R.; Hartinger, J.; Martino, M. M.; Lorentz, K. M.; Wolbank, S.; Hofmann, A.; Largo, R. A.; Marschall, J. S.; Groppa, E.; Gianni-Barrera, R.; Ehrbar, M.; Hubbell, J. A.; Redl, H.; Banfi, A. Long-lasting fibrin matrices ensure stable and functional angiogenesis by highly tunable, sustained delivery of recombinant VEGF164. *Proc. Natl. Acad. Sci. U. S. A.* **2014**, *111* (19), 6952–7.

(175) Hubbell, J. A.; Frey, P.; Lorentz, K. Tg-aprotinin fusion proteins and matrices thereof. WO 2011025957 A2, March 3, 2011.

(176) Redl, H.; Fuerst, W.; Kneidinger, R.; Helgerson, S. L.; Looker, D.; Inman, E. M.; Richards, J. P.; Wong, C. Fibrin/fibrinogen-binding conjugate. US 7091325 B2, August 15, 2006.

(177) Singh, S.; Dodt, J.; Volkers, P.; Hethershaw, E.; Philippou, H.; Ivaskевичius, V.; Imhof, D.; Oldenburg, J.; Biswas, A. Structure functional insights into calcium binding during the activation of coagulation factor XIII A. *Sci. Rep.* **2019**, *9* (1), 11324.

(178) Henderson, S. J.; Stafford, A. R.; Leslie, B. A.; Kim, P. Y.; Vaezzadeh, N.; Ni, R.; Fredenburgh, J. C.; Weitz, J. I. Zinc delays clot lysis by attenuating plasminogen activation and plasmin-mediated fibrin degradation. *Thromb Haemost* **2015**, *113* (6), 1278–88.

(179) Smith, S. A.; Morrissey, J. H. Fibrin sealant. US 8821861 B2, September 2, 2014.

(180) Hadjipanayi, E.; Kuhn, P. H.; Moog, P.; Bauer, A. T.; Kuekrek, H.; Mirzoyan, L.; Hummel, A.; Kirchhoff, K.; Salgin, B.; Isenburg, S.; Dornseifer, U.; Ninkovic, M.; Machens, H. G.; Schilling, A. F. The Fibrin Matrix Regulates Angiogenic Responses within the Hemostatic Microenvironment through Biochemical Control. *PLoS One* **2015**, *10* (8), e0135618.

(181) Zisch, A. H.; Schenk, U.; Schense, J. C.; Sakiyama-Elbert, S. E.; Hubbell, J. A. Covalently conjugated VEGF–fibrin matrices for endothelialization. *J. Controlled Release* **2001**, *72* (1–3), 101–13.

(182) Sahni, A.; Francis, C. W. Vascular endothelial growth factor binds to fibrinogen and fibrin and stimulates endothelial cell proliferation. *Blood* **2000**, *96* (12), 3772–8.

(183) Martino, M. M.; Briquez, P. S.; Ranga, A.; Lutolf, M. P.; Hubbell, J. A. Heparin-binding domain of fibrin(ogen) binds growth factors and promotes tissue repair when incorporated within a synthetic matrix. *Proc. Natl. Acad. Sci. U. S. A.* **2013**, *110* (12), 4563–4568.

(184) Ahmed, T. A.; Dare, E. V.; Hincke, M. Fibrin: a versatile scaffold for tissue engineering applications. *Tissue Eng. Part B Rev.* **2008**, *14* (2), 199–215.

(185) Noori, A.; Ashrafi, S. J.; Vaez-Ghaemi, R.; Hatamian-Zaremi, A.; Webster, T. J. A review of fibrin and fibrin composites for bone tissue engineering. *Int. J. Nanomedicine* **2017**, *12*, 4937–4961.

(186) Li, Y.; Meng, H.; Liu, Y.; Lee, B. P. Fibrin Gel as an Injectable Biodegradable Scaffold and Cell Carrier for Tissue Engineering. *Scientific World Journal* **2015**, *2015*, 685690.

(187) Hauptstein, N.; Pouyan, P.; Kehrein, J.; Dirauf, M.; Driessen, M. D.; Raschig, M.; Licha, K.; Gottschaldt, M.; Schubert, U. S.; Haag, R.; Meinel, L.; Sottriffer, C.; Lühmann, T. Molecular Insights into Site-Specific Interferon- α 2a Bioconjugates Originated from PEG, LPG, and PETox. *Biomacromolecules* **2021**, *22* (11), 4521–4534.

(188) Lühmann, T.; Gutmann, M.; Moscaroli, A.; Raschig, M.; Béhé, M.; Meinel, L. Biodistribution of Site-Specific PEGylated Fibroblast Growth Factor-2. *ACS Biomaterials Science & Engineering* **2020**, *6* (1), 425–432.

(189) Lühmann, T.; Schmidt, M.; Leiske, M. N.; Spieler, V.; Majdanski, T. C.; Grube, M.; Hartlieb, M.; Nischang, I.; Schubert, S.; Schubert, U. S.; Meinel, L. Site-Specific POxylation of Interleukin-4. *ACS Biomaterials Science & Engineering* **2017**, *3* (3), 304–312.

(190) Lühmann, T.; Spieler, V.; Werner, V.; Ludwig, M. G.; Fiebig, J.; Mueller, T. D.; Meinel, L. Interleukin-4-Clicked Surfaces Drive M2Macrophage Polarization. *Chembiochem* **2016**, *17* (22), 2123–2128.

(191) Wu, F.; Braun, A.; Lühmann, T.; Meinel, L. Site-Specific Conjugated Insulin-like Growth Factor-I for Anabolic Therapy. *ACS Biomater. Sci. Eng.* **2018**, *4* (3), 819–825.

(192) *Fibrin Sealant Market By Product Type, by End User and by Region: Industry Analysis, Market Share, Revenue Opportunity, Competition and Forecast 2020 to 2027*. FutureWise Research. <https://www.futurewiseresearch.com/healthcare-market-research/Fibrin-Sealant-Market/194> (accessed 2021-11-08).

Recommended by ACS

Self-Assembled Fibrinogen Hydro- and Aerogels with Fibrin-like 3D Structures

Dominik Hense, Oliver I. Strube, *et al.*

AUGUST 19, 2021
BIOMACROMOLECULES

READ 

Control Release and Diffusion-Reaction Kinetics of Genipin-Eluting Fibers Using an *in Vitro* Aneurysm Flow Model

Emily Augustine, Christopher J. Bettinger, *et al.*

OCTOBER 01, 2021
ACS BIOMATERIALS SCIENCE & ENGINEERING

READ 

Plasma–Alginate Composite Material Provides Improved Mechanical Support for Stem Cell Growth and Delivery

Nicholas Edwin Clay, Shanmugasundaram Natesan, *et al.*

SEPTEMBER 23, 2019
ACS APPLIED BIO MATERIALS

READ 

How Do Amphiphilic Biopolymers Gel Blood? An Investigation Using Optical Microscopy

Ian C. MacIntire, Srinivasa R. Raghavan, *et al.*

JULY 17, 2020
LANGMUIR

READ 

Get More Suggestions >

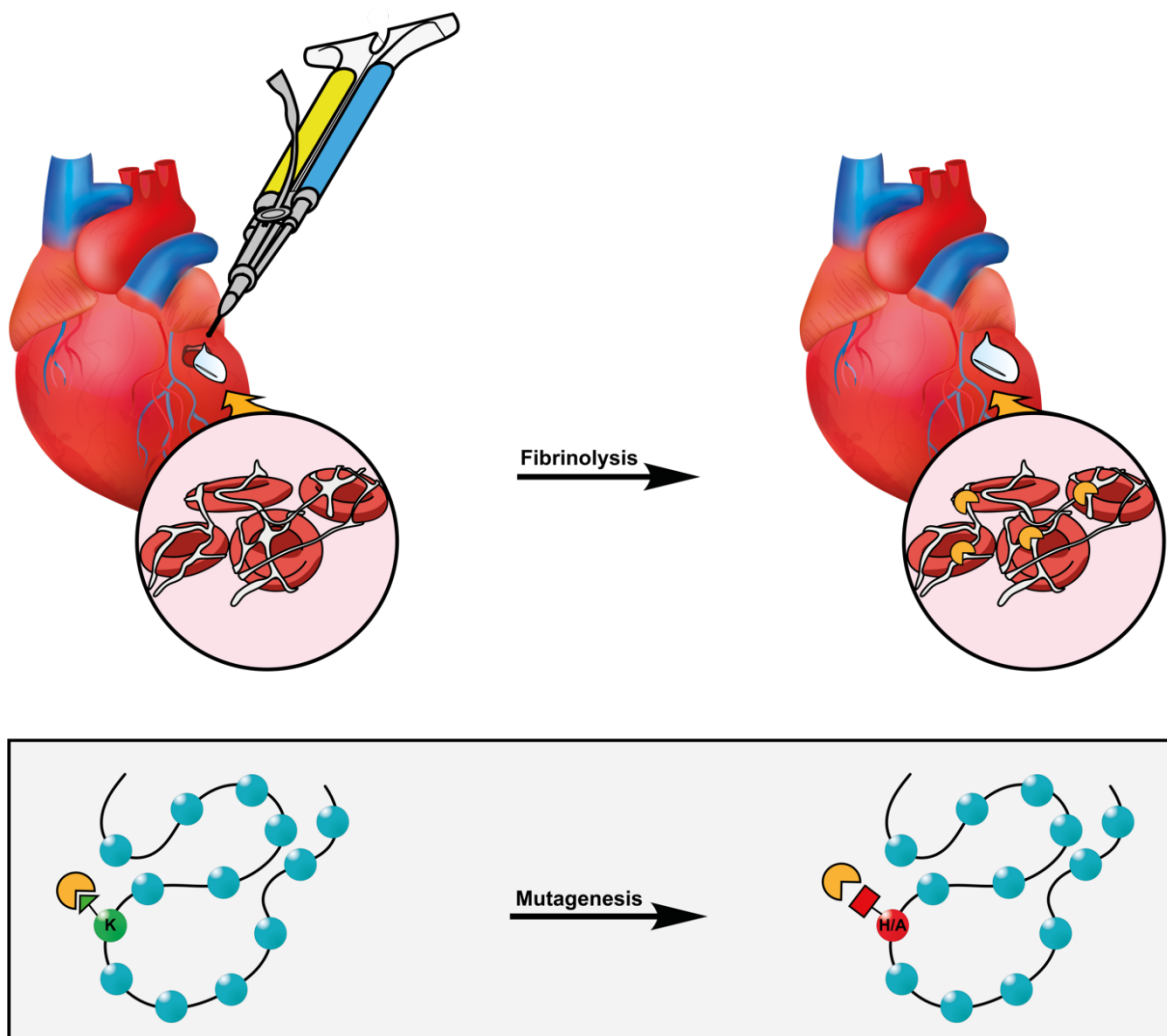
7. Chapter 4: Molecular Engineering of Fibrinogen for Improved Stability towards Plasmin Degradation

Matthias Beudert¹, Marc Drießen¹, Rafael Worschech¹, Lars Schönemann², Anna-Sophia Stecher¹, Tessa Lühmann¹, Lorenz Meinel^{1,3}

¹Institute of Pharmacy and Food Chemistry, Julius-Maximilians-University Würzburg, Am Hubland, 97074 Würzburg, Germany

²Rudolf -Virchow Center – Center for Integrative and Translational Bioimaging, University of Würzburg, Würzburg, Germany

³Helmholtz Institute for RNA-based Infection Research, Josef-Schneider-Straße 2, DE-97080 Würzburg, Germany



Introduction

Closure of wounds and the subsequent tissue regeneration are amongst the most important abilities of the human body. In the last phase of this process, the so-called secondary hemostasis, fibrinogen (Fbg) plays a pivotal role in the formation of the fibrin clot after its activation by thrombin.¹⁻³ Fbg is a longitudinal hexameric protein whose shape is reminiscent of a dumbbell. The soluble protein consists of three separate chains where two pairs of each form a complex of approximately 340 kDa molecular weight in total (A α - (66.5 kDa), B β - (52 kDa), and γ -chain (46.5 kDa)).⁴⁻⁶ In nature, Fbg exists in heterogenous populations of different forms. Both the α - and γ -chain have different isoforms formed through alternative splicing. The α -chain (Uniprot-P02671) comprises two different forms, the isoform E (α E; molecular weight: ~93 kDa)⁷ and the isoform 2 (A α , here referred to as α). Fbg α E accounts for around 1-2% of the Fbg population in the human body. There are also indications that Fbg containing α E might be less susceptible to proteolytic degradation making it an interesting candidate for increasing the half-life of fibrin clots towards plasmin.^{7, 8} The γ -chain (Uniprot-P02679) exists in two different isoforms, referred to as γ - and γ' -chain. In nature, the γ' -chain exists primarily as heterodimer (γ/γ') and only about 0.5% as homodimer γ'/γ' in human plasma.⁹⁻¹¹ The presence of γ' can have an impact on the structure and function of Fbg and the fibrin clot.⁹ During hemostasis the N-termini of both α - and β -chain are processed by the enzyme thrombin which leads to the formation of the fibrin network which is described in **chapter III** in more detail.^{12, 13} Due to its natural role and mechanics, fibrin has been used as biomaterial in different fields of medicine.^{14, 15} One of the most important applications is the use in so-called fibrin sealants to facilitate wound closure in surgeries with acute bleeding.¹⁶⁻¹⁸ The utilization of fibrin for bleeding control has several advantages compared to other available wound glues biocompatibility, and versatility.^{6, 19, 20}

However, there are still shortcomings associated with the product that constrain the broader use of fibrin sealants. In this regard, one challenge, especially during excessive bleeding, is the fast resorption of the fibrin clot at the injury site due to proteolytic degradation, called fibrinolysis.^{21, 22} Even though fibrinolysis is an essential process in the body to prevent the formation of intravascular clots or to degrade the clot during tissue regeneration, blood-borne proteases also attack fibrin glues and thereby reduce the stability of the wound sealant. The process of fibrinolysis is mediated mainly by the enzyme plasmin.^{23, 24}

Active plasmin is a serine protease that is derived from its zymogen plasminogen.^{25, 26} The activity of plasminogen is highly coordinated in an interplay of a multitude of different activators including urokinase-type plasminogen activators (uPA, urokinase) and inhibitors (e.g. α_2 -antiplasmin) that are secreted by cells.^{27, 28} After activation, plasmin degrades the fibrin clot

rapidly. Fbg used in fibrin sealants is often derived from pooled human plasma and therefore already contains small amounts of plasminogen.^{22, 29} Upon contact of the sealant with the injury site, this plasminogen is activated by proteases released from the cells and might amplify the sealant resorption in combination with endogenous plasmin.²²

Over the years, different approaches have been developed to tackle this problem. Currently, the most successful approach has been the addition of protease inhibitors to the sealant, which locally limit plasmin activity. The most common plasmin inhibitor used for these applications is aprotinin (bovine pancreatic trypsin inhibitor). Aprotinin is a peptide serine-protease inhibitor with a molecular weight of 6.5 kDa, that has been shown to successfully inhibit different proteases including plasmin.³⁰⁻³² It is also the only inhibitor that is currently used in fibrin sealants formulations that are already approved by the US food and drug administration (U.S. FDA) (e.g. TISSEEL[®], Baxter, Deerfield, USA).^{33, 34} However, the use of aprotinin also has some shortcomings, such as the potential for allergic or anaphylactic reactions.^{35, 36} In addition, aprotinin diffuses quickly from the injury site due to its small molecular weight. Thus, plasmin inhibition only has a relatively short time frame.²²

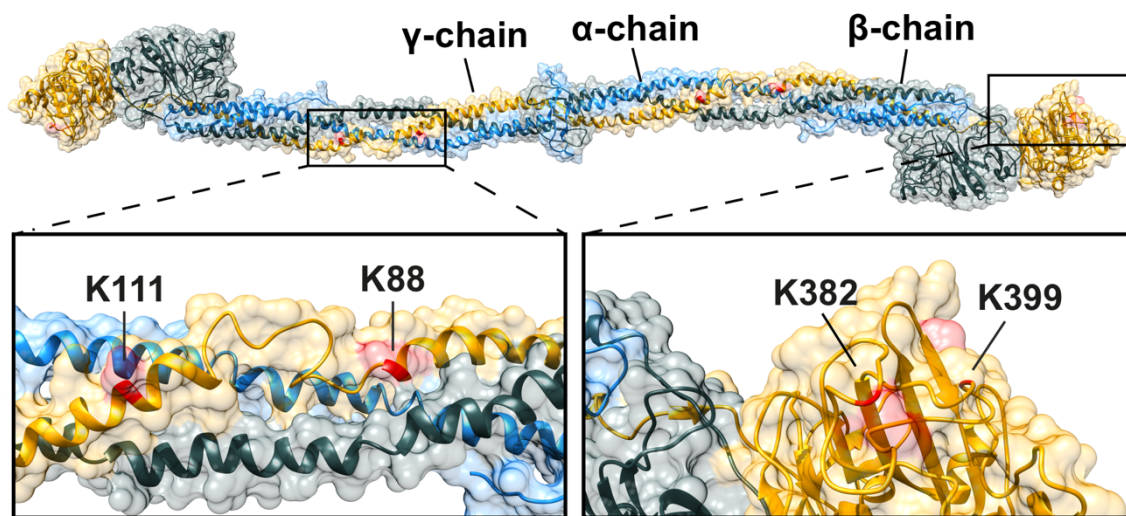
For decades protein engineering has been used to tune biophysical and mechanical properties of proteins depending on different needs and applications.³⁷ Increasing protein stability such as thermostability, has been studied extensively over the years by using genetic engineering e.g. via directed evolution.^{38, 39} Our aim was to develop a recombinant Fbg through site-directed mutagenesis with improved stability towards plasmin degradation. Therefore, we identified plasmin cleavage sites in Fbg and exchanged the AA P1 (AA residues in the substrate that undergo cleavage) to limit cleavage efficiency. After expression of rFbg in Chinese Hamster Ovary (CHO) cells, we demonstrated that AA exchange reduced cleavage by plasmin.

Results

Design of recombinant Fbg for Improved Stability towards Plasmin

Plasmin fibrinolysis occurs at multiple cleavage sites in all chains (α -, β - and γ -chain).⁴⁰⁻⁴³ In order to investigate the influence of mutations (AA exchange) and their location, with respect to the complex structure, on proteolytic degradation, we chose plasmin cleavage sites in different parts of the quaternary structure of Fbg. Mutation sites are located in the α -helical domain as well as the random coil domain (known as D domain⁴⁴; Figure 1A). We chose to insert mutations only in the γ -chain to increase degradation stability of the complex by keeping one complete chain intact, that additionally facilitates factor XIII lateral crosslinking.⁴⁵ The four different cleavage sites, either in the α -helical or D domain also allowed us to study their influence on the structure of Fbg. The mutation sites are QLI(**K**)AIQ; ATL(**K**)SRM (both α -helical domain); TYS(**K**)AST; ATW(**K**)TRW (both D domain) (Fig. 1A, B, S1). The ideal substrate of plasmin contains either an arginine (Arg, R) or a lysine (Lys, K) residue at Position P1.⁴⁶ In order to test the influence of the AA exchange in these sequences on plasmin cleavage, we synthesized the four different sequences changing K to the polar AA serine (Ser, S) proof of principle by using solid-phase peptide synthesis (SPPS). After purification, peptides were incubated with plasmin and cleavage efficiency was analyzed using HPLC. Peptide sequences including S instead of K showed a significant reduction in cleavage efficiency compared to the original sequences.⁴⁷ After this proof of principle, we introduced the aforementioned mutations in the γ -chain by using site-directed mutagenesis. To test the influence of different Fbg forms, we furthermore built two different expression plasmids, one containing $\alpha\alpha$ -, $\beta\beta$ - and γ -chain (rFbg) and one containing αE -, $\beta\beta$ - and γ' -chain (recombinant fibrinogen isoforms, rFbgi).

A



B

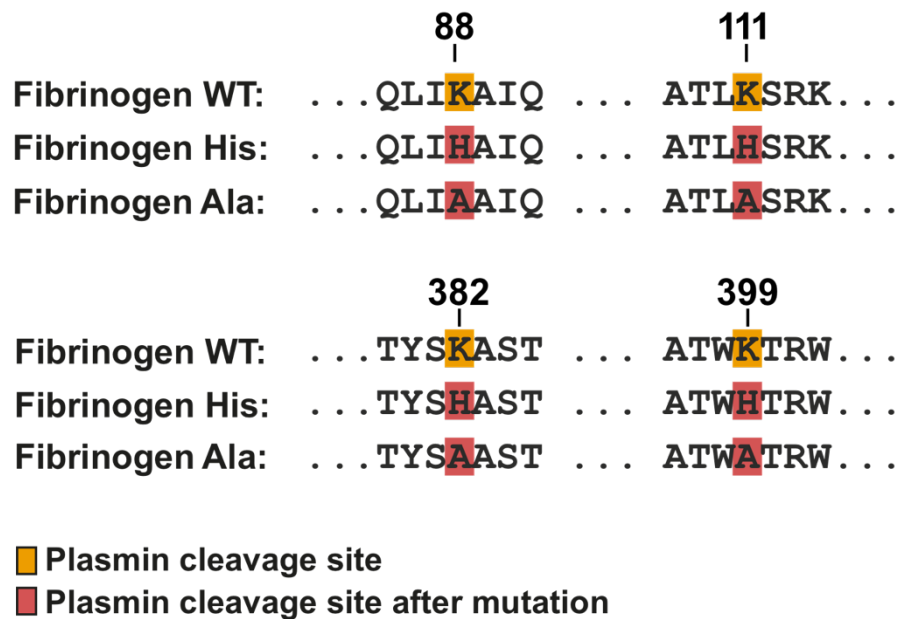


Figure 1: Schematic depiction of the Fbg modifications. (A) Structure of Fbg with the target AA positions in the 3D structure (PDB: 3GHG⁵) colored in red, α -chain colored in blue, β -chain colored in grey and γ -chain colored in yellow. (B) AA sequence of the plasmin target sites. The catalytic residue (orange) and the modified AAs of the mutants (red).

Production of rFbg and rFbgi

The production of rFbg and rFbgi and was performed using eukaryotic protein expression in CHO cells. The construction of expression plasmid pcDNA4-TO-FBG was achieved by using ligation-independent cloning (SLIC; Fig. S2). The plasmid encodes for all three chains, α , β

and γ -chain. All chains are set in row and are under control of the human cytomegalovirus (CMV) promoter. Bovine growth hormone (bGH) polyadenylation signal was added to the end of each gene to assure transcription termination (Fig. 2). Expression plasmids were built for both, wild type (WT) and variants carrying all four mutations.

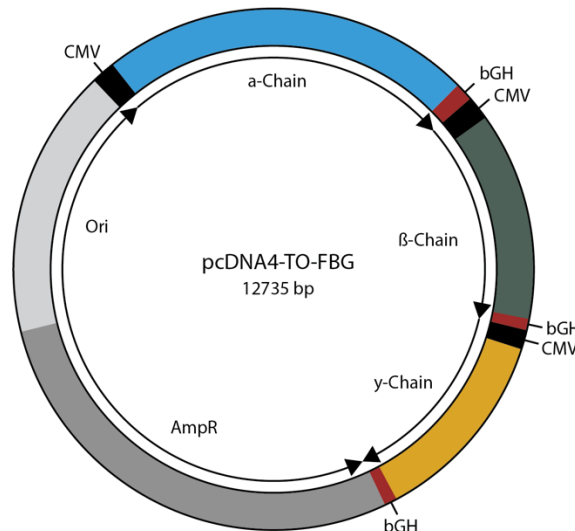


Figure 2: Map of the Fbg expression plasmid pcDNA4-TO-fbg. The plasmid consists of the different genes for each chain of Fbg α , β and γ , each controlled by the CMV promoter. BGH polyadenylation signal and transcription termination sequences were added to each gene cassette.

After the expression and purification of rFbgi, the non-reduced SDS-PAGE analysis showed a band at over 300 kDa for WT which can be attributed to the native hexamer form of Fbg. However, no high molecular band was visible for the expression for Ser-Fbg indicating that the introduction of S instead of K at the four mutations sites lead to either degradation or truncation of the γ -chain and therefore prevents Fbg production and assembly (Fig S3). According to literature, S can act as a helix breaker in secondary protein structures.⁴⁸ As two of the four mutations are located in the middle of the α -helical part of Fbg, these mutations could lead to the interruption of the helix and therefore disrupt the formation of the quaternary structure.

To mimic the physicochemical properties of the target AAs we chose histidine (His, H) and Alanine (Ala, A) as substitutes for K. A is known to be abundant in α -helices and is regarded the most stabilizing AA for helices.⁴⁹ H mimics the positive charge of the natural lysine residue and therefore might stabilize or at least not disrupt the structure of Fbg. After the insertion of the new mutations into the plasmid using gibson assembly, the new mutants of both rFbg and rFbgi were produced in CHO cells and showed a high purity after size exclusion chromatography (SEC, Fig. 3A, B). Non-reduced SDS-PAGE analysis showed a band for all four variants (His-rFbgi, Ala-rFbgi, rFbg, His-rFbg, Ala-rFbg) at a high molecular weight of over

300 kDa (Fig 3B, S4B, C). This suggests that the insertion of these mutations did not impair protein expression and the Fbg hexamer was built.

Structural Analysis of rFbg

To further verify the structure of the Fbg mutants, reduced SDS-PAGE was performed. Both β - and γ -chain were visible on the gel with molecular weights of around 52 kDa and 46.5 kDa as well as the native form at over 300 kDa (Fig 3B, S4). Furthermore, the presence and sequence of the different chains was confirmed by high resolution ESI-MS (Figure S5-10). This shows that the introduction of the different mutations did not impair gene expression, that the γ -chain could be produced and that the general approach can be used in the future. However, the band of the α -chain (α -chain: 66.5 kDa; α E: 93 kDa) was not visible on the SDS-PAGE under reducing conditions. Instead, another band emerged at around 44 kDa for both rFbg and rFbgi indicating a truncation of the α -chain during the production or purification process (Fig 3B, S4). Furthermore, the native Fbg band was slightly lower compared to the control also indicating a truncation of the protein (Fig. 3B).

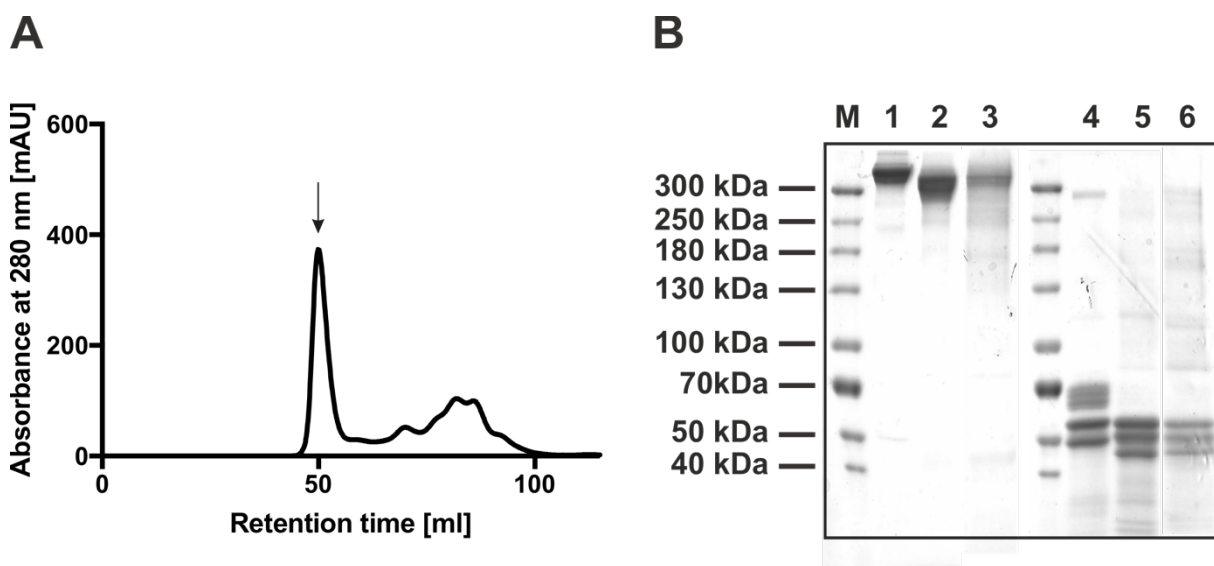
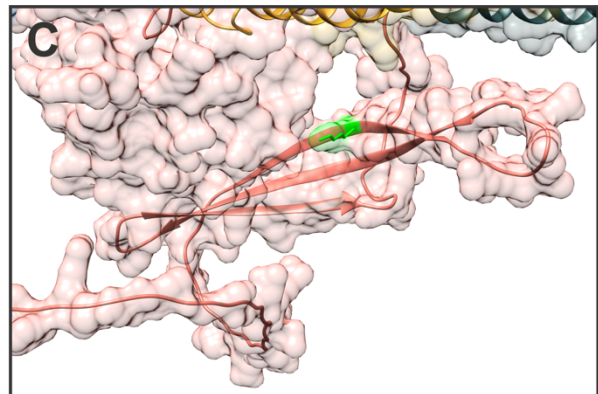
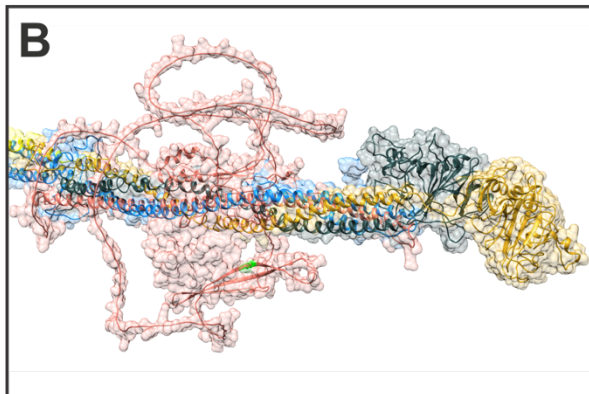
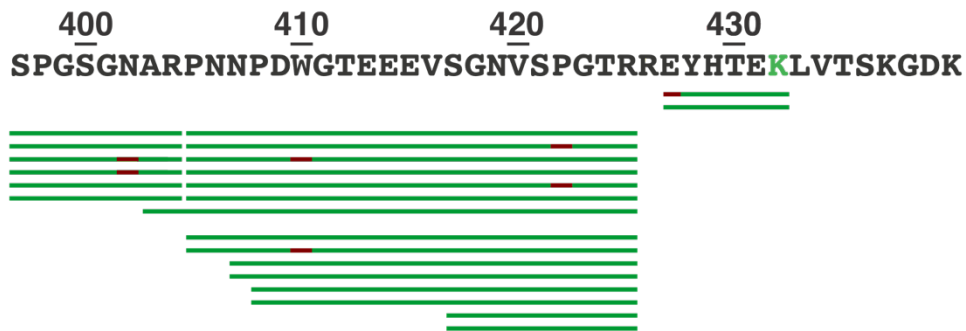


Figure 3: Analysis of rFbgi variants. (A) Exemplary size exclusion chromatography (SEC) chromatogram of His-rFbgi. (B) SDS-PAGE of Fbg control (1), His-rFbgi (2), Ala-rFbgi (3) under non-reduced conditions and Fbg control (4), His-rFbgi (5), Ala-rFbgi (6) under reduced conditions.

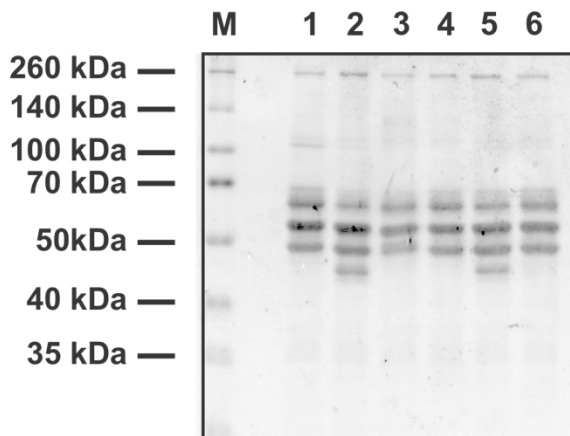
Fbg in general is susceptible to proteolytic degradation during the production.⁵⁰ CHO cells are known to secrete proteases during cell culture which can lead to proteolytic degradation of the α -chain. However, every CHO cell line has its own unique protease expression pattern which makes it difficult to identify the responsible protease. For the optimization of the approach, we focused on the rFbg ($A\alpha$ -, $B\beta$ - and γ -chain) from this point on because this form of Fbg is generally used as part of fibrin glues.

To verify that the new band at around 44 kDa is a truncated form of the α -chain and to locate the exact site of truncation, we performed an in-gel digestion with trypsin for a mass spectrometry (MS) characterization of the fragment. High resolution electrospray ionization (ESI) MS analysis showed a high alignment with the native α -chain and a truncation of the chain at K432 (Fig 4A, B, C, S11). These results also match with the molecular weight of the band in the SDS-PAGE (Fig 3 B) and suggested the degradation by a serine protease. It has also been described before, that the addition of the serine protease inhibitor aprotinin during CHO cell expression led to the production of functional Fbg.⁵¹ To limit the observed degradation, we applied the same approach as described previously and exchanged K432 to H in the α -chain gene cassette to inhibit proteolytic cleavage of the mutation site (rFbg432). In addition, we built an expression plasmid in which all K inside 20 AA up/downstream of the cleavage site K432 (K432, K437, K440, K446, K448: rFbg5xKtoH) were exchanged to H to prevent the emergence of a new cleavage site due to evolutionary pressure. However, SDS-PAGE analysis after CHO cell protein expression of both His-rFbg432 and His-rFbg5xKtoH revealed that the α -chain is still degraded during the process (Fig. S12). Other enzymes that have been reported to degrade the Fbg α -chain are matrix metalloproteinases (MMPs). The literature analysis of MMP cleavages sites as well as the influence of different MMPs on Fbg showed a degradation pattern resembling the ones of both rFbg and rFbgi and a potential cleavage site at K432 (e. g. MMP 2, 3, 12, 14).^{41, 52-54}

A



D



E

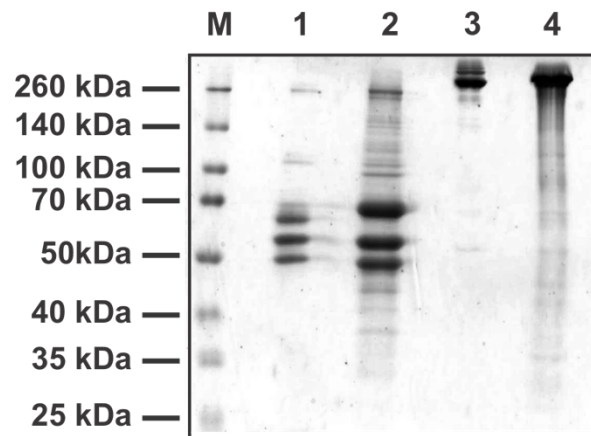


Figure 4: Improvement of rFbg expression. (A) Cutout (AA397-440) of MS-analysis of in gel digest of the truncated α -chain (Full analysis Figure S11). (B-C) Alignment of the Fbg crystal structure (PDB: 3GHG) with the predicted structure of the Fbg α -chain by AlphaFold^{55, 56} (P02671) in red with the target AA K432 highlighted in green. (D) SDS-PAGE of the screening of different protease inhibitors on the degradation of Fbg in CHO cell culture supernatant after two days of incubation; 1: Fbg control in Tris-buffer, 2: Fbg, 3: Fbg + EDTA; 4: Fbg + 1,10 Phenantroline, 5: Fbg + GM6001, 6: Fbg + UK 370106. (E) SDS-PAGE of His-rFbg432 with the addition of UK 370106 during expression; 1: Fbg control reduced, 2: His-rFbg432 reduced, 3: Fbg control non-reduced, 4: His-rFbg432 non-reduced.

Therefore, we screened different serine-protease and MMP inhibitors on their influence on the α -chain degradation to find a suitable compound for the inhibition of α -chain degradation. We incubated commercially available human Fbg with the supernatant taken from the CHO cells used for the expression and incubated the protein at 37 °C for several days. The analysis using SDS-PAGE showed the same degradation pattern for Fbg as seen during the expression. The truncated α -chain is also visible after the addition of the serin protease inhibitor aprotinin which could be an explanation why the inserted mutation at 432 did not have an impact on the degradation (Fig. S13). However, an intact α -chain was detected even a couple of days after the addition of either EDTA, 1,10-Phenanthroline or the MMP inhibitor UK 370106 (Fig. 4D, S13). This shows that the degradation of rFbg during CHO cell expression is likely the result of an overexpression of MMPs, either secreted or cell-bound, and a subsequent cleavage of the α -chain.

Hence, we expressed His-rFbg432 with the addition of 25 μ M of UK 370106. Reduced SDS-PAGE analysis showed three bands at around 68 kDa, 52 kDa and 46.5 kDa similar to the ones in commercially available Fbg. This indicates that the addition of the UK 370106 lead to the production of a fully intact α -chain (Fig 4E). The slight difference in molecular weight of the α -chain compared to the control could be the results of a difference in the complex glycosylation pattern of rFbg. The sequence of the α -chain was verified using high resolution ESI-MS (Fig. S14).

Analysis of Plasmin Digest of the γ -Chain of rFbg Mutants

Due to the truncated α -chain, gel formation with rFbg was not possible as of yet. The production of the intact complex (compare above) is still ongoing. Therefore, we performed plasmin digests in solution with WT as well as both Ala- and His-rFbg mutants to investigate if the inserted mutations are limiting proteolytic efficiency of plasmin at the respective cleavage sites. Plasmin was added to the Fbg solution (1 mg/mL) to a final concentration of 0.5 U/mL. The mixture was then incubated for 24 h to ensure complete cleavage of Fbg. Using high-resolution ESI-MS, we could detect the four different cleavage sites K88, K111, K382, K399 in the WT. However, no cleavage was detected in either of the two mutants for all four mutations showing that the AA exchange from K to A or H does limit proteolytic efficiency of plasmin in rFbg (Fig. 5, S5-6, S15). At some positions both cleaved and non-cleaved peptides were detected, however, no cleavage at the target sites did contain a mutation. This might be due to residual WT-Fbg peptides either on the column (carryover) or through residual WT-Fbg at any point in the workup. We believe that this cannot be an expression or cell line artifact since CHO cells do not produce WT-Fbg naturally and the expression plasmid only contains the mutated form of the γ -chain. However, this analysis was done only qualitatively due to the high

costs for the expression and the truncation of the α -chain. Therefore, these experiments must be repeated in the future with the fully intact rFbg to confirm and quantify the cleavage.

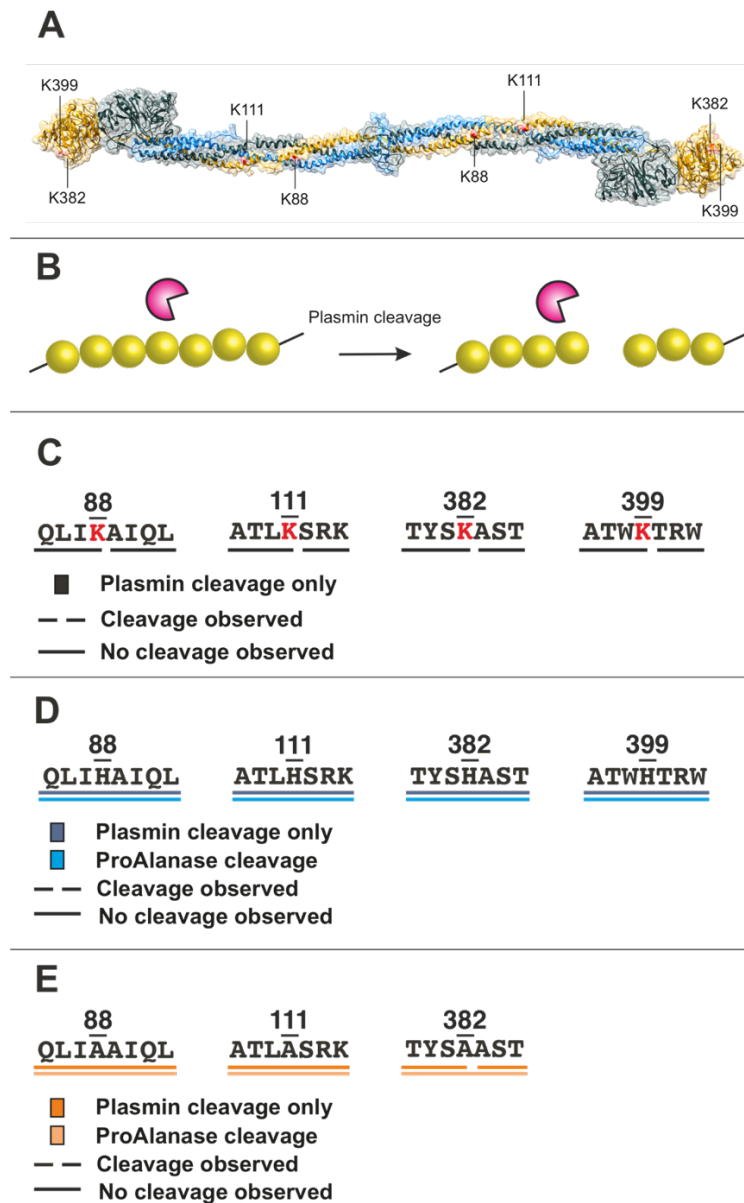


Figure 5: Plasmin cleavage analysis of rFbg variants. (A) Structure of Fbg with the target AAs positions in the 3D structure (PDB: 3GHG⁵) colored in red. (B) Plasmin cleaves target site in Fbg. Analysis of plasmin cleavage of target sites in WT-Fbg (C), His-rFbg (D) and Ala-rFbg (E). The presented cleavage sites are C-terminal to K. P1 of targeted cleavage sites are colored in red. Peptide fragments detected after plasmin (dark color) and after additional ProAlanase cleavage (light color) are shown. Position 382 shows a partial cleavage for the mutants (both cleaved and non-cleaved peptides detected). Position 399 could only be detected in His-rFbg and WT-Fbg.

Time Dependent Analysis of Plasmin Digestion of Fbg

After proving that the AA exchange from K to either H or A does impair plasmin mediated degradation of the γ -chain, we wanted to analyze which cleavage sites are cut in intact fibrin gels during the early phase of fibrinolysis. These sites could be potential targets for site-directed mutagenesis in the future to stabilize and limit Fbg degradation directly at the start. For this, fibrin gels (Sigma-Aldrich, 20 mg/mL) were cast, and a plasmin solution (0.005 mU/ml) was added on top of the gels and incubated for up to 2 h. At different time points the supernatant was collected and plasmin was inactivated by the addition of PSMF and heating. Afterwards, the solutions were purified using a C18 gravity column (Strata X, Phenomenex, Torrance, CA) and 100 fmol of ProteoMass™ Angiotensin II MALDI-MS Standard (Sigma-Aldrich, Steinheim, Germany) were added as an internal standard to each sample to quantify the cleavage of plasmin restriction sites. The time course of plasmin cleavage was analyzed using high resolution ESI-MS. For the analysis, we used the specificity of plasmin described in literature (cleavage C-terminal of R/K, similar to trypsin). However, an untargeted search revealed several non-tryptic cleavage sites. Thus, plasmin apparently cleaves both C- and N-terminal of R/K. In addition, some recurrent interfaces were observed showing AAs other than R/K in P1 and P1' positions.

The analysis shows that cleavage of fibrin gels in the earlier stages is most prominent within the α -chain which is consistent with reports from literature. The data supports the reports that cleavage begins in the α C region of Fbg with the most prominent cleavage at positions 602 (K|MADE) and 620 (K|RGHA). Next, cleavage sites further down the α C region are cleaved leading to the complete removal of this part of Fbg (e.g. positions 527 (K|TFPG), 511 (R|HRHP), 226 (K|MKPV) and 239 (K|SQLQ)). At the same time, cleavage in the α -helical region of the α -chain begins (e.g. positions 101 (K|DSHS) and 123 (R|DNTY)) (Figure 6A, D).⁴²
⁴³ However, we were able to detect a multitude of different cleavage sites with this approach that were not mentioned in the literature before (Figure S1). Furthermore, this approach enables a much more sensitive readout and analysis compared to methods such as high performance liquid chromatography (HPLC) and Sodium Dodecyl Sulfate – PolyAcrylamid Gel Electrophoresis (SDS-PAGE). In accordance with literature cleavage of the β -chain starts at the N-terminus highlighted by positions 52 (K|REEA) and 72 (R|ARPA) (Figure 6B, E). Subsequently, the α -helical part between fragment D and E is cleaved by plasmin (e.g. 153 (K|DLWQ) and 160 (K|QVKD)) (Figure 6B, E).^{42, 43}

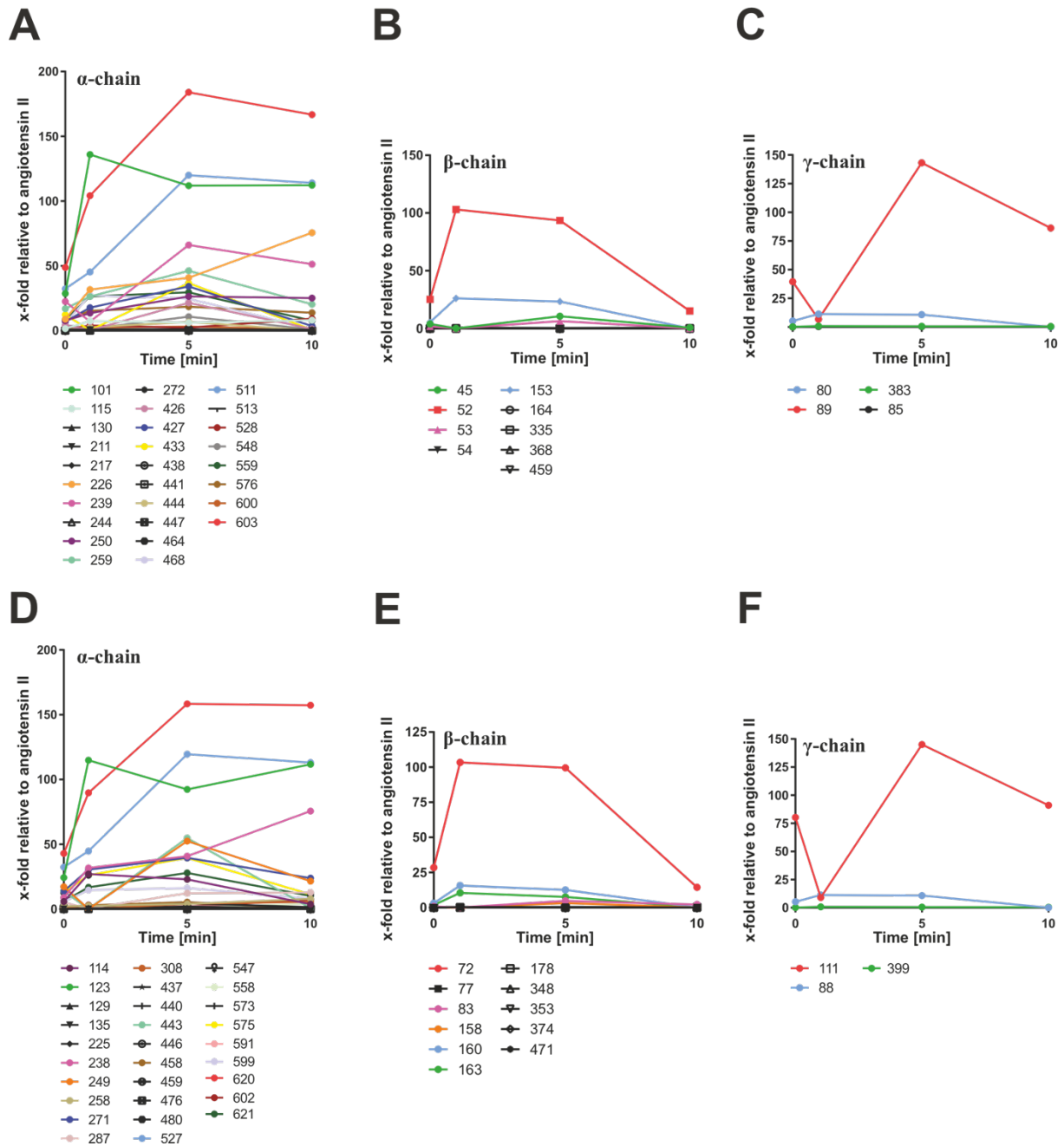


Figure 6: Temporal analysis of the plasmin cleavage sites of fibrin gels. The signal intensity of the identified peptides was normalized to the standard angiotensin II, after that an intensity of all detected peptides either starting (A, B, C) or ending (D, E, F) at the indicated position were summed up. (A, D) Analysis of the cleavage sites of the α -chain over time by signals from peptides starting (A) or ending (D) with the indicated position. (B) Analysis of the cleavage sites of the β -chain over time by signals from peptides starting with the indicated position. (E) Analysis of the cleavage sites of the β -chain over time by signals from peptides ending with the indicated position. (C) Analysis of the cleavage sites of the γ -chain over time by signals from peptides starting with the indicated position. (F) Analysis of the cleavage sites of the γ -chain over time by signals from peptides ending with the indicated position.

Strikingly, only one additional cleavage site was found for γ -chain (Fig 6C, F) supporting our initial hypothesis for the use of the γ -chain for the insertion of mutations. With only five cleavage sites detected during the early stages of plasmin degradation, less mutations are needed to potentially protect a complete chain in the fibrin complex. However, as described above for the analysis of plasmin degradation of the γ -chain after the AA exchange, the analysis of plasmin cleavage sites in Fbg was done qualitatively. Therefore, these experiments must be repeated in the future for a confirmation and a quantitative readout of the data.

Conclusion

The fast resorption of fibrin sealants due to plasmin cleavage is still a major problem in hemorrhage control. However, there are only few approaches that have been studied over the past decades. Here, we report a novel approach using molecular engineering to limit plasmin-induced cleavage of Fbg. Plasmin cleavage sites in both helical and random coil domains of Fbg were exchanged using site-directed mutagenesis. The γ -chain was successfully produced in CHO cells, indicating that the insertion of mutations in different structures of the protein does not impact its folding or expression. MS analysis showed that plasmin cleavage of those sites was restricted proving that the AA exchange at plasmin restriction sites limits the cleavage by enzyme. In addition, a process for the production of rFbg in ExpiCHO™ cells was developed by screening and subsequent use of different MMP inhibitors during expression. Furthermore, we developed a potential time-resolved screening protocol for the elucidation of plasmin cleavage sites for a potential AA exchange for further generations of Fbg variants. Nonetheless, different experiments must be repeated in the future for a quantitative readout of the experiments. The approach for the production of a molecular engineered Fbg, reported here, could be used in the future to generate a new generation of fibrin sealants with an improved stability towards plasmin degradation. By varying both the number of mutations at plasmin cleavage sites as well as their location in the quaternary structure of the protein, fibrin gel resorption could potentially be fine-tuned for specific application. In the future, the ability of the different recombinant Fbg variants to form fibrin gels must be verified. Furthermore, the influence of the mutations on the gel structure needs to be analyzed. Most importantly, the effect of the mutations on the resorption time of fibrin gels must be investigated in order to further develop the platform for a potential use as wound sealant in the future.

Materials and Methods

Materials

Restriction enzymes were purchased from New England Biolabs (NEB, Frankfurt a. M., Germany)^[2] and used according to manufacturer's instructions. For PCRs, Phusion™ High-Fidelity DNA Polymerase from Thermo Fisher Scientific (Waltham, USA)^[3] was used, also according to manufacturer's instructions. Custom oligonucleotides were purchased from Sigma-Aldrich (St. Louis, USA)^[4], desalted and lyophilized, and solubilized to 100 μM in H₂O upon arrival. The ExpiCHO™ expression system, comprising Gibco ExpiCHO-S cells, Gibco ExpiCHO™ Expression Medium, Gibco ExpiFectamine™ CHO reagent, ExpiCHO™ Feed, ExpiFectamine™ Enhancer and Gibco OptiPRO™ Serum-Free Complexation Medium were purchased from Thermo Fisher Scientific (Waltham, USA). Spectra™ Prestained Multicolor High Range Protein Ladder (40 – 300 kDa), Spectra™ Prestained Multicolor Broad Range Protein Ladder (40 – 300 kDa) and PageRuler™ (10 – 170 kDa), Coomassie Brilliant Blue G250, SuperSignal™ West Pico PLUS Chemiluminescent Substrate, Bradford Protein Assay Kit, Mammalian Cell Lysis Buffer, 1-Step™ Ultra TMB ELISA Substrate Solution were from Thermo Fisher Scientific (Dreieich, Germany). HiTrap™ Capto MMC, Superdex™ 200 Hiload 16/600 and Superdex™ 75 10/300 GL were from Cytiva (Buckinghamshire, GB).

Methods

Site-directed mutagenesis

The γ-chain vector DNA was amplified using PCR with primers designed in order to insert mutations at different positions in the sequence (FGG-Lys88-S-FW: 5'-GCAGCTGATC AGCGCCATCC AGCTGACCTA CAACCCCGAC GAGG-3'; FGG-Lys88-S-RV: 5'-GGTCAGCTGG ATGGCGCTGA TCAGCTGCTT CACTTCGCTG GTC-3'; FGG-Lys111-S-FW: 5'-CCGCCACCCT GAGCTCCCGG AAGATGCTGG AAGAGATC-3'; FGG-Lys111-S-RV: 5'-CGGGAGCTCA GGGTGGCGGC GTCGATCATG TTG-3'; FGG-Lys356-S-FW: 5'-CTACAGCAGC GCCAGCACCC CCAACGGCTA CGACAAC-3'; FGG-Lys356-S-RV: 5'- GTGCTGGCGC TGCTGTAGGT GCCGCCCTGG TAGTACACG-3'; FGG-Lys373-S-FW: 5'-CACCTGGAGC ACCCGGTGGT ACAGCATGAA GAAAACCAC-3'; FGG-Lys373-S-RV: 5'-CCGGGTGCTC CAGGTGGCCC AGATGATGCC GTTGT-3'). The amplified cDNA was transformed into *E. coli* dH5α and mutations of target residues were verified by sanger sequencing.

Gibson Assembly

For the insertion of the different mutations into the γ -chain, a part of the DNA sequence of the γ -chain was purchased from Thermo Fisher Scientific (Waltham, USA). In order to perform Gibson assembly pairs of primer for both the vector containing the γ -chain as well as the synthesized gene were designed (FGG Insert Fw: 5'-GAGAACAAGA CCAGCGAAGT GAA-3'; FGG Insert Rv: 5'-CTTCATGGTG GTTTTCTTCA TGC-3'; FGG Vector Fw: 5'-GTACAGCATG AAGAAAACCA CCA-3'; FGG Vector Rv: 5'-CTTCACTTCG CTGGTCTTGT TCT-3'). The amplified cDNA was purified using PCR purification kits (E.Z.N.A[®] Kits, Omega Bio-tek, Inc., Norcross, USA) and inserted into the vector pcDNA3 and transformed into *E. coli* dh5 α . Successful cloning was verified by sanger sequencing (Eurofins Genomics, Ebersberg, Germany).

Building of expression plasmids

All cloning steps were performed via SLIC, using PCR-amplified inserts and vectors opened with restriction enzymes. First, the open reading frame (ORF) for Fbg α -chain was cloned into the *Xba*I-opened pcDNA[™]4/TO/myc-His A^[5] vector, either without a stop-codon to incorporate the vector-encoded myc-His tag or with a stop-codon for untagged versions. The ORFs for Fbg β - and γ -chain have been cloned into the *Eco*RI-opened pcDNA[™]3 vector^[6]. In a second step, the FGB- and FGG-ORFs were PCR-amplified together with the surrounding CMV promoter and bGH poly(A)signals (using oligonucleotides #7 and #8, or #9 and #10, respectively) and inserted in a single SLIC-reaction into the pcDNA4/TO/FGA construct, opened by restriction with *Sap*I-enzyme (cuts in the vector backbone between the ColE1 origin of replication and the bleomycin resistance gene).

Clones were screened by a combination of colony-PCRs^[7] and analytical restriction analysis^[8] and verified by sequencing all three ORFs^[9].

Cell Culture

ExpiCHO[™] cells were cultured according to manufacturer's protocol. In short, cells were maintained in 125 mL flask in ExpiCHO[™] Expression Medium at 37 °C, 8% CO₂ and 130 rpm without the use of antibiotics. For general maintenance cells were passaged every 3-4 days when a density of approximately 6 x 10⁶ cells/mL was reached.

Production of rFbg and rFbgi

Fbg variants were expressed according to the user manual (Thermo Fisher Scientific, Waltham, USA). Briefly, ExpiCHO[™] cells (Thermo Fisher Scientific, Waltham, USA) were cultured to a final density of 10 x 10⁶ cells/mL. Plasmids encoding for the different Fbg variants (0.8 μ g/mL of culture) as well as ExpiFectamine[™] CHO (Thermo Fisher Scientific, Waltham,

USA) were diluted in 5 mL of cold OptiPro™ medium (Thermo Fisher Scientific, Waltham, USA) and incubated for 5 min at room temperature (RT). The ExpiFectamine™ CHO/DNA complex was transferred to the shaker flask and incubated at 37 °C and 8% CO₂ and 130 rpm. After 24 h of incubation, ExpiFectamine™ CHO Enhancer and ExpiFectamine™ CHO Feed (Thermo Scientific, Waltham, USA) were added to the culture flask. The culture flasks were transferred to an incubator at 32 °C and 8% CO₂ with shaking at 130 rpm. This step was repeated after 4 days of incubation. After another incubation step of up to 7 days at 32 °C and 8% CO₂ and 130 rpm cells were harvested and centrifuged at 3000 rpm for 15 min.

For the production of rFbg with the addition of UK 370106, the inhibitor was added to the medium to a final concentration of 25 µM. Every day, cells were centrifuged at 1100 rpm for 4 min. The supernatant was removed, EDTA was added to a final concentration of 2 mM, and it was stored at -80 °C until further use. Purification was done as described before with the addition of 2 mM EDTA to every buffer used during the process.

Purification of rFbg and rFbgi

WT and mutants of both rFbg and rFbgi were purified from the supernatant of ExpiCHO™ cells. After filtration of the supernatant using a microfiltration membrane (Filtropur S 0.2 µM, Polyethersulfon-Membran, Sarstedt, Nuembrecht, Germany) the solution containing the recombinant protein was purified by ion exchange (AiEx) chromatography using a fast protein liquid chromatography system with a Capto MMC column (GE Healthcare Äkta Explorer, Life sciences, Freiburg, Germany) equilibrated in 20 mM phosphate buffer (pH 7) containing 150 mM sodium chloride (NaCl). The protein was eluted from the column with a linear gradient using a 200 mM arginine buffer (pH 8.5) with 500 mM NaCl. After buffer exchange to a 10 mM arginine buffer (pH 8.5) containing 150 mM NaCl recombinant Fbg was purified in a second step using SEC (Hiload 16/600 Superdex 200 PG, GE Healthcare, Life sciences, Freiburg, Germany) with 10 mM arginine buffer (pH 8.5) containing 150 mM NaCl. Protein concentration was determined using bicinchoninic acid (BCA) or Bradford assay according to manufacturer's manual. The recombinant protein was stored at -80 °C.

SDS-Page

Purified proteins and conjugates were analyzed using Tris-glycine SDS-PAGE either with or without the addition of β-mercaptoethanol as described before.⁵⁷ Gels were stained with Coomassie Brilliant Blue G250 and documented using FluorChem FC2 imaging system (Protein Simple, Santa Clara, USA).

Formation of fibrin gels

Lyophilized Fbg (Sigma-Aldrich, St. Louis, USA) was dissolved in ddH₂O and dialyzed against 10 mM Tris/HCl, 150 mM NaCl (pH 7.5) over night at RT. Gelation of Fbg (20 mg/mL) was started by the addition of thrombin (Merck KGaA, Darmstadt, Germany) (1 U/mL), factor XIIIa (fibrogamin[®], CSL Behring) (50 mU/mL) as well as CaCl₂ (10 mM). 100 µL of the Fbg solution were transferred to a 96 well plate and incubated at RT for at least 2 h. Afterwards gels were stored at 4 °C upon further experiments.

Plasmin digest

In order to analyze plasmin digestion of mutated restriction sites, 100 µL of human plasmin (Merck KGaA, Darmstadt, Germany) (0.5 U/mL) were added to 100 µg of Fbg and rFbg (Ala and His) and incubated for 24 h at 37 °C and 130 rpm in order to ensure complete cleavage. Afterwards, samples were stored at -80 °C. For the analysis of the time-dependent cleavage site determination and quantification of plasmin, fibrin gels (20 mg/mL) were incubated with different plasmin concentrations on top of the gels ranging from 0.005 mU/mL – 0.5 U/mL. Samples were taken at different points in time from 1 min to 24 h. PMSF (1 mM) was added to the sample and heated at 95 °C for 10 min to ensure plasmin inactivation. Samples were stored at -80 °C.

Screening of inhibitors for Fbg expression

ExpiCHO[™] cells were cultured to a density of 6 x 10⁶ cells/mL. Afterwards, cells were centrifuged for 4 min at 1000 rpm at RT and the supernatant was collected. Commercially available Fbg (Sigma-Aldrich, St. Louis, USA) was mixed with the supernatant to a final concentration of 3.3 mg/mL and a volume of 200 µL. The mixture incubated at 37 °C and 750 rpm and samples were taken at 0, 24 and 48 h, respectively. For the screening the different inhibitors were added to the mixture (final concentrations: PMSF: 1 mM; Aprotinin: 50 µg/mL; GM6001: 25 µM; EDTA: 4 mM; 1,10-Phenanthroline: 1 mM; UK 370106: 100 µM). As control Fbg was incubated in 10 mM Tris/HCl, 150 mM NaCl (pH 7.5) under the same conditions. For the visualization of Fbg degradation, 20 µL of the mixtures were analyzed using SDS-PAGE.

High resolution mass spectrometry analysis

Sample preparation - In-gel digestion

Samples were diluted with Nupage Sample buffer[™] (Thermo Fisher Scientific, Waltham, USA). In a next step dithiothreitol was added to the samples to a final concentration of 50 mM for the reduction of disulfide bonds. After denaturation of the proteins at 70 °C for 10 min, iodoacetamide (IAA) was added to a final concentration of 120 mM and the samples were

incubated for 20 min in the dark. SDS-PAGE was performed (*vide supra*) and the band of interest was cut out of the gel and stored at -80 °C until further use.

In case of in-gel digestion, gel bands were cut out and subsequently destained with 30% acetonitrile. Afterwards they were shrunk with 100% acetonitrile. In the next step they were dried using a vacuum concentrator.

Per slide, 0.1 µg of trypsin were used, and the digest was performed overnight at 37 °C in 0.05 M NH₄HCO₃ (pH 8). Peptides extraction from the gel slices was done using 5% formic acid.

ProAla digest was performed by incubating the gel-slice with 0.1% Formic acid, containing 0.2 µg of ProAla for 1.5 h. Peptides were extracted as above.

Sample preparation – In-solution digestion

Proteins were digested either with plasmin alone (*vide supra*) or with plasmin and ProAla (ProAla) (Promega, Madison, USA) with slight differences in handling. For all digests, samples were brought to a concentration of 0.2 µg/µL in 50 mM Tris buffer. For “plasmin only” samples were immediately purified (see below). For ProAla (Promega, Madison, USA), 50 µL of 8M Guanidinium Hydrochloride were added to 10 µg (50 µL) of protein stock solution and briefly heated to ensure denaturation. To enable specific ProAla digest the solution was acidified using 900 µL of 32 mM HCl. After pH was checked to be in the range of 1-1.5, ProAla was added (1:50 ProAla:Protein; 0.25 µg), proteolysis was allowed to continue for 2.5 h. Afterwards, pH was set to slightly basic by addition of 0.5 -1 mL of 2 M Tris buffer. In the next step, the samples were immediately purified.

Prior to purification, samples were reduced and alkylated as follows:

Tris(2-carboxyethyl)phosphine (TCEP) was added to a final concentration of 20 mM. Samples were heated to 60 °C for 5 min and IAA was added to a final concentration of 40 mM during cooling. The samples were allowed to fully cool in the dark for 20 min. Immediately after, the samples were loaded on 1 mL Strata X33 syringe columns (10 mg bed; Phenomenex, Torrance, CA). For all steps only gravitational flow was used. The columns were activated with 3 mL 100% ACN and then washed with 3 mL 100% deionized water. Then the sample was added. Afterwards, the column was washed with 5 mL 0.4% formic acid in ddH₂O. Elution was performed with 0.5 mL 0.4 % formic acid in 80% ACN. The eluted samples were frozen in liquid nitrogen and freeze dried. For analysis, samples were resuspended in 50 µL 0.2% formic acid, 2% acetonitrile and used for liquid chromatography (LC)-MS/MS analysis immediately.

LC-MS

NanoLC-MS/MS analysis were done with a LTQ-Orbitrap Velos Pro (Thermo Fisher Scientific, Waltham, USA) using a PicoView Ion Source (New Objective, Littleton, USA) that was connected with an EASY-nLC 1000 (Thermo Fisher Scientific, Waltham, USA). First, peptides

were applied to a precolumn (trap column, 2 cm x 150 μ M ID) with 3 μ m C18 ReproSil (Thermo Fisher Scientific, Waltham, USA). Subsequently, they were eluted to self-packed capillary columns (30 cm x 150 μ m ID) with 1.9 μ m ReproSil-Pur 120 C18-AQ (Thermo Fisher Scientific, Waltham, USA). Separation of peptides was done using either a 30, 60 or 120-min linear gradient from 3-30% acetonitrile and 0.1% formic acid. The flow rate was set to 500 nL/min. Gradients were used as follows: 30 min gradients were used for in-gel digested samples, 60 min gradients for time resolved plasmin cleavage site determination and quantification, 120 min gradients for all other in solution digests.

The acquisition of MS and MS/MS scans was done as previously described.⁵⁸ In brief, an Orbitrap analyzer (resolution of 30,000 at m/z 400) was used to obtain MS scan. For the acquisition of MS/MS scans, a resolution of 7500 at m/z 400 in combination with HCD fragmentation with 30% normalized collision energy were applied. MS/MS fragmentation of precursor ions (TOP5) was performed in data-dependent scans with a dynamic exclusion of 7 seconds and a repeat count of 1; charge exclusion (z=1) was applied. The intensity threshold for the selection of precursor ions was set to a value of 50,000. Automatic gain control (AGC) was set to a target value of 1×10^6 for MS scans and a value of 5×10^4 for MS/MS scans. Internal mass calibration was facilitated by using background ions from decamethylcyclpentasiloxane (m/z of 371.10124 for $[M+H]^+$) as lock mass in all runs.

Data Analysis

Data analysis was performed using PMI-Byos (Protein Metrics inc., Cupertino United states). For quality control, data was searched against databases containing all human proteins (uniprot reference proteome). When the target protein was identified searches detailed below were performed against custom databases containing either the WT sequences of α -, β - and γ -chain of Fbg, or in the case of γ -chain analysis only the γ -sequence. For determination of successful expression after inhibitor addition, the isoform sequence (P02671-2|FIBA_HUMAN Isoform 2) from uniprot was used.

Samples were searched using PMI-Preview (Protein Metrics inc., Cupertino United states) first, and suggested modifications were included in the main search. In all cases decoys were added. Results were filtered and only peptide matches with a scoring of > 100 were considered.

Settings for individual searches varied and were as follows:

Determination of cleavage efficiency in mutants:

All datafiles were searched in batches of 3 (separated by protease used for digest), with the settings described below.

A. Plasmin Only digest (γ):

Precursor Tolerance of 15 ppm, fragment mass tolerance of 20 ppm, digestion C-terminal of K (non-specific); Allowed modifications were: Oxidation (C, H, M, P, W, Y), Acetyl (N-term), Deamidation (NQ), fixed Carbamidomethyl (C), Dioxidation (M, W) Decarbamidomethyl (C). They are concurrent with PMI-Byos recommendations for sequence variant analysis workflows (two rare and common modifications allowed).

B. Plasmin and ProAlanase digest (γ):

Precursor Tolerance of 15 ppm, fragment mass tolerance of 20 ppm, digestion C-terminal of A and P (non-specific); Allowed modifications were: Acetyl (N-term), fixed Carbamidomethyl (C). They are concurrent with PMI-Byos recommendations for sequence variant analysis workflows (two rare and common modifications allowed).

In addition to that, a “quality control” assessment of the experiments was performed. Both sets of digests were searched against a database containing all three Fbg chains.

Settings were as follows: 5 ppm precursor and 20 ppm fragment tolerance, digestion C-terminal of APKR, set to semi-specific with up to 5 missed cleavages. Modifications were drastically reduced compared to the gamma chain searches (compare attached file). Data was filtered as above.

α -chain in-gel digest:

A. Tryptic digest:

A custom database of all three chains, their mutants and other proteins was used.

Settings: 5 ppm precursor and 20 ppm fragment tolerance, digestion C-terminal of R/K, fully specific with up to 2 missed cleavages allowed, one common and one rare modification allowed.

Modifications, see attached file

B. ProAlanase digest:

A custom database of all three chains, their mutants and other proteins was used.

Settings: 5 ppm precursor and 20 ppm fragment tolerance, digestion C-terminal of P/A, non-specific with up to 2 missed cleavages allowed, one common and one rare modification allowed.

Modifications, see attached file

α -chain expression with protease inhibitors in-gel digest:

The database contained isoform 2 of the alpha chain and the other two chains.

Settings: 5 ppm precursor and 20 ppm fragment tolerance, digestion C-terminal of R/K, fully specific with up to 3 missed cleavages allowed, three common and two rare modifications allowed.

Time resolved cleavage site determination and quantification:

This search was performed using MaxQuant (V1.6.17.0) using a database containing all three Fbg chains, and in addition plasminogen, prothrombin, Factor FXIIIa and angiotensin peptide, common contaminants were added. Datafiles of 6 consecutive points in time were searched in batch. We used the instrument specific standard settings, specific trypsin digest but allowing up to 7 missed cleavages to account for differences between plasmin and trypsin, match between runs feature, allowed for up to 5 modifications. Allowed modifications were: Oxidation (M), Acetyl (N-term), Deamidation (NQ), Phospho (STY) and fixed Carbamidomethyl (C).

Bioinformatic analysis was performed using Perseus (V 4.1.3). We filtered the results as follows: removing contaminants, at least one intensity >0. We then normalized all intensities to the angiotensin intensity of the respective datafile. This excluded the last two points in time, as the angiotensin intensity was too low to be confirmed. We then extracted information for each of the respective Fbg chains. For each chain separately and per timepoint, we summed up intensities of all peptides, either regarding their start or end position. The sum of intensities for all peptides starting or ending at certain cleavage site, allowed us to develop a timepoint, not dependent on a single peptide, but on a certain cleavage site.

Supporting Information

Supporting Figure

Fibrinogen α -chain

10	20	30	40	50
MFSMRIVCLV	LSVVGTAWTA	DSGEGDFLAE	GGGVRGPEVV	ERHQ SACKDS
60	70	80	90	100
DWPFCSDEDW	NYKCPSGCRM	KGLIDEVNQD	FTNRINKLKN	SLFEYQKNNK
110	120	130	140	150
DSHSLTTNIM	EILGDFSSA	NNRDNNTYNV	SEDLRSRIEV	LKRK VIEKVQ
160	170	180	190	200
HIQLLQKNVR	AQLVDMKRLE	VDIDIKIRSC	RGSCSRALAR	EVDLKD YEDQ
210	220	230	240	250
QKQLEQVIAK	DLLPSDRQH	LPLIKMKPVP	DLVPGNFESQ	LQKVPPEWKA
260	270	280	290	300
LTDMPQME	LERPGGNEIT	GGSTSYGTG	SETESPENPS	SAGSWNSGSS
310	320	330	340	350
GPGSTGNRNP	GSSGTGGTAT	WKPGSSGPGS	TGSWNSGSSG	TGSTGNQNGP
360	370	380	390	400
SPRPGSTGTW	NPGSSERGSA	GHWTSESSVS	GSTGQWHSSES	GSFRPDSPGS
410	420	430	440	450
GNARPNPDW	GTFEEVSGNV	SPGTRREYHT	EKLVTSKGDK	ELRTGKQKVT
460	470	480	490	500
SGSTTTTRRS	CSKTVTKTVI	GPDGHKEVTK	EVVTS EDGSD	CPEAMD LGTL
510	520	530	540	550
SGIGTLDGFR	HRHPDEAAFF	DTASTGKTFP	GGFSPMLGEF	VSETESRGSE
560	570	580	590	600
SGIFTNTKES	SSHHPGIAEF	PSRCKSSSYS	KQFTSSTSYN	RGDSTFESKS
610	620	630	640	
YKMADEAGSE	ADHEGTHSTK	RGHAKSRPVR	GIHTSPLGKP	SLSP

Fibrinogen α -chain isoform αE

631-866:

640	650	660	670	680
DCDDVLQTHP	SGTQSGIFNI	KLPGSSKIFS	VYCDQETSLG	GWLLIQORMD
690	700	710	720	730
GSLNFNRTWQ	DYKRGFGSLN	DEGEGEFWLG	NDYLHLLTQR	GSVLRVELED
740	750	760	770	780
WAGNEAYA EY	HFRVGSEAEG	YALQVSSYEG	TAGDALIEGS	VEEGA EYTSH
790	800	810	820	830
NNMQFSTFDR	DADQWEENCA	EVYGGGWYWN	NCQAANLNGI	YYPGGSYDPR
840	850	860		
NNSPYEIENG	VVWVSFRGAD	YSLRAVRMKI	RPLVTQ	

Fibrinogen β -chain

```

10          20          30          40          50
MKRMVSWSFH KLKTMKHLILL LLLCVFLVKS QGVNDNEEGF FSARGHRPLD
60          70          80          90         100
KKREEAPSLR PAPPPISSGGG YRARPAKAAA TQKKVERKAP DAGGCLHADP
110         120         130         140         150
DLGVLCPGTC QLQEALLQQE RPIRNSVDEL NNNVEAVSQT SSSSFQYMYL
160         170         180         190         200
LKDLWQKRQK QVLDNENVVN EYSSELEKHQ LYIDETVNSN IPTNLRVLR
210         220         230         240         250
ILENLRSKIQ KLESVSAQM EYCPTCTVS CNIPVVSQKE CEEIIRKQGE
260         270         280         290         300
TSEMYLIQPD SSVKPYRVYC DMNTENGGWT VIQNRQDGSV DFGRKWDQYK
310         320         330         340         350
QGFQVATNT DGKNYCGLPG EYWLGNKIS QLTRMGPTEL LIEMEDWKGD
360         370         380         390         400
KVKAHYGGFT VQNEANKYQI SVNKYRGTAG NALMDGASQL MGENRTMTIH
410         420         430         440         450
NGMFFSTYDR DNDGWLTS DP RKQCSKEDGG GWWYNRCHAA NPNGRYYWGG
460         470         480         490
QYTWDMAKHG TDDGVVWMNW KGSWYSMRKM SMKIRPFFPQ Q

```

Fibrinogen γ -chain

```

10          20          30          40          50
MSWSLHPRNL ILYFYALLFL SSTCVAYVAT RDNCCILDER FGSYCPTTCG
60          70          80          90         100
IADFLSTYQT KVDKDLQSL EILHQVENT SEVKQLIKAI QLTYNPDESS
110         120         130         140         150
KPNMIDAATL KSRKMLEEIM KYEASILTHD SSIRYLQEIY NSNNQKIVNL
160         170         180         190         200
KEKVAQLEAQ CQEPCKDTVQ IHDITGKDCQ DIANKGAKQS GLYFIKPLKA
210         220         230         240         250
NQQFLVYCEI DGSGNGWTVF QKRLDGSVDF KKNWIQYKEG FGHLSPGTGT
260         270         280         290         300
EFWLGNEKIH LISTQSAIPY ALRVELEDWN GRTSTADYAM FKVGPEADKY
310         320         330         340         350
RLTYYAFAGG DAGDAFDGFD FGDDPSDKFF TSHNGMQFST WDNDNDKFEG
360         370         380         390         400
NCAEQDQSGW WMNKCHAGHL NGVYYQGGTY SKASTPNGYD NGIIWATWT
410         420         430
RWYSMKKTTM KIIPFNRLTI GEGQOHHLGG AKQAGDV

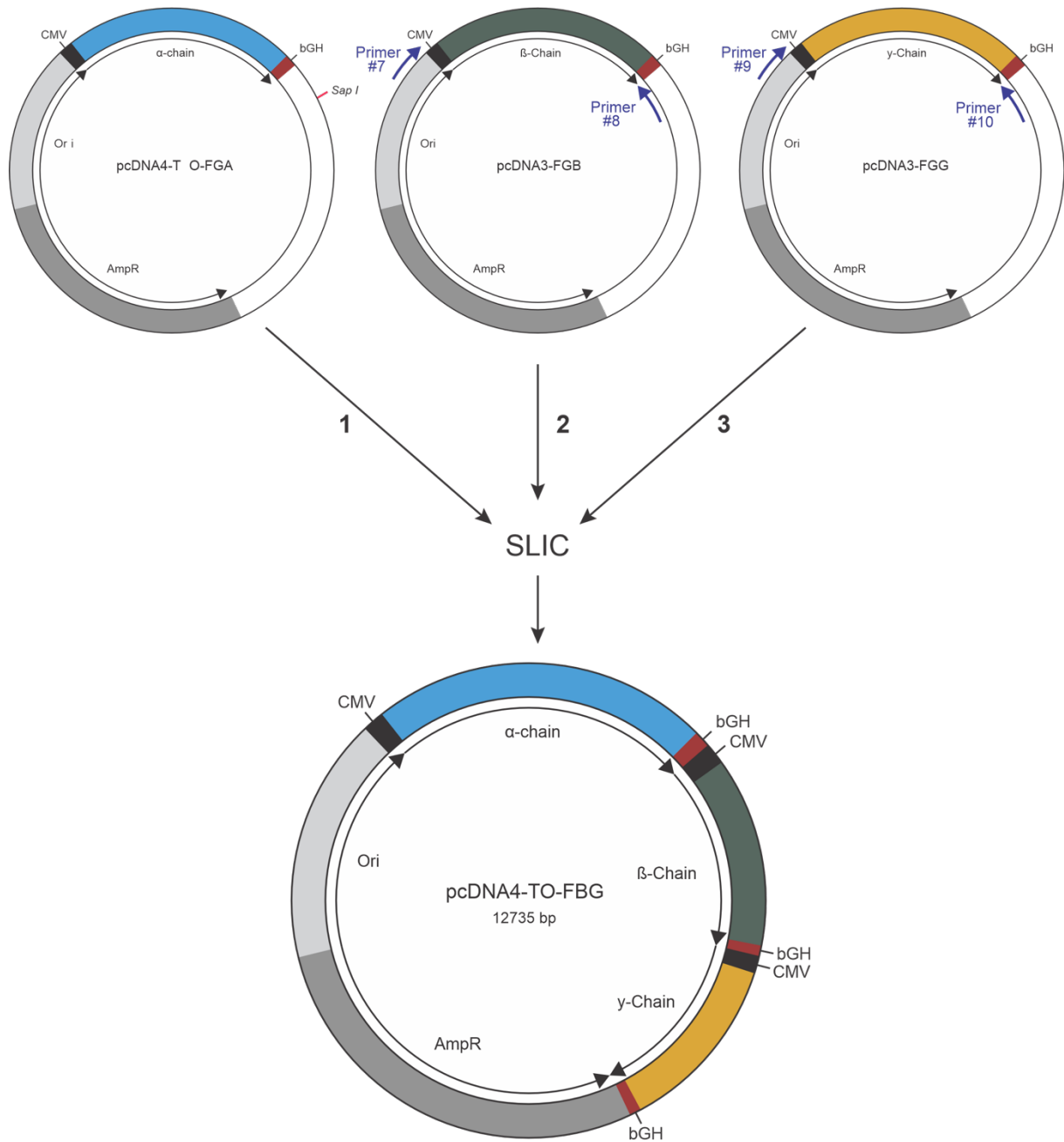
```

Fibrinogen γ -chain isoform γ' :

434-437: AGDV — VRPEHPAETEYDSLYPEDDL

- Cleavage sites only found in literature
- Cleavage sites only found MS experiments
- Cleavage sites found in literature and MS experiments
- Mutation sites found in this study

Figure S1: Sequence of the Fbg chains, α (Uniprot-FB02671), β (Uniprot-FB02675) and γ (Uniprot-FB02679), with cleavage and mutations sites highlighted in different colors.⁴⁰⁻⁴³



1. *SapI* restriction digest
2. PCR, dephosphorylation
3. PCR, dephosphorylation

Figure S2: Construction of Fbg expression plasmid.

Table 1: Listing of the different plasmids

Date / Name	FGA	FGB	FGG	tag
pcDNA4/TO/FG	wt, isoform α -E	wt, isoform 1	wt, isoform γ'	C-terminal myc-His (FGA)
pcDNA4/TO/FG_wt_no tag	wt, isoform α -E	wt, isoform 1	wt, isoform γ'	-
pcDNA4/TO/FG_mut_mycHis	wt, isoform α -E	wt, isoform 1	K88S, K111S, K382S, K399S, isoform γ'	C-terminal myc-His (FGA)
pcDNA4/TO/FG_mut_no tag	wt, isoform α -E	wt, isoform 1	K88S, K111S, K382S, K399S, isoform γ'	-
pcDNA4/TO/FG_new_wt	wt, isoform α	wt, isoform 1	wt, isoform γ	-
pcDNA4/TO/FG_new_HisM4	wt, isoform α	wt, isoform 1	K88H, K111H, K382H, K399H, isoform γ	-
pcDNA4/TO/FG_new_AlaM3	wt, isoform α	wt, isoform 1	K88A, K111A, K382A, K399A, isoform γ	-
pcDNA4/TO/FG_K432H_wt	K432H, isoform α	wt, isoform 1	wt, isoform γ	-
pcDNA4/TO/FG_5xKtoH_wt	5xKtoH*, isoform α	wt, isoform 1	wt, isoform	-
pcDNA4/TO/FG_K432H_HisM4	K432H, isoform α	wt, isoform 1	K88H, K111H, K382H, K399H, isoform γ	-
pcDNA4/TO/FG_5xKtoH_HisM4	5xKtoH*, isoform α	wt, isoform 1	K88H, K111H, K382H, K399H, isoform γ	-

Table 2: Oligonucleotides used for PCR-amplifications:

Amplicon	oligonucleotides	template
FGA-ORF, wt, isoform α E, without stop-codon	#1 #2	"FGA-Bio-His"
FGA-ORF, wt, isoform α E, with stop-codon	#1 #68	"FGA-Bio-His"
FGA-ORF, wt, isoform A α	#198 #201	pcMV6-XL4-FGA_new
FGA-ORF, K432H mutagenesis	#302 #304	pcDNA4/TO/FGA_new
FGA-ORF, 5xKtoH mutagenesis	#303 #305	pcDNA4/TO/FGA_new
FGB-ORF, wt, isoform 1	#3 #4	„FGB“
FGG-ORF, wt, isoform γ'	#5 #6	„FGG“
FGG-ORF, K88S, K111S, K382S, K399S, isoform γ'	#5 #6	"FGG mutation"
FGG-ORF, wt, isoform γ	received ORF already in pcDNA3	
FGG-ORF, K88H, K111H, K382H, K399H, isoform γ	received ORF already in pcDNA3	
FGG-ORF, K88A, K111A, K382A, K399A, isoform γ	received ORF already in pcDNA3	
FGB-operon (incl. CMV promoter and bGH poly(A)signal)	#7 #8	pcDNA3-FGB
FGG-operon (incl. CMV promoter and bGH poly(A)signal)	#9 #10	pcDNA3-FGG, pcDNA3-FGG_mut, pcDNA3-FGG_HisM4, or pcDNA3-FGG_AlaM3

Table 3: Oligonucleotide sequences:

oligonucleotide	direction	sequence
#1	forward	TGGCGGCCGCTCGAGTCTAGGCCACCATGGTGTCCATGC
#2	reverse	TTGTTCGAAGGGCCCTCTAGCCTGAGTGACCAGGGGC
#3	forward	GCCGCCAGTGTGCTGGAATTGCCACCATGGTCCGGATGG
#4	reverse	TGATGGATATCTGCAGAATTTCACTGCTGAGGAAAGAATGGCC
#5	forward	GCCGCCAGTGTGCTGGAATTGCCACCATGGTCTGGTCCC
#6	reverse	TGATGGATATCTGCAGAATTTCACAGGTCGTCCTCGGGG
#7	forward	GTATTGGGCGCTCTTCCGCTGTACGGGCCAGATATACGCG
#8	reverse	CGCGTATATCTGGCCCGTACCCATAGAGCCCACCGCATCC
#9	forward	GGATGCGGTGGGCTCTATGGGTACGGGCCAGATATACGGG
#10	reverse	GAGTCAGTGAGCGAGGAAGCCCATAGAGCCCACCGCATCC
#68	reverse	TGTTCGAAGGGCCCTCTAGATCAAGCCTGAGTGACCAGGGGCC
#198	Reverse	TTGTTCGAAGGGCCCTCTAGCTAGGGGGACAGGGAAG
#201	forward	TAAGAAGGAGATATAACCATGGAAGCAGCAGTCG
#302	forward	CATCTGGTCACTTCTAAAGGAGATAAAGAGC
#303	reverse	CATCTGGTCACTTCTCATGGAGATCATGAGCTCAGGACTGTGCATGAGCATGTCACCTCTGGTAGCACAACC
#304	forward	CCTTTAGAAGTGACCAGATGTTCTGTGTGGTACTCTC
#305	reverse	CCATGAGAAGTGACCAGATGTTCTGTGTGGTACTCTC

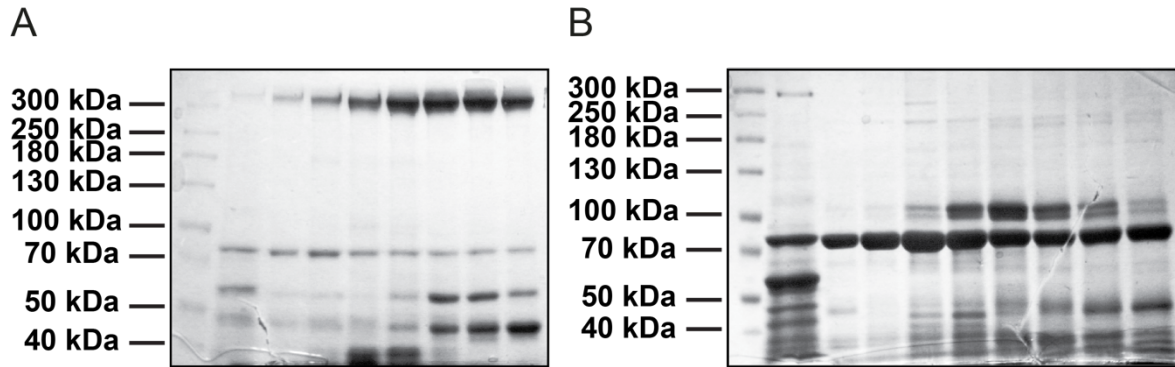


Figure S3: Analysis of recombinant Fbg expression in CHO cells. (A) SDS-PAGE (5-12%) WT-rFbgi after the first purification using AiEx (B) Ser-rFbgi after the first purification using AiEx.

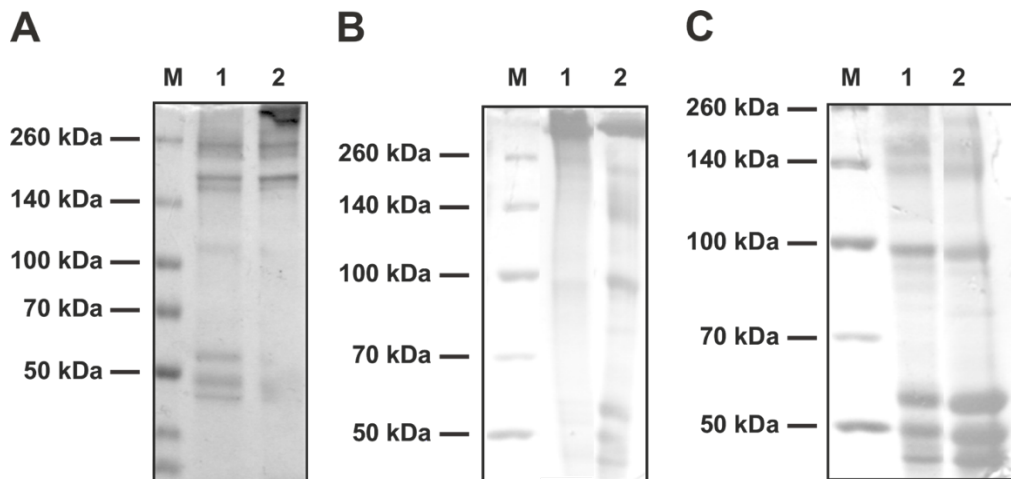
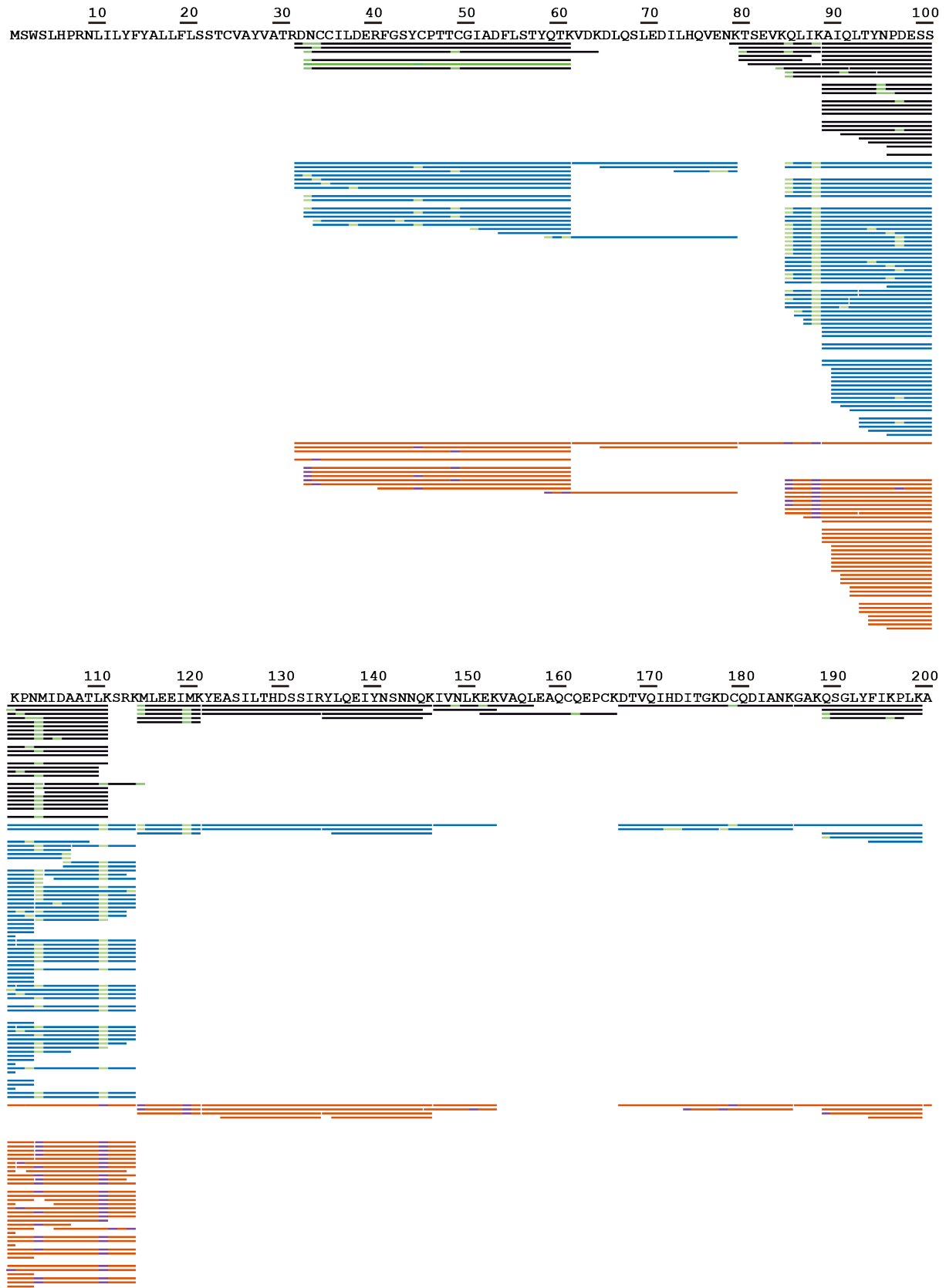


Figure S4: SDS-PAGE analysis of the expression of rFbg, His-rFbg and Ala-rFbg. (A) SDS-Page of WT rFbg: M: Marker; 1: rFbg reduced; 2: rFbg non-reduced. (B) SDS-PAGE of rFbg variants: M: Marker; 1: His-rFbg non-reduced; 2: Ala-rFbg non-reduced. (C) SDS-PAGE of rFbg variants: M: Marker; 1: His-rFbg reduced; 2: Ala-rFbg reduced.



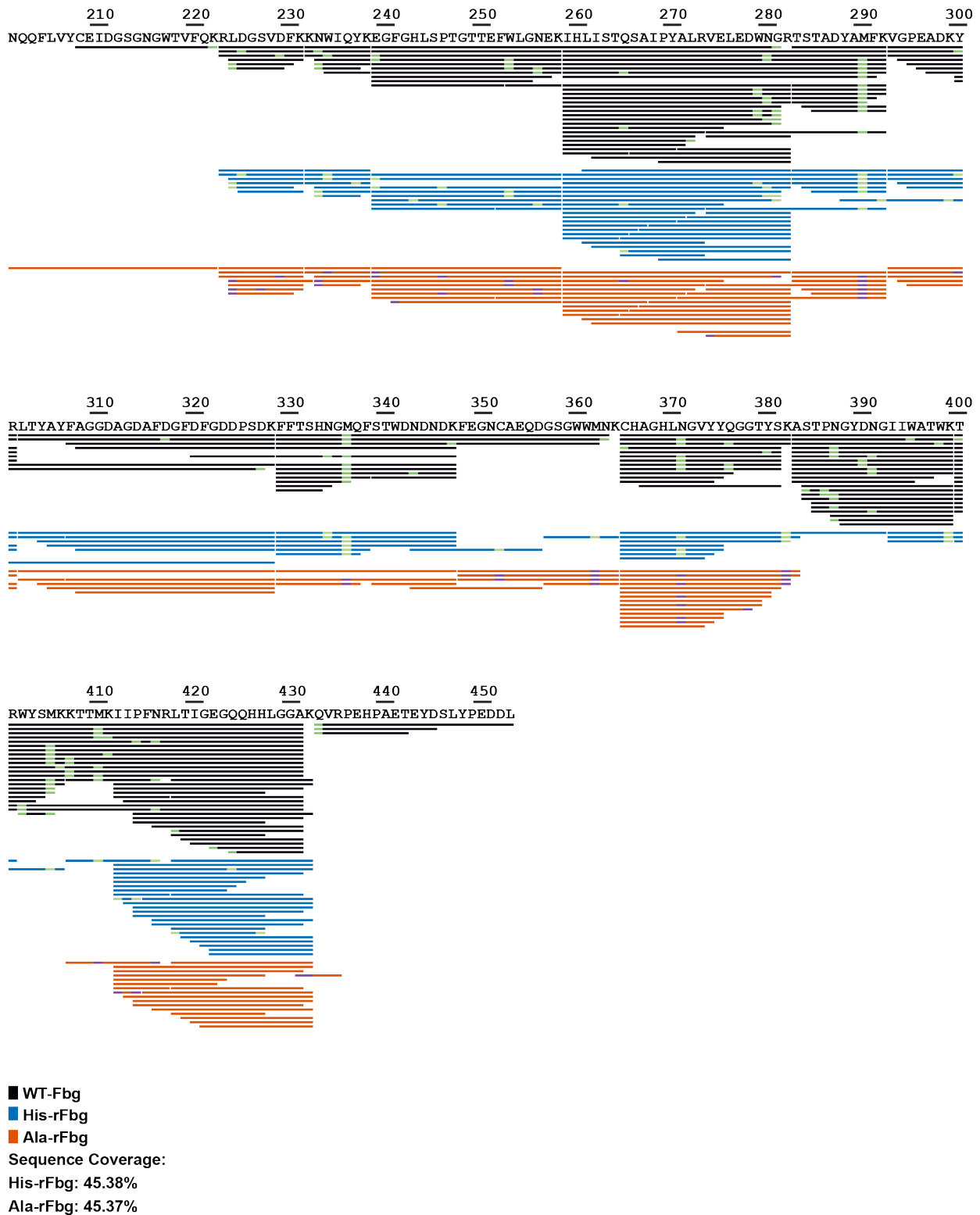


Figure S5: NanoLC-MS/MS analysis of rFbg, His- and Ala-rFbg γ -chain after plasmin digest. Suggested modifications are highlighted in light green (WT- and His-rFbg) or dark blue (Ala-rFbg). Opposing colors of peptide fragments to the normal coloring scheme (Black – Green; Blue – Green, Red – Purple) are the result of the selection of the respective fragments in the software.

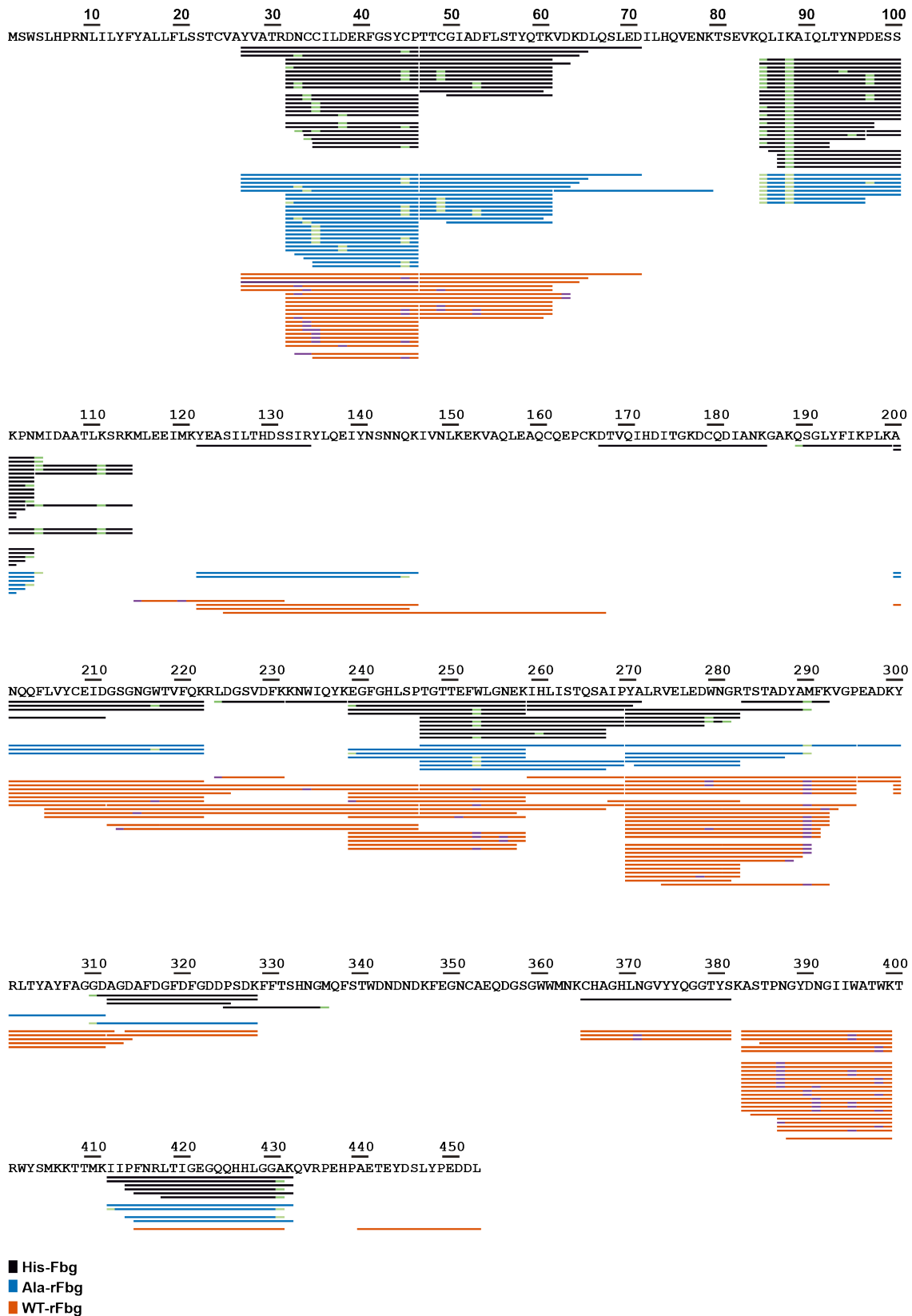
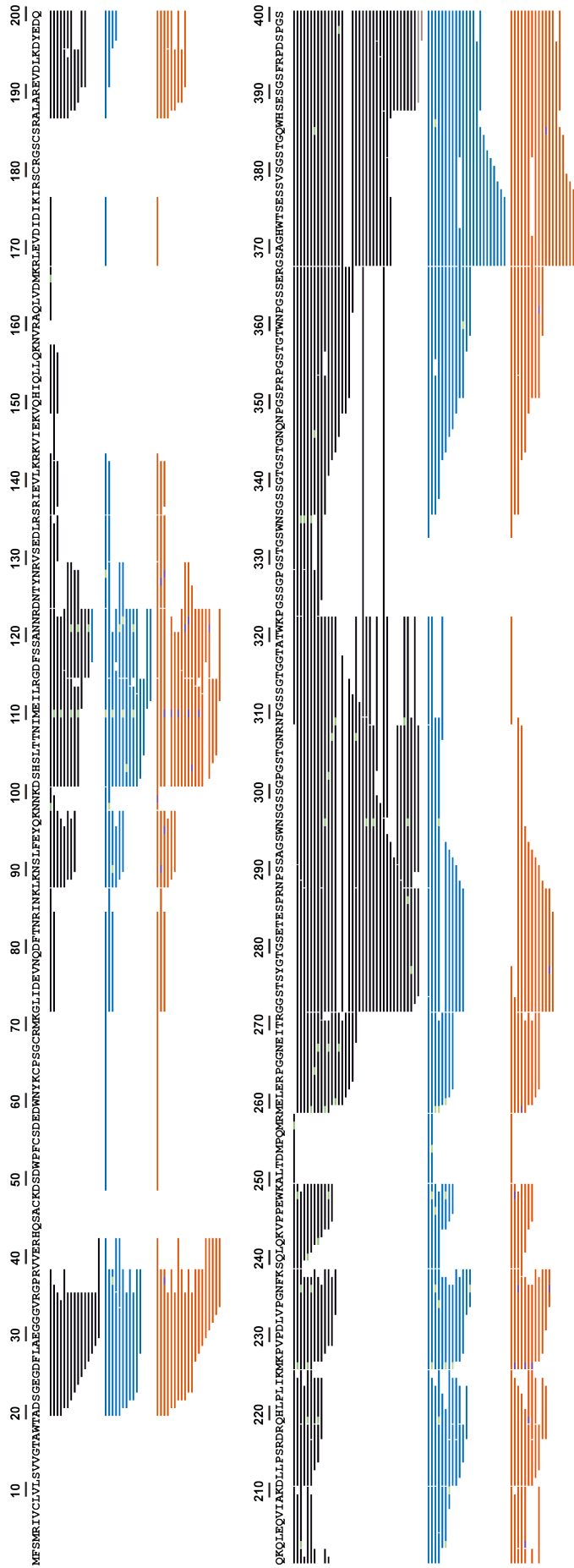


Figure S6: NanoLC-MS/MS analysis of rFbg, His- and Ala-rFbg γ -chain after plasmin and subsequent ProAla digest. Suggested modifications are highlighted in light green (His- and Ala-rFbg) or dark blue (WT-rFbg). Opposing colors of peptide fragments to the normal coloring scheme (Black – Green; Blue – Green, Red – Purple) are the result of the selection of the respective fragments in the software.



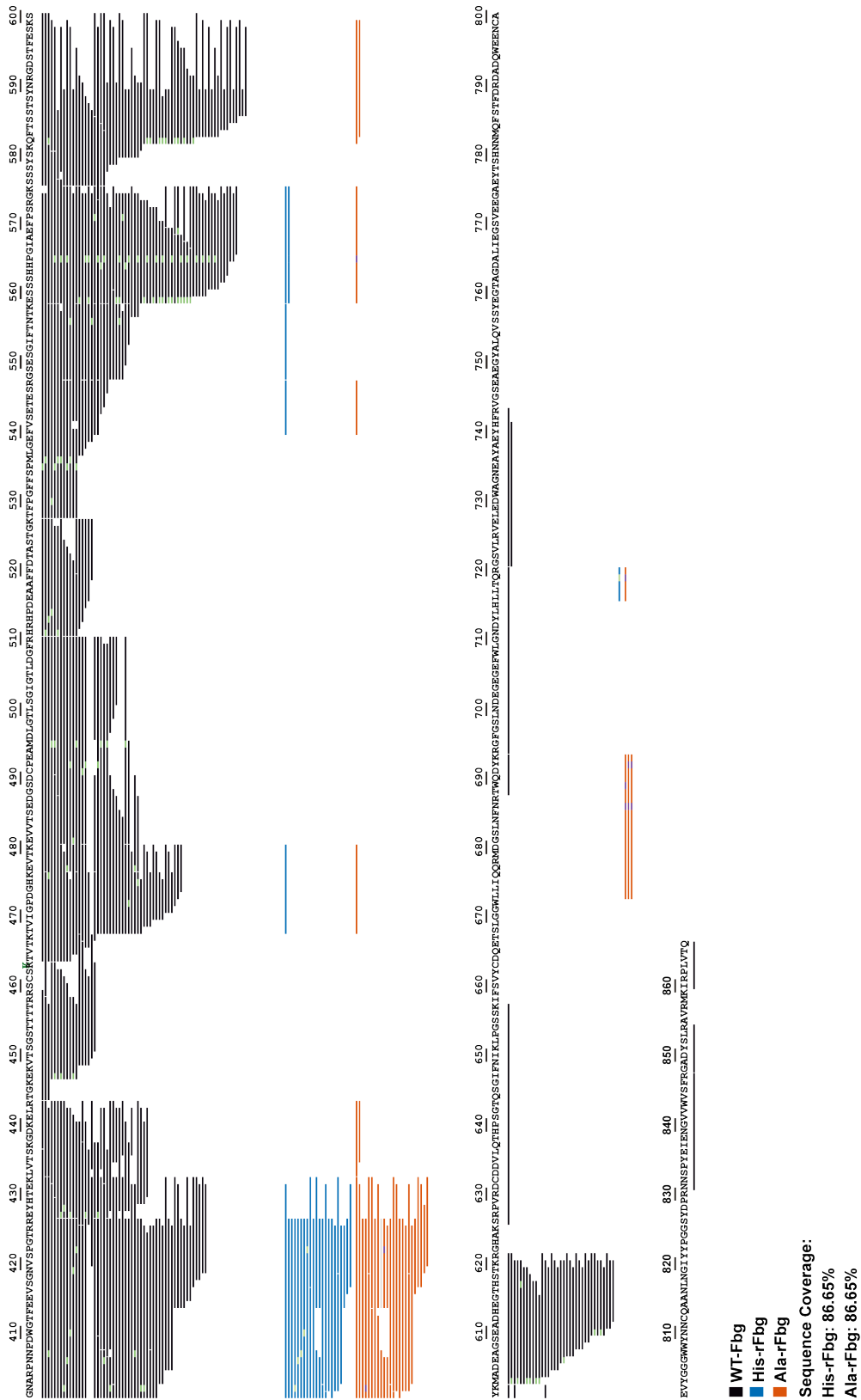


Figure S7: NanoLC-MS/MS analysis of WT-Fbg, His- and Ala-rFbg α -chain after plasmin digest. Suggested modifications are highlighted in light green (WT-Fbg- and His-rFbg) or dark blue (Ala-rFbg). Opposing colors of peptide fragments to the normal coloring scheme (Black – Green; Blue – Green, Red – Purple) are the result of the selection of the respective fragments in the software.

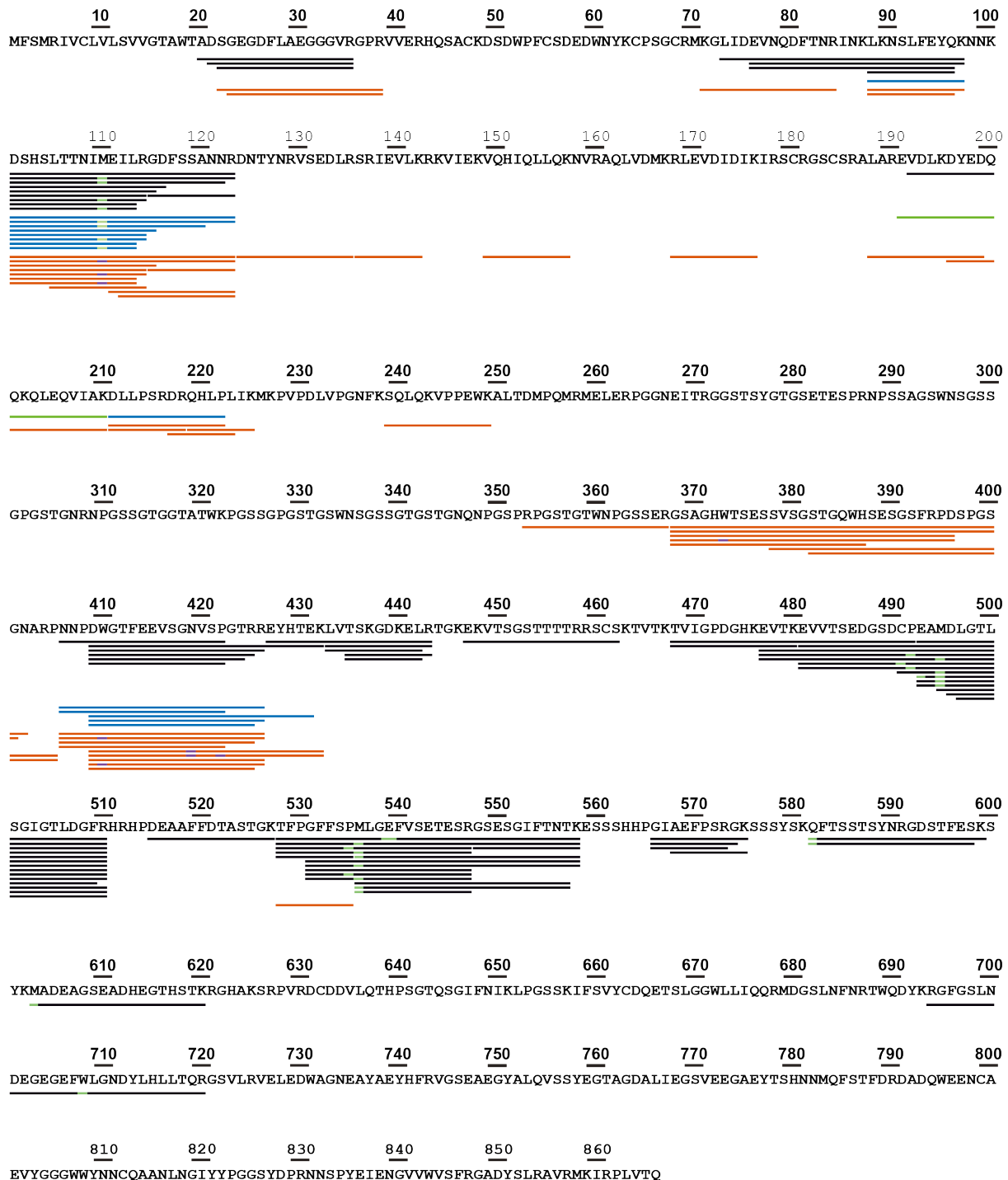


Figure S8: NanoLC-MS/MS analysis of WT-Fbg, His- and Ala-rFbg α -chain after plasmin and subsequent ProAla digest. Suggested modifications are highlighted in light green (Ala- and His-rFbg) or dark blue (WT-Fbg). Opposing colors of peptide fragments to the normal coloring scheme (Black – Green; Blue – Green, Red – Purple) are the result of the selection of the respective fragments in the software.

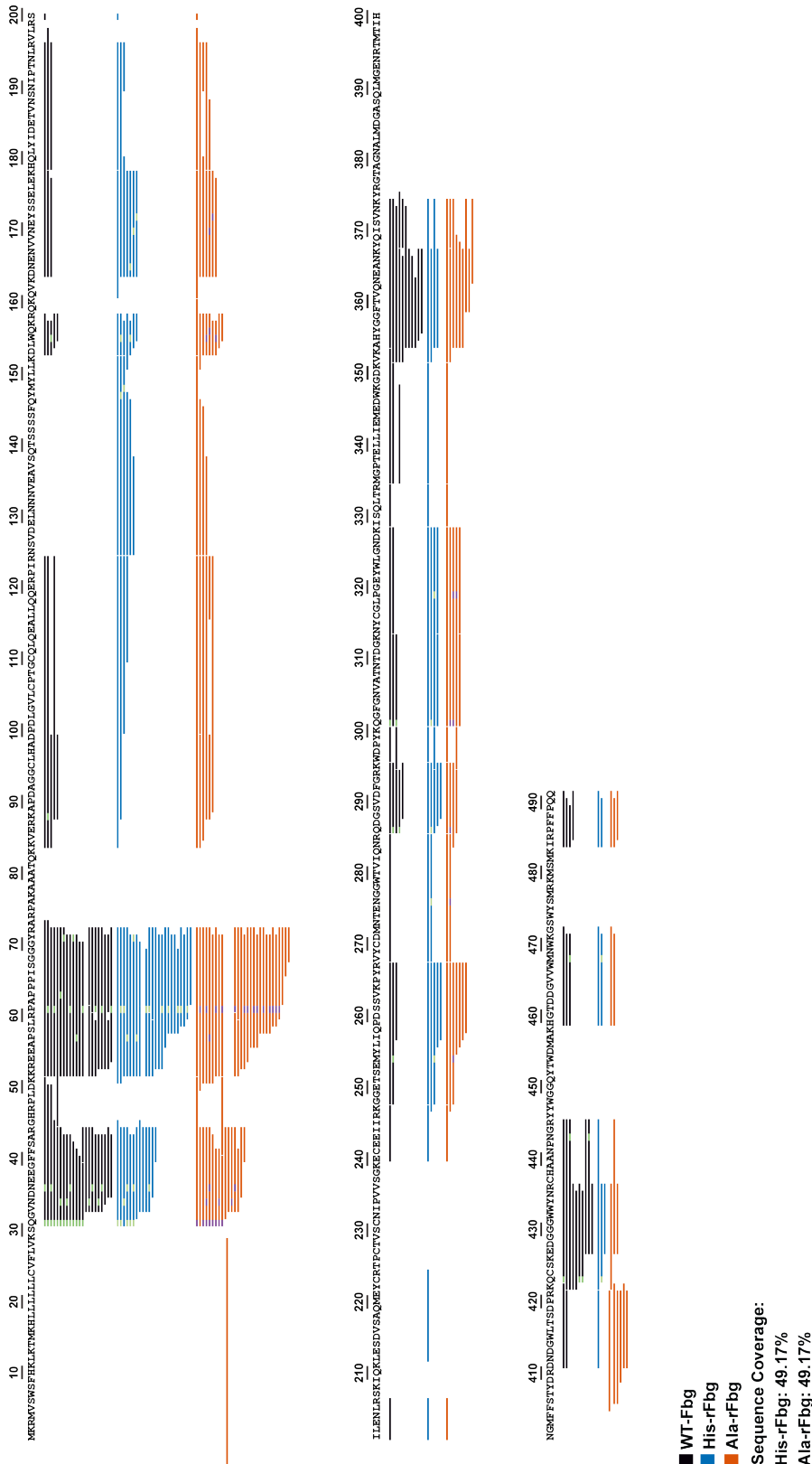
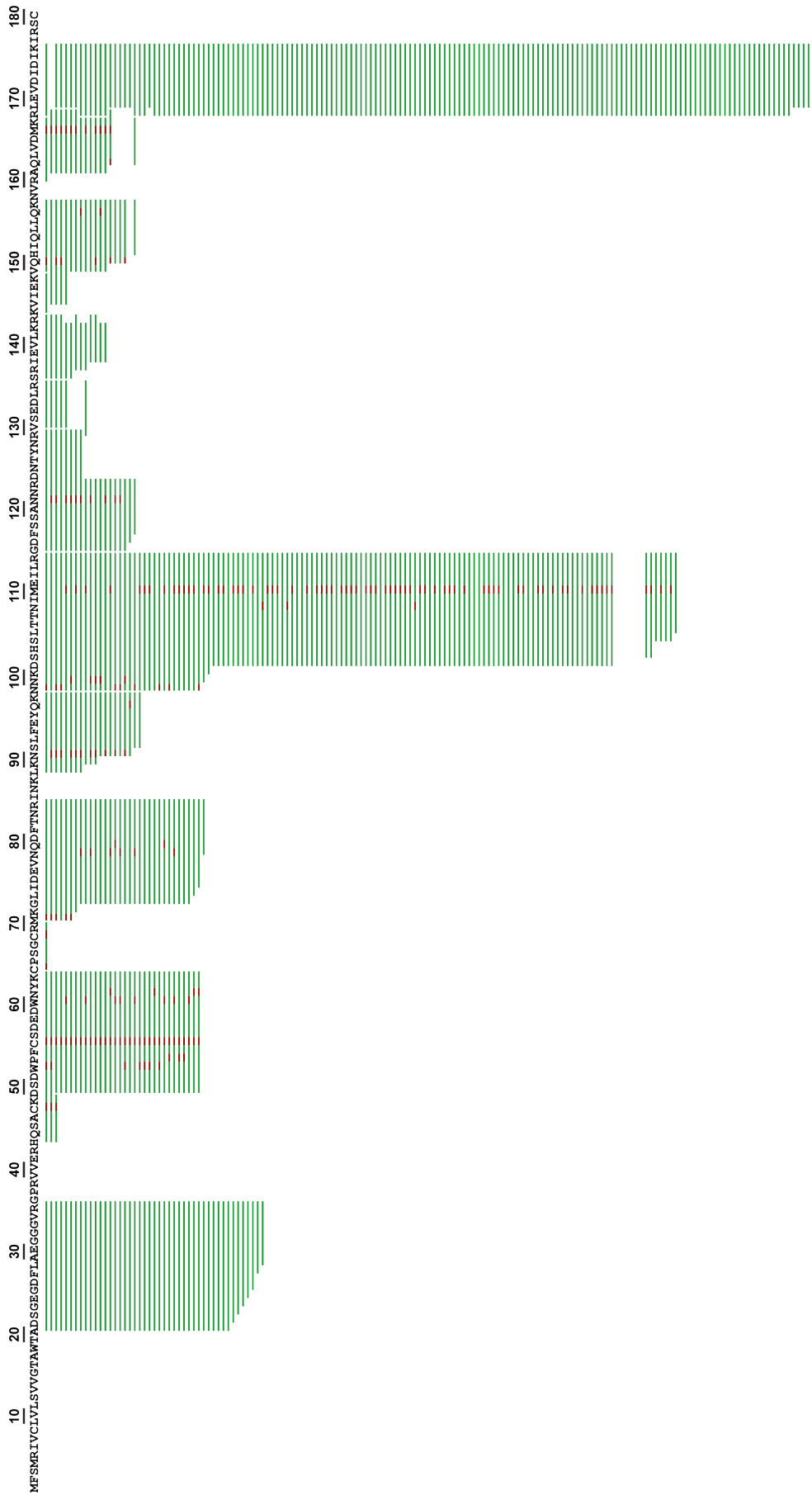


Figure S9: NanoLC-MS/MS analysis of WT-Fbg, His- and Ala-rFbg β -chain after plasmin digest. Suggested modifications are highlighted in light green (WT-Fbg- and His-rFbg) or dark blue (Ala-rFbg). Opposing colors of peptide fragments to the normal coloring scheme (Black – Green; Blue – Green, Red – Purple) are the result of the selection of the respective fragments in the software.



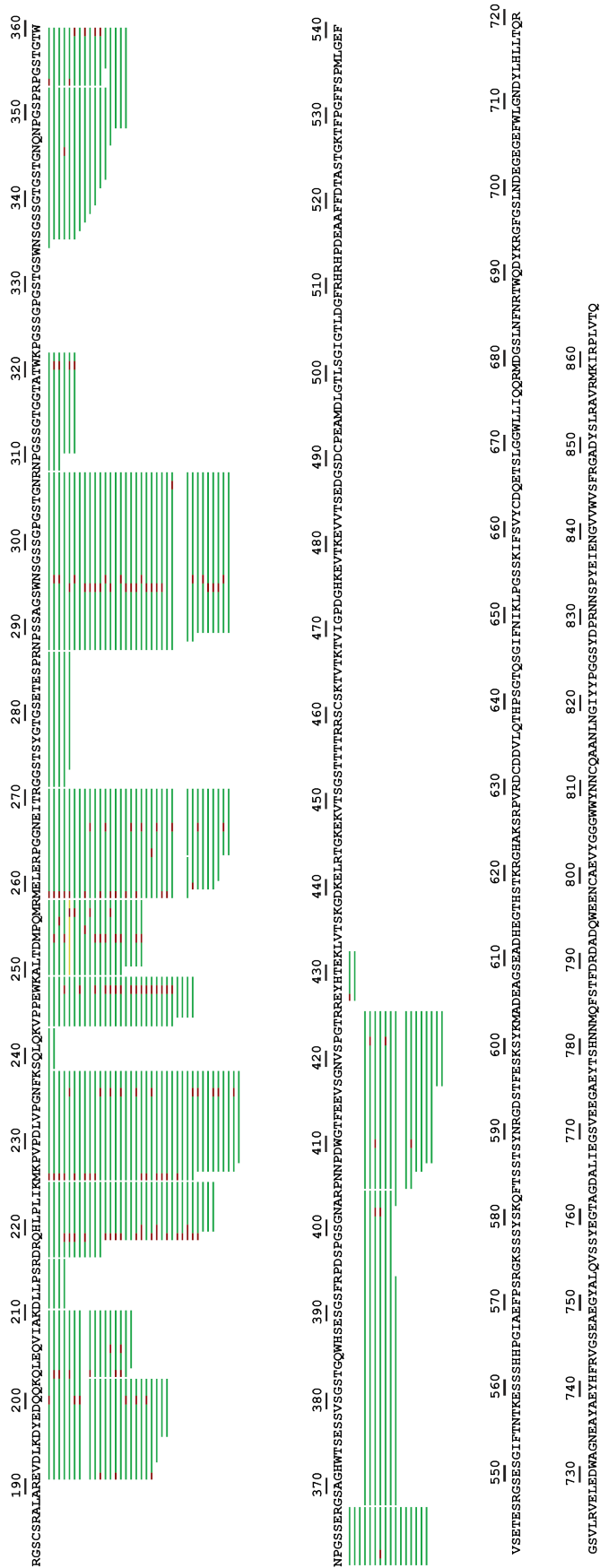


Figure S11: NanoLC-MS/MS analysis of the in-gel digest of His-rFbg α -chain.

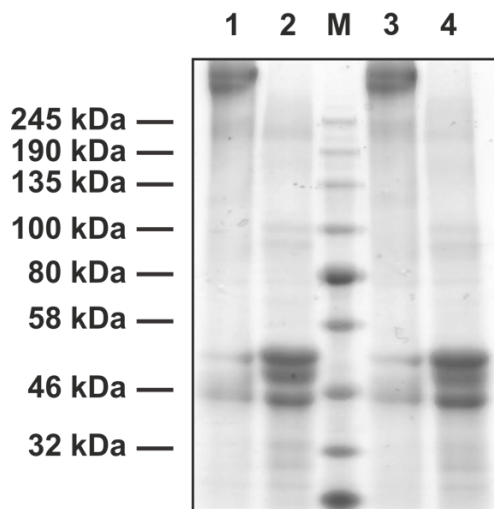


Figure S12: SDS-PAGE analysis of the expression of His-rFbg432 and His-rFbg5xKtoH. M: Marker; 1: His-rFbg432 non-reduced. 2: His-rFbg432 reduced. 3: His-rFbg5xKtoH non-reduced. 4: His-rFbg5xKtoH reduced.

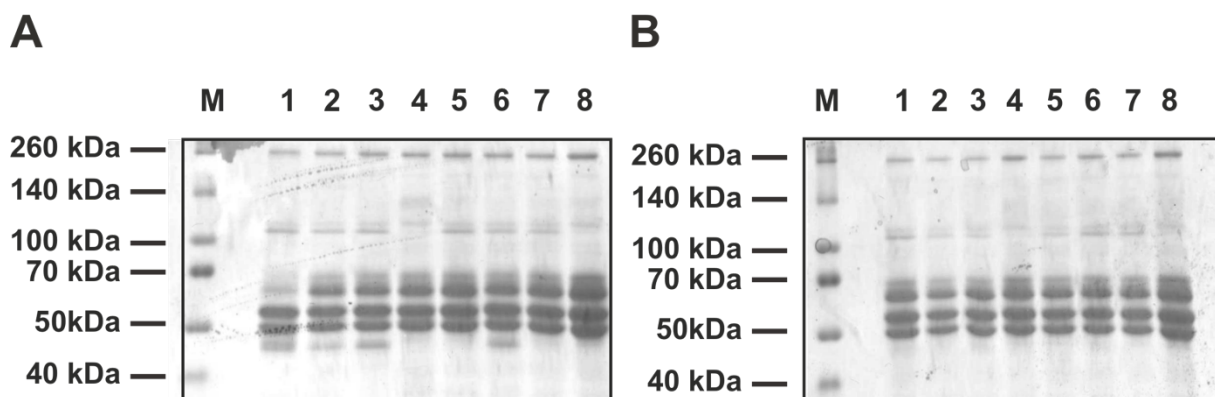


Figure S13: Screening of different inhibitors for the expression of rFbg. (A) SDS-PAGE of Fbg incubated with ExpiCHO™ cell supernatant and different inhibitors after 2 h: M: Marker; 1: Fbg 2: Fbg + PMSF 3: Fbg + Aprotinin; 4: Fbg + EDTA; 5: Fbg + 1,10 Phenanthroline; 6: Fbg + GM6001; 7: Fbg + UK 370106; 8: Fbg control. (B) SDS-PAGE of Fbg incubated with ExpiCHO™ cell supernatant and different inhibitors after 14 h: M: Marker; 1: Fbg 2: Fbg + PMSF 3: Fbg + Aprotinin; 4: Fbg + EDTA; 5: Fbg + 1,10 Phenanthroline; 6: Fbg + GM6001; 7: Fbg + UK 370106; 8: Fbg control.

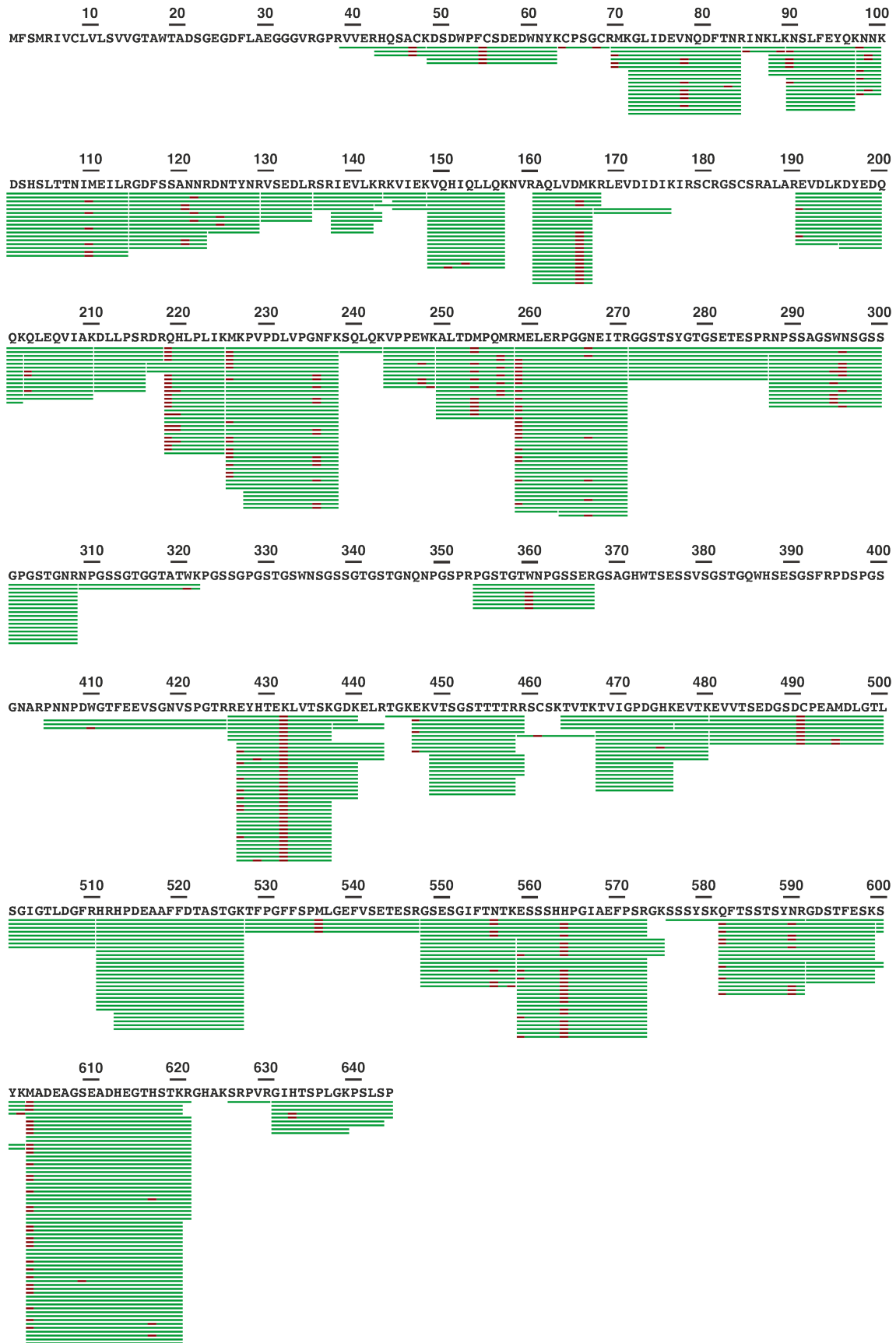


Figure S14: NanoLC-MS/MS analysis of the in-gel digest of His-rFbgK432 α -chain with the addition of UK 370106 during production.

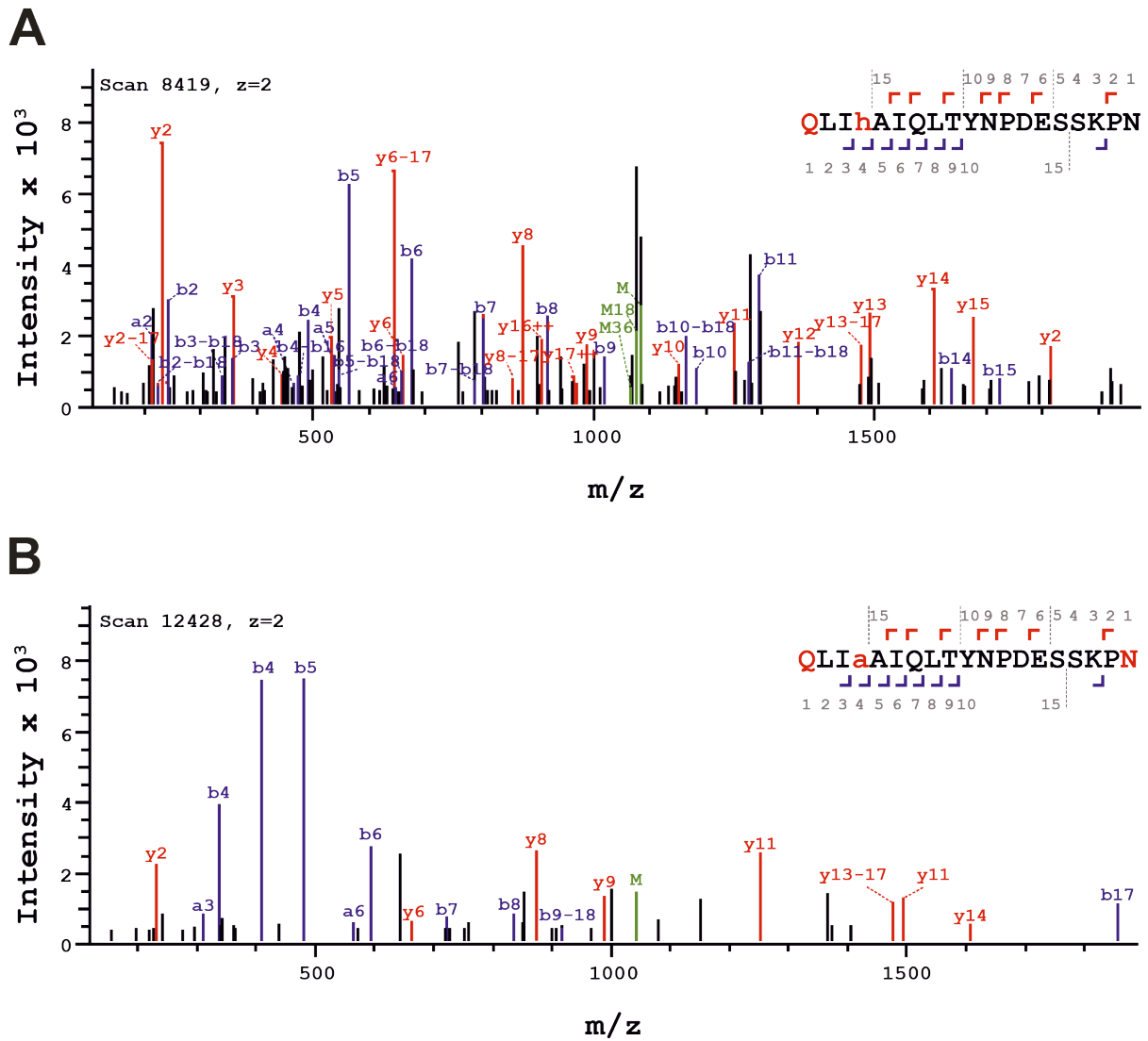


Figure S15: NanoLC-MS/MS analysis of (A) His- and (B) Ala-rFbg γ -chain after plasmin digest.

References:

1. Sørensen, B.; Tang, M.; Larsen, O. H.; Laursen, P. N.; Fenger-Eriksen, C.; Rea, C. J., The role of fibrinogen: a new paradigm in the treatment of coagulopathic bleeding. *Thromb Res* **2011**, *128 Suppl 1*, S13-6.
2. Gale, A. J., Continuing education course #2: current understanding of hemostasis. *Toxicol Pathol* **2011**, *39* (1), 273-80.
3. Kattula, S.; Byrnes, J. R.; Wolberg, A. S., Fibrinogen and Fibrin in Hemostasis and Thrombosis. *Arteriosclerosis, Thrombosis, and Vascular Biology* **2017**, *37* (3), e13-e21.
4. Mosesson, M. W., Fibrinogen and fibrin structure and functions. *J Thromb Haemost* **2005**, *3* (8), 1894-904.
5. Kollman, J. M.; Pandi, L.; Sawaya, M. R.; Riley, M.; Doolittle, R. F., Crystal Structure of Human Fibrinogen. *Biochemistry* **2009**, *48* (18), 3877-3886.
6. Roberts, I. V.; Bukhary, D.; Valdivieso, C. Y. L.; Tirelli, N., Fibrin Matrices as (Injectable) Biomaterials: Formation, Clinical Use, and Molecular Engineering. *Macromolecular Bioscience* **2020**, *20* (1), 1900283.
7. Fu, Y.; Grieninger, G., Fib420: a normal human variant of fibrinogen with two extended alpha chains. *Proceedings of the National Academy of Sciences* **1994**, *91* (7), 2625-2628.
8. Soria, J.; Mirshahi, S.; Mirshahi, S. Q.; Varin, R.; Pritchard, L. L.; Soria, C.; Mirshahi, M., Fibrinogen α C domain: Its importance in physiopathology. *Res Pract Thromb Haemost* **2019**, *3* (2), 173-183.
9. Cantero, M.; Rojas, H.; Anglés-Cano, E.; Marchi, R., Fibrin γ/γ' influences the secretion of fibrinolytic components and clot structure. *BMC Molecular and Cell Biology* **2019**, *20* (1), 47.
10. Meh, D. A.; Siebenlist, K. R.; Mosesson, M. W., Identification and Characterization of the Thrombin Binding Sites on Fibrin*. *Journal of Biological Chemistry* **1996**, *271* (38), 23121-23125.
11. Wolfenstein-Todel, C.; Mosesson, M. W., Human plasma fibrinogen heterogeneity: evidence for an extended carboxyl-terminal sequence in a normal gamma chain variant (gamma'). *Proc Natl Acad Sci U S A* **1980**, *77* (9), 5069-73.
12. Greenberg, C. S.; Miraglia, C. C.; Rickles, F. R.; Shuman, M. A., Cleavage of blood coagulation factor XIII and fibrinogen by thrombin during in vitro clotting. *J Clin Invest* **1985**, *75* (5), 1463-70.
13. Riedel, T.; Suttner, J.; Brynda, E.; Houska, M.; Medved, L.; Dyr, J. E., Fibrinopeptides A and B release in the process of surface fibrin formation. *Blood* **2011**, *117* (5), 1700-1706.
14. Joo, J. Y.; Amin, M. L.; Rajangam, T.; An, S. S. A., Fibrinogen as a promising material for various biomedical applications. *Molecular & Cellular Toxicology* **2015**, *11* (1), 1-9.
15. Solovieva, E. V.; Fedotov, A. Y.; Mamonov, V. E.; Komlev, V. S.; Panteleyev, A. A., Fibrinogen-modified sodium alginate as a scaffold material for skin tissue engineering. *Biomed Mater* **2018**, *13* (2), 025007.
16. Spotnitz, W. D., Fibrin Sealant: Past, Present, and Future: A Brief Review. *World Journal of Surgery* **2010**, *34* (4), 632-634.
17. Spotnitz, W. D., Fibrin Sealant: The Only Approved Hemostat, Sealant, and Adhesive—a Laboratory and Clinical Perspective. *ISRN Surgery* **2014**, *2014*, 203943.
18. Jackson, M. R., Fibrin sealants in surgical practice: An overview. *Am J Surg* **2001**, *182* (2 Suppl), 1s-7s.
19. Zhang, Y., Applications of Fibrin Tissue Sealant. *IOP Conference Series: Earth and Environmental Science* **2021**, *632* (5), 052098.
20. Spotnitz, W. D., Fibrin Sealant: The Only Approved Hemostat, Sealant, and Adhesive—a Laboratory and Clinical Perspective. *ISRN Surg* **2014**, *2014*, 203943.

21. Smith, J. D.; Chen, A.; Ernst, L. A.; Waggoner, A. S.; Campbell, P. G., Immobilization of aprotinin to fibrinogen as a novel method for controlling degradation of fibrin gels. *Bioconjug Chem* **2007**, *18* (3), 695-701.
22. Lorentz, K. M.; Kontos, S.; Frey, P.; Hubbell, J. A., Engineered aprotinin for improved stability of fibrin biomaterials. *Biomaterials* **2011**, *32* (2), 430-438.
23. Chapin, J. C.; Hajjar, K. A., Fibrinolysis and the control of blood coagulation. *Blood reviews* **2015**, *29* (1), 17-24.
24. Bannish, B. E.; Chernysh, I. N.; Keener, J. P.; Fogelson, A. L.; Weisel, J. W., Molecular and Physical Mechanisms of Fibrinolysis and Thrombolysis from Mathematical Modeling and Experiments. *Scientific Reports* **2017**, *7* (1), 6914.
25. Keragala, C. B.; Medcalf, R. L., Plasminogen: an enigmatic zymogen. *Blood* **2021**, *137* (21), 2881-2889.
26. Schaller, J.; Gerber, S. S., The plasmin-antiplasmin system: structural and functional aspects. *Cell Mol Life Sci* **2011**, *68* (5), 785-801.
27. Katz, J. M.; Tadi, P., Physiology, Plasminogen Activation. In *StatPearls*, StatPearls Publishing Copyright © 2021, StatPearls Publishing LLC.: Treasure Island (FL), **2021**.
28. Whyte, C. S.; Mutch, N. J., uPA-mediated plasminogen activation is enhanced by polyphosphate. *Haematologica* **2020**, *106* (2), 522-531.
29. DePalma, L.; Criss, V. R.; Luban, N. L., The preparation of fibrinogen concentrate for use as fibrin glue by four different methods. *Transfusion* **1993**, *33* (9), 717-20.
30. Scheule, A. M.; Beierlein, W.; Wendel, H. P.; Eckstein, F. S.; Heinemann, M. K.; Ziemer, G., Fibrin sealant, aprotinin, and immune response in children undergoing operations for congenital heart disease. *J Thorac Cardiovasc Surg* **1998**, *115* (4), 883-9.
31. Kassell, B.; Laskowski, M., Sr., The basic trypsin inhibitor of bovine pancreas. V. The disulfide linkages. *Biochem Biophys Res Commun* **1965**, *20* (4), 463-8.
32. Kang, H. M.; Kalnoski, M. H.; Frederick, M.; Chandler, W. L., The kinetics of plasmin inhibition by aprotinin in vivo. *Thromb Res* **2005**, *115* (4), 327-40.
33. Baxter Healthcare Corporation; Package Insert - TISSEEL, n.d. U.S. Food and Drug Administration Web site <https://www.fda.gov/media/71674/download> (accessed Dez 13, 2022).
34. Lindsey, K.; Clinical Review - Tisseel STN: 103980/5601, n.d.. U.S. Food & Drug Administration Web site. <https://www.fda.gov/media/83108/download> (accessed Dez 13, 2022).
35. Beierlein, W.; Scheule, A. M.; Antoniadis, G.; Braun, C.; Schosser, R., An immediate, allergic skin reaction to aprotinin after reexposure to fibrin sealant. *Transfusion* **2000**, *40* (3), 302-305.
36. Shirai, T.; Shimota, H.; Chida, K.; Sano, S.; Takeuchi, Y.; Yasueda, H., Anaphylaxis to aprotinin in fibrin sealant. *Intern Med* **2005**, *44* (10), 1088-9.
37. Lutz, S.; Iamurri, S. M., Protein Engineering: Past, Present, and Future. *Methods Mol Biol* **2018**, *1685*, 1-12.
38. Modarres, H. P.; Mofrad, M. R.; Sanati-Nezhad, A., Protein thermostability engineering. *RSC Advances* **2016**, *6* (116), 115252-115270.
39. Huang, P.; Chu, S. K. S.; Frizzo, H. N.; Connolly, M. P.; Caster, R. W.; Siegel, J. B., Evaluating Protein Engineering Thermostability Prediction Tools Using an Independently Generated Dataset. *ACS Omega* **2020**, *5* (12), 6487-6493.
40. Yuan, H.; Vance, K. M.; Junge, C. E.; Geballe, M. T.; Snyder, J. P.; Hepler, J. R.; Yepes, M.; Low, C. M.; Traynelis, S. F., The serine protease plasmin cleaves the amino-terminal domain of the NR2A subunit to relieve zinc inhibition of the N-methyl-D-aspartate receptors. *J Biol Chem* **2009**, *284* (19), 12862-73.
41. Bini, A.; Wu, D.; Schnuer, J.; Kudryk, B. J., Characterization of stromelysin 1 (MMP-3), matrilysin (MMP-7), and membrane type 1 matrix metalloproteinase (MT1-MMP)

- derived fibrin(ogen) fragments D-dimer and D-like monomer: NH₂-terminal sequences of late-stage digest fragments. *Biochemistry* **1999**, *38* (42), 13928-36.
42. Henschen, A.; Mcdonagh, J., Chapter 7 Fibrinogen, fibrin and factor XIII. *New Comprehensive Biochemistry* **1986**, *13*, 171-241.
 43. Hudson, N. E., Biophysical Mechanisms Mediating Fibrin Fiber Lysis. *Biomed Res Int* **2017**, *2017*, 2748340.
 44. Mosesson, M. W.; Siebenlist, K. R.; Meh, D. A., The structure and biological features of fibrinogen and fibrin. *Ann N Y Acad Sci* **2001**, *936*, 11-30.
 45. Standeven, K. F.; Carter, A. M.; Grant, P. J.; Weisel, J. W.; Chernysh, I.; Masova, L.; Lord, S. T.; Ariëns, R. A. S., Functional analysis of fibrin γ -chain cross-linking by activated factor XIII: determination of a cross-linking pattern that maximizes clot stiffness. *Blood* **2007**, *110* (3), 902-907.
 46. Hervio, L. S.; Coombs, G. S.; Bergstrom, R. C.; Trivedi, K.; Corey, D. R.; Madison, E. L., Negative selectivity and the evolution of protease cascades: the specificity of plasmin for peptide and protein substrates. *Chemistry & Biology* **2000**, *7* (6), 443-452.
 47. Stecher, A.-S., Untersuchungen zur Stabilität von rekombinantem Fibrinogen und Fibrinogen-abgeleiteten Peptiden. Wuerzburg, J.-M.-U., Ed. Unpublished Master Thesis 2018.
 48. Tendulkar, A. V.; Wangikar, P. P., Characterization and sequence prediction of structural variations in α -helix. *BMC Bioinformatics* **2011**, *12* (1), S20.
 49. López-Llano, J.; Campos, L. A.; Sancho, J., Alpha-helix stabilization by alanine relative to glycine: roles of polar and apolar solvent exposures and of backbone entropy. *Proteins* **2006**, *64* (3), 769-78.
 50. Hirashima, M.; Imamura, T.; Yano, K.; Kawamura, R.; Meta, A.; Tokieda, Y.; Nakashima, T., High-level expression and preparation of recombinant human fibrinogen as biopharmaceuticals. *J Biochem* **2016**, *159* (2), 261-70.
 51. Lord, S. T., Method for recombinant fibrinogen production. US6037457, **2000**
 52. Hiller, O.; Lichte, A.; Oberpichler, A.; Kocourek, A.; Tschesche, H., Matrix Metalloproteinases Collagenase-2, Macrophage Elastase, Collagenase-3, and Membrane Type 1-Matrix Metalloproteinase Impair Clotting by Degradation of Fibrinogen and Factor XII*. *Journal of Biological Chemistry* **2000**, *275* (42), 33008-33013.
 53. Bini, A.; Itoh, Y.; Kudryk, B. J.; Nagase, H., Degradation of cross-linked fibrin by matrix metalloproteinase 3 (stromelysin 1): hydrolysis of the gamma Gly 404-Ala 405 peptide bond. *Biochemistry* **1996**, *35* (40), 13056-63.
 54. Eckhard, U.; Huesgen, P. F.; Schilling, O.; Bellac, C. L.; Butler, G. S.; Cox, J. H.; Dufour, A.; Goebeler, V.; Kappelhoff, R.; Keller, U. A. D.; Klein, T.; Lange, P. F.; Marino, G.; Morrison, C. J.; Prudova, A.; Rodriguez, D.; Starr, A. E.; Wang, Y.; Overall, C. M., Active site specificity profiling of the matrix metalloproteinase family: Proteomic identification of 4300 cleavage sites by nine MMPs explored with structural and synthetic peptide cleavage analyses. *Matrix Biol* **2016**, *49*, 37-60.
 55. Jumper, J.; Evans, R.; Pritzel, A.; Green, T.; Figurnov, M.; Ronneberger, O.; Tunyasuvunakool, K.; Bates, R.; Židek, A.; Potapenko, A.; Bridgland, A.; Meyer, C.; Kohl, S. A. A.; Ballard, A. J.; Cowie, A.; Romera-Paredes, B.; Nikolov, S.; Jain, R.; Adler, J.; Back, T.; Petersen, S.; Reiman, D.; Clancy, E.; Zielinski, M.; Steinegger, M.; Pacholska, M.; Berghammer, T.; Bodenstein, S.; Silver, D.; Vinyals, O.; Senior, A. W.; Kavukcuoglu, K.; Kohli, P.; Hassabis, D., Highly accurate protein structure prediction with AlphaFold. *Nature* **2021**, *596* (7873), 583-589.
 56. Varadi, M.; Anyango, S.; Deshpande, M.; Nair, S.; Natassia, C.; Yordanova, G.; Yuan, D.; Stroe, O.; Wood, G.; Laydon, A.; Židek, A.; Green, T.; Tunyasuvunakool, K.; Petersen, S.; Jumper, J.; Clancy, E.; Green, R.; Vora, A.; Lutfi, M.; Figurnov, M.; Cowie, A.; Hobbs, N.; Kohli, P.; Kleywegt, G.; Birney, E.; Hassabis, D.; Velankar, S., AlphaFold Protein Structure Database: massively

- expanding the structural coverage of protein-sequence space with high-accuracy models. *Nucleic Acids Research* **2021**.
57. Germershaus, O.; Schultz, I.; Lühmann, T.; Beck-Broichsitter, M.; Högger, P.; Meinel, L., Insulin-like growth factor-I aerosol formulations for pulmonary delivery. *European Journal of Pharmaceutics and Biopharmaceutics* **2013**, *85* (1), 61-68.
58. Hör, J.; Garriss, G.; Di Giorgio, S.; Hack, L.-M.; Vanselow, J. T.; Förstner, K. U.; Schlosser, A.; Henriques-Normark, B.; Vogel, J., Grad-seq in a Gram-positive bacterium reveals exonucleolytic sRNA activation in competence control. *The EMBO Journal* **2020**, *39* (9), e103852.

8. Materials & Methods

All the individual chapters (1-4) include their own material and methods segment in the main text or in the supporting information (SI). There are no other materials & methods that were used outside the ones stated in the chapters.

9. Discussion & Outlook

Due to the vast progress in material as well as biomedical and pharmaceutical sciences over the last decades, the form, role, and value of hydrogels changed drastically. While hydrogels were initially used mainly as implants or contact lenses^{4, 27}, nowadays so-called smart hydrogels, designed with unique properties including self-healing¹⁵⁷, conductive¹⁵⁸ or shape-memory behaviour¹⁵⁹, are being developed. These approaches paved the way for new applications in entirely different fields ranging from drug delivery, biotechnology and tissue engineering to the microelectronics sector.^{28, 160-165} The selection of the polymers is as diverse as the applications themselves comprising a multitude of different synthetic and natural polymer classes. The choice depends on many different factors and can have a huge impact on the performance of the material and the application. However, there is no holistic solution for all the different areas and fields that need to be addressed. Hence, there is still a need for more suitable systems for the multitude of unique approaches, emphasizing the importance for the development of novel and sophisticated hydrogels.

This work focused on the development and improvement of hydrogel systems for three different areas of biomedical research – biofabrication, drug delivery and wound sealants – based on the synthetic polymer classes of poly(2-oxazoline)s and poly(2-oxazine)s as a versatile alternative to current bioinks such as PEG, as well as the protein Fbg – the current gold standard in wound sealants.¹⁶⁶

9.1 Thermogelling POx/POzi Hydrogels for Drug Delivery and Biofabrication

Over the last decade the field of biofabrication has gained increasing attention due to the advantages such as the possibilities of generating more complex 3D tissue models or the future generation of tissue transplants (**See Introduction, Chapter I and II**). However, there is still the need for new functional and fitting bioinks besides the currently used systems like PEG to further push the progress and development in this field.^{167, 168}

One class that has generated interest in this regard is the class of poly(2-oxazoline)s.¹⁶⁹ Recently, a physical thermogelling hydrogel based on a diblock copolymer PMeOx-b-PnPrOzi was developed that shows promising properties for an application as a bioink including cytocompatibility and a pronounced shear thinning behavior. However, its use especially in long-term 2D or 3D cell culture is limited due to the physical gelation mechanism which leads to the dissolution of the scaffolds in aqueous solutions.⁴⁵ Nonetheless, there is a multitude of

different modification strategies that can be applied to modify and enhance polymer properties such as long-term stability or the bioactivity.

We used this approach to incorporate chemical crosslinking to facilitate a dual gelation mechanism resulting in long-term stability of the hydrogels. We introduced furan and/or maleimide moieties to the polymer backbone establishing chemical crosslinking via Diels-Alder chemistry. The modification did not have a negative effect on the printability of the polymer. Furthermore, chemical crosslinking facilitated long-term stability in aqueous solutions without the addition of further components to the system enabling a use of this system in cell culture. In a next step, we incorporated RGD-peptides into the POx/POzi hydrogels which resulted in cell adhesion of fibroblast cells on the top of the gels.

However, there is still need and room for improvement and development for this system. One of the most crucial points is the crosslinking kinetics of the Diels-Alder chemistry. Especially for more complex printing experiments that require a longer time frame, the onset of chemical crosslinking during the printing process could lead to uneven printing, higher shear stress for the cells or clogging of the syringe. To tackle this problem, different printheads that allow the mixing of the two components directly at the extrusion of the hydrogel could be used preventing premature crosslinking during the printing process. Another area for potential improvement of the bioink is the printability. Recently, it has been shown that the addition of a nanoclay improves the printability of the basic PMeOx-b-PnPrOzi hydrogel by improving the yield point.¹⁷⁰ Despite this improvement, this system was not applicable in long-term cell culture due to the lack of chemical-crosslinking. However, a combination of nanoclay with the furan and maleimide modified hydrogel platform could drastically improve the printability of the system while retaining form and stability in cell culture. Lastly, due to the small pore size of the cross-linked hydrogels no cell adhesion was visible inside the gels in 3D cell culture despite the incorporation of RGD-motifs. By using cleavable peptide linkers, e.g., matrix metalloprotease-sensitive peptide sequences, the mesh size of the polymer network could be adjusted after printing, either by the addition of exogenous proteases or the expression of endogenous protease from the cells, thereby creating their own niche.

Another potential application of the PMeOx-b-PnPrOzi system is the sustained and targeted delivery of biological cues both in drug delivery for patients as well as in biofabrication for the maturation of cells post-printing. Recent advances in science have led to a huge variety of different new therapeutics. However, often conventional drug dosing forms can result in severe off target effects or limit the efficacy of those drugs. Hence, there is a need for novel drug delivery systems to overcome these challenges. Hydrogels have been used for drug delivery for decades due to their unique properties including high water content and ability to

incorporate drugs. These properties are further enhanced by the emerging technique of 3D printing which enables the development of more complex 3D structures and patterns that can tune the release of drugs according to specific applications.¹⁷¹ They can facilitate spatial and temporal control over the release and thereby, e.g., increase the bioavailability of drugs at the site of action while reducing off target effects.^{67, 162, 172, 173} Due to its thermoresponsive behavior, printability, and its chemical versatility, the PMeOx-b-PnPrOzi polymer is a promising alternative to other widely used polymers such as PEG and a candidate for the incorporation and delivery of biologics such as growth factors. Using a different modification approach, we introduced an omega-chain-end DBCO functionality to the polymer. After that, we coupled IGF-1, an U.S. FDA approved growth factor¹⁷⁴, site-specifically to the polymer by applying both a bioinspired enzymatic and a biorthogonal conjugation using an MMP-sensitive peptide linker. By using this approach, we showed that receptor binding and, therefore, bioactivity of IGF-I are not impaired by the linker or the polymer. Furthermore, the polymer-drug conjugate could be printed, and IGF-I was released by MMPs from the hydrogel. We were also able to print IGF-PSL-POx with spatial control over its distribution inside the 3D scaffold.

This starting point offers different opportunities for future studies and developments. IGF-I has been previously shown to have positive effects on cardiac cells including differentiation of cardiac progenitor cells, revascularization, proliferation or cell survival.¹⁷⁵⁻¹⁷⁷ This is why injectable scaffolds loaded with IGF-I have recently gained interest in the field of cardiac tissue engineering.¹⁷⁵ Therefore, the here presented IGF-I delivery system could be tested for a potential use in cardiac tissue repair. Moreover, reduced levels of IGF-I have also been connected to impaired wound healing, e.g., in diabetic wounds.¹⁷⁸ The IGF-POx-b-POzi hydrogel system could be developed as wound sealant for the simultaneously delivery of essential growth factors for wound closure and regeneration directly at the target site. Another possible application is the use of the presented hydrogels for cartilage tissue regeneration during diseases such as osteoarthritis. IGF-I has been shown to enhance chondrocyte proliferation and has been investigated for cartilage repair and tissue engineering before.^{179, 180} However, there is still a lack of suitable systems for the controlled delivery of IGF-I at the target site for cartilage repair.¹⁸¹ The IGF-I-loaded hydrogels described here, could be applied directly at the site of interest via injection or as transplant and release IGF-I in controlled manner due to increased MMP levels. Furthermore, the delivery of IGF-I could be used in the field of tissue engineering and biofabrication for the targeted delivery of much needed biological cues during the maturation process.

In addition, the structure of the printed scaffold has a huge influence on the release profile of the drug due to both the diffusion of the proteases in the hydrogel as well as the diffusion of the target protein drug out of the hydrogel.^{182, 183} The mesh size of polymer networks strongly

influences the diffusion process of proteins inside the hydrogel.¹⁸⁴ By varying different parameters such as weight percentage of the polymer, crosslinking degree as well as kinetics, the changing release profile could be studied and adapted depending on target applications. In addition, no release from more sophisticated printed POx-constructs was tested as of right now. Therefore, complex structures should be printed to investigate the influence of 3D structures and the spatial control over the drug distribution on the drug release. Moreover, the different modifications – maleimide or furan together with DBCO – could be introduced to PMeOx-b-PnPrOzi polymer reducing the components of the system and open up new possibilities for applications, e.g., in biofabrication.

At the moment, the system has only been tested for the model protein IGF-I. To improve and test the versatility of this approach, different proteins could be coupled to the polymer in further studies. Different proteins such as bone morphogenic protein 2 (BMP-2), a growth factor that plays an important role in bone and cartilage development and regeneration^{185, 186}, have intrinsic transglutaminase (TG) binding sites¹⁸⁷ and could be incorporated into the hydrogel by using the same approach as for IGF-I. Furthermore, molecular engineering can be applied to modify other biologics without an intrinsic TG-responsive site. Recently, a factor XIIIa recognition site was introduced at the C-terminus of mIL-4 for the site-specific conjugation to different polymers including poly-(2-ethyl-2-oxazolin).⁸⁰ Another promising approach is amber codon expansion which has been used, e.g., to incorporate unnatural AAs into interferon α -2a for a subsequent site-specific coupling to different polymers without affecting its biological activity.⁷³ Both possibilities could be used to attach a variety of different proteins to PMeOx-b-PnPrOzi polymer to further expand the current toolbox.

Applying these concepts for different proteins open up the opportunity for the simultaneous incorporation of different proteins or drugs into the hydrogel network, enabling co-delivery of different drugs. Co-administration of dual drugs with synergistic effects has recently gained interest, especially in the field of cancer research. The co-delivery of two different drugs can be an important tool to tackle problems like multi-drug resistance of tumor cells which highly restricts adequate cancer treatment.¹⁸⁸ This concept could also be applied in the field of biofabrication using the targeted delivery of different biological cues in separated compartments for the stimulation and maturation of different cell types.

9.2 Development of Improved Fibrin Sealants for Wound Closure

The last part of this work focuses on the development and improvement of another hydrogel that has been of interest for years due to its application in hemorrhage control – the current generations of fibrin wound sealants. Alongside the rising population world-wide, the number of hundreds of million surgeries performed each year will only increase.⁸⁴ However, these

surgeries not only lead to increased morbidity and mortality^{85, 189}, but also contribute to enormous costs for our entire healthcare system.^{190, 191} Today, there is a huge variety of different devices available for surgeons to control major bleeding such as sutures and clips, but also tissue sealants, adhesives, and hemostats. Especially the latter group has been emerging as a valuable addition to the toolbox with increasing interest in the development of novel wound sealants.⁸⁷ Potentially the most important material in this group is fibrin. This is also reflected by the approval of fibrin-based products as hemostat, sealant and adhesive – the only material thus far.⁹⁷ However, there are still several shortcomings that limit the more widespread use of fibrin-based materials. One of the biggest problems in this regard is the fast *in vivo* resorption of the sealant due to the endogenous protease plasmin.⁹⁸ In the current generation of fibrin sealants this issue is typically addressed by the addition of the protease inhibitor aprotinin.¹⁹²⁻¹⁹⁴ However, the addition of aprotinin entails the possibility for allergic reactions.¹⁹⁵⁻¹⁹⁷ We used molecular engineering in order to impair plasmin cleavage of Fbg by exchanging targeted AA in plasmin cleavage sites in the protein. Furthermore, we created a mammalian expression vector containing the genes for the three different Fbg chains – α , β - and γ . We showed that the AA exchange in different parts of the protein, α -helical and globular part, did not affect protein expression. We were also able to detect qualitatively that the AA exchange from K to H/A did limit plasmin cleavage efficiency of targeted sites. In combination with the presented time-dependent screening method, this approach might be used for the production of fibrin sealants with increased stability towards plasmin degradation in the future. These findings open up a variety of different possibilities for further experiments and studies that have to be performed hereafter. First, as already mentioned above, both the plasmin cleavage efficiency after AA exchange as well as the time-dependent screening were performed qualitatively. Therefore, these experiments and results must be repeated and confirmed for the quantification of the data. Next, gel formation of the rFbg variants must be tested in order to verify the full bioactivity. In addition, the influence of the currently inserted mutations on the plasmin cleavage of fibrin networks has to be evaluated. Potentially, new AA exchanges must be performed to measure an impact of these mutations on the long-term stability of the gels. There are different approaches that could potentially be applied. By eradicating each plasmin cleavage site from one chain, e.g., the γ -chain, one complete strand of Fbg could be preserved and lead to increased stability of the fibrin network over a longer period. The γ -chain is a promising candidate as it has the lowest number of plasmin cleavage sites (**Chapter IV**) and additionally facilitates factor XIII dependent intermolecular crosslinking, thereby potentially enhancing the stability of the network.^{198, 199} A second method is the selection of AA that are presented on the surface of the protein. These residues tend to be more susceptible and accessible for protease cleavage. In this setup it would be interesting to

investigate the influence of the location of the mutations on plasmin cleavage in general. Another approach is the use of the presented time-dependent screening method for the selection additional residues for further AA exchanges. By deleting plasmin cleavage sites that are cleaved directly at the beginning of the degradation process, the onset of mechanical breakdown of the fibrin gels could be delayed. Additionally, it is interesting to analyze the maximum number of AA that could be exchanged without affecting the structure of the protein, its bioactivity, the structure of the clot as a whole or its mechanical properties.

In the current generation of fibrin sealants, Fbg is used in concentration of up to 106 mg/ml.¹⁹² Therefore, another important point is the optimization of the protein expression in Chinese hamster ovary (CHO) cells to maximize the protein yield and reduce production costs for a potential use as wound sealant. The most promising approach in this regard is the establishment of a high-level stable expression cell line. While transient expression systems as described in this work are more adaptable and beneficial for basic research and screenings, stable cell lines allow high-level expression of targeted proteins under controlled conditions without the need of transfection agents. Therefore, establishing a high-level expression cell line for the most promising Fbg versions would be ideal for further potential *in vivo* studies in the future.

Lastly, a way to improve future generation of fibrin sealants is the incorporation of biological cues to enhance hemostasis and tissue regeneration. Fbg contains several TG responsive sequences or other binding domains such as heparin binding domains that can be used for growth the incorporation of growth factors.²⁰⁰⁻²⁰² As already described above, TG-responsive peptide sequences could be incorporated into biological moieties for the covalent attachment to the fibrin network. Still, this approach is limited to the existing binding domains and sequences in the protein. By incorporating unnatural AA into the protein using amber codon expansion, biological moieties could be site-specifically coupled to Fbg through biorthogonal conjugation methods.

In conclusion, the emergence and development of novel biomaterials especially over the last centuries has led to groundbreaking products that contributed to our current lifestyle, e.g., in form of implants or for advances in research and science. However, as a result of the constantly rising number and age of the population and the associated health issues, new innovations and approaches in the field of biomaterials will be needed in the future for a multitude of different biomedical areas. In this thesis, a highly versatile hydrogel platform was developed that can be used in multiple areas such as biofabrication as well as drug delivery and can be adapted depending on target applications. Furthermore, a novel approach was deployed to further enhance stability of fibrin sealants towards plasmin degradation, that can

help in the future to prolong the hemostatic effect of the sealants and thereby expand their current usage in clinics.

10. References

References that were used in **1. Introduction** and **6. Discussion & Outlook** are listed in this section. The references from the individual chapters are listed directly at the end of each chapter.

1. Huebsch, N.; Mooney, D. J., Inspiration and application in the evolution of biomaterials. *Nature* **2009**, *462* (7272), 426-432.
2. Ratner, B. D.; Zhang, G., 1.1.2 - A History of Biomaterials. In *Biomaterials Science (Fourth Edition)*, Wagner, W. R.; Sakiyama-Elbert, S. E.; Zhang, G.; Yaszemski, M. J., Eds. Academic Press: 2020; pp 21-34.
3. Wichterle, O.; LÍM, D., Hydrophilic Gels for Biological Use. *Nature* **1960**, *185* (4706), 117-118.
4. Nicolson, P. C.; Vogt, J., Soft contact lens polymers: an evolution. *Biomaterials* **2001**, *22* (24), 3273-83.
5. Marin, E.; Boschetto, F.; Pezzotti, G., Biomaterials and biocompatibility: An historical overview. *Journal of Biomedical Materials Research Part A* **2020**, *108* (8), 1617-1633.
6. Park, J. B.; Lakes, R. S., Introduction to Biomaterials. In *Biomaterials: An Introduction*, Springer US: Boston, MA, 1992; pp 1-6.
7. Ratner, B. D., Biomaterials: Been There, Done That, and Evolving into the Future. *Annual Review of Biomedical Engineering* **2019**, *21* (1), 171-191.
8. Green, J. J.; Elisseeff, J. H., Mimicking biological functionality with polymers for biomedical applications. *Nature* **2016**, *540* (7633), 386-394.
9. Kamperman, T.; Koerselman, M.; Kelder, C.; Hendriks, J.; Crispim, J. F.; de Peuter, X.; Dijkstra, P. J.; Karperien, M.; Leijten, J., Spatiotemporal material functionalization via competitive supramolecular complexation of avidin and biotin analogs. *Nature Communications* **2019**, *10* (1), 4347.
10. Mosiewicz, K. A.; Kolb, L.; van der Vlies, A. J.; Martino, M. M.; Lienemann, P. S.; Hubbell, J. A.; Ehrbar, M.; Lutolf, M. P., In situ cell manipulation through enzymatic hydrogel photopatterning. *Nat Mater* **2013**, *12* (11), 1072-8.
11. Yang, C.; Tibbitt, M. W.; Basta, L.; Anseth, K. S., Mechanical memory and dosing influence stem cell fate. *Nat Mater* **2014**, *13* (6), 645-52.
12. Markert, E. K.; Levine, A. J.; Vazquez, A., Proliferation and tissue remodeling in cancer: the hallmarks revisited. *Cell Death Dis* **2012**, *3* (10), e397.
13. Lu, P.; Takai, K.; Weaver, V. M.; Werb, Z., Extracellular matrix degradation and remodeling in development and disease. *Cold Spring Harb Perspect Biol* **2011**, *3* (12).
14. Humphrey, J. D.; Dufresne, E. R.; Schwartz, M. A., Mechanotransduction and extracellular matrix homeostasis. *Nature Reviews Molecular Cell Biology* **2014**, *15* (12), 802-812.
15. Bloom, A. B.; Zaman, M. H., Influence of the microenvironment on cell fate determination and migration. *Physiol Genomics* **2014**, *46* (9), 309-14.
16. Zhu, J.; Clark, R. A. F., Fibronectin at select sites binds multiple growth factors and enhances their activity: expansion of the collaborative ECM-GF paradigm. *J Invest Dermatol* **2014**, *134* (4), 895-901.
17. von der Mark, K.; Park, J.; Bauer, S.; Schmuki, P., Nanoscale engineering of biomimetic surfaces: cues from the extracellular matrix. *Cell Tissue Res* **2010**, *339* (1), 131-53.
18. Prince, E.; Kumacheva, E., Design and applications of man-made biomimetic fibrillar hydrogels. *Nature Reviews Materials* **2019**, *4* (2), 99-115.

19. Yue, B., Biology of the extracellular matrix: an overview. *J Glaucoma* **2014**, *23* (8 Suppl 1), S20-S23.
20. Gutmann, M.; Braun, A.; Seibel, J.; Lühmann, T., Bioorthogonal Modification of Cell Derived Matrices by Metabolic Glycoengineering. *ACS Biomaterials Science & Engineering* **2018**, *4* (4), 1300-1306.
21. Bellis, S. L., Advantages of RGD peptides for directing cell association with biomaterials. *Biomaterials* **2011**, *32* (18), 4205-10.
22. Zapp, C.; Minsky, B. B.; Boehm, H., Tuning RGD Motif and Hyaluronan Density to Study Integrin Binding. *Frontiers in Physiology* **2018**, *9*.
23. de Castro Brás, L. E.; Frangogiannis, N. G., Extracellular matrix-derived peptides in tissue remodeling and fibrosis. *Matrix Biol* **2020**, *91-92*, 176-187.
24. Lutolf, M. P.; Hubbell, J. A., Synthetic biomaterials as instructive extracellular microenvironments for morphogenesis in tissue engineering. *Nat Biotechnol* **2005**, *23* (1), 47-55.
25. Der Hydrogel und das kristallinische Hydrat des Kupferoxydes. *Zeitschrift für Chemie und Industrie der Kolloide* **1907**, *1* (7), 213-214.
26. Rabinovich, D., Otto Wichterle: An Eye for Hydrogels. *Chemistry International* **2015**, *37* (2), 19-19.
27. Kopecek, J., Hydrogels: From soft contact lenses and implants to self-assembled nanomaterials. *Journal of Polymer Science Part A: Polymer Chemistry* **2009**, *47* (22), 5929-5946.
28. Jayakumar, A.; Jose, V. K.; Lee, J.-M., Hydrogels for Medical and Environmental Applications. *Small Methods* **2020**, *4* (3), 1900735.
29. Khan, F.; Atif, M.; Haseen, M.; Kamal, S.; Khan, M. S.; Shahid, S.; Nami, S. A. A., Synthesis, classification and properties of hydrogels: their applications in drug delivery and agriculture. *Journal of Materials Chemistry B* **2022**, *10* (2), 170-203.
30. Chai, Q.; Jiao, Y.; Yu, X., Hydrogels for Biomedical Applications: Their Characteristics and the Mechanisms behind Them. *Gels (Basel, Switzerland)* **2017**, *3* (1), 6.
31. Mantha, S.; Pillai, S.; Khayambashi, P.; Upadhyay, A.; Zhang, Y.; Tao, O.; Pham, H. M.; Tran, S. D., Smart Hydrogels in Tissue Engineering and Regenerative Medicine. *Materials (Basel, Switzerland)* **2019**, *12* (20), 3323.
32. Williams, D. F., On the mechanisms of biocompatibility. *Biomaterials* **2008**, *29* (20), 2941-2953.
33. Taghipour, Y. D.; Hokmabad, V. R.; Del Bakhshayesh, A. R.; Asadi, N.; Salehi, R.; Nasrabadi, H. T., The Application of Hydrogels Based on Natural Polymers for Tissue Engineering. *Curr Med Chem* **2020**, *27* (16), 2658-2680.
34. ter Horst, B.; Moiemmen, N. S.; Grover, L. M., 6 - Natural polymers: biomaterials for skin scaffolds. In *Biomaterials for Skin Repair and Regeneration*, García-Gareta, E., Ed. Woodhead Publishing: 2019; pp 151-192.
35. Catoira, M. C.; Fusaro, L.; Di Francesco, D.; Ramella, M.; Boccafoschi, F., Overview of natural hydrogels for regenerative medicine applications. *Journal of Materials Science: Materials in Medicine* **2019**, *30* (10), 115.
36. Reddy, M. S. B.; Ponnamma, D.; Choudhary, R.; Sadasivuni, K. K., A Comparative Review of Natural and Synthetic Biopolymer Composite Scaffolds. *Polymers* **2021**, *13* (7), 1105.
37. Madduma-Bandarage, U. S. K.; Madihally, S. V., Synthetic hydrogels: Synthesis, novel trends, and applications. *Journal of Applied Polymer Science* **2021**, *138* (19), 50376.
38. Liu, F.; Wang, X., Synthetic Polymers for Organ 3D Printing. *Polymers (Basel)* **2020**, *12* (8).
39. Benwood, C.; Chrenek, J.; Kirsch, R. L.; Masri, N. Z.; Richards, H.; Teetzen, K.; Willerth, S. M., Natural Biomaterials and Their Use as Bioinks for Printing Tissues. *Bioengineering* **2021**, *8* (2), 27.
40. Jayawarna, V.; Ali, M.; Jowitt, T. A.; Miller, A. F.; Saiani, A.; Gough, J. E.; Ulijn, R. V., Nanostructured Hydrogels for Three-Dimensional Cell Culture Through Self-

- Assembly of Fluorenylmethoxycarbonyl–Dipeptides. *Advanced Materials* **2006**, *18* (5), 611-614.
41. Dodero, A.; Pianella, L.; Vicini, S.; Alloisio, M.; Ottonelli, M.; Castellano, M., Alginate-based hydrogels prepared via ionic gelation: An experimental design approach to predict the crosslinking degree. *European Polymer Journal* **2019**, *118*, 586-594.
 42. Mihajlovic, M.; Staropoli, M.; Appavou, M.-S.; Wyss, H. M.; Pyckhout-Hintzen, W.; Sijbesma, R. P., Tough Supramolecular Hydrogel Based on Strong Hydrophobic Interactions in a Multiblock Segmented Copolymer. *Macromolecules* **2017**, *50* (8), 3333-3346.
 43. You, Y.; Yang, J.; Zheng, Q.; Wu, N.; Lv, Z.; Jiang, Z., Ultra-stretchable hydrogels with hierarchical hydrogen bonds. *Scientific Reports* **2020**, *10* (1), 11727.
 44. Falcone, N.; Shao, T.; Sun, X.; Kraatz, H.-B., Systematic exploration of the pH dependence of a peptide hydrogel. *Canadian Journal of Chemistry* **2018**, *97* (6), 430-434.
 45. Lorson, T.; Jaksch, S.; Lübtow, M. M.; Jüngst, T.; Groll, J.; Lühmann, T.; Luxenhofer, R., A Thermogelling Supramolecular Hydrogel with Sponge-Like Morphology as a Cytocompatible Bioink. *Biomacromolecules* **2017**, *18* (7), 2161-2171.
 46. Farrugia, B. L.; Kempe, K.; Schubert, U. S.; Hoogenboom, R.; Dargaville, T. R., Poly(2-oxazoline) Hydrogels for Controlled Fibroblast Attachment. *Biomacromolecules* **2013**, *14* (8), 2724-2732.
 47. Wang, X., Advanced Polymers for Three-Dimensional (3D) Organ Bioprinting. *Micromachines (Basel)* **2019**, *10* (12).
 48. Lang, K.; Chin, J. W., Bioorthogonal Reactions for Labeling Proteins. *ACS Chemical Biology* **2014**, *9* (1), 16-20.
 49. Hauptstein, J.; Forster, L.; Nadernezhad, A.; Horder, H.; Stahlhut, P.; Groll, J.; Blunk, T.; Teßmar, J., Bioink Platform Utilizing Dual-Stage Crosslinking of Hyaluronic Acid Tailored for Chondrogenic Differentiation of Mesenchymal Stromal Cells. *Macromol Biosci* **2022**, *22* (2), e2100331.
 50. Occhetta, P.; Visone, R.; Russo, L.; Cipolla, L.; Moretti, M.; Rasponi, M., VA-086 methacrylate gelatine photopolymerizable hydrogels: A parametric study for highly biocompatible 3D cell embedding. *J Biomed Mater Res A* **2015**, *103* (6), 2109-17.
 51. Khetan, S.; Burdick, J. A., Patterning network structure to spatially control cellular remodeling and stem cell fate within 3-dimensional hydrogels. *Biomaterials* **2010**, *31* (32), 8228-8234.
 52. Sawicki, L. A.; Kloxin, A. M., Design of thiol–ene photoclick hydrogels using facile techniques for cell culture applications. *Biomaterials Science* **2014**, *2* (11), 1612-1626.
 53. Bagheri, A.; Jin, J., Photopolymerization in 3D Printing. *ACS Applied Polymer Materials* **2019**, *1* (4), 593-611.
 54. Zhang, J.; Dumur, F.; Xiao, P.; Graff, B.; Bardelang, D.; Gignes, D.; Fouassier, J. P.; Lalevée, J., Structure Design of Naphthalimide Derivatives: Toward Versatile Photoinitiators for Near-UV/Visible LEDs, 3D Printing, and Water-Soluble Photoinitiating Systems. *Macromolecules* **2015**, *48* (7), 2054-2063.
 55. Sharifi, S.; Sharifi, H.; Akbari, A.; Chodosh, J., Systematic optimization of visible light-induced crosslinking conditions of gelatin methacryloyl (GelMA). *Scientific Reports* **2021**, *11* (1), 23276.
 56. Sinha, R. P.; Häder, D. P., UV-induced DNA damage and repair: a review. *Photochem Photobiol Sci* **2002**, *1* (4), 225-36.
 57. Cadamuro, F.; Russo, L.; Nicotra, F., Biomedical Hydrogels Fabricated Using Diels–Alder Crosslinking. *European Journal of Organic Chemistry* **2021**, *2021* (3), 374-382.
 58. Ruiz-Pardo, C.; Silva-Gutiérrez, L.; Lizardi-Mendoza, J.; López-Franco, Y.; Peniche-Covas, C.; Argüelles-Monal, W., Chitosan Hydrogels Based on the Diels-Alder Click Reaction: Rheological and Kinetic Study. *Polymers (Basel)* **2022**, *14* (6).

59. García-Astrain, C.; Gandini, A.; Peña, C.; Algar, I.; Eceiza, A.; Corcuera, M.; Gabilondo, N., Diels–Alder “click” chemistry for the cross-linking of furfuryl-gelatin-polyetheramine hydrogels. *RSC Advances* **2014**, *4* (67), 35578-35587.
60. Bi, B.; Ma, M.; Lv, S.; Zhuo, R.; Jiang, X., In-situ forming thermosensitive hydroxypropyl chitin-based hydrogel crosslinked by Diels-Alder reaction for three dimensional cell culture. *Carbohydrate Polymers* **2019**, *212*, 368-377.
61. Wei, H.-L.; Yang, Z.; Zheng, L.-M.; Shen, Y.-M., Thermosensitive hydrogels synthesized by fast Diels–Alder reaction in water. *Polymer* **2009**, *50* (13), 2836-2840.
62. Kirchhof, S.; Strasser, A.; Wittmann, H.-J.; Messmann, V.; Hammer, N.; Goepferich, A. M.; Brandl, F. P., New insights into the cross-linking and degradation mechanism of Diels–Alder hydrogels. *Journal of Materials Chemistry B* **2015**, *3* (3), 449-457.
63. Guaresti, O.; Basasoro, S.; González, K.; Eceiza, A.; Gabilondo, N., In situ cross-linked chitosan hydrogels via Michael addition reaction based on water-soluble thiol-maleimide precursors. *European Polymer Journal* **2019**, *119*, 376-384.
64. Jalalvandi, E.; Hanton, L. R.; Moratti, S. C., Schiff-base based hydrogels as degradable platforms for hydrophobic drug delivery. *European Polymer Journal* **2017**, *90*, 13-24.
65. Azagarsamy, M. A.; Marozas, I. A.; Spaans, S.; Anseth, K. S., Photoregulated Hydrazone-Based Hydrogel Formation for Biochemically Patterning 3D Cellular Microenvironments. *ACS Macro Letters* **2016**, *5* (1), 19-23.
66. Guimarães, C. F.; Marques, A. P.; Reis, R. L., Pushing the Natural Frontier: Progress on the Integration of Biomaterial Cues toward Combinatorial Biofabrication and Tissue Engineering. *Advanced Materials* **2022**, *34* (33), 2105645.
67. He, W.; Reaume, M.; Hennenfent, M.; Lee, B. P.; Rajachar, R., Biomimetic hydrogels with spatial- and temporal-controlled chemical cues for tissue engineering. *Biomaterials Science* **2020**, *8* (12), 3248-3269.
68. Fisher, S. A.; Baker, A. E. G.; Shoichet, M. S., Designing Peptide and Protein Modified Hydrogels: Selecting the Optimal Conjugation Strategy. *Journal of the American Chemical Society* **2017**, *139* (22), 7416-7427.
69. Nanda, J. S.; Lorsch, J. R., Chapter Eight - Labeling a Protein with Fluorophores Using NHS Ester Derivatization. In *Methods in Enzymology*, Lorsch, J., Ed. Academic Press: 2014; Vol. 536, pp 87-94.
70. Dempsey, D. R.; Jiang, H.; Kalin, J. H.; Chen, Z.; Cole, P. A., Site-Specific Protein Labeling with N-Hydroxysuccinimide-Esters and the Analysis of Ubiquitin Ligase Mechanisms. *Journal of the American Chemical Society* **2018**, *140* (30), 9374-9378.
71. Gil Alvaradejo, G.; Glassner, M.; Hoogenboom, R.; Delaittre, G., Maleimide end-functionalized poly(2-oxazoline)s by the functional initiator route: synthesis and (bio)conjugation. *RSC Advances* **2018**, *8* (17), 9471-9479.
72. Christie, R. J.; Fleming, R.; Bezabeh, B.; Woods, R.; Mao, S.; Harper, J.; Joseph, A.; Wang, Q.; Xu, Z.-Q.; Wu, H.; Gao, C.; Dimasi, N., Stabilization of cysteine-linked antibody drug conjugates with N-aryl maleimides. *Journal of Controlled Release* **2015**, *220*, 660-670.
73. Hauptstein, N.; Pouyan, P.; Kehrein, J.; Dirauf, M.; Driessen, M. D.; Raschig, M.; Licha, K.; Gottschaldt, M.; Schubert, U. S.; Haag, R.; Meinel, L.; Sottriffer, C.; Lühmann, T., Molecular Insights into Site-Specific Interferon- α 2a Bioconjugates Originated from PEG, LPG, and PEtOx. *Biomacromolecules* **2021**, *22* (11), 4521-4534.
74. Hou, W.; Zhang, X.; Liu, C.-F., Progress in Chemical Synthesis of Peptides and Proteins. *Transactions of Tianjin University* **2017**, *23* (5), 401-419.
75. Mbua, N. E.; Guo, J.; Wolfert, M. A.; Steet, R.; Boons, G. J., Strain-promoted alkyne-azide cycloadditions (SPAAC) reveal new features of glycoconjugate biosynthesis. *Chembiochem* **2011**, *12* (12), 1912-21.
76. Lobba, M. J.; Fellmann, C.; Marmelstein, A. M.; Maza, J. C.; Kissman, E. N.; Robinson, S. A.; Stahl, B. T.; Urnes, C.; Lew, R. J.; Mogilevsky, C. S.; Doudna, J.

- A.; Francis, M. B., Site-Specific Bioconjugation through Enzyme-Catalyzed Tyrosine–Cysteine Bond Formation. *ACS Central Science* **2020**, *6* (9), 1564-1571.
77. Beerli, R. R.; Hell, T.; Merkel, A. S.; Grawunder, U., Sortase Enzyme-Mediated Generation of Site-Specifically Conjugated Antibody Drug Conjugates with High In Vitro and In Vivo Potency. *PLOS ONE* **2015**, *10* (7), e0131177.
78. Lexhaller, B.; Ludwig, C.; Scherf, K. A., Identification of Isopeptides Between Human Tissue Transglutaminase and Wheat, Rye, and Barley Gluten Peptides. *Scientific Reports* **2020**, *10* (1), 7426.
79. Nikolajsen, C. L.; Dyrlyund, T. F.; Poulsen, E. T.; Enghild, J. J.; Scavenius, C., Coagulation factor XIIIa substrates in human plasma: identification and incorporation into the clot. *J Biol Chem* **2014**, *289* (10), 6526-6534.
80. Haas, D.; Hauptstein, N.; Dirauf, M.; Driessen, M. D.; Ruopp, M.; Schubert, U. S.; Lühmann, T.; Meinel, L., Chemo-Enzymatic PEGylation/POxylation of Murine Interleukin-4. *Bioconjugate Chemistry* **2022**, *33* (1), 97-104.
81. Braun, A. C.; Gutmann, M.; Mueller, T. D.; Lühmann, T.; Meinel, L., Bioresponsive release of insulin-like growth factor-I from its PEGylated conjugate. *J Control Release* **2018**, *279*, 17-28.
82. Mandal, A.; Clegg, J. R.; Anselmo, A. C.; Mitragotri, S., Hydrogels in the clinic. *Bioeng Transl Med* **2020**, *5* (2), e10158-e10158.
83. Correa, S.; Grosskopf, A. K.; Lopez Hernandez, H.; Chan, D.; Yu, A. C.; Stapleton, L. M.; Appel, E. A., Translational Applications of Hydrogels. *Chemical Reviews* **2021**, *121* (18), 11385-11457.
84. Meara, J. G.; Leather, A. J. M.; Hagander, L.; Alkire, B. C.; Alonso, N.; Ameh, E. A.; Bickler, S. W.; Conteh, L.; Dare, A. J.; Davies, J.; Mérisier, E. D.; El-Halabi, S.; Farmer, P. E.; Gawande, A.; Gillies, R.; Greenberg, S. L. M.; Grimes, C. E.; Gruen, R. L.; Ismail, E. A.; Kamara, T. B.; Lavy, C.; Lundeg, G.; Mkandawire, N. C.; Raykar, N. P.; Riesel, J. N.; Rodas, E.; Rose, J.; Roy, N.; Shrime, M. G.; Sullivan, R.; Verguet, S.; Watters, D.; Weiser, T. G.; Wilson, I. H.; Yamey, G.; Yip, W., Global Surgery 2030: evidence and solutions for achieving health, welfare, and economic development. *The Lancet* **2015**, *386* (9993), 569-624.
85. Ramirez Manuel G, C. G. F., Ramirez Manuel A, The Economic Burden of Bleeds and Transfusions in Selected Surgeries: A Retrospective Multi Center Analysis from the Us Perspective. *Am J Biomed Sci & Res.* **2019**, *2*(5).
86. Matz, D.; Teuteberg, S.; Wiencierz, A.; Soysal, S. D.; Heizmann, O., Do antibacterial skin sutures reduce surgical site infections after elective open abdominal surgery? - Study protocol of a prospective, randomized controlled single center trial. *Trials* **2019**, *20* (1), 390.
87. Taboada, G. M.; Yang, K.; Pereira, M. J. N.; Liu, S. S.; Hu, Y.; Karp, J. M.; Artzi, N.; Lee, Y., Overcoming the translational barriers of tissue adhesives. *Nature Reviews Materials* **2020**, *5* (4), 310-329.
88. Spotnitz, W. D.; Burks, S., Hemostats, sealants, and adhesives: components of the surgical toolbox. *Transfusion* **2008**, *48* (7), 1502-16.
89. Hickman, D. A.; Pawlowski, C. L.; Sekhon, U. D. S.; Marks, J.; Gupta, A. S., Biomaterials and Advanced Technologies for Hemostatic Management of Bleeding. *Adv Mater* **2018**, *30* (4).
90. Kumar, A.; Domb, A. J., Polymerization Enhancers for Cyanoacrylate Skin Adhesive. *Macromolecular Bioscience* **2021**, *21* (10), 2100143.
91. Sultan, A.; Mohamed, A., Efficacy and Safety of Using N-Butyl Cyanoacrylate in Cranial Fixation Following Trauma and Other Pathologies. *Turk Neurosurg* **2018**, *28* (3), 416-420.
92. Robicsek, F.; Rielly, J. P.; Marroum, M. C., The use of cyanoacrylate adhesive (Krazy Glue) in cardiac surgery. *J Card Surg* **1994**, *9* (3), 353-6.

93. Vote, B. J.; Elder, M. J., Cyanoacrylate glue for corneal perforations: a description of a surgical technique and a review of the literature. *Clinical & Experimental Ophthalmology* **2000**, *28* (6), 437-442.
94. Ge, L.; Chen, S., Recent Advances in Tissue Adhesives for Clinical Medicine. *Polymers (Basel)* **2020**, *12* (4).
95. Sanders, L.; Nagatomi, J., Clinical applications of surgical adhesives and sealants. *Crit Rev Biomed Eng* **2014**, *42* (3-4), 271-92.
96. Spotnitz, W. D., Fibrin Sealant: The Only Approved Hemostat, Sealant, and Adhesive-a Laboratory and Clinical Perspective. *ISRN Surg* **2014**, *2014*, 203943.
97. Spotnitz, W. D., Fibrin Sealant: Past, Present, and Future: A Brief Review. *World Journal of Surgery* **2010**, *34* (4), 632-634.
98. Lorentz, K. M.; Kontos, S.; Frey, P.; Hubbell, J. A., Engineered aprotinin for improved stability of fibrin biomaterials. *Biomaterials* **2011**, *32* (2), 430-8.
99. Roberts, I. V.; Bukhary, D.; Valdivieso, C. Y. L.; Tirelli, N., Fibrin Matrices as (Injectable) Biomaterials: Formation, Clinical Use, and Molecular Engineering. *Macromolecular Bioscience* **2020**, *20* (1), 1900283.
100. Malda, J.; Visser, J.; Melchels, F. P.; Jüngst, T.; Hennink, W. E.; Dhert, W. J. A.; Groll, J.; Huttmacher, D. W., 25th Anniversary Article: Engineering Hydrogels for Biofabrication. *Advanced Materials* **2013**, *25* (36), 5011-5028.
101. Levato, R.; Jungst, T.; Scheuring, R. G.; Blunk, T.; Groll, J.; Malda, J., From Shape to Function: The Next Step in Bioprinting. *Advanced Materials* **2020**, *32* (12), 1906423.
102. Dalton, P. D.; Woodfield, T. B. F.; Mironov, V.; Groll, J., Advances in Hybrid Fabrication toward Hierarchical Tissue Constructs. *Advanced Science* **2020**, *7* (11), 1902953.
103. Groll, J.; Burdick, J. A.; Cho, D. W.; Derby, B.; Gelinsky, M.; Heilshorn, S. C.; Jüngst, T.; Malda, J.; Mironov, V. A.; Nakayama, K.; Ovsianikov, A.; Sun, W.; Takeuchi, S.; Yoo, J. J.; Woodfield, T. B. F., A definition of bioinks and their distinction from biomaterial inks. *Biofabrication* **2018**, *11* (1), 013001.
104. Heid, S.; Boccaccini, A. R., Advancing bioinks for 3D bioprinting using reactive fillers: A review. *Acta Biomaterialia* **2020**, *113*, 1-22.
105. Mézel, C.; Souquet, A.; Hallo, L.; Guillemot, F., Bioprinting by laser-induced forward transfer for tissue engineering applications: jet formation modeling. *Biofabrication* **2010**, *2* (1), 014103.
106. Dudman, J. P. R.; Ferreira, A. M.; Gentile, P.; Wang, X.; Ribeiro, R. D. C.; Benning, M.; Dalgarno, K. W., Reliable inkjet printing of chondrocytes and MSCs using reservoir agitation. *Biofabrication* **2020**, *12* (4), 045024.
107. Detsch, R.; Blob, S.; Zehnder, T.; Boccaccini, A. R., Evaluation of cell inkjet printing technique for biofabrication. *BioNanoMaterials* **2016**, *17* (3-4), 185-191.
108. Gao, G.; Kim, B. S.; Jang, J.; Cho, D.-W., Recent Strategies in Extrusion-Based Three-Dimensional Cell Printing toward Organ Biofabrication. *ACS Biomaterials Science & Engineering* **2019**, *5* (3), 1150-1169.
109. Miri, A. K.; Mirzaee, I.; Hassan, S.; Mesbah Oskui, S.; Nieto, D.; Khademhosseini, A.; Zhang, Y. S., Effective bioprinting resolution in tissue model fabrication. *Lab Chip* **2019**, *19* (11), 2019-2037.
110. Hölzl, K.; Lin, S.; Tytgat, L.; Van Vlierberghe, S.; Gu, L.; Ovsianikov, A., Bioink properties before, during and after 3D bioprinting. *Biofabrication* **2016**, *8* (3), 032002.
111. Schwab, A.; Levato, R.; D'Este, M.; Piluso, S.; Eglin, D.; Malda, J., Printability and Shape Fidelity of Bioinks in 3D Bioprinting. *Chemical Reviews* **2020**, *120* (19), 11028-11055.
112. Gillispie, G.; Prim, P.; Copus, J.; Fisher, J.; Mikos, A. G.; Yoo, J. J.; Atala, A.; Lee, S. J., Assessment methodologies for extrusion-based bioink printability. *Biofabrication* **2020**, *12* (2), 022003.

113. Pössl, A.; Hartzke, D.; Schmidts, T. M.; Runkel, F. E.; Schlupp, P., A targeted rheological bioink development guideline and its systematic correlation with printing behavior. *Biofabrication* **2021**, *13* (3).
114. Ying, G.-L.; Jiang, N.; Maharjan, S.; Yin, Y.-X.; Chai, R.-R.; Cao, X.; Yang, J.-Z.; Miri, A. K.; Hassan, S.; Zhang, Y. S., Aqueous Two-Phase Emulsion Bioink-Enabled 3D Bioprinting of Porous Hydrogels. *Advanced Materials* **2018**, *30* (50), 1805460.
115. Theus, A. S.; Ning, L.; Hwang, B.; Gil, C.; Chen, S.; Wombwell, A.; Mehta, R.; Serpooshan, V., Bioprintability: Physiomechanical and Biological Requirements of Materials for 3D Bioprinting Processes. *Polymers (Basel)* **2020**, *12* (10).
116. Galarraga, J. H.; Kwon, M. Y.; Burdick, J. A., 3D bioprinting via an in situ crosslinking technique towards engineering cartilage tissue. *Scientific Reports* **2019**, *9* (1), 19987.
117. Montero, F. E.; Rezende, R. A.; da Silva, J. V. L.; Sabino, M. A., Development of a Smart Bioink for Bioprinting Applications. *Frontiers in Mechanical Engineering* **2019**, *5*.
118. Seeliger, W.; Aufderhaar, E.; Diepers, W.; Feinauer, R.; Nehring, R.; Thier, W.; Hellmann, H., Recent Syntheses and Reactions of Cyclic Imidic Esters. *Angewandte Chemie International Edition in English* **1966**, *5* (10), 875-888.
119. Tomalia, D. A.; Sheetz, D. P., Homopolymerization of 2-alkyl- and 2-aryl-2-oxazolines. *Journal of Polymer Science Part A-1: Polymer Chemistry* **1966**, *4* (9), 2253-2265.
120. Bassiri, T. G.; Levy, A.; Litt, M., Polymerization of cyclic imino ethers. I. Oxazolines. *Journal of Polymer Science Part B: Polymer Letters* **1967**, *5* (9), 871-879.
121. Kagiya, T.; Narisawa, S.; Maeda, T.; Fukui, K., Ring-opening polymerization of 2-substituted 2-oxazolines. *Journal of Polymer Science Part B: Polymer Letters* **1966**, *4* (7), 441-445.
122. Levy, A.; Litt, M., Polymerization of cyclic imino ethers. II. Oxazines. *Journal of Polymer Science Part B: Polymer Letters* **1967**, *5* (9), 881-886.
123. Kelly, A. M.; Wiesbrock, F., Strategies for the Synthesis of Poly(2-Oxazoline)-Based Hydrogels. *Macromolecular Rapid Communications* **2012**, *33* (19), 1632-1647.
124. Morgese, G.; Verbraeken, B.; Ramakrishna, S. N.; Gombert, Y.; Cavalli, E.; Rosenboom, J.-G.; Zenobi-Wong, M.; Spencer, N. D.; Hoogenboom, R.; Benetti, E. M., Chemical Design of Non-Ionic Polymer Brushes as Biointerfaces: Poly(2-oxazine)s Outperform Both Poly(2-oxazoline)s and PEG. *Angewandte Chemie International Edition* **2018**, *57* (36), 11667-11672.
125. Hahn, L.; Karakaya, E.; Zorn, T.; Sochor, B.; Maier, M.; Stahlhut, P.; Forster, S.; Fischer, K.; Seiffert, S.; Pöpller, A.-C.; Detsch, R.; Luxenhofer, R., An Inverse Thermogelling Bioink Based on an ABA-Type Poly(2-oxazoline) Amphiphile. *Biomacromolecules* **2021**, *22* (7), 3017-3027.
126. Nahm, D.; Weigl, F.; Schaefer, N.; Sancho, A.; Frank, A.; Groll, J.; Villmann, C.; Schmidt, H.-W.; Dalton, P. D.; Luxenhofer, R., A versatile biomaterial ink platform for the melt electrowriting of chemically-crosslinked hydrogels. *Materials Horizons* **2020**, *7* (3), 928-933.
127. Podevyn, A.; Arys, K.; de la Rosa, V. R.; Glassner, M.; Hoogenboom, R., End-group functionalization of poly(2-oxazoline)s using methyl bromoacetate as initiator followed by direct amidation. *European Polymer Journal* **2019**, *120*, 109273.
128. Ochsenhirt, S. E.; Kokkoli, E.; McCarthy, J. B.; Tirrell, M., Effect of RGD secondary structure and the synergy site PHSRN on cell adhesion, spreading and specific integrin engagement. *Biomaterials* **2006**, *27* (20), 3863-3874.
129. Le Saux, G.; Magenau, A.; Böcking, T.; Gaus, K.; Gooding, J. J., The Relative Importance of Topography and RGD Ligand Density for Endothelial Cell Adhesion. *PLOS ONE* **2011**, *6* (7), e21869.
130. Li, J.; Chen, Y.; Kawazoe, N.; Chen, G., Ligand density-dependent influence of arginine-glycine-aspartate functionalized gold nanoparticles on osteogenic and adipogenic differentiation of mesenchymal stem cells. *Nano Research* **2018**, *11* (3), 1247-1261.

131. Frith, J. E.; Mills, R. J.; Cooper-White, J. J., Lateral spacing of adhesion peptides influences human mesenchymal stem cell behaviour. *J Cell Sci* **2012**, *125* (Pt 2), 317-27.
132. Rossi, E.; Gerges, I.; Tocchio, A.; Tamplenizza, M.; Aprile, P.; Recordati, C.; Martello, F.; Martin, I.; Milani, P.; Lenardi, C., Biologically and mechanically driven design of an RGD-mimetic macroporous foam for adipose tissue engineering applications. *Biomaterials* **2016**, *104*, 65-77.
133. Lee, E. J.; Ahmad, K.; Pathak, S.; Lee, S.; Baig, M. H.; Jeong, J. H.; Doh, K. O.; Lee, D. M.; Choi, I., Identification of Novel FNIN2 and FNIN3 Fibronectin-Derived Peptides That Promote Cell Adhesion, Proliferation and Differentiation in Primary Cells and Stem Cells. *Int J Mol Sci* **2021**, *22* (6).
134. Boateng, S. Y.; Lateef, S. S.; Mosley, W.; Hartman, T. J.; Hanley, L.; Russell, B., RGD and YIGSR synthetic peptides facilitate cellular adhesion identical to that of laminin and fibronectin but alter the physiology of neonatal cardiac myocytes. *Am J Physiol Cell Physiol* **2005**, *288* (1), C30-8.
135. Cimmino, C.; Rossano, L.; Netti, P. A.; Ventre, M., Spatio-Temporal Control of Cell Adhesion: Toward Programmable Platforms to Manipulate Cell Functions and Fate. *Front Bioeng Biotechnol* **2018**, *6*, 190.
136. Winkler, J.; Abisoye-Ogunniyan, A.; Metcalf, K. J.; Werb, Z., Concepts of extracellular matrix remodelling in tumour progression and metastasis. *Nature Communications* **2020**, *11* (1), 5120.
137. Bruno, B. J.; Miller, G. D.; Lim, C. S., Basics and recent advances in peptide and protein drug delivery. *Ther Deliv* **2013**, *4* (11), 1443-67.
138. Anselmo, A. C.; Gokarn, Y.; Mitragotri, S., Non-invasive delivery strategies for biologics. *Nature Reviews Drug Discovery* **2019**, *18* (1), 19-40.
139. Vigata, M.; Meinert, C.; Hutmacher, D. W.; Bock, N., Hydrogels as Drug Delivery Systems: A Review of Current Characterization and Evaluation Techniques. *Pharmaceutics* **2020**, *12* (12).
140. Sercombe, L.; Veerati, T.; Moheimani, F.; Wu, S. Y.; Sood, A. K.; Hua, S., Advances and Challenges of Liposome Assisted Drug Delivery. *Frontiers in Pharmacology* **2015**, *6*.
141. Jash, A.; Ubeyitogullari, A.; Rizvi, S. S. H., Liposomes for oral delivery of protein and peptide-based therapeutics: challenges, formulation strategies, and advances. *Journal of Materials Chemistry B* **2021**, *9* (24), 4773-4792.
142. Pudlarz, A.; Szemraj, J., Nanoparticles as Carriers of Proteins, Peptides and Other Therapeutic Molecules. *Open Life Sci* **2018**, *13*, 285-298.
143. Li, J.; Mooney, D. J., Designing hydrogels for controlled drug delivery. *Nat Rev Mater* **2016**, *1* (12), 16071.
144. Hoare, T. R.; Kohane, D. S., Hydrogels in drug delivery: Progress and challenges. *Polymer* **2008**, *49* (8), 1993-2007.
145. Hsiao, W.-K.; Lorber, B.; Reitsamer, H.; Khinast, J., 3D printing of oral drugs: a new reality or hype? *Expert Opinion on Drug Delivery* **2018**, *15* (1), 1-4.
146. Larush, L.; Kaner, I.; Fluksman, A.; Tamsut, A.; Pawar, A. A.; Lesnovski, P.; Benny, O.; Magdassi, S., 3D printing of responsive hydrogels for drug-delivery systems. *Journal of 3D Printing in Medicine* **2017**, *1* (4), 219-229.
147. Jamróz, W.; Szafraniec, J.; Kurek, M.; Jachowicz, R., 3D Printing in Pharmaceutical and Medical Applications – Recent Achievements and Challenges. *Pharm Res* **2018**, *35* (9), 176.
148. Awad, A.; Trenfield, S. J.; Goyanes, A.; Gaisford, S.; Basit, A. W., Reshaping drug development using 3D printing. *Drug Discovery Today* **2018**, *23* (8), 1547-1555.
149. Mohapatra, S.; Kar, R. K.; Biswal, P. K.; Bindhani, S., Approaches of 3D printing in current drug delivery. *Sensors International* **2022**, *3*, 100146.
150. Zhu, X.; Li, H.; Huang, L.; Zhang, M.; Fan, W.; Cui, L., 3D printing promotes the development of drugs. *Biomedicine & Pharmacotherapy* **2020**, *131*, 110644.

151. Kotta, S.; Nair, A.; Alsabeelah, N., 3D Printing Technology in Drug Delivery: Recent Progress and Application. *Curr Pharm Des* **2018**, *24* (42), 5039-5048.
152. Hauptstein, J.; Forster, L.; Nadermezhad, A.; Groll, J.; Teßmar, J.; Blunk, T., Tethered TGF- β 1 in a Hyaluronic Acid-Based Bioink for Bioprinting Cartilaginous Tissues. *Int J Mol Sci* **2022**, *23* (2).
153. Han, Z.; Wang, P.; Mao, G.; Yin, T.; Zhong, D.; Yiming, B.; Hu, X.; Jia, Z.; Nian, G.; Qu, S.; Yang, W., Dual pH-Responsive Hydrogel Actuator for Lipophilic Drug Delivery. *ACS Applied Materials & Interfaces* **2020**, *12* (10), 12010-12017.
154. Kim, Y. K.; Kim, E.-J.; Lim, J. H.; Cho, H. K.; Hong, W. J.; Jeon, H. H.; Chung, B. G., Dual Stimuli-Triggered Nanogels in Response to Temperature and pH Changes for Controlled Drug Release. *Nanoscale Research Letters* **2019**, *14* (1), 77.
155. Chandrawati, R., Enzyme-responsive polymer hydrogels for therapeutic delivery. *Exp Biol Med (Maywood)* **2016**, *241* (9), 972-9.
156. Freeman, F. E.; Pitacco, P.; van Dommelen, L. H. A.; Nulty, J.; Browe, D. C.; Shin, J.-Y.; Alsberg, E.; Kelly, D. J., 3D bioprinting spatiotemporally defined patterns of growth factors to tightly control tissue regeneration. *Science Advances* **2020**, *6* (33), eabb5093.
157. Liu, Y.; Hsu, S.-h., Synthesis and Biomedical Applications of Self-healing Hydrogels. *Frontiers in Chemistry* **2018**, *6*.
158. Liu, K.; Wei, S.; Song, L.; Liu, H.; Wang, T., Conductive Hydrogels—A Novel Material: Recent Advances and Future Perspectives. *Journal of Agricultural and Food Chemistry* **2020**, *68* (28), 7269-7280.
159. Löwenberg, C.; Balk, M.; Wischke, C.; Behl, M.; Lendlein, A., Shape-Memory Hydrogels: Evolution of Structural Principles To Enable Shape Switching of Hydrophilic Polymer Networks. *Accounts of Chemical Research* **2017**, *50* (4), 723-732.
160. Chen, G.; Tang, W.; Wang, X.; Zhao, X.; Chen, C.; Zhu, Z., Applications of Hydrogels with Special Physical Properties in Biomedicine. *Polymers (Basel)* **2019**, *11* (9).
161. Buwalda, S. J.; Boere, K. W. M.; Dijkstra, P. J.; Feijen, J.; Vermonden, T.; Hennink, W. E., Hydrogels in a historical perspective: From simple networks to smart materials. *Journal of Controlled Release* **2014**, *190*, 254-273.
162. Li, J.; Mooney, D. J., Designing hydrogels for controlled drug delivery. *Nature Reviews Materials* **2016**, *1* (12), 16071.
163. Milcovich, G.; Lettieri, S.; Antunes, F. E.; Medronho, B.; Fonseca, A. C.; Coelho, J. F. J.; Marizza, P.; Perrone, F.; Farra, R.; Dapas, B.; Grassi, G.; Grassi, M.; Giordani, S., Recent advances in smart biotechnology: Hydrogels and nanocarriers for tailored bioactive molecules depot. *Advances in Colloid and Interface Science* **2017**, *249*, 163-180.
164. El-Sherbiny, I. M.; Yacoub, M. H., Hydrogel scaffolds for tissue engineering: Progress and challenges. *Global cardiology science & practice* **2013**, *2013* (3), 316-342.
165. Liu, Y.; Liu, J.; Chen, S.; Lei, T.; Kim, Y.; Niu, S.; Wang, H.; Wang, X.; Foudeh, A. M.; Tok, J. B. H.; Bao, Z., Soft and elastic hydrogel-based microelectronics for localized low-voltage neuromodulation. *Nature Biomedical Engineering* **2019**, *3* (1), 58-68.
166. Srinivasan, P. K.; Sperber, V.; Afify, M.; Tanaka, H.; Fukushima, K.; Kögel, B.; Gremse, F.; Tolba, R., Novel synthetic adhesive as an effective alternative to Fibrin based adhesives. *World J Hepatol* **2017**, *9* (24), 1030-1039.
167. Panwar, A.; Tan, L. P., Current Status of Bioinks for Micro-Extrusion-Based 3D Bioprinting. *Molecules* **2016**, *21* (6), 685.
168. Chimene, D.; Lennox, K. K.; Kaunas, R. R.; Gaharwar, A. K., Advanced Bioinks for 3D Printing: A Materials Science Perspective. *Annals of Biomedical Engineering* **2016**, *44* (6), 2090-2102.
169. Lorson, T.; Lübtow, M. M.; Wegener, E.; Haider, M. S.; Borova, S.; Nahm, D.; Jordan, R.; Sokolski-Papkov, M.; Kabanov, A. V.; Luxenhofer, R., Poly(2-oxazoline)s

- based biomaterials: A comprehensive and critical update. *Biomaterials* **2018**, *178*, 204-280.
170. Hu, C.; Hahn, L.; Yang, M.; Altmann, A.; Stahlhut, P.; Groll, J.; Luxenhofer, R., Improving printability of a thermoresponsive hydrogel biomaterial ink by nanoclay addition. *Journal of Materials Science* **2021**, *56* (1), 691-705.
 171. Bittner, S. M.; Guo, J. L.; Mikos, A. G., Spatiotemporal Control of Growth Factors in Three-Dimensional Printed Scaffolds. *Bioprinting* **2018**, *12*.
 172. Leijten, J.; Seo, J.; Yue, K.; Santiago, G. T.; Tamayol, A.; Ruiz-Esparza, G. U.; Shin, S. R.; Sharifi, R.; Noshadi, I.; Álvarez, M. M.; Zhang, Y. S.; Khademhosseini, A., Spatially and Temporally Controlled Hydrogels for Tissue Engineering. *Mater Sci Eng R Rep* **2017**, *119*, 1-35.
 173. Abueva, C. D. G.; Chung, P.-S.; Ryu, H.-S.; Park, S.-Y.; Woo, S. H., Photoresponsive Hydrogels as Drug Delivery Systems. *Medical Lasers* **2020**, *9* (1), 6-11.
 174. Fintini, D.; Brufani, C.; Cappa, M., Profile of mecasermin for the long-term treatment of growth failure in children and adolescents with severe primary IGF-1 deficiency. *Ther Clin Risk Manag* **2009**, *5* (3), 553-9.
 175. Rosellini, E.; Barbani, N.; Frati, C.; Madeddu, D.; Massai, D.; Morbiducci, U.; Lazzeri, L.; Falco, A.; Graiani, G.; Lagrasta, C.; Audenino, A.; Cascone, M. G.; Quaini, F., IGF-1 loaded injectable microspheres for potential repair of the infarcted myocardium. *J Biomater Appl* **2021**, *35* (7), 762-775.
 176. Bocchi, L.; Savi, M.; Graiani, G.; Rossi, S.; Agnetti, A.; Stillitano, F.; Lagrasta, C.; Baruffi, S.; Berni, R.; Frati, C.; Vassalle, M.; Squarcia, U.; Cerbai, E.; Macchi, E.; Stilli, D.; Quaini, F.; Musso, E., Growth factor-induced mobilization of cardiac progenitor cells reduces the risk of arrhythmias, in a rat model of chronic myocardial infarction. *PLoS One* **2011**, *6* (3), e17750.
 177. Frati, C.; Savi, M.; Graiani, G.; Lagrasta, C.; Cavalli, S.; Prezioso, L.; Rossetti, P.; Mangiaracina, C.; Ferraro, F.; Madeddu, D.; Musso, E.; Stilli, D.; Rossini, A.; Falco, A.; Angelis, A. D.; Rossi, F.; Urbanek, K.; Leri, A.; Kajstura, J.; Anversa, P.; Quaini, E.; Quaini, F., Resident cardiac stem cells. *Curr Pharm Des* **2011**, *17* (30), 3252-7.
 178. Lin, M.-J.; Lu, M.-C.; Chang, H.-Y., Sustained Release of Insulin-Like Growth Factor-1 from Bombyx mori L. Silk Fibroin Delivery for Diabetic Wound Therapy. *International Journal of Molecular Sciences* **2021**, *22* (12), 6267.
 179. Cho, H.; Kim, J.; Kim, S.; Jung, Y. C.; Wang, Y.; Kang, B. J.; Kim, K., Dual delivery of stem cells and insulin-like growth factor-1 in coacervate-embedded composite hydrogels for enhanced cartilage regeneration in osteochondral defects. *J Control Release* **2020**, *327*, 284-295.
 180. Elisseeff, J.; McIntosh, W.; Fu, K.; Blunk, B. T.; Langer, R., Controlled-release of IGF-I and TGF-beta1 in a photopolymerizing hydrogel for cartilage tissue engineering. *J Orthop Res* **2001**, *19* (6), 1098-104.
 181. Wen, C.; Xu, L.; Xu, X.; Wang, D.; Liang, Y.; Duan, L., Insulin-like growth factor-1 in articular cartilage repair for osteoarthritis treatment. *Arthritis Research & Therapy* **2021**, *23* (1), 277.
 182. Dreiss, C. A., Hydrogel design strategies for drug delivery. *Current Opinion in Colloid & Interface Science* **2020**, *48*, 1-17.
 183. Sharpe, L. A.; Daily, A. M.; Horava, S. D.; Peppas, N. A., Therapeutic applications of hydrogels in oral drug delivery. *Expert Opin Drug Deliv* **2014**, *11* (6), 901-15.
 184. Rehmann, M. S.; Skeens, K. M.; Kharkar, P. M.; Ford, E. M.; Maverakis, E.; Lee, K. H.; Kloxin, A. M., Tuning and Predicting Mesh Size and Protein Release from Step Growth Hydrogels. *Biomacromolecules* **2017**, *18* (10), 3131-3142.
 185. Lin, H.; Tang, Y.; Lozito, T. P.; Oyster, N.; Wang, B.; Tuan, R. S., Efficient in vivo bone formation by BMP-2 engineered human mesenchymal stem cells encapsulated in a projection stereolithographically fabricated hydrogel scaffold. *Stem Cell Research & Therapy* **2019**, *10* (1), 254.

186. Deng, Z. H.; Li, Y. S.; Gao, X.; Lei, G. H.; Huard, J., Bone morphogenetic proteins for articular cartilage regeneration. *Osteoarthritis and Cartilage* **2018**, *26* (9), 1153-1161.
187. Beazley, K. E.; Nurminskaya, M., BMP2 cross-linked by transglutaminase 2 to collagen-plla scaffold promotes osteogenic differentiation in mesenchymal stem cells. *Biotechnol Lett* **2014**, *36* (9), 1901-7.
188. Li, Y.; Thambi, T.; Lee, D. S., Co-Delivery of Drugs and Genes Using Polymeric Nanoparticles for Synergistic Cancer Therapeutic Effects. *Adv Healthc Mater* **2018**, *7* (1).
189. Stokes, M. E.; Ye, X.; Shah, M.; Mercaldi, K.; Reynolds, M. W.; Rupnow, M. F. T.; Hammond, J., Impact of bleeding-related complications and/or blood product transfusions on hospital costs in inpatient surgical patients. *BMC Health Services Research* **2011**, *11* (1), 135.
190. Shander, A., Financial and clinical outcomes associated with surgical bleeding complications. *Surgery* **2007**, *142* (4 Suppl), S20-5.
191. Christensen, M. C.; Krapf, S.; Kempel, A.; von Heymann, C., Costs of excessive postoperative hemorrhage in cardiac surgery. *J Thorac Cardiovasc Surg* **2009**, *138* (3), 687-93.
192. Baxter Healthcare Corporation; Package Insert - TISSEEL, n.d. U.S. Food and Drug Administration Web site <https://www.fda.gov/media/71674/download> (accessed Dez 12, 2022).
193. Epstein, J. S.; March 21, 2008 Approval Letter - ARTISS, **2008**. U.S. Food and Drug Administration Web site. <http://wayback.archive-it.org/7993/20170723024803/https://www.fda.gov/BiologicsBloodVaccines/BloodBloodProducts/ApprovedProducts/LicensedProductsBLAs/FractionatedPlasmaProducts/ucm073064.htm> (accessed Dez 12, 2022).
194. CSL Behring GmbH; Beriplast P Combi-Set. <https://portal.dimdi.de/amispb/doc/pei/Web/2601182-spcen-20130401.pdf> (accessed Dez 12, 2022).
195. Kon, N. F.; Masumo, H.; Nakajima, S.; Tozawa, R.; Kimura, M.; Maeda, S., [Anaphylactic reaction to aprotinin following topical use of biological tissue sealant]. *Masui* **1994**, *43* (10), 1606-10.
196. Beierlein, W.; Scheule, A. M.; Antoniadis, G.; Braun, C.; Schosser, R., An immediate, allergic skin reaction to aprotinin after reexposure to fibrin sealant. *Transfusion* **2000**, *40* (3), 302-5.
197. Oswald, A.-M.; Joly, L.-M.; Gury, C.; Disdet, M.; Leduc, V.; Kanny, G., Fatal Intraoperative Anaphylaxis Related to Aprotinin after Local Application of Fibrin Glue. *Anesthesiology* **2003**, *99* (3), 762-763.
198. Siebenlist, K. R.; Mosesson, M. W., Progressive cross-linking of fibrin gamma chains increases resistance to fibrinolysis. *J Biol Chem* **1994**, *269* (45), 28414-9.
199. Duval, C.; Allan, P.; Connell, S. D.; Ridger, V. C.; Philippou, H.; Ariëns, R. A., Roles of fibrin α - and γ -chain specific cross-linking by FXIIIa in fibrin structure and function. *Thromb Haemost* **2014**, *111* (5), 842-50.
200. Sahni, A.; Francis, C. W., Vascular endothelial growth factor binds to fibrinogen and fibrin and stimulates endothelial cell proliferation. *Blood* **2000**, *96* (12), 3772-8.
201. Martino, M. M.; Briquez, P. S.; Ranga, A.; Lutolf, M. P.; Hubbell, J. A., Heparin-binding domain of fibrin(ogen) binds growth factors and promotes tissue repair when incorporated within a synthetic matrix. *Proceedings of the National Academy of Sciences* **2013**, *110* (12), 4563-4568.
202. Tada, S.; Kitajima, T.; Ito, Y., Design and Synthesis of Binding Growth Factors. *International Journal of Molecular Sciences* **2012**, *13* (5), 6053-6072.

Declaration of Authorship

Statement of individual author contributions and of legal second publication rights:

From Thermogelling Hydrogels towards Functional Bioinks: Controlled Modification and Cytocompatible Crosslinking					
Hahn L.*, Beudert M.*, Gutmann M., Keßler L., Stahlhut P., Fischer L., Karakaya E., Lorson T., Thievensen I., Detsch R., Lühmann T., Luxenhofer R.					
<i>Macromolecular Bioscience</i> , 2021, https://doi.org/10.1002/mabi.202100122					
*Contributed equally to this manuscript					
Participated in	Author Initials, Responsibility decreasing from left to right				
Study Design Methods Development	HL, BM, LR, LT	GM, LoT			
Data Collection	HL, BM	GM, KL	SP, KE	FL	
Data Analysis and Interpretation	HL, BM, LR, LT	GM, SP, KE	TI, DR		
Manuscript Writing Writing of Introduction Writing of Materials & Methods Writing of Discussion Writing of First Draft Writing of Supporting Information	HL, BM, LR, LT	GM	FL, KE, TI, DR		

Merging Bioresponsive Release of Insulin-like Growth Factor I with 3D Printable Thermogelling Hydrogels					
Beudert M., Hahn, L., Horn A.H.C., Hauptstein N., Sticht H., Meinel, L., Luxenhofer R., Gutmann M., Lühmann T.					
<i>Journal of Controlled Release</i> , 2022, DOI: 10.1016/j.jconrel.2022.04.028					
Participated in	Author Initials, Responsibility decreasing from left to right				
Study Design Methods Development	BM, GM, LT	HL, LR, AHCH, HS	ML, NH		
Data Collection	BM, GM	HL, AHCH NH			
Data Analysis and Interpretation	BM, GM, LT	HL, NH, AHCH, HS	ML, LR		
Manuscript Writing Writing of Introduction Writing of Materials & Methods Writing of Discussion Writing of First Draft Writing of Supporting Information	BM, GM, LT	HL, NH, AHCH	HS, ML, LR		

Fibrin Sealants – Challenges and Solutions					
Beudert M., Gutmann M., Lühmann T., Meinel L. <i>ACS Biomaterials Science & Engineering</i> , 2022 , DOI: 0.1021/acsbmaterials.1c01437					
Participated in	Author Initials, Responsibility decreasing from left to right				
Study Design Methods Development	BM, GM, ML	LT			
Data Collection					
Data Analysis and Interpretation					
Manuscript Writing Writing of Introduction Writing of Materials & Methods Writing of Discussion Writing of First Draft Writing of Supporting Information	BM, GM, ML	LT			

Molecular Engineering of Fibrinogen for Improved Stability of Fibrin Sealants towards Plasmin Degradation					
Beudert M., Drießen M., Schönemann L., Worschech R., Stecher A., Lühmann T., Meinel L. <i>Unpublished Manuscript</i>					
Participated in	Author Initials, Responsibility decreasing from left to right				
Study Design Methods Development	BM, ML, LT	DM, SL	WR	SA	
Data Collection	BM, DM	SL	WR		
Data Analysis and Interpretation	BM, ML	DM	SL, WR		
Manuscript Writing Writing of Introduction Writing of Materials & Methods Writing of Discussion Writing of First Draft Writing of Supporting Information	BM, ML	LT, DM, SL			



Declaration of Authorship

The doctoral researcher confirms that he has obtained permission from both the publishers (copyright) and the co-authors for legal second publication.

The doctoral researcher and the primary supervisor confirm the correctness of the above-mentioned assessment.

Matthias Beudert 16.12.2022 Würzburg

Doctoral Researcher's Name Date Place Signature

Prof. Dr. Tessa Lühmann 16.12.2022 Würzburg

Primary Supervisor's Name Date Place Signature

Statement of individual author contributions to figures/tables included in the manuscripts:

From Thermogelling Hydrogels towards Functional Bioinks: Controlled Modification and Cytocompatible Crosslinking					
Hahn L.*, Beudert M.*, Gutmann M., Keßler L., Stahlhut P., Fischer L., Karakaya E., Lorson T., Thievessen I., Detsch R., Lühmann T., Luxenhofer R., <i>Macromolecular Bioscience</i> , 2021 , https://doi.org/10.1002/mabi.202100122 *Contributed equally to this manuscript					
Figure	Author Initials , Responsibility decreasing from left to right				
1	BM	HL	GM	LT, LR	
2	HL	BM	KL	LT, LR	
3	HL	BM	KL	LR	
4	HL	BM	SP	GM, LT, LR	
5	HL, BM				
6	BM	GM, HL	FL, TI	TL, LR	
7	BM	GM	HL	TL, LR	
TOC	Author Initials , Responsibility decreasing from left to right				
	BM	HL	GM	LT, LR	

Merging Bioresponsive Release of Insulin-like Growth Factor I with 3D Printable Thermogelling Hydrogels					
Beudert M., Hahn, L., Horn A.H.C., Hauptstein N., Sticht H., Meinel, L., Luxenhofer R., Gutmann M., Lühmann T. <i>Journal of Controlled release</i> , 2022 , DOI: 10.1016/j.jconrel.2022.04.028					
Figure	Author Initials , Responsibility decreasing from left to right				
1	BM, GM	HL, LT	LR	ML, AHCH, HS	
2	AHCH, HS	BM	GM	TL	
3	BM	GM	LT	LR, ML, HL	
4	GM	BM	NH, LT	LR, ML	
5	BM, GM	LT	LR, ML		
6	BM	GM, LH	LT, LR, ML		
TOC	Author Initials , Responsibility decreasing from left to right				
	GM	MB	LT	LR, ML	

Fibrin Sealants – Challenges and Solutions					
Beudert M., Gutmann M., Lühmann T., Meinel L. <i>ACS Biomaterials Science & Engineering</i> 2022 , DOI: 0.1021/acsbmaterials.1c01437					
Figure	Author Initials , Responsibility decreasing from left to right				
1	GM	BM	ML	LT	
2	BM	GM	ML	LT	
3	BM	GM	ML	LT	
4	GM, BM	ML	LT		
Table	Author Initials , Responsibility decreasing from left to right				
1	BM	GM	ML	LT	
2	BM	GM	ML	LT	
TOC	Author Initials , Responsibility decreasing from left to right				
	GM, BM	ML	LT		

Molecular Engineering of Fibrinogen for Improved Stability of Fibrin Sealants towards Plasmin Degradation

Beudert M., Drießen M., Schönemann L., Worschech R., Stecher A., Lühmann T., Meinel L.
Unpublished Manuscript

Figure	Author Initials, Responsibility decreasing from left to right				
1	BM	SA	ML, TL		
2	BM	SL	ML, TL		
3	BM	ML, LT			
4	BM	WR	DM	ML, LT	
5	BM	DM	ML, LT		
6	DM	MB	WR	ML, LT	
TOC	Author Initials, Responsibility decreasing from left to right				
	BM	GM	ML, LT		

I also confirm my primary supervisor's acceptance.

Matthias Beudert 16.12.2022 Würzburg

Doctoral Researcher's Name Date Place Signature

Affidavit

I hereby confirm that my thesis entitled *Bioinspired Modification and Functionalization of Hydrogels for Applications in Biomedicine* is the result of my own work. I did not receive any help or support from commercial consultants. All sources and / or materials applied are listed and specified in the thesis.

Furthermore, I confirm that this thesis has not yet been submitted as part of another examination process neither in identical nor in similar form.

Würzburg, 16.12.2022

Place

Date

Signature

Eidesstattliche Erklärung

Hiermit erkläre ich an Eides statt, die Dissertation *Biologisch-inspirierte Modifizierung und Funktionalisierung von Hydrogelen für Anwendungen in der Biomedizin* eigenständig, d.h. insbesondere selbständig und ohne Hilfe eines kommerziellen Promotionsberaters, angefertigt und keine anderen als die von mir angegebenen Quellen und Hilfsmittel verwendet zu haben.

Ich erkläre außerdem, dass die Dissertation weder in gleicher noch in ähnlicher Form bereits in einem anderen Prüfungsverfahren vorgelegen hat.

Würzburg, 16.12.2021

Ort

Datum

Unterschrift

